ERDC/ITL TR-16-1

Information and Technology Laboratory

US Army Corps of Engineers®
Engineer Research and Development Center

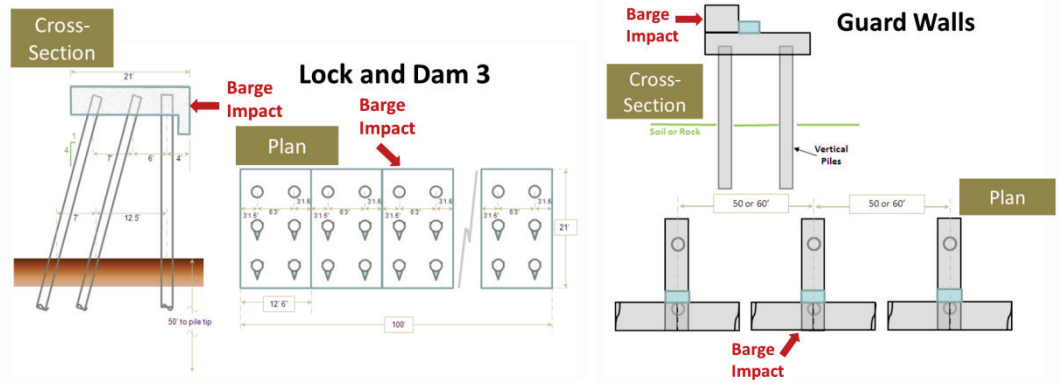
ERDC
INNOVATIVE SOLUTIONS for a safer, better world

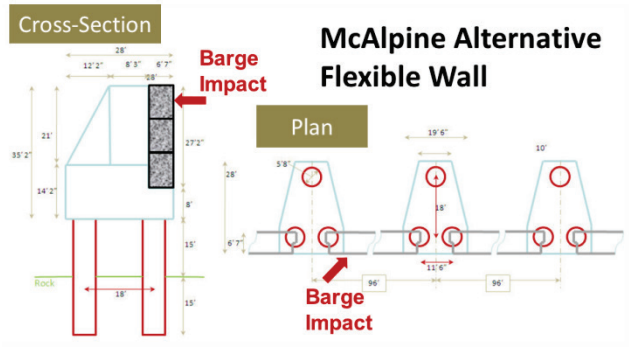
Navigation Systems Research Program

Simplified Dynamic Structural Time-History Response Analysis of Flexible Approach Walls Founded on Clustered Pile Groups Using Impact_Deck

Barry C. White, José Ramón Arroyo, and Robert M. Ebeling

July 2016





Approved for public release; distribution is unlimited.

The US Army Engineer Research and Development Center (ERDC) solves the nation's toughest engineering and environmental challenges. ERDC develops innovative solutions in civil and military engineering, geospatial sciences, water resources, and environmental sciences for the Army, the Department of Defense, civilian agencies, and our nation's public good. Find out more at www.erdc.usace.army.mil.

To search for other technical reports published by ERDC, visit the ERDC online library at http://acwc.sdp.sirsi.net/client/default.

ERDC/ITL TR-16-1
July 2016

Simplified Dynamic Structural Time-History Response Analysis of Flexible Approach Walls Founded on Clustered Pile Groups Using Impact_Deck

Barry C. White and Robert M. Ebeling

Information Technology Laboratory
U.S. Army Engineer Research and Development Center
3909 Halls Ferry Road
Vicksburg, MS 39180-6199

José Ramón Arroyo

Department of General Engineering
University of Puerto Rico
Mayagüez, PR 00681

Final report

Approved for public release; distribution is unlimited.

Prepared for U.S. Army Corps of Engineers
441 G. Street NW
Washington, DC 20314-1000

Under Work Unit Number 448769

Abstract

Flexible approach walls are being considered for retrofits, replacements, or upgrades to Corps lock structures that have exceeded their economic lifetime. This report discusses a new engineering software tool to be used in the design or evaluation of flexible approach walls founded on clustered pile groups and subjected to barge train impact events.

This software tool, Impact_Deck, is used to perform a dynamic, time-domain analysis of three different types of pile-founded flexible approach walls: an impact deck, an alternative flexible approach wall, and a guard wall. Dynamic loading is performed using Impact_Force time histories (Ebeling et al. 2010). This report covers the numerical methods used to create this tool, a discussion of the graphical user interface for the tool, and an analysis of results for the three wall systems.

The results of analyzing the three wall systems reveals that dynamic evaluations should be performed for these structures because of inertial effects occurring in the wall superstructure and substructure. These inertial effects can cause overall and individual response forces that are greater than the peak force from the Impact_Force time history.

This report also discusses the advantages of load sharing between multiple pile groups in an approach wall substructure. In the case of Lock and Dam 3, the peak reaction force for any individual pile group was 11% of the peak impact load.

DISCLAIMER: The contents of this report are not to be used for advertising, publication, or promotional purposes. Citation of trade names does not constitute an official endorsement or approval of the use of such commercial products. All product names and trademarks cited are the property of their respective owners. The findings of this report are not to be construed as an official Department of the Army position unless so designated by other authorized documents.

DESTROY THIS REPORT WHEN NO LONGER NEEDED. DO NOT RETURN IT TO THE ORIGINATOR.

Contents

Abstract ii

Figures and Tables vi

Preface xiii

Unit Conversion Factors xv

1 Dynamic Structural Time-History Response Analysis of a Flexible Approach Wall Supported by Clustered Pile Groups during Impact with a Barge Train 1

1.1 Introduction - Glancing Impact Blows and Flexible Approach Wall Structural Systems 1

1.2 Examples of the Next Generation Flexible Approach Walls 1

1.2.1 Lock and Dam 3 1

1.2.2 McAlpine flexible wall 3

1.2.3 Guard walls 4

1.3 Overview of Dynamic Time-History Response Analysis of a Flexible Beam Supported Over Elastic-Plastic Spring Supports 4

1.4 Report Contents 8

2 Impact Deck Approach Wall – Lock and Dam 3 Example 11

2.1 Introduction 11

2.2 Lock and Dam 3 – Physical Model 11

2.3 Lock and Dam 3 – Construction Drawings 18

2.4 Lock and Dam 3 – Mathematical Model 18

2.5 Nonlinear force-deflection relationship for the spring supports 31

2.6 Solving for the motion of the structure 32

2.7 Validation of Impact_Deck Computer Program 32

2.8 Numerical Example of the Elastic-Plastic Response Using Impact_Deck 34

2.9 Impact_Deck GUI results 36

2.10 Final Remarks 56

3 An Approach Wall with Impact Beams on Nontraditional Pile Supported Bents – McAlpine Example 57

3.1 Introduction 57

3.2 Alternative Flexible Approach Wall – Physical Model 57

3.3 McAlpine Alternative Flexible Approach Wall – Mathematical Model 58

3.4 Nonlinear force-deflection relationship for the springs supports 60

3.5 Solving for the motion of the structure 62

3.6 Validation of Impact_Deck Computer Program 63

3.7 Numerical Example of the Elastic-Plastic Response Using Impact_Deck 66

3.8 Impact_Deck GUI results 67

3.9 Final Remarks 84

4 Traditional Impact Beam Guard Walls 85

4.1 Introduction 85
4.2 Guard Walls – Physical Model 85
4.3 Guard wall – Mathematical Model 86
4.4 Nonlinear force-deflection relationship for the springs supports 88
4.5 Solving for the motion of the structure 90
4.6 Validation of Impact_Deck Computer Program 90
4.7 Numerical Example of the Elastic-Plastic Nonlinear Response Using Impact_Deck 92
4.8 Impact_Deck GUI results 93
4.9 Final Remarks 110

5 Impact_Deck Graphical User Interface (GUI) 111
5.1 Introduction 111
5.2 Geometry Tab 112
5.3 Impact Time History Tab 118
5.4 Beam Properties Tab 119
5.5 Pile Cluster Spring Tab 121
5.6 Analyze Tab 123
5.7 Output Tab 126
5.7.1 FEO Nodal Output 127
5.7.2 FEO Element Output 133
5.7.3 FEO Pile Group Response 138
5.7.4 Run Information 143
5.8 Example: Geometry Input for the Impact Deck at Lock and Dam 3 144
5.9 Final Remarks 148

6 Conclusions and Recommendations 149

References 153

Appendix A: Lock and Dam 3 – Equations of Motion for the Mathematical Model 155

Appendix B: McAlpine Alternative Flexible Wall – Equations of Motion for the Mathematical Model 165

Appendix C: Guard wall – Equations of Motion for the Mathematical Model 179

Appendix D Push-over analysis for batter-pile bent system 189

Appendix E: Formulation for the rotational spring stiffness for the McAlpine flexible approach wall clustered group of vertical piles model 224

Appendix F: HHT-α method 232

Appendix G: Wilson-θ Method 235

Appendix H: Member End Release Details for Load Applied at the End Release Node 238

Appendix I: Rayleigh Damping 240

Appendix J: Key Impact_Deck Program Variables 245

Report Documentation Page

Figures and Tables

Figures

Figure 1.1 Front-end cells of Lock and Dam 3. 2
Figure 1.2 Lock and Dam 3 cross-section and plan view. 3
Figure 1.3 McAlpine flexible walls. 4
Figure 1.4 Guard wall schematic drawing. 5
Figure 1.5 Barge train impacting at a fixed impact position along the simply supported, flexible impact beam mathematical model with the barge train oriented at an approach angle θ to the wall's X_{Global} axis (plan view). 6
Figure 1.6 Example of an impact pulse-force time history. 6
Figure 1.7 Barge impact point force moving along the wall from initial contact time t_1 to final contact time t_2. 7
Figure 2.1 Front end cell of Lock and Dam 3. 12
Figure 2.2 Pinned connection between the circular cell and the Impact Deck at Lock and Dam 3. 13
Figure 2.3 Arrangement of piles at Lock and Dam 3. 13
Figure 2.4 Impact Deck supported over piles at Lock and Dam 3. 14
Figure 2.5 An upstream view starting at the concrete cell of the pile-founded flexible approach wall at Lock and Dam 3. 14
Figure 2.6 Precast bases before installation. 15
Figure 2.7 Precast bases during installation. 15
Figure 2.8 Precast bases connected to piles. 16
Figure 2.9 Construction joint between concrete block segments (axial, shear and moment transfer connection). 16
Figure 2.10 Construction joints. 17
Figure 2.11 Massive concrete circular cell. 17
Figure 2.12 Pile-founded flexible impact deck structure. 18
Figure 2.13 Lock and Dam 3 guide wall plan view 1 of 2. 19
Figure 2.14 Lock and Dam 3 guide wall plan view 2 of 2. 20
Figure 2.15 Lock and Dam 3 guide wall detail of pile layout and end cell. 21
Figure 2.16 Lock and Dam 3 guide wall section view. 22
Figure 2.17 Lock and Dam 3 guide wall plan – 5. 23
Figure 2.18 Lock and Dam 3 guide wall plan – 6. 24
Figure 2.19 Lock and Dam 3 flexible approach wall. 25
Figure 2.20 (a) Typical 3-D segment of the impact-deck beam element, (b) Impact force applied to the Impact Deck, (c) Typical 3-D beam element. 25
Figure 2.21 Typical 2-D beam element used in Impact_Deck 26
Figure 2.22 Lock and Dam 3 mathematical model. 27
Figure 2.23 First beam element used in Lock and Dam 3 mathematical model. 27
Figure 2.24 Last beam element used in Lock and Dam 3 mathematical model. 27

Figure 2.25 Description of two beam elements connected at the inter-monolith connection....28
Figure 2.26 Beam elements numbering in a typical internal monolith....28
Figure 2.27 Cross-section of Lock and Dam 3....29
Figure 2.28 Transverse and longitudinal push-over results for a single row of three piles aligned in the transverse direction....30
Figure 2.29 Force-displacement relation of the spring support....32
Figure 2.30 Force time history of Winfield Test # 10....33
Figure 2.31 Validation of Impact_Deck against SAP2000....34
Figure 2.32 Dynamic response of the transverse spring located at *x = 402.896 ft.*....35
Figure 2.33 Dynamic response of the transverse spring located at *x = 402.896 ft.*....36
Figure 2.34 Reprint of the Figure 4-4 transverse direction of loading push-over analyses from Ebeling et al. (2012); fixed head results in green and pinned head results in blue....37
Figure 2.35 Impact_Deck GUI Table of maximum nodal displacements for the L&D3 example impact deck....39
Figure 2.36 Transverse nodal displacement time histories for node 86....40
Figure 2.37 Longitudinal nodal displacement time histories for node 137....40
Figure 2.38 Rotational nodal displacement time histories for node 93....41
Figure 2.39 Transverse wall displacements at 0.26 sec....42
Figure 2.40 Longitudinal wall displacements at 0.21 sec....42
Figure 2.41 Rotational wall displacements at 0.26 sec....43
Figure 2.42 Impact_Deck GUI table of element minimum and maximum axial forces for the L&D3 example impact deck....43
Figure 2.43 Impact_Deck GUI table of element minimum and maximum shear forces for the L&D3 example impact deck....44
Figure 2.44 Impact_Deck GUI table of element minimum and maximum moments for the L&D3 example impact deck....44
Figure 2.45 Axial-force time histories for element 82....45
Figure 2.46 Axial-force time histories for element 81....46
Figure 2.47 Shear-force time histories for element 82....46
Figure 2.48 Shear-force time histories for element 81....47
Figure 2.49 Moment time histories for element 81....47
Figure 2.50 Moment time histories for element 82....48
Figure 2.51 Wall axial forces at 0.2 sec....48
Figure 2.52 Wall shear forces at 0.2 sec....49
Figure 2.53 Wall moments at 0.18 sec....49
Figure 2.54 Table of pile group response maximum forces and moments and their time....50
Figure 2.55 Table of pile group response maximum displacements and their time....51
Figure 2.56 Table of pile group responses for each pile group individually and summed (not shown) at time 0.26 sec....51
Figure 2.57 Transverse pile group responses for the pile group at node 85 and at time 0.24 sec....52

Figure 2.58 Longitudinal pile group responses for the pile group at node 85 and at time 0.24 sec. 52
Figure 2.59 Rotational pile group response for the pile group at node 85 and at time 0.24 sec. 53
Figure 2.60 Time-history plot of transverse input forces, total force response for all the pile groups, and an individual pile group response forces. 54
Figure 3.1 McAlpine alternative flexible approach wall. 58
Figure 3.2 McAlpine flexible approach wall mathematical model. 59
Figure 3.3 (a) Typical 3-D segment of the Impact Deck beam element, (b) Impact force applied to the Impact Deck, (c) Typical 3-D beam element. 60
Figure 3.4 Typical 2-D beam element used in Impact_Deck. 60
Figure 3.5 Plan view of the flexible wall pile layout. 61
Table 3.1 Primary loading curve for the transverse spring model for a McAlpine alternative flexible wall bent (3 piles). 62
Figure 3.6 Force time history of Winfield Test # 10. 64
Figure 3.7 Validation of Impact_Deck against SAP2000 – Transverse displacement at node 1. 64
Figure 3.8 Validation of Impact_Deck against SAP2000 – Transverse displacement at node 23. 65
Figure 3.9 Validation of Impact_Deck against SAP2000 – Transverse displacement at node 12'. 65
Figure 3.10 Validation of Impact_Deck against SAP2000 – Rotation at node 12 and 12'. 66
Figure 3.11 Dynamic transverse response of node 12 and 12'. 68
Figure 3.12 Dynamic response of the rotational spring at node 12 and 12'. 68
Figure 3.13 Dynamic response of the transverse spring located at $x = 84.5$ *ft.* 69
Figure 3.14 Impact_Deck GUI table of maximum nodal displacements for the McAlpine flexible wall. 70
Figure 3.15 Transverse nodal displacement time histories for node 21. 70
Figure 3.16 Longitudinal nodal displacement time histories for node 22. 71
Figure 3.17 Rotational nodal displacement time histories for node 22. 71
Figure 3.18 Transverse wall displacements at 0.252 sec. 72
Figure 3.19 Longitudinal wall displacements at 0.192 sec. 72
Figure 3.20 Rotational wall displacements at 0.22 sec. 73
Figure 3.21 Impact_Deck GUI table of element minimum and maximum axial forces for the McAlpine flexible wall example. 74
Figure 3.22 Axial-force time histories for element 21. 75
Figure 3.23 Axial-force time histories for element 20. 75
Figure 3.24 Shear-force time histories for element 21. 76
Figure 3.25 Shear-force time histories for element 20. 76
Figure 3.26 Moment time histories for element 31. 77
Figure 3.27 Moment time histories for element 21. 77
Figure 3.28 Wall axial forces at 0.2 sec. 78
Figure 3.29 Wall shear forces at 0.220 sec. 78
Figure 3.30 Wall moments at 0.220 sec. 79

Figure 3.31 Table of pile group response maximum displacements. 79
Figure 3.32 Response forces for the pile groups at time 0.2200 sec. 80
Figure 3.33 Response forces for the pile groups at time 0.2800 sec. 80
Figure 3.34 Pile group response for the pile group at node 2 and at time 0.298 sec. 81
Figure 3.35 Time-history plot of transverse input forces, total force response for all the pile groups, and an individual pile group response forces. 82
Figure 4.1 Guard wall schematic drawing. 86
Figure 4.2 Guard flexible approach wall mathematical model. 87
Figure 4.3 (a) Typical 3-D segment of the Impact Deck beam element, (b) Impact force applied to the Impact Deck, (c) Typical 3-D beam element. 87
Figure 4.4 Typical 2-D beam element used in Impact_Deck. 88
Figure 4.5 Force-displacement relations from push-over analysis of a single guard wall pile. 89
Figure 4.6 Force time history of Winfield Test # 10. 91
Figure 4.7 Validation of Impact_Deck against SAP2000 – Transverse displacement at node 1. 91
Figure 4.8 Validation of Impact_Deck against SAP2000 – Transverse displacement at node 6. 92
Figure 4.9 Dynamic transverse response of node 1. 93
Figure 4.10 Dynamic transverse response of spring at node 6. 94
Figure 4.11 Plastic force-displacement of the transverse spring at node 6. 94
Figure 4.12 Impact_Deck GUI pile group longitudinal and transverse spring model backbone curves. 95
Figure 4.13 Impact_Deck GUI table of maximum nodal displacements for the guard wall. 96
Figure 4.14 Transverse nodal displacement time histories for node 51. 97
Figure 4.15 Longitudinal nodal displacement time histories for node 51. 97
Figure 4.16 Rotational nodal displacement time histories for node 50. 98
Figure 4.17 Transverse wall displacements at 0.332 sec. 98
Figure 4.18 Longitudinal wall displacements at 0.41 sec. 99
Figure 4.19 Rotational wall displacements at 0.286 sec. 99
Figure 4.20 Impact_Deck GUI table of element minimum and maximum axial forces for the guard wall Example. 100
Figure 4.21 Axial force time histories for element 51. 101
Figure 4.22 Axial force time histories for element 50. 101
Figure 4.23 Shear force time histories for element 51. 102
Figure 4.24 Shear force time histories for element 50. 102
Figure 4.25 Moment time histories for element 51. 103
Figure 4.26 Moment time histories for element 50. 103
Figure 4.27 Wall axial forces at 0.410 sec. 104
Figure 4.28 Wall shear forces at 0.714 sec. 104
Figure 4.29 Wall moments at 0.716 sec. 105
Figure 4.30 Table of pile group response maximum displacements. 105
Figure 4.31 Forces at the three pile group nodes at time 0.332 sec. 106

Figure 4.32 Transverse pile group response for the pile group at node 51 and at time 0.332 sec. 106
Figure 4.33 Time-history plot of transverse input forces, total force response for all the pile groups, and an individual pile group response forces. 108
Figure 5.1 Introducing Impact_Deck. 111
Figure 5.2 Geometry for a flexible wall. 112
Figure 5.3 Geometry for a guard wall. 113
Figure 5.4 Geometry for an Impact_Deck. 113
Figure 5.5 Zooming in the input plot section. 116
Figure 5.6 The zoomed view. 116
Figure 5.7 Selected nodes are highlighted. 116
Figure 5.8 Entering an offset to copy selected nodes. 117
Figure 5.9 Confirming the offset copy (which can be performed multiple times). 117
Figure 5.10 Selected nodes are copied at the offset position. 118
Figure 5.11 Input for an impact time history. 119
Figure 5.12 Extending a time history with 0.0 value. 119
Figure 5.13 Beam properties tab as it appears for a flexible wall. 120
Figure 5.14 Beam properties tab as it appears for an impact deck or guard wall. 120
Figure 5.15 Beam properties tab as it appears for a flexible wall. 121
Figure 5.16 Beam properties tab as it appears for an Impact_Deck. 122
Figure 5.17 Analyze tab input for analysis method and specified output. 124
Figure 5.18 Selecting finite element nodes where data will be captured. 125
Figure 5.19 Output tab for selecting and viewing select data. 126
Figure 5.20 Output tab with selected data. 127
Figure 5.21 FEO nodal output window showing maximum nodal values for all the nodes. 128
Figure 5.22 Graph of node 70 X-displacement vs time. 129
Figure 5.23 Graph of node 70 Y-displacement vs time. 129
Figure 5.24 Graph of node 70 Z-displacement vs time. 130
Figure 5.25 Animated graph of wall X-displacement. 132
Figure 5.26 Animated graph of wall Y-displacement. 132
Figure 5.27 Animated graph of wall Z-displacement. 133
Figure 5.28 FEO element output window showing maximum and minimum force and moments acting on all the elements. 134
Figure 5.29 Graph showing element 60 axial force vs time. 135
Figure 5.30 Graph showing element 60 moment force-length vs time. 135
Figure 5.31 Graph showing element 60 shear force vs time. 136
Figure 5.32 Animated graph of axial forces acting on the wall. 137
Figure 5.33 Animated graph of moments acting on the wall. 137
Figure 5.34 Animated graph of shears acting on the wall. 138
Figure 5.35 Pile Group Response Maximum and Minimum Forces and Moments. 139
Figure 5.36 Pile Group Response Peak Deflections. 140

Figure 5.37 Pile Group Response Maximum and Minimum Forces and Moments..... 140
Figure 5.38 Animated plot of node 85 X-force and displacement vs time. 141
Figure 5.39 Animated plot of node 85 Y-force and displacement vs time..... 142
Figure 5.40 Animated plot of node 85 Z-force and displacement vs time. 142
Figure 5.41 Output run information with selected FEO node output..... 144
Figure 5.42 Add node at position 0.0 ft as an inter-monolith node..... 145
Figure 5.43 Add interpolated nodes from 3.3541666 ft to 101.4791666 ft..... 146
Figure 5.44 Selecting nodes with a left-mouse, click-drag. 146
Figure 5.45 Selected nodes are shown with vertical lines..... 146
Figure 5.46 Selected nodes can be copied multiple times with the copy selected nodes button.....147
Figure 5.47 The copy selected nodes dialog lets the user specify an offset. 147
Figure 5.48 Select OK the number of times that the selected nodes need to be copied. 147
Figure 5.49 Finally, Add the Final Node. 148
Figure A.1 Shape function for axial displacement effect..... 157
Figure A.2 Shape function for transverse displacement and rotation effect..... 159
Figure A.3 Force-displacement relation of the spring support..... 164
Figure B.1 Shape function for axial displacement effect..... 167
Figure B.2 Shape function for transverse displacement and rotation effect..... 169
Figure B.3 Force-displacement relation of the spring support. 174
Figure B.4 Typical McAlpine flexible wall system. 175
Figure B.5 McAlpine flexible wall mathematical model. 175
Figure B.6 Transformation of beam element coordinate system (Local-Global). 178
Figure C.1 Shape function for axial displacement effect..... 181
Figure C.2 Shape function for transverse displacement and rotation effect..... 183
Figure C.3 Force-displacement relation of the spring support. 188
Figure D.1 Pipe pile approach wall..... 189
Figure D.2 CPGA analytical model. 190
Figure D.3 Simple interaction diagram for 24-inch-diameter pipe pile..... 191
Figure D.4 (After Figure 3 Yang 1966) Coefficient of critical buckling strength..... 193
Figure D.5 (After Figure 9 Yang 1966) Coefficient decrement of buckling strength. 193
Figure D.6, (After Figure 7 Yang 1966) Coefficient of horizontal load capacity. 197
Figure D.7 (After Figure 2 Yang 1966) Effective embedment of pile at buckling. 202
Figure D.8 Load – displacement plot for pipe pile system..... 222
Figure E.1. Plan view of the McAlpine flexible alternative approach wall system. 224
Figure E.2 Relation between Global-Axis and central support Local-Axis. 225
Figure E.3 Location of the Center of Rigidity. 225
Figure E.4 Definition of the forces and distances generated when the pile cap rotate. 228
Figure E.5 Rotational angle definition when the pile cap rotate..... 229
Figure G.1 Linear variation of acceleration over normal and extended time steps. 235
Figure I.1 (a) Mass-proportional damping; (b) stiffness-proportional damping..... 240

Tables

Table 2.1 Primary loading curve for the transverse spring model of a single pile group with a leading vertical pile followed by two batter piles (Lock and Dam 3). 38

Table 2.2 Primary loading curve for the longitudinal spring model of a single pile group with a leading vertical pile followed by two batter piles (Lock and Dam 3). 38

Table 2.3 Maximum nodal displacements for the Impact_Deck example problem. 39

Table 2.4 Extreme forces/moments for the Impact_Deck example problem. 45

Table 2.5 Transverse forces with respect to time. 54

Table 3.1 Primary loading curve for the transverse spring model for a McAlpine alternative flexible wall bent (3 piles). 62

Table 3.2 Primary loading curve for the longitudinal spring model for a McAlpine alternative flexible wall bent (3 piles). 62

Table 3.3 Primary loading curve for a spring model for a single 6-ft diameter DIP pile. 62

Table 3.4 Maximum nodal displacements for the McAlpine flexible wall example problem. 70

Table 3.5 Extreme forces/moments for the Impact_Deck example problem. 74

Table 3.6 Transverse forces with respect to time. 82

Table 4.1 Primary loading curve for the transverse spring model for a bent with two vertical piles. 89

Table 4.2 Primary loading curve for the longitudinal spring model for a bent with two vertical piles. 90

Table 4.3 Maximum nodal displacements for the guard wall example problem. 96

Table 4.4 Extreme Forces/Moments for the Impact Deck Example Problem. 100

Table 4.5 Transverse forces with respect to time. 107

Table D.1 Euler critical buckling load – translating pile top – pinned head condition 195

Table D.2 Euler critical buckling load – translating pile top – fixed head condition. 196

Table D.3 Euler critical buckling load – translating pile top – pinned head condition. 209

Table D.4 Euler critical buckling load – translating pile top – fixed head condition. 210

Table F.1. HHT-α Method. 234

Table G.1 Wilson's Method: Nonlinear Systems 237

Preface

More than 50% of the U.S. Army Corps of Engineers' locks and their approach walls have continued past their economic lifetimes. As these structures wear out, they must be retrofitted, replaced, or upgraded with a lock extension. Innovative designs must be considered for the Corps hydraulic structures, particularly flexible approach walls, and new tools for evaluating these designs must be developed.

This technical report describes an engineering methodology for the dynamic structural response analysis of a flexible approach wall consisting of a series of impact beams or impact decks supported by clustered pile groups during barge train impact loading. This engineering methodology is implemented in a PC-based FORTRAN program and Visual Modeler named Impact_Deck, which is also discussed in this report. The engineering formulation for Impact_Deck uses an impact-force time history acting on the clustered pile group founded flexible impact beams or impact decks to characterize the impact event. This impact-force time history may be obtained using a companion program Impact_Force (Ebeling et al. 2010).

This report was authorized by Headquarters, U.S. Army Corps of Engineers (HQUSACE), and was written from October 2013 to March 2014. It was published under the Navigation Systems Research Program, Work Unit "Flexible Approach Walls." Jeff McKee was the HQUSACE Navigation Business Line Manager.

The Program Manager for the Navigation Systems Research Program was Charles Wiggins, Coastal and Hydraulics Laboratory (CHL), U.S. Army Engineer Research and Development Center (ERDC). Jeff Lillycrop was Technical Director, CHL-ERDC. The research was led by Dr. Robert M. Ebeling, Information Technology Laboratory (ITL), ERDC, under the general supervision of Dr. Reed L. Mosher, Director, ITL-ERDC; Patti S. Duett, Deputy Director, ITL-ERDC. This work effort was also done under the general supervision of Dr. Robert M. Wallace, Chief, Computational Science and Engineering Division (CSED), ITL, during the initial formulation and programming stage. During the data interpretation and report writing stages, Elias Arredondo, Dr. Kevin Abraham, and Dr. Jerrell R. Ballard were Acting Division Chiefs. Dr. Ballard is the CSED

Chief for the final stage of the publication process. Dr. Ebeling was the Principal Investigator of the "Flexible Approach Walls" work unit.

This report was written by Barry C. White of ITL-ERDC, Professor José Ramón Arroyo, University of Puerto Rico at Mayagüez, and Dr. Ebeling of ITL-ERDC. White is with the Computational Analysis Branch (CAB), of which Elias Arredondo is Chief.

Impact_Deck software formulation was developed by Arroyo and Ebeling. Input specifications for the pertinent engineering features and boundary conditions of the three different wall types to be analyzed by this software were provided by Ebeling, White, and Arroyo. Programming for the engineering formulation was led by Arroyo, with support from White and Ebeling. The Graphical User Interface (GUI) comprised of the Visual Modeler and an extensive and detailed Output Visualization software package was developed by White with support from Arroyo and Ebeling. Example problem input definition was provided by Ebeling, Arroyo, and White. Initial engineering program validation and example problem engineering assessments were led by Arroyo. Initial engineering formulation documentation was created by Arroyo, with support by Ebeling and White. Example problem output was collected and interpreted by White and Arroyo. White was lead on the final organization of this report, including the compilation, recasting, and reduction of the engineering formulation description and example problems using the Impact_Deck processor, with the aid of Arroyo. Having provided the Visual Pre- and Post-Processor for Impact_Deck, White led in writing the user interface and output visualization sections for the report. White also provided additional example problems for verification and to support observations highlighting the unique engineering advantages of each of the three flexible approach wall systems, with the aid of the Visual Pre- and Post-Processor. These unique features were interpreted from the data results by Ebeling and White.

At the time of publication, COL Bryan S. Green was Commander, ERDC, and Dr. Jeffery P. Holland was the Director.

Unit Conversion Factors

Multiply	By	To Obtain
cubic feet	0.02831685	cubic meters
cubic inches	1.6387064 E-05	cubic meters
cubic yards	0.7645549	cubic meters
degrees (angle)	0.01745329	radians
feet	0.3048	meters
foot-pounds force	1.355818	joules
inches	0.0254	meters
inch-pounds (force)	0.1129848	newton meters
knots	0.5144444	meters per second
microns	1.0 E-06	meters
miles (nautical)	1,852	meters
miles (U.S. statute)	1,609.347	meters
miles per hour	0.44704	meters per second
pounds (force)	4.448222	newtons
pounds (force) per foot	14.59390	newtons per meter
pounds (force) per inch	175.1268	newtons per meter
pounds (force) per square foot	47.88026	pascals
pounds (force) per square inch	6.894757	kilopascals
pounds (mass)	0.45359237	kilograms
pounds (mass) per cubic foot	16.01846	kilograms per cubic meter
pounds (mass) per cubic inch	2.757990 E+04	kilograms per cubic meter
pounds (mass) per square foot	4.882428	kilograms per square meter
pounds (mass) per square yard	0.542492	kilograms per square meter
slugs	14.59390	kilograms
square feet	0.09290304	square meters
square inches	6.4516 E-04	square meters
tons (force)	8,896.443	newtons
tons (force) per square foot	95.76052	kilopascals
tons (2,000 pounds, mass)	907.1847	kilograms
tons (2,000 pounds, mass) per square foot	9,764.856	kilograms per square meter
yards	0.9144	meters

1 Dynamic Structural Time-History Response Analysis of a Flexible Approach Wall Supported by Clustered Pile Groups during Impact with a Barge Train

1.1 Introduction - Glancing Impact Blows and Flexible Approach Wall Structural Systems

A glancing blow impact event of a barge train impacting an approach wall as it aligns itself with a lock is an event of short duration. The contact time between the impact corner of the barge train and the approach wall can range from one second to several seconds. In order to reduce construction costs as well as to reduce damage to barges during glancing blow impacts with lock approach walls, the next generation of Corps approach walls are more flexible than the massive, stiff-to-rigid structures constructed in the past. A flexible approach wall or flexible approach wall system is one in which the wall/system has the capacity to absorb impact energy by deflecting or "flexing" during impact, thereby affecting the dynamic impact forces developing during the impact event. Pile-founded approach wall structural systems are characterized as flexible structures. This report summarizes an engineering methodology as well as the corresponding software for performing a dynamic structural response analysis. The analysis is of a flexible impact approach wall deck or impact beam system supported by piles representing using an elastic-plastic spring model of each of the clustered pile groups to a barge train impact event. The PC-based software used for conducting the dynamic structural response analysis is referred to as Impact_Deck. A pulse-force time history of the barge train impacting the flexible approach wall is used to dynamically load the model. The PC-based software Impact_Force (Ebeling et al. 2010) is used to develop the pulse-force time history required by the Impact_Deck software.

1.2 Examples of the Next Generation Flexible Approach Walls

1.2.1 Lock and Dam 3

Lock and Dam No. 3 (Lock and Dam 3) is a lock and dam located near Red Wing, Minnesota on the Upper Mississippi River around river mile 796.9.

It was constructed and placed in operation July 1938. The site underwent major rehabilitation from 1988 through 1991. In recent years, a guide wall extension was added to the project.

The structure consists of eight reinforced concrete monoliths of 104 ft 10 in. each. It was constructed by joining eight concrete blocks of 12 ft 6 in. with a free end of 37.5 in. at both ends. Each block is supported over two rows of piles with three piles per row. That results in a monolith supported by 48 piles, where 36 of these piles are battered with a batter of 1:4. Over the piles, the monolith's dimensions are 5 ft in height and 22 ft in width. One end of the deck is pinned and connected to a massive circular concrete cell and the other end is free. The inter-monolith connections are connected by using four reinforcing steel bars just to transfer the axial and shear force and no flexural moment transfer. The piles have a diameter of 2 ft, and are symmetrically located at each concrete block. The weight of each precast concrete beam is approximately 6,919 tons. Some of the drawings/plans of this flexible impact deck are shown in Appendix D. Examples of this type of Corps flexible approach wall is shown in Figures 1.1 and 1.2 for Lock and Dam 3.

Figure 1.1 Front-end cells of Lock and Dam 3.

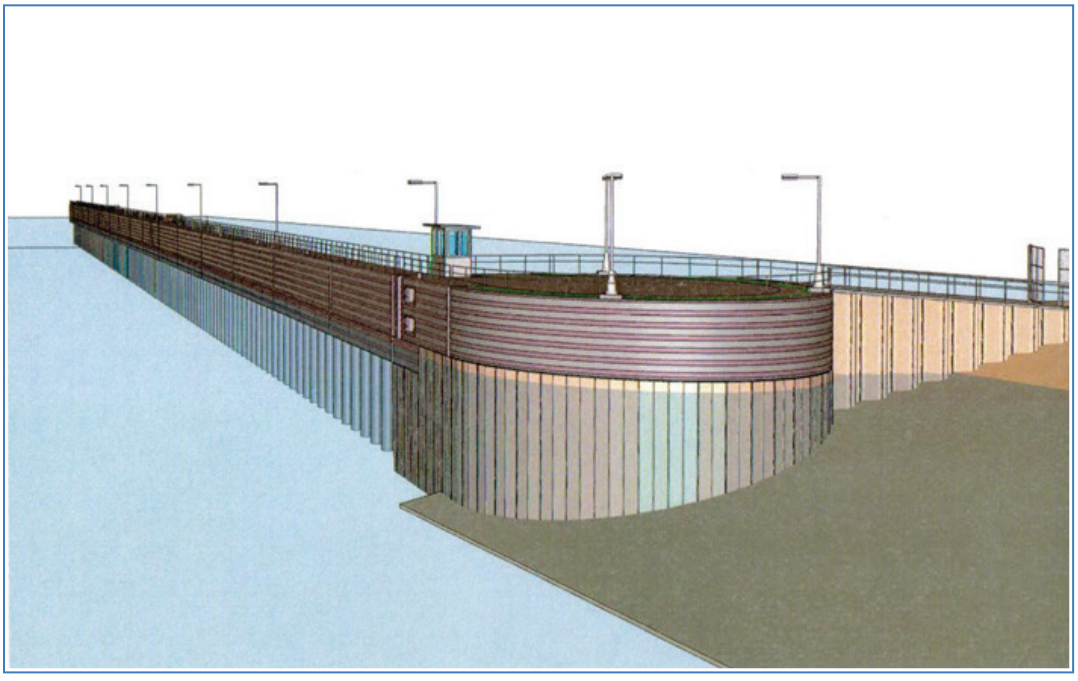
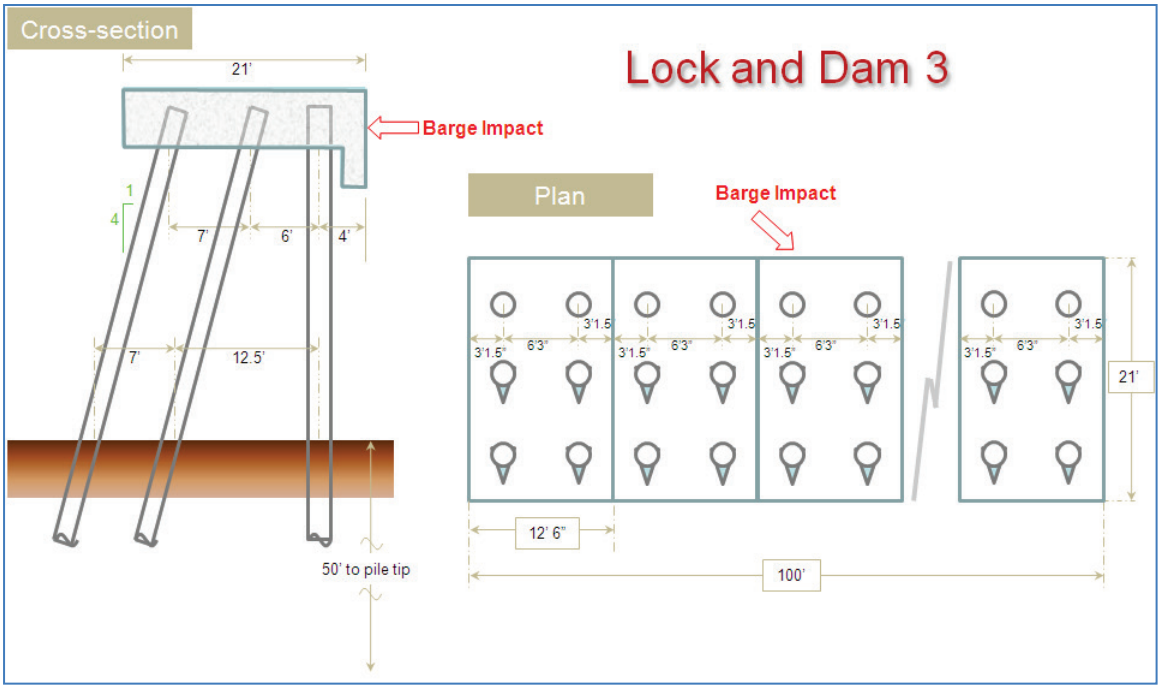


Figure 1.2 Lock and Dam 3 cross-section and plan view.

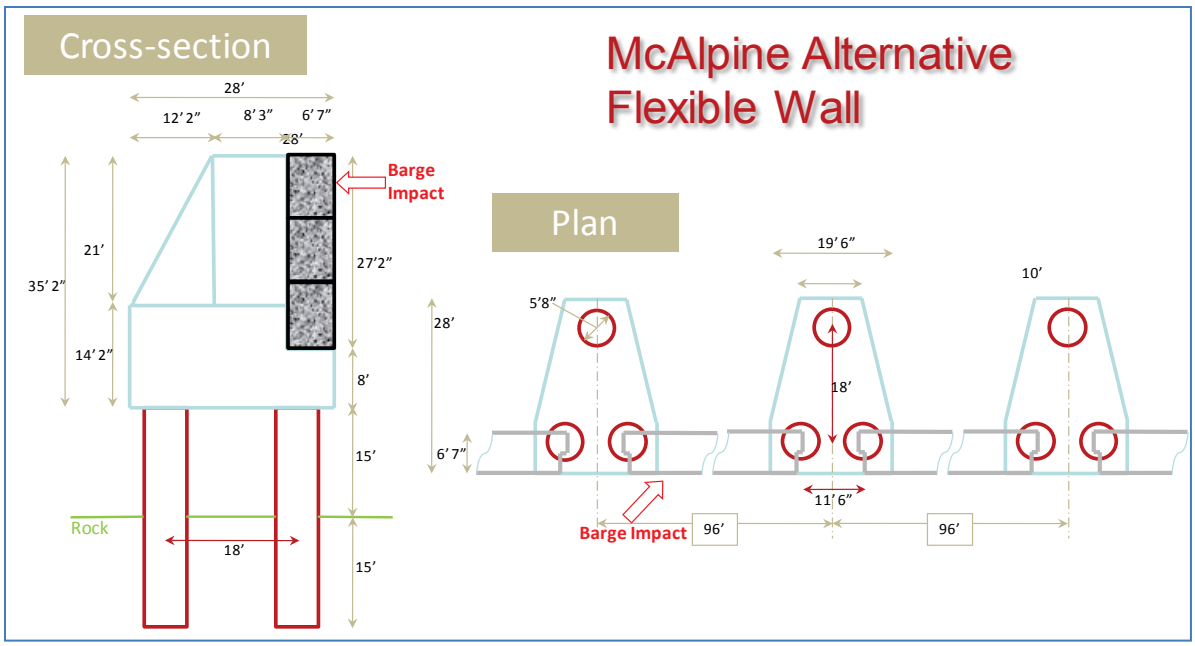


1.2.2 McAlpine flexible wall

McAlpine Locks and Dam are located in downtown Louisville, Kentucky. The dam is at mile 604.4 of the Ohio River and the locks are in the Louisville and Portland Canal on the Kentucky side of the river. The 56 ft x 600 ft auxiliary lock was completed in 1921. The 110 ft x 1200 ft main chamber opened in 1961. A new lock chamber (110 ft x 1200 ft) began operation in 2009.

The alternative flexible approach wall structure discussed in this section consists of a continuous elastic concrete beam with segments spanning approximately 96 ft in length. The continuity of the beam is achieved by means of shear key at each pile group support. That means the beams just transfer the longitudinal and transverse forces with no moment transfer at each pile support. The axial and transverse forces at the end of the beams are transferred to the pile cap by means of a shear key. The shear key has a length of 11.5 ft. The length of the shear key is the distance between two consecutive concrete beams. The shear key is part of the massive pile cap that rests over the pile group. The pile group consists of three piles, each one with a diameter of 5 ft 8 in. They are arranged in a triangular scheme to absorb the torsion generated at the pile group due to the eccentricity between the center of the pile group and the location of the end of the beams that rest over the pile group. A plan view drawing and a cross-section view are presented in Figure 1.3.

Figure 1.3 McAlpine flexible walls.



1.2.3 Guard walls

This kind of flexible approach wall can be found at numerous Corps locks. The structure consists of a continuous elastic concrete beam with a span of approximately 50 or 60 ft long, each segment. The continuity of the beam is achieved by means of shear key at each pile-group support. That means the beams just transfer the longitudinal and transverse forces with no moment transfer at each pile support. The axial and transverse forces at the ends of the beams are transferred to the pile cap by means of a shear key. The shear key is a concrete block between the end and start of two consecutive flexible beams constraining the motion of the beam to the motion of the pile bent. The length of the shear key is equal to the width of the pile cap of the pile group. The shear key is part of the massive pile cap that rests over the pile group. The pile group consists of two aligned piles, each with a diameter of 5 ft 8 in. The two piles are arranged in such a way that no torsion is transferred to the pile group. A plan view drawing and a cross-section view are presented in Figure 1.4.

1.3 Overview of Dynamic Time-History Response Analysis of a Flexible Beam Supported Over Elastic-Plastic Spring Supports

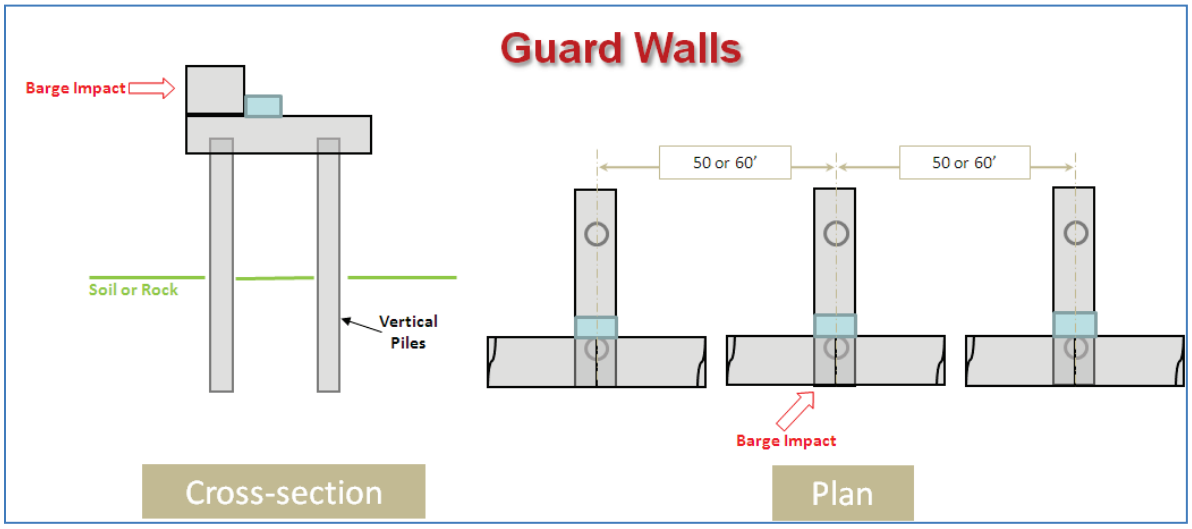
Due to the flexibility and the mass of the new generation flexible approach walls, the impact event can be a dynamic event from the point of view of the mathematical structural model. In structural dynamics the mathematical

model of bodies of finite dimensions undergoing translatory motion are governed by Newton's Second Law of Motion, expressed as

$$\sum F = m \bullet a \tag{1.1}$$

where F are forces, m is mass, and a is acceleration at each time step *t* during motion.

Figure 1.4 Guard wall schematic drawing.



In the mathematical model, the forces acting on the flexible wall mass at each time step *t* are (1) the impact force at time step *t*, (2) the elastic restoring forces (of the beam), and (3) the damping forces (of the beam). This report discusses an engineering methodology that uses Equation 1.1 to compute the dynamic structural response of a flexible impact beam supported over flexible supports of the mathematical model to the impact-force time history. The impact event is idealized as shown in Figure 1.5 for the mathematical beam and impact event model of the force time history, $F_{normal\text{-}wall}(t)$ is developed by scaling of existing pulse-force time histories recorded during the full-scale barge impact experiments conducted at Winfield Lock & Dam (Ebeling et al. 2010) and the Pittsburgh Prototype tests (Patev et al. 2003). The force time history shown in Figure 1.6 denotes the component of the pulse force time history acting normal to the wall. Initial barge train contact with the wall starts at time t_1 and ends at time t_2. The solution to this dynamic problem will be a succession of solutions at user-specified time steps starting at time t_1. These solution time steps are dictated by the time step the user selects for the barge train impact-force time history created using the PC-based software

Impact_Force (Ebeling et al. 2010). Due to the nature of dynamic structural response of some types of beams with consideration of both the duration and frequency characteristics of the impact-force time history, the peak response of the simply supported, flexible impact beam may occur during impact (i.e., between times t_1 and t_2) or after impact concluded (i.e., after time t_2). The engineering methodology discussed in this report and corresponding software are capable of addressing both types of dynamic structural systems responses.

Figure 1.5 Barge train impacting at a fixed impact position along the simply supported, flexible impact beam mathematical model with the barge train oriented at an approach angle θ to the wall's X_{Global} axis (plan view).

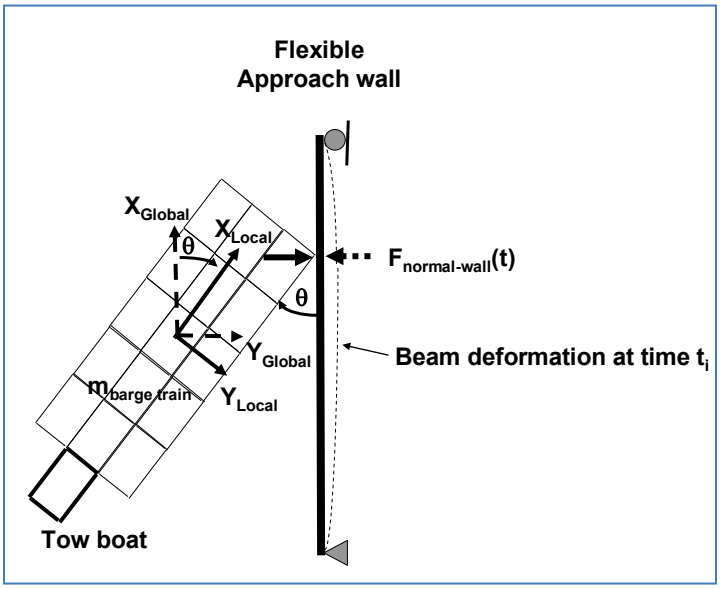
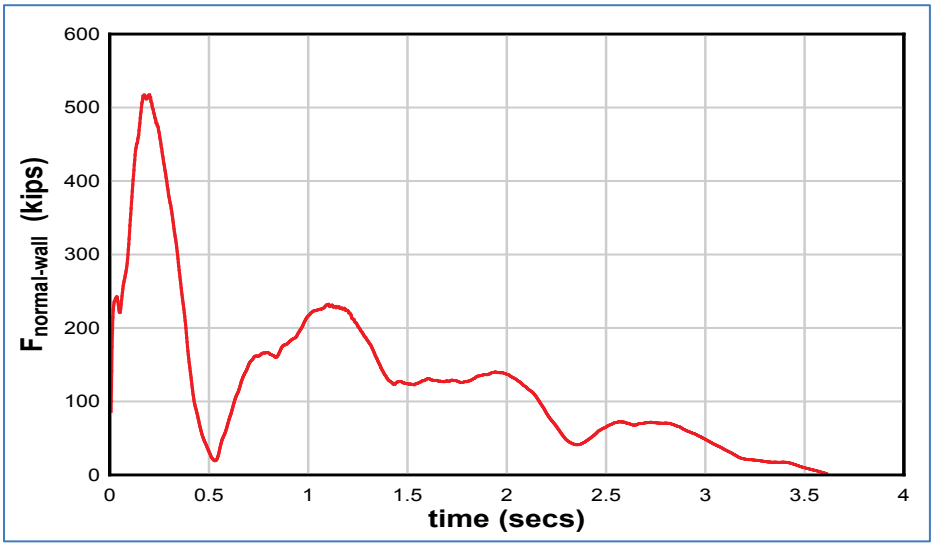


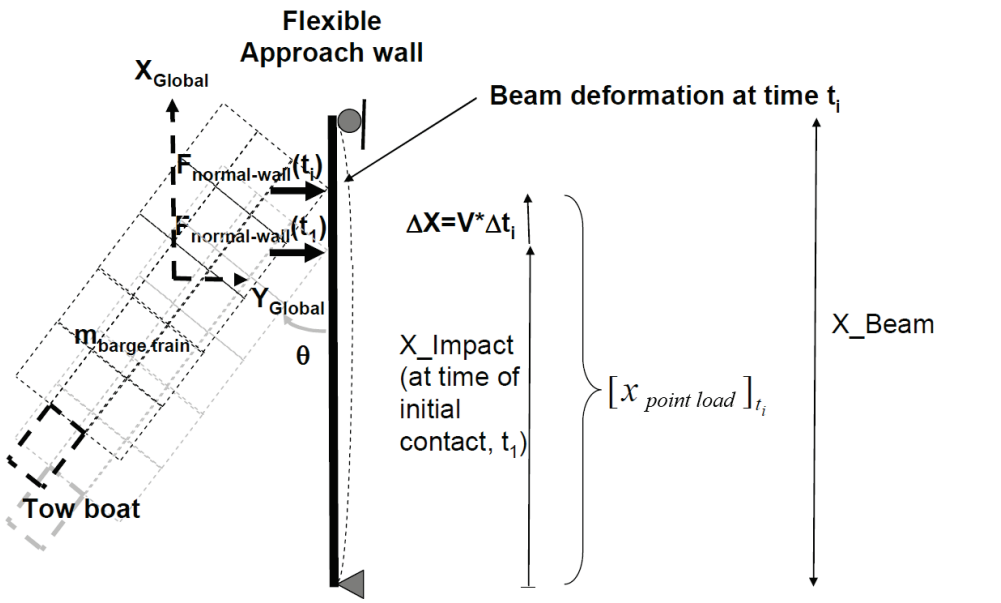
Figure 1.6 Example of an impact pulse-force time history.



An alternative formulation incorporated within the PC-based program Impact_Deck allows for the specification of a barge train having an initial contact with the impact beam at a position designated X_Impact (in PC-program Impact_Deck input terminology) at time t_1 and moving in contact at a constant velocity (V) along the beam as shown in Figure 1.7. The position of the impact point force moves with time after contact. The time after contact is designated as an increment in time Δt_i, and it occurs at an absolute time of $[t_1 + \Delta t_i]$. The change in position of the contact force is designated a distance ΔX from initial contact point X_Impact and is given by

$$\Delta X = V \bullet \Delta t_i \tag{1.2}$$

Figure 1.7 Barge impact point force moving along the wall from initial contact time t_1 to final contact time t_2.



The position of the point load along the beam at time t_i is

$$[x_{\text{point load}}]_{t_i} = X_\text{Impact} + \Delta X \tag{1.3}$$

Substituting from Equation 1.2, Equation 1.3 becomes

$$[x_{point\ \ load}]_{t_i} = [X_\text{Impact} \quad + V \bullet \Delta t_i] \tag{1.4}$$

Thus, the normal force time history of Figure 6 moves along the beam from time t_1 to time t_2 according to the user-specified velocity (V).

1.4 Report Contents

The engineering methodology discussed in this report is implemented in a PC-based FORTRAN program named Impact_Deck, which is also discussed in this report. A pulse-force time history (normal to the flexible approach wall) is used in this dynamic time-history response analysis to represent the demand made of the flexible beam supported over elastic-plastic springs during the impact event. The impact-force time history to be used in the Impact_Deck analysis is created by the companion PC-based program Impact_Force (Ebeling et al. 2010). The engineering formulation for Impact_Force uses the impulse momentum principle to convert the linear momentum of a barge train into a pulse-force time history acting normal to the approach wall.

The engineering formulation developed for and implemented in Impact_Deck assumes that the District engineer will have knowledge of

1. Length, modulus of elasticity, cross-sectional area, moment of inertia and mass per unit length (equal to the weight per unit length divided by the gravitational constant, including hydrodynamic added mass for the beam) of the flexible impact beam
2. Point of initial impact
3. Velocity *(V)* the barge train moves along the approach wall during impact
4. Dynamic coefficient of friction between the wall and the barge train
5. Force-displacement relationship of a pile group
6. Impact pulse-force time history normal to the impact beam

The engineering formulation developed for Impact_Force assumes that the District engineer will have knowledge of

1. Size, the weight (and mass) of the barge train (including hydrodynamic added mass)
2. Barge approach velocity (often expressed in local barge coordinates)
3. Approach angle (the angle measured from the face of the wall to the side of the barge train)

This information will be required for the usual, unusual, and extreme design load cases.

Sections 2-4 describe the relationships that comprise the engineering formulation used to solve Newton's Second Law of Motion for the dynamic response of a flexible impact beam supported on groups of piles and subjected to a barge train impact. The groups of piles are modeled as stiff elastic-plastic springs. The barge train impact is modeled using a representative pulse-force time history applied normal to the point of contact between the barge train and the flexible approach wall. In this initial engineering formulation implemented in Impact_Deck, the numerical solution of Newton's Second Law of Motion for the impact pulse-force time history is applied to the flexible impact beam. The numerical solution makes use of the Wilson's θ method to solve the equations of motion of the multiple degrees of freedom (MDOF) system in the time domain. Each section discusses the results of this analysis for a different structural system. The analysis in section 2 is for the Lock and Dam 3 guide wall structural system; section 3 is for the McAlpine flexible wall structural system; and section 4 is for a typical guard wall structural system.

Section 5 introduces the user to the Graphical User Interface (GUI), Engineering Processor, and Visual Post-Processor named Impact_Deck. An example problem presents the features for input and the output visualization.

Section 6 presents the conclusions of this report based on the Impact_Deck computer software.

Appendix A discusses the formulation for a structural impact deck founded on rows of pile groups. This type of flexible approach wall structural system was used for the Lock and Dam 3 approach wall extension. Each pile group cluster consists of an in-line row of vertical and batter piles.

Appendix B discusses the formulation for a flexible approach wall founded on a triangular formation of three vertical piles modeled using Impact_Deck. The McAlpine lock alternative flexible approach wall structural system is an example of this type of flexible-impact structure.

Appendix C discusses the formulation for a simply supported flexible-impact beam supported by two groups of clustered vertical piles modeled

using Impact_Deck. Guard walls are an example of this type of flexible-impact structure. Each pile-group cluster consists of an in-line row of vertical piles.

Appendix D discusses the formulation for a two-translational spring model of a row of piles that is used in Impact_Deck. This appendix discusses the non-linear, force-deflection relationship for primary loading and for unload-reload response of the clustered group of piles using the push-over method of analysis and CPGA[1] software applied to the Lock and Dam 3 approach wall extension problem.

Appendix E discusses the formulation for a single rotational spring model of a clustered group of vertical piles. This type of flexible approach wall structural system, proposed for use at McAlpine Locks and Dam, is referred to as the "alternative" flexible approach wall system.

Appendix F discusses the numerical method formulation for the time integration of the Equation of Motion by HHT-α.

Appendix G discusses the numerical method formulation for the time integration of the Equation of Motion by the Wilson-θ method.

Appendix H summarizes the member end release details used in Impact_Deck for a load applied at the end release node.

Appendix I summarizes the Raleigh Damping formulation for the three flexible approach walls.

Appendix J summarizes the Impact_Deck ASCII input file.

Appendix K lists key Impact_Deck FORTRAN program variables.

[1] CPGA is CASE software for the Pile Group Analysis.

2 Impact Deck Approach Wall – Lock and Dam 3 Example

2.1 Introduction

This chapter summarizes an engineering methodology using the Impact_Deck software for performing a dynamic structural response analysis of a flexible impact deck supported over groups of clustered piles and subjected to a barge train impact event. This example is based on the real-world example at Lock and Dam 3 on the Mississippi River in Minnesota.

This example models a glancing blow impact event of a barge train impacting an approach wall as it aligns itself with a lock is an event of short duration; the contact time between the impact corner of the barge train and the approach wall can be as short as a second or as long as several seconds. The next generation of Corps approach walls is more flexible than the massive, stiff-to-rigid structures constructed in the past in order to reduce construction costs as well as to reduce damage to barges during glancing blow impacts with lock approach walls. A flexible approach wall or flexible approach wall system is one in which the wall has the capacity to absorb impact energy by deflecting or "flexing" during impact, thereby affecting the dynamic impact forces that develop during the impact event.

2.2 Lock and Dam 3 – Physical Model

Lock and Dam 3 is located in Welch Township, Minnesota, on the Upper Mississippi River, approximately 6 miles upstream from Red Wing, Minnesota (around river mile 796).

Artist renderings, idealized cut-away sections, and pictures of Lock and Dam 3 are shown in Figures 2.1 through 2.12, as well as in Figures D.1 and D.2 (Appendix D). The impact deck of the flexible guide wall consists of eight reinforced concrete monoliths. Each monolith is approximately 104 ft 10 in. in length[1]. Each impact-deck monolith was constructed by joining together eight concrete precast block segments that are 12 ft 6 in. in length. Each 12 ft 6 in. block segment is supported over two rows of

[1] The cited dimensions and those shown on construction drawings may deviate slightly from as-built conditions.

piles, with three piles per row. The front row of piles is vertical and the back two rows of piles have a batter of 1:4. The piles are concrete-filled pipe piles having a diameter of 2 ft and a vertical height of approximately 72 ft (Figure D.1). Figure 2.6 shows one of the pre-cast 12 ft 6 in. bases for each block segment prior to installation. The base is hung from the top of the piles (Figure 2.8). The impact-deck monolith is then cast on top of eight neighboring block segments. Figure 2.2 shows the relationship of the two and a half precast bases (the areas above the piles but below the monolith, separated by vertical lines) to the overtopping monolith and supporting pile groups. That results in an impact-deck monolith being supported by 48 flexible piles, where 16 of these piles are vertical and another 32 of these piles are battered. Over the piles, the impact-deck monolith has dimensions of 5 ft height and 22 ft width.

Each end of adjoining monoliths is structurally detailed to provide for shear and axial load transfer but no moment transfer between monoliths using shear bars that are close to the line through the cross-section center. The ends of each monolith are 37.5 in. from the last supporting pile group.

One end of the flexible guide wall impact deck (consisting of eight monoliths) is pin-connected to a massive circular concrete cell and the other end, adjacent to the existing approach wall, is free. The weight of impact deck (all eight monoliths) is approximately 627,655 kg (6,919 tons).

Figure 2.1 Front end cell of Lock and Dam 3.

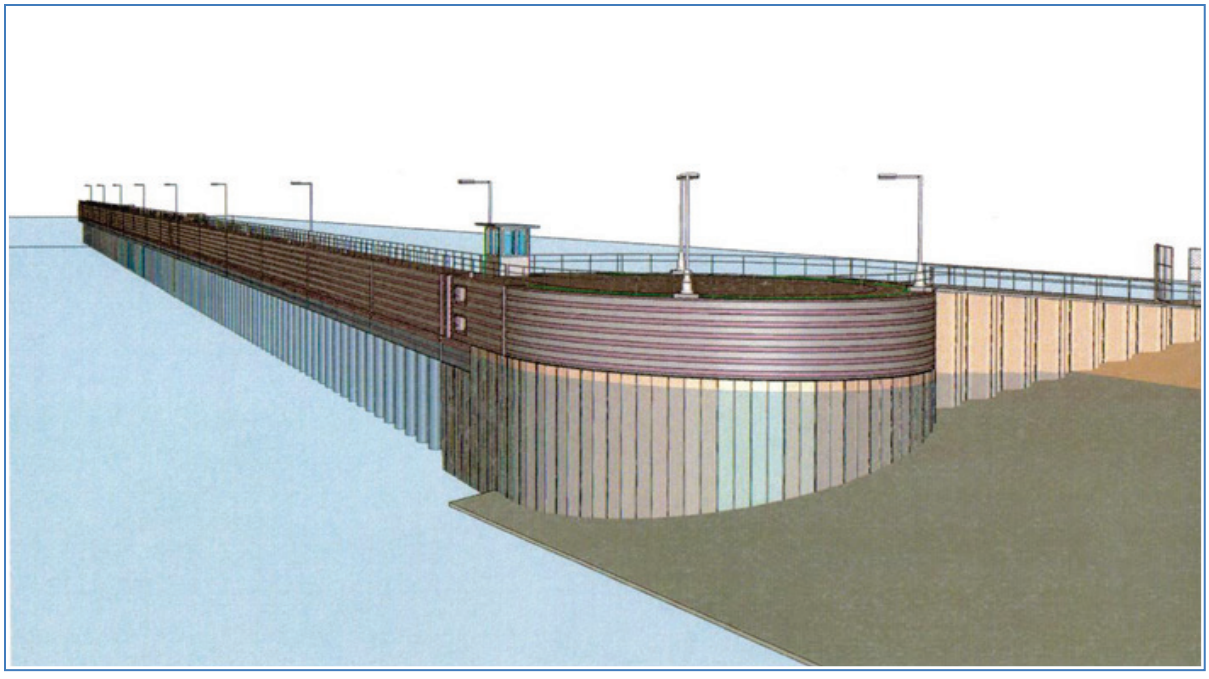


Figure 2.2 Pinned connection between the circular cell and the Impact Deck at Lock and Dam 3.

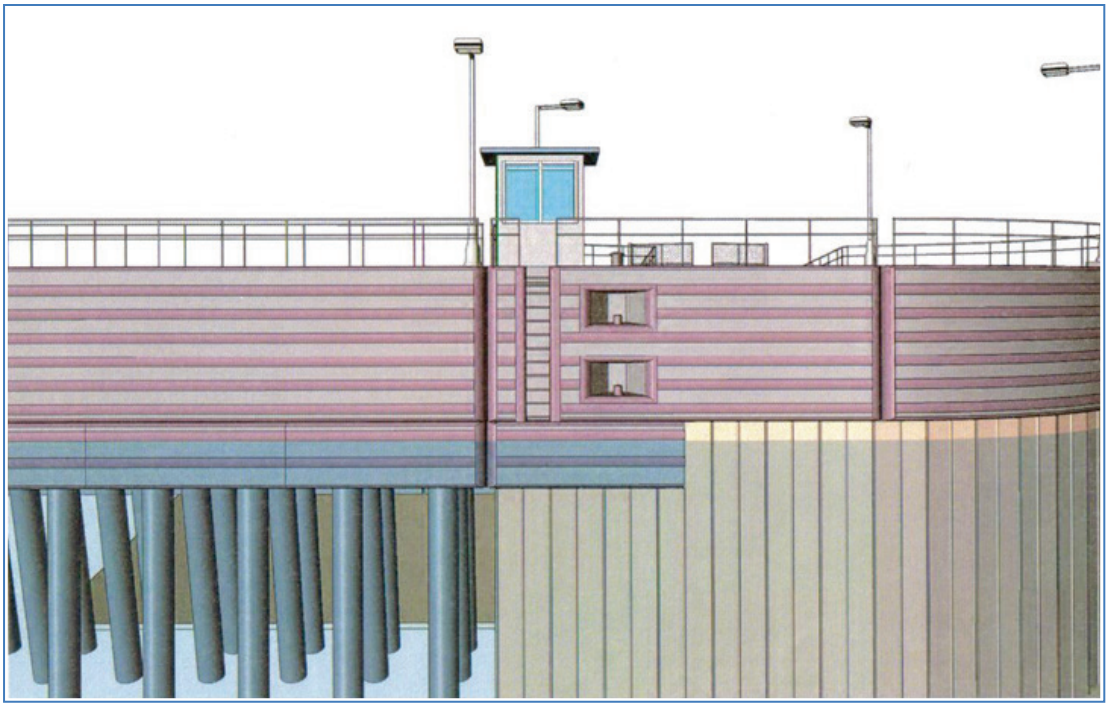


Figure 2.3 Arrangement of piles at Lock and Dam 3.

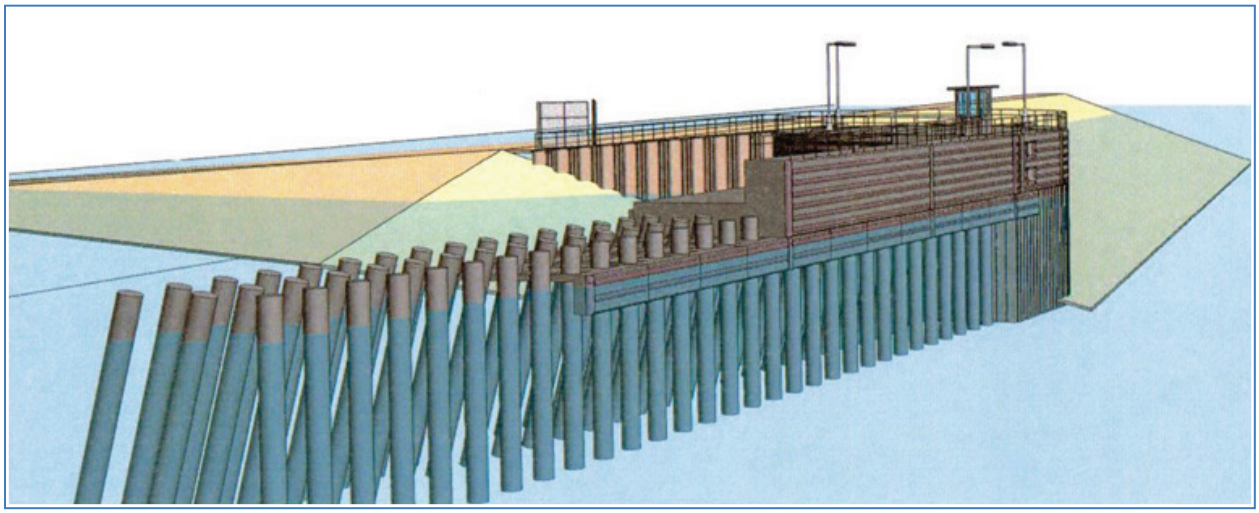


Figure 2.4 Impact Deck supported over piles at Lock and Dam 3.

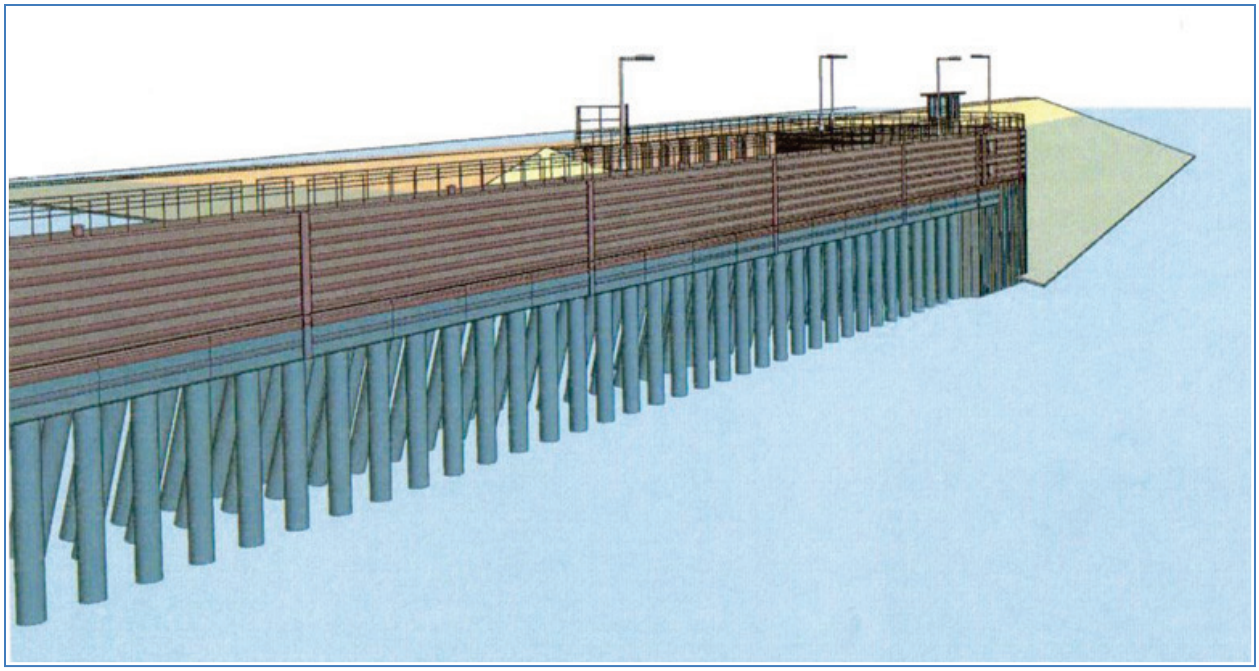


Figure 2.5 An upstream view starting at the concrete cell of the pile-founded flexible approach wall at Lock and Dam 3.



Figure 2.6 Precast bases before installation.



Figure 2.7 Precast bases during installation.



Figure 2.8 Precast bases connected to piles.



Figure 2.9 Construction joint between concrete block segments (axial, shear and moment transfer connection).



Figure 2.10 Construction joints.



Figure 2.11 Massive concrete circular cell.



Figure 2.12 Pile-founded flexible impact deck structure.



2.3 Lock and Dam 3 – Construction Drawings

In Figures 2.13-2.18, some general construction drawings are provided that demonstrate the pile arrangement, the inter-monolith arrangement, and circular concrete cell location. Figure 2.14 shows the plan view and pile layout for the concrete cell at the start of the guide wall. Figure 2.5 is a picture of this completed concrete cell. A typical cross section of the flexible impact deck structural system is presented in Figure 2.15. This figure also shows a close-up, plan view of a 12 ft 6 in. long precast base segment. Figure 2.6 is a picture of this precast base segment.

2.4 Lock and Dam 3 – Mathematical Model

Lock and Dam 3 can be considered as a beam element because its length is much greater than the other two directions. The length is 838.66 ft and the height and width are 5 ft and 22 ft, respectively. The model can be seen in Figure 2.19.

Figure 2.13 Lock and Dam 3 guide wall plan view 1 of 2.

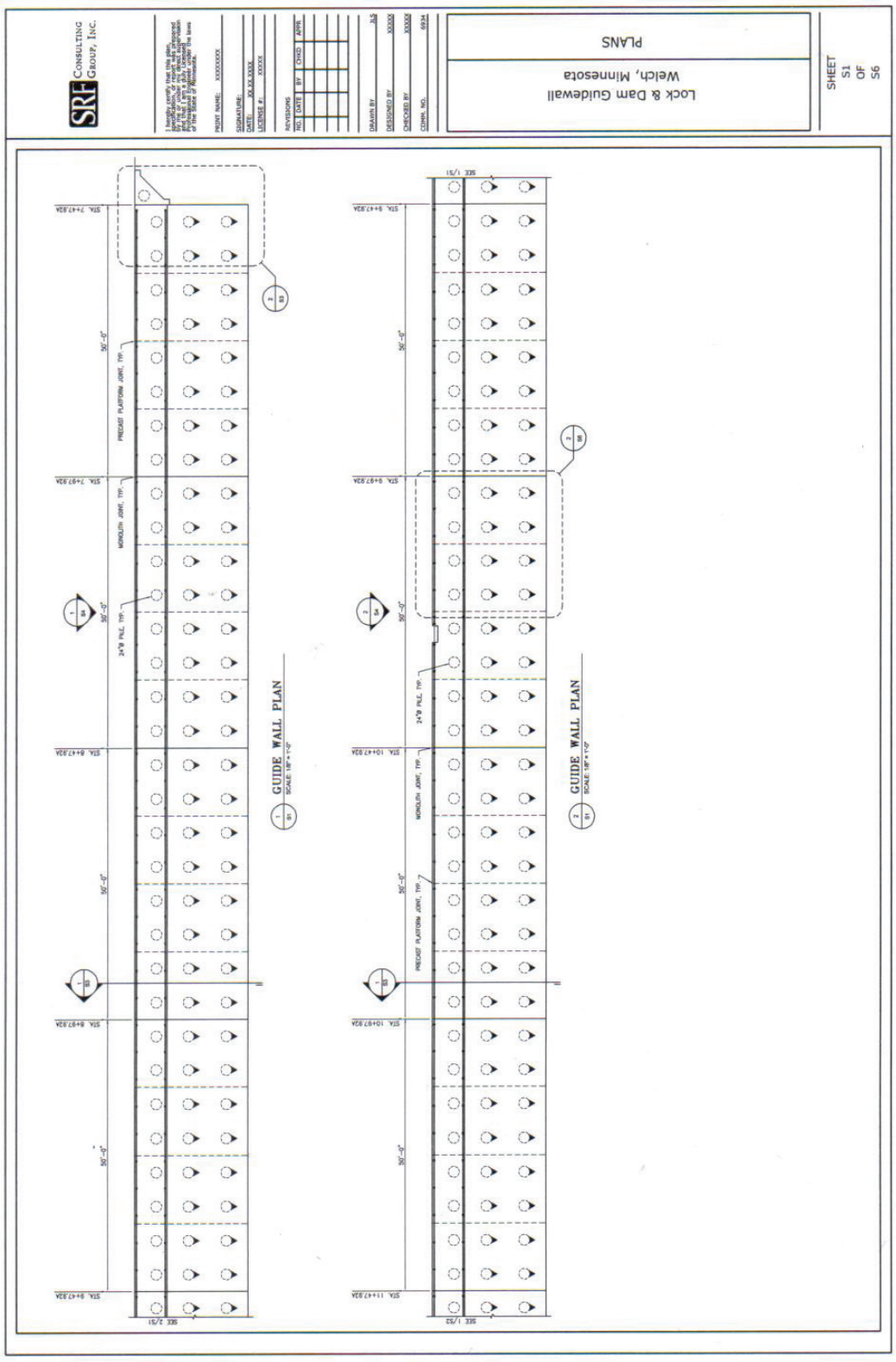


Figure 2.14 Lock and Dam 3 guide wall plan view 2 of 2.

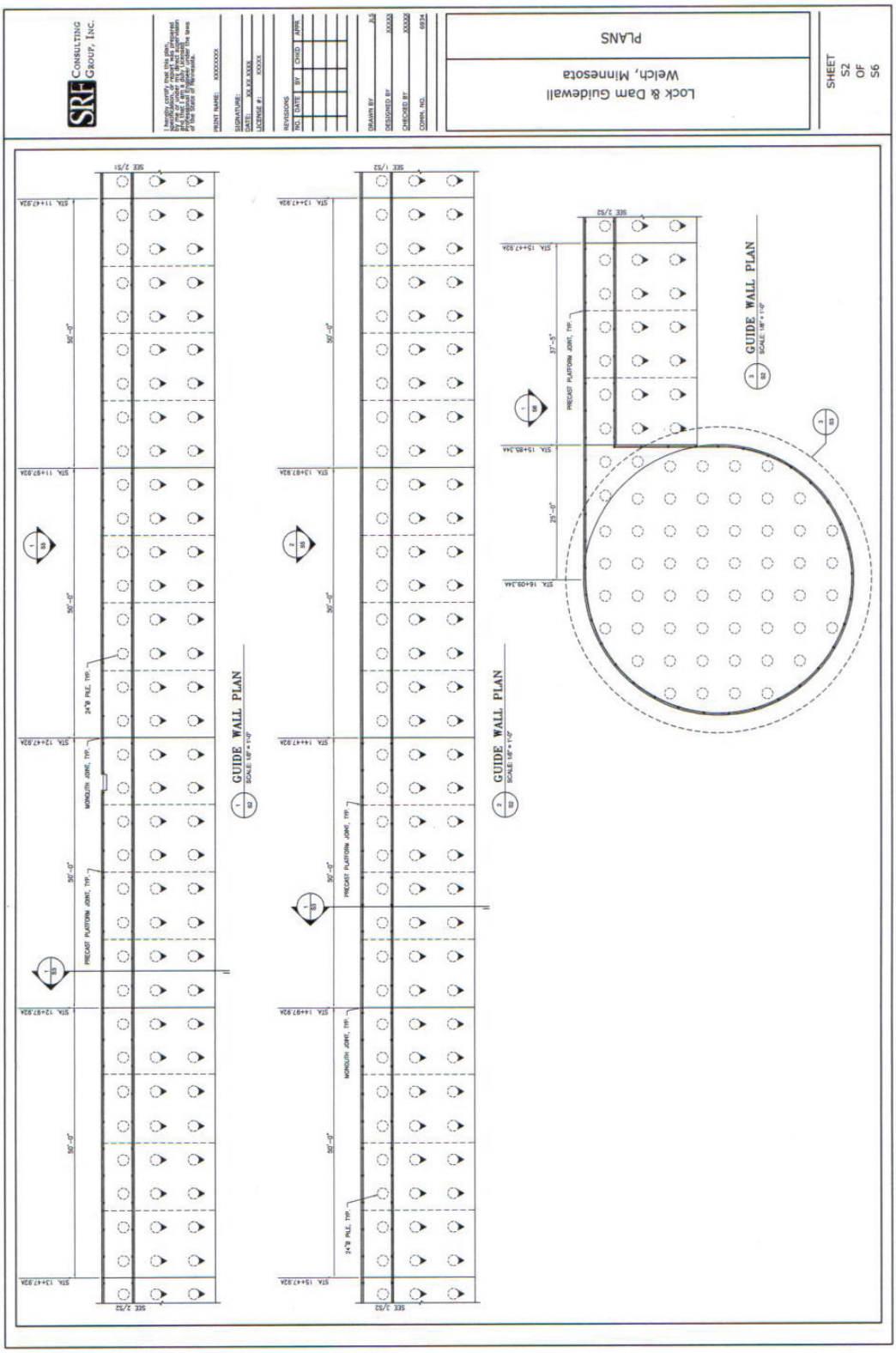


Figure 2.15 Lock and Dam 3 guide wall detail of pile layout and end cell.

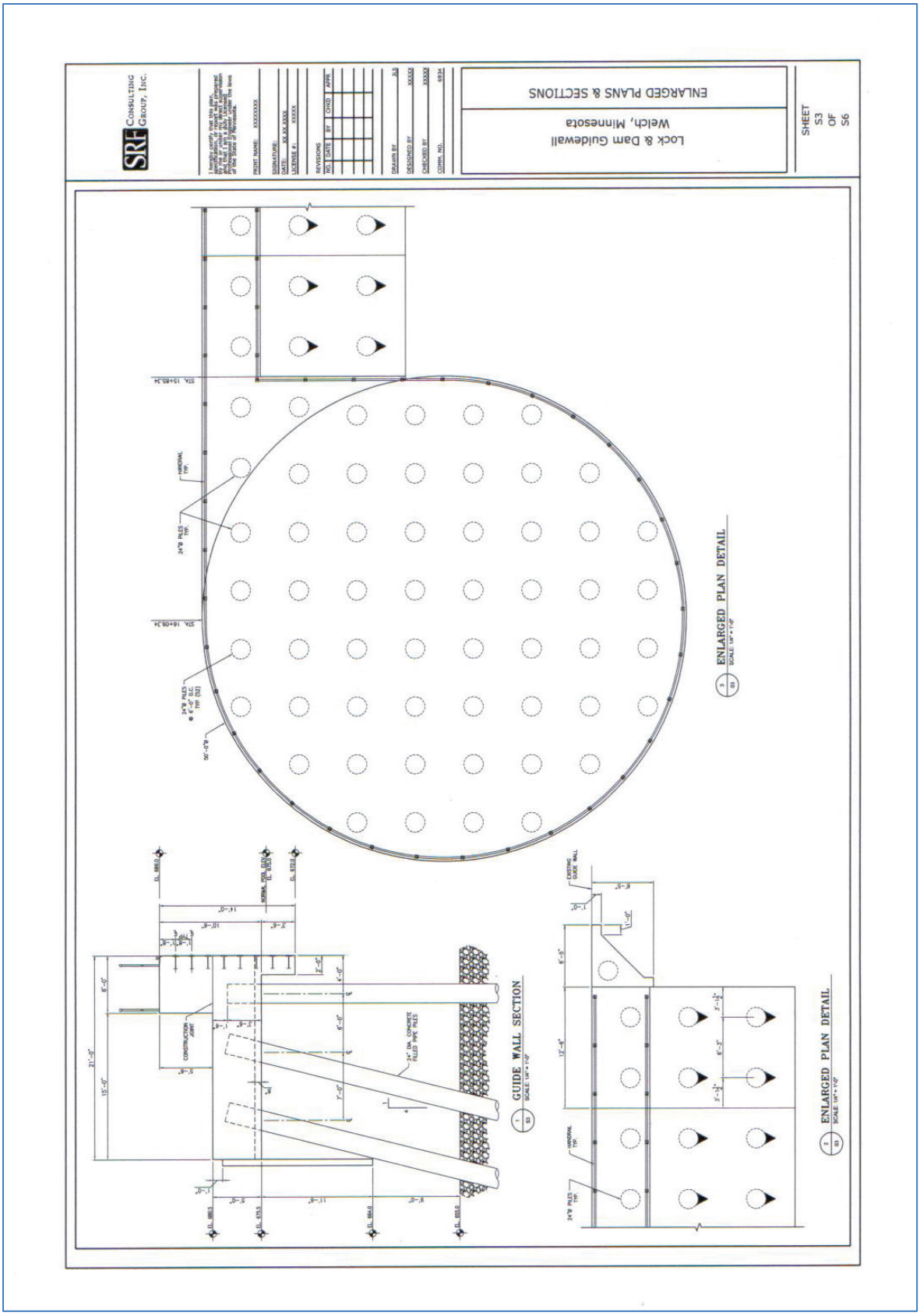


Figure 2.16 Lock and Dam 3 guide wall section view.

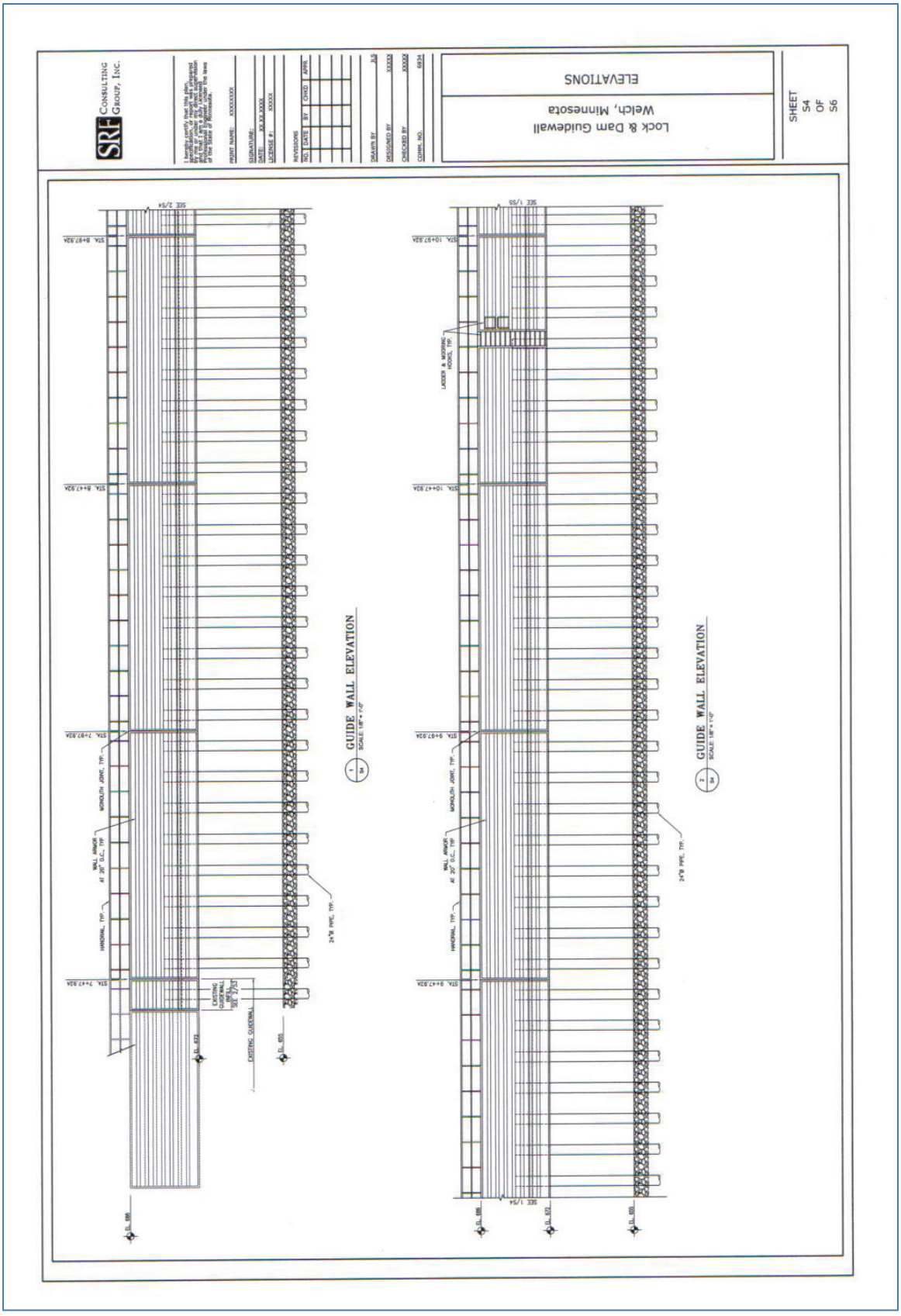


Figure 2.17 Lock and Dam 3 guide wall plan – 5.

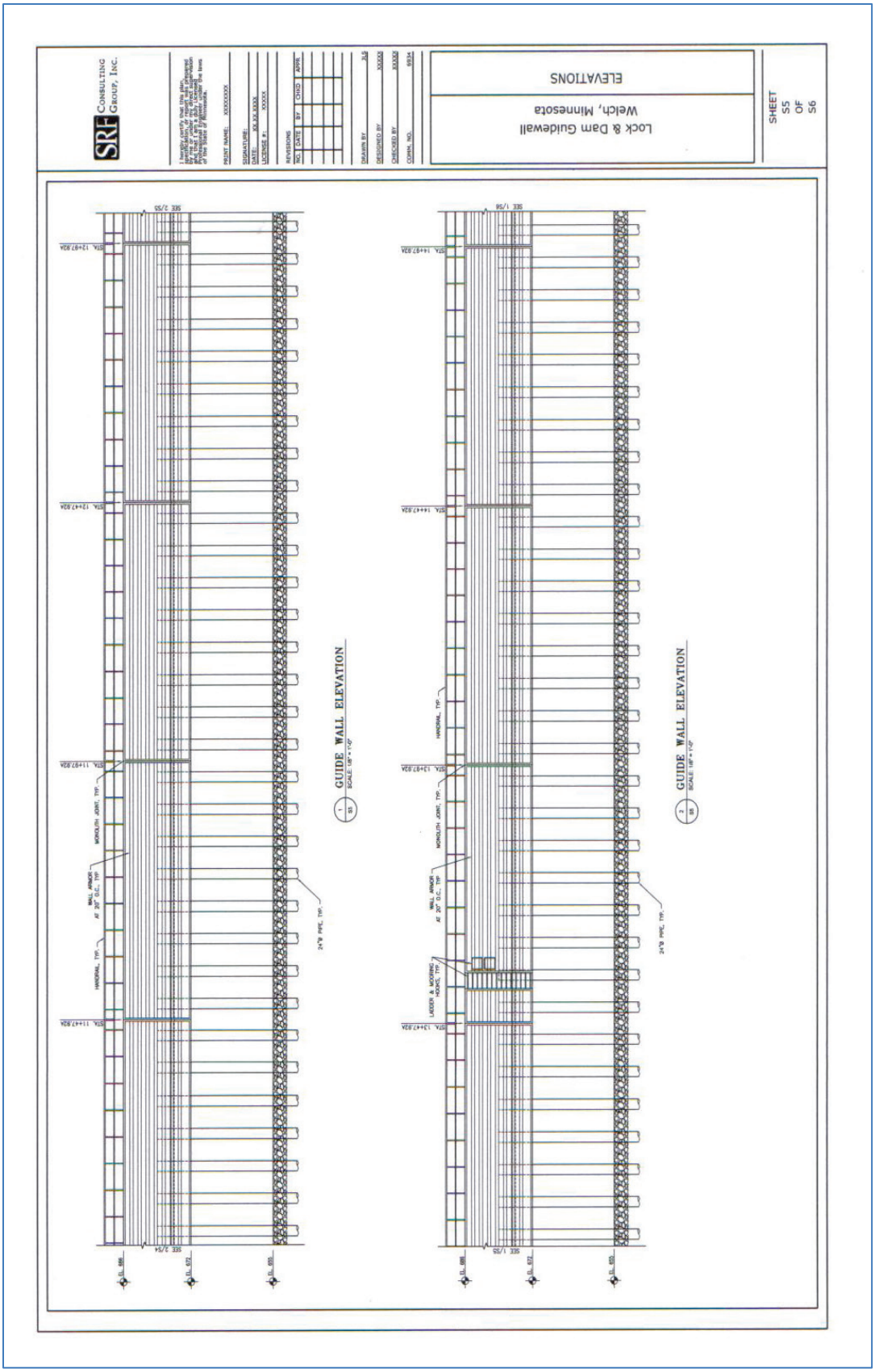
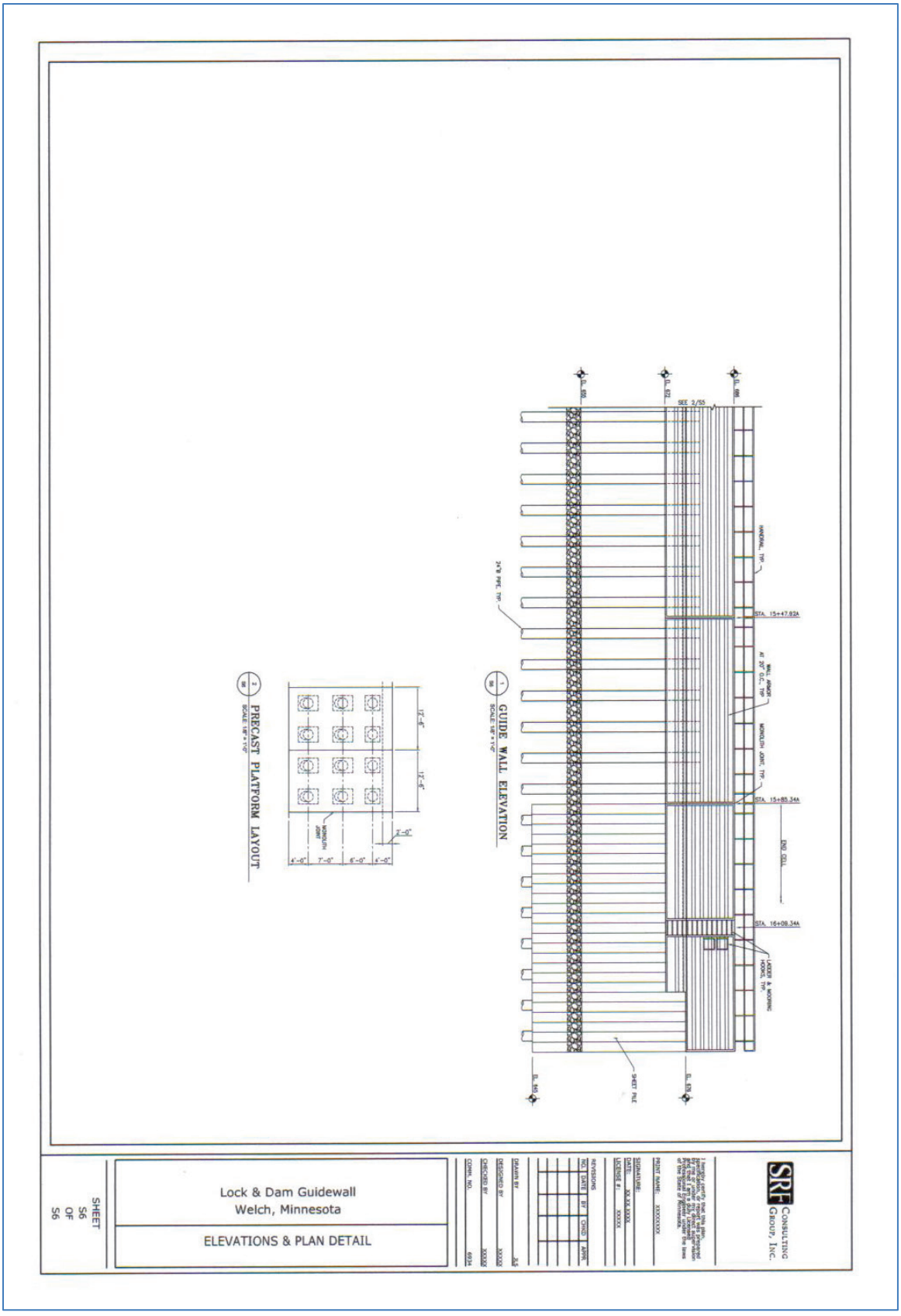


Figure 2.18 Lock and Dam 3 guide wall plan – 6.



The mathematical model can be done using 3-D beam elements. A 3-D beam element has 6 degrees of freedom per node, producing 12 degrees of freedom per element. The degrees of freedom per node are 3 translations and 3 rotations as seen in Figure 2.20. The applied normal force $F_x(t)$ is the impact-force time history developed using the PC-based software Impact_Force. The applied parallel force $F_y(t)$ is a (decimal) fraction of the normal force calculated using the dynamic coefficient of friction between the barge and the impact deck surfaces. Note the armor rubbing surfaces cast into the impact deck face can be seen in detail in Figure 2.10.

Figure 2.19 Lock and Dam 3 flexible approach wall.

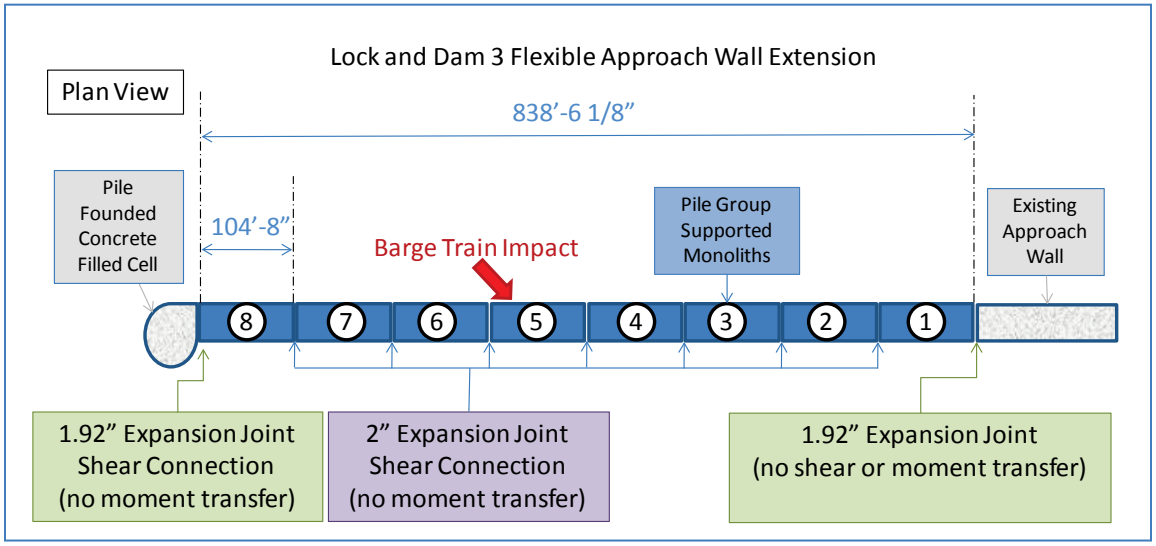
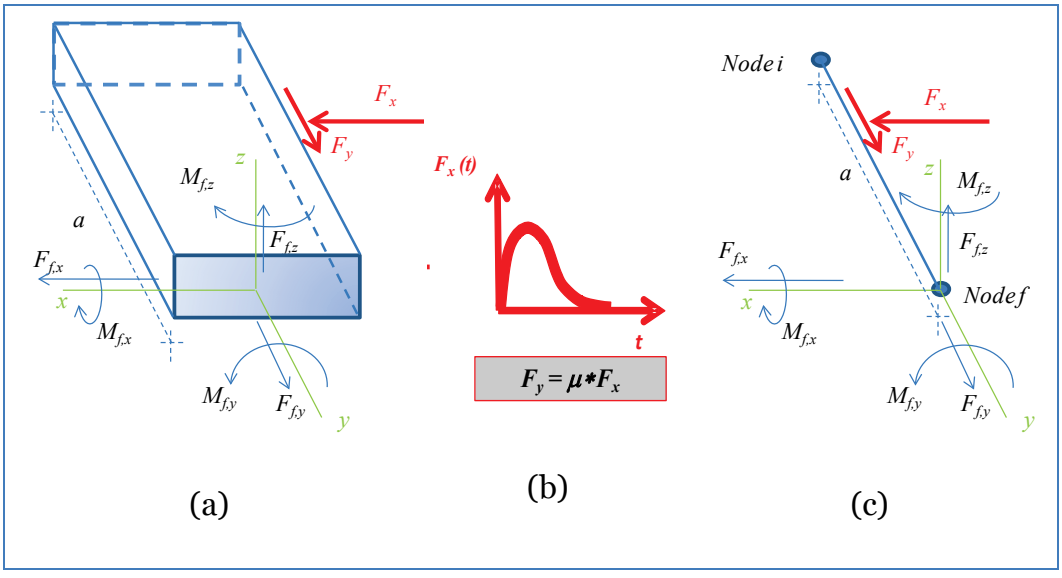
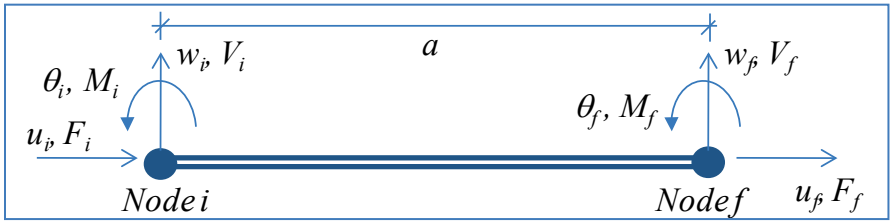


Figure 2.20 (a) Typical 3-D segment of the impact-deck beam element, (b) Impact force applied to the Impact Deck, (c) Typical 3-D beam element.



If the model used to describe the beam is developed in the plane, the beam element has 3 degrees of freedom per node and 6 degrees of freedom per element. The degrees of freedom per node are 2 translations and 1 rotation, as seen in Figure 2.21. Based on the notation of Figure 2.20, the force and moment conditions for node *i* are $F_{i,x} = V_i$, $M_{i,x} = 0$, $F_{i,y} = F_i$, $M_{i,y} = 0$, $F_{i,z} = 0$, and $M_{i,z} = M_i$, and for node *f* are $F_{f,x} = V_f$, $M_{f,x} = 0$, $F_{f,y} = F_f$, $M_{f,y} = 0$, $F_{f,z} = 0$, and $M_{f,z} = M_f$. Basically, to transform a 3-D beam element to a 2-D (plane element), the moment about the "*x*" axis, the moment about the "*y*" axis, and the force in the "*z*" directions are equal to zero.

Figure 2.21 Typical 2-D beam element used in Impact_Deck



The Impact_Deck PC-based computer program is based on beam elements loaded and deformed in the plane "*y*-*x*". The mathematical model is presented in Figure 2.22. The connection of the impact deck to the concrete circular cell is assumed as pinned and the end of the last monolith is assumed to be free. The inter-monolith connection is considered as an internal pin where the moment is zero (i.e., no moment transfer). The normal and shear impact force (time history) is applied along the beam elements and has a variation in time and position. The load moves with a constant velocity, so the position of the load varies linearly with respect to time. The impact deck is supported by equally spaced nonlinear springs in the global "*x*" and "*y*" directions. These nonlinear springs represent the reaction provided by each row of three piles through soil-structure interaction with the foundation soil(s).

A description of the beam element used for the first element (i.e., element that is pinned and connected to the rigid circular cell) is presented in Figure 2.23. At node 1, which is at the cell to monolith number 8 interface (left side in Figure 2.19), the element has zero displacements (for these two DOFs) and also, a zero bending moment. The other force, moment, displacement, and rotations are not equal to zero.

Figure 2.22 Lock and Dam 3 mathematical model.

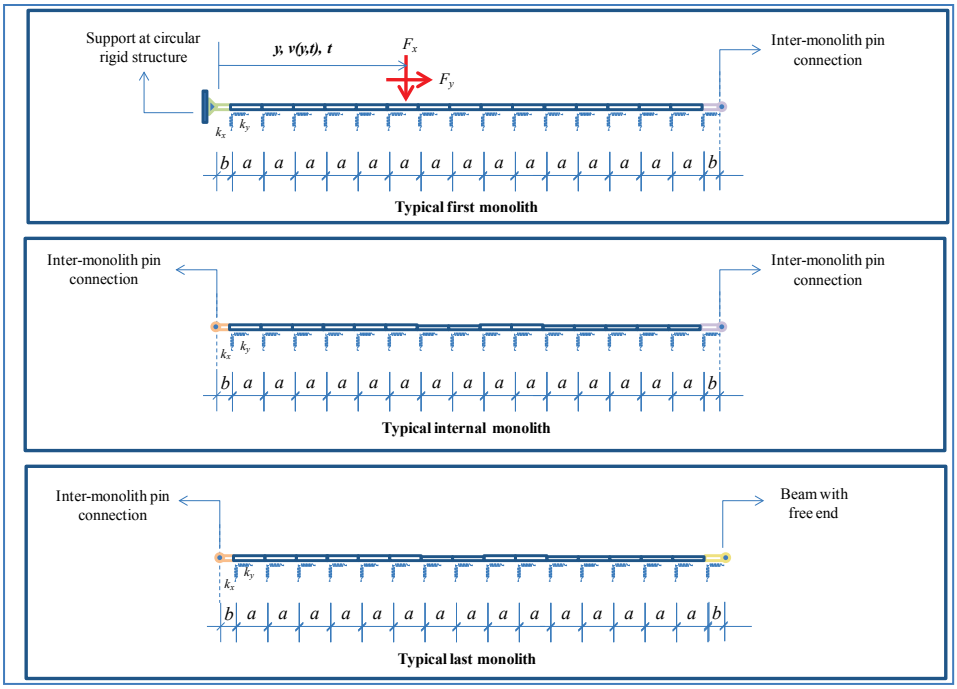
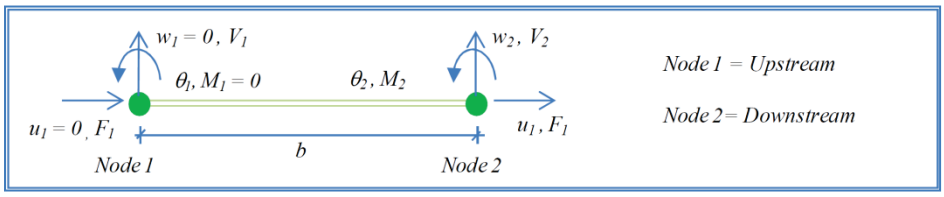
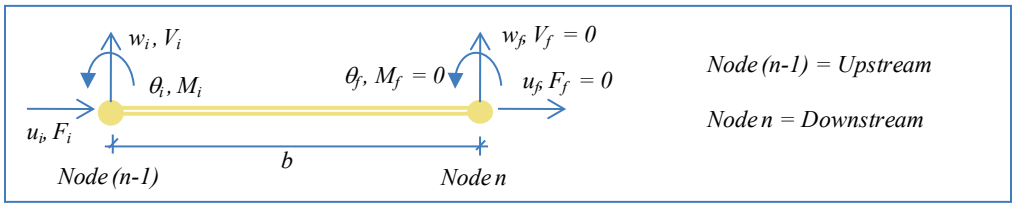


Figure 2.23 First beam element used in Lock and Dam 3 mathematical model.



A description of the beam element used for the last element (i.e., element adjacent to the existing approach wall) is presented in Figure 2.24. The force, moment, rotation, and displacement at node *(n-1)* are similar to node *i* of the typical beam element. At node *n*, located at the monolith number 1 to the existing approach wall interface on the right side in Figure 2.19, the forces and moment (at node *n*) are equal to zero (i.e., free beam end).

Figure 2.24 Last beam element used in Lock and Dam 3 mathematical model.



A description of the beam element used for the inter-monolith pin connection is presented in Figure 2.25. At the inter-monolith pin connection (node *s*), the bending moment is equal to zero; but the other forces, moments, displacements, and rotations are not equal to zero.

Figure 2.25 Description of two beam elements connected at the inter-monolith connection.

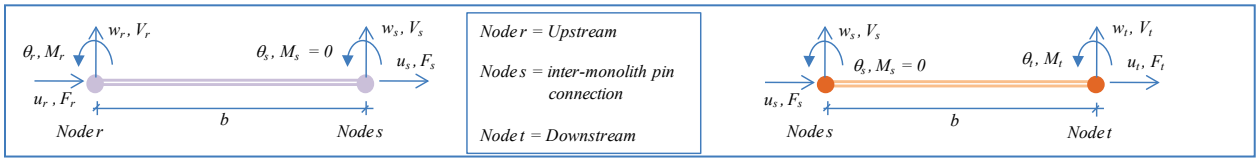
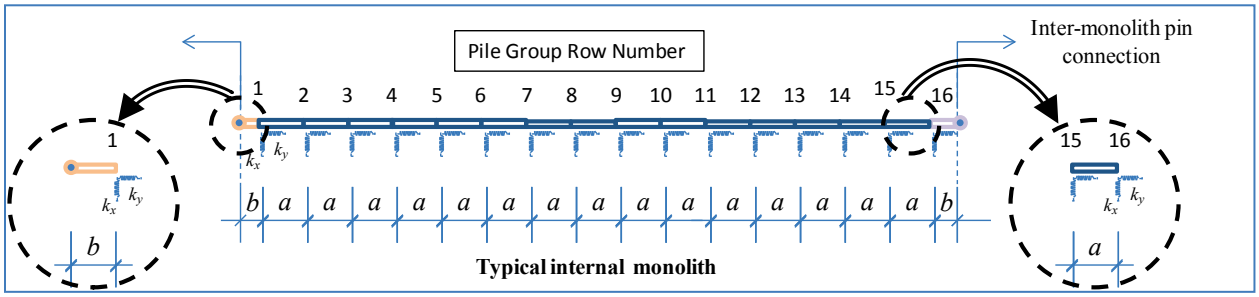


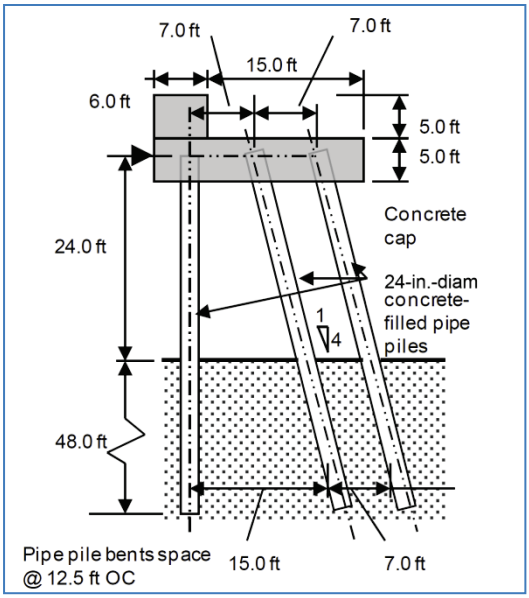
Figure 2.26 shows a typical internal monolith and the locations of the connected inter-monolith beam elements. Observe that the individual pile group row number (i.e., at the location of each pair of springs) is also shown in this Figure and labeled as numbers 1 through 16.

Figure 2.26 Beam elements numbering in a typical internal monolith.



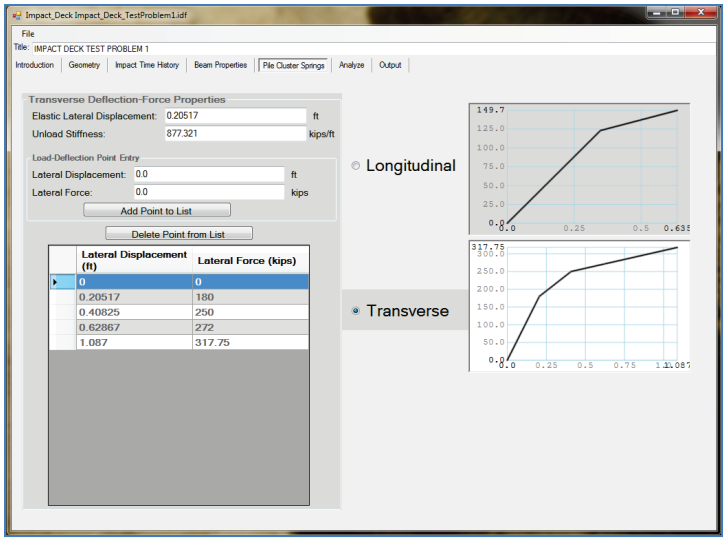
The behavior of a single row of three piles under static lateral load was conducted to determine the force-versus-displacement relationship for the nonlinear springs used in the Lock and Dam 3 model. A description of the cross-section of Lock and Dam 3 is presented in Figure 2.27 with the three batter piles that resist the lateral load. The system has two battered piles with an inclination of 1 horizontal to 4 vertical and one vertical pile. The piles extend 24 ft above ground surface and are embedded a vertical distance of 48 ft into the ground. Each pipe pile is 24 in. in diameter and is filled with concrete.

Figure 2.27 Cross-section of Lock and Dam 3.

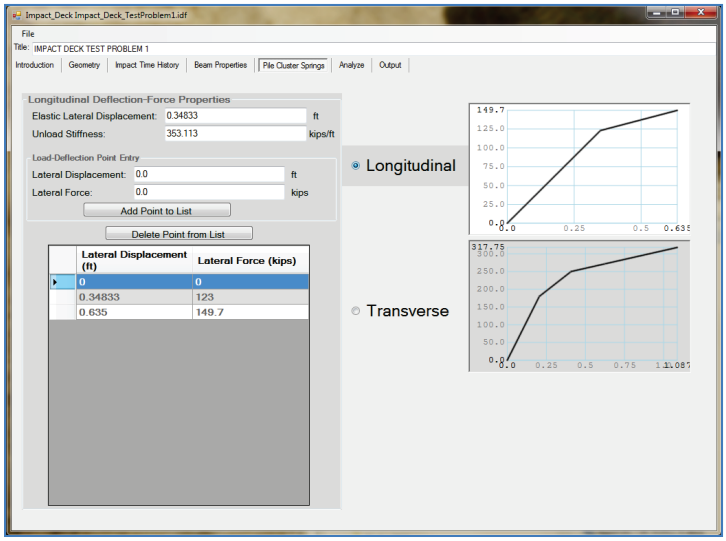


Two separate push-over analyses were conducted to define the pair of nonlinear impact deck springs representing the soil-structure interaction responses in the transverse and longitudinal directions of an individual batter pile group using the computer program CPGA. The transverse push-over result shown in Figure 2.28a is consistent with those reported in the Ebeling et al. (2012) Figure 4.4 (or Figure B.8). The resulting nonlinear force-versus-displacement relationship for loading in the transverse direction is a result of the development of plastic hinging at various locations within the individual piles, and of the development of (soil-to-pile interface) tension and/or pile tip (end) bearing soil failures of individual piles within the batter pile system as the applied lateral load is increased on the single batter pile group. Details of this push-over analysis are discussed in section 4 of Ebeling et al. (2012). Figure 2.28a, force-versus-displacement curve (with a white background, shows that a horizontal force of 180 kips results in a lateral displacement of 0.2 ft (2.46 in.); a force of 250 kips results in a lateral displacement of 0.41 ft (4.9 in.); a force of 272 kips results in a lateral displacement of 0.63 ft (7.5 in.); and a force of 317.75 kips results in a lateral displacement of 1.1 ft (13 in.). The data describing this curve is shown as a table in this user interface (Figure 2.28a). The curve used to define the elastic loading phase of the load-unload nonlinear process that will be discussed in section 2.5.

Figure 2.28 Transverse and longitudinal push-over results for a single row of three piles aligned in the transverse direction.



a) Transverse direction



b) Longitudinal direction

The longitudinal push-over results are shown in Figure 2.28b. The resulting nonlinear force-versus-displacement relationship is a result of the development of plastic hinging, first occurring at the pile cap and then at a point along the pile located below the mud line within the individual piles of the three-pile group as the lateral load is applied to the single batter pile group in the longitudinal direction (i.e., perpendicular to the line of piles). The Figure 2.28b force-versus-displacement curve (with a white background) shows a horizontal force of 123 kips resulting in a lateral displacement of 0.35 ft (4.18 in.), and a force of 149.7 kips resulting in a lateral displacement of 0.64 ft (7.6 in.). The curve used to define the

elastic loading phase of the load-unload nonlinear process will be discussed in section 2.5.

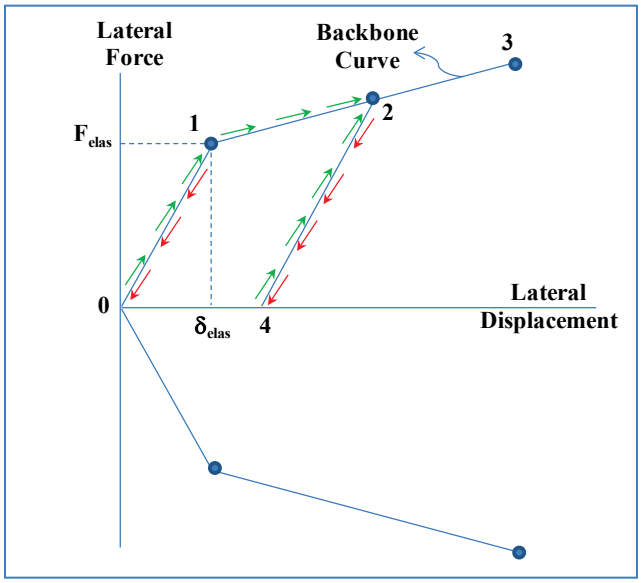
The ultimate push-over capacity of the pile group in the transverse direction is 317.75 kips as compared to a capacity of 149.7 kips in the longitudinal direction, a factor of 2.1. For the same level of horizontal displacement, the push-over curve in the longitudinal direction is of lower magnitude force than in the transverse direction. This is because for longitudinal loading each of the three piles responds more like "vertical" piling under a lateral load. Vertical pile push-over response behavior is discussed in detail in section 3 of Ebeling et al. (2012). It is observed that vertical pile behavior under lateral loading occurs without the soil-to-pile failures and the "pole-vaulting" actions that are unique to a batter pile group subjected to an applied line of loading in the transverse direction (i.e., in line with the three-pile group). These push-over results are further discussed in section 2.9.

2.5 Nonlinear force-deflection relationship for the spring supports

Impact_Deck has the capability to calculate the response of the spring supports during the time-history analysis even if the springs possess plastic behavior in their force-displacement relationship of an individual pile group. The spring is considered as "linear" if the load in the spring is below the elastic displacement δ_{elas} and the elastic force F_{elas} as shown in Figure 2.29. If the load is reduced, and the force-displacement is below point 1, the unloading path follows the same path as the previous loading phase. The loading phase in this figure is depicted as the green arrows and the unloading phase by the red arrows. However, if the load is greater than the elastic displacement and is in the loading stage, the load will follow the path shown using the green arrows until it reaches the maximum force-displacement value, labeled as point 2 in this figure. If unloading occurs from this point, it will unload following the user-specified slope that follows the unload path starting at point 2 and moves in the direction of point 4. If the pile group nonlinear "spring" is never again subjected to a force as large as that corresponding to point 2 on this figure, the force-displacement response will remain along a line from points 2 to 4, until zero force is reached. However, a plastic permanent deflection equal to the distance from the origin to point 4, lateral displacements will result for the pile group. Another scenario is if the load should increase again and go above the point 2 force magnitude, the load-displacement response will follow along the "original backbone curve" moving from point 2 towards point 3. If the force

reaches a maximum value somewhere between point 2 and 3 and starts to decrease again, the load-deflection will follow the same unload slope as the slope between points 2 and 4, but start from the new maximum force-deflection point. Lastly, if the force-deflection value is greater than that corresponding to point 3, Impact_Deck assigns a zero value to this spring because the maximum force value was reached and failure will occur.

Figure 2.29 Force-displacement relation of the spring support.



2.6 Solving for the motion of the structure

The equations of motion for a flexible approach wall structure comprised of decks supported on clustered pile groups and their end-release computations for the Lock and Dam 3 model and other similar structural systems, is given in Appendix A. Appendix I discusses the Rayleigh damping feature of the structural model, with section I.2 giving information specific to the Lock and Dam 3 model. The numerical methods to be used in the solution of the equations of motion are either HHT-α or Wilson-θ, which are discussed in Appendix F and G, respectively.

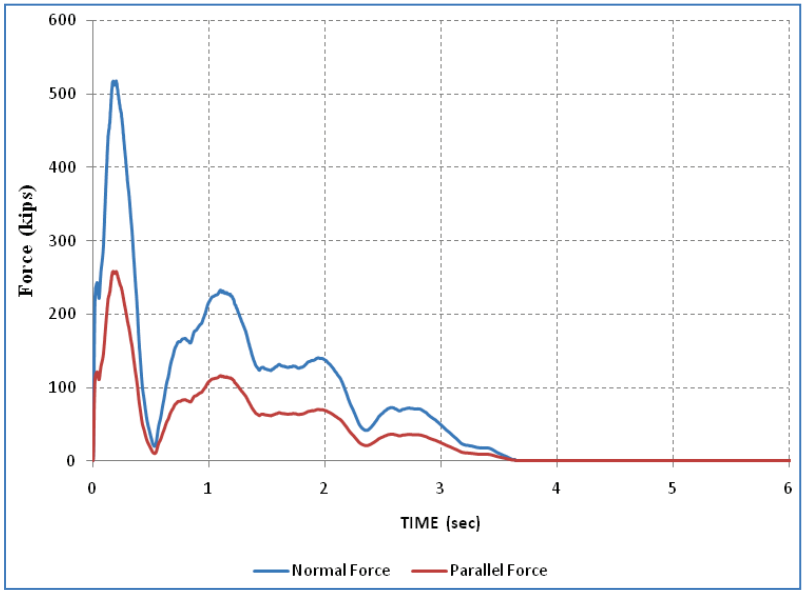
2.7 Validation of Impact_Deck Computer Program

The validation of Impact_Deck computer program using the Lock and Dam 3 model was made against the results obtained from the computer program SAP2000. The beam for validation has a total length of 838.666 ft long. In the validation procedure, the beam was modeled with 137 nodes and 136 beam elements. The 7 inter-monolith pin connections (i.e., no bending

moment transfer between adjacent monoliths) were included in the model. A set of linear springs was located at the node where the pile supports were placed.[1] The strength of the concrete was assumed as $f'c = 5{,}000\ psi$ with a corresponding modulus of elasticity for the concrete of $E = 580{,}393.25\ kips/ft^2$. The beam cross-sectional area and the beam second moment of area (moment of inertia) were 110.0 ft^2 and 4436.666 ft^4, respectively. The mass per linear foot of beam was calculated as $\bar{m}$ = 0.5127 kip *sec^2/ft. A damping factor of 0.02 (i.e., 2% of the critical damping) was used in both computer program models. The impact-force time history was the Winfield test # 10 (generated using Impact_Force, Ebeling et al. 2010) and shown in Figure 2.30. The tangential-force time history was set equal to the transverse-force time history multiplied by a dynamic coefficient of friction of 0.5. The impact load was kept stationary at a point 402.896 ft along the impact deck due to restrictions in loading for SAP2000. The load-deflection relationship was assumed as the one presented in Figure C-4 of Ebeling et al. (2012).

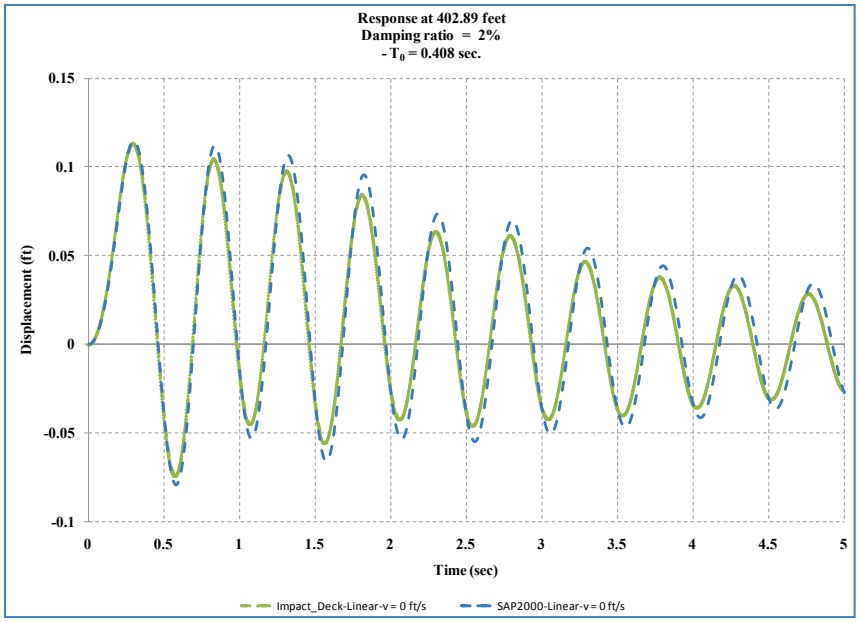
Figure 2.31 shows the results obtained for the node where the load was applied at 402.896 ft along the impact deck. The results are consistent between the two programs.

Figure 2.30 Force time history of Winfield Test # 10.



[1] The SAP2000 analysis is restricted to a linear spring model for each group of clustered piles.

Figure 2.31 Validation of Impact_Deck against SAP2000.



2.8 Numerical Example of the Elastic-Plastic Response Using Impact_Deck

In this section, results from a numerical example are shown that demonstrate the plastic behavior capability of the nonlinear impact deck clustered pile springs. Plastic response can develop if the limiting elastic displacement specified by the user (i.e., Point 1 in Figure 2.29) is low enough to force the springs to enter into the zone of plastic response. The input data for the Impact_Deck computer program for Lock and Dam 3 model included the total length of the beam at 838.666 ft long with 137 nodes and 136 beam elements. The 7 inter-monolith pin connections (i.e., no bending moment transfer between adjacent monoliths) were included in the model. A set of springs was located at the node where the pile supports were placed. The strength of the concrete was assumed as $f'c = 5{,}000\ psi$ producing a modulus of elasticity for the concrete of $E = 580{,}393.25\ kips/ft^2$. The beam cross-sectional area and the beam second moment of area (moment of inertia) were $110.0\ ft^2$ and $4436.666\ ft^4$, respectively. The mass per linear foot of beam was calculated as $\bar{m} = 0.5127\ kip\ *sec^2/ft$. A damping factor of 0.02 (i.e., 2% of the critical damping) was used. The impact-force time history applied was the Winfield test # 10 as shown in Figure 2.30. The tangential-force time history was set equal to the transverse-force time history but multiplied by a dynamic coefficient of friction of 0.5. In this example, the load was assumed to be in motion along the impact deck at a velocity of $v = 3\ ft/sec$, starting at the node located at $x = 402.896\ ft$. The spring stiffnesses assigned in this analysis did not make

use of the Ebeling et al. (2012) Appendix A push-over analysis results for the 6-ft-diameter vertical piling because the Winfield Test # 10 loads could not be guaranteed to bring the computed stiffnesses into the zone of plastic deformation. In an effort to illustrate the effects of plastic deformation, the force-displacement relationship (backbone curve) was assumed to have the following slopes (stiffness), $k_1 = 540.0$ *kip/ft*, $k_2 = 215.0$ *kip/ft*, $k_3 = 100.46$ *kip/ft*, and the stiffness when it is in the plastic unload path of $k_{unload} = 3.33 * k_1$. The limit for the elastic displacement was assumed as $\delta_{elastic} = 0.0633$ *ft*. The force-displacement relationship (backbone curve) had a second break point (second to third slope) at a displacement of 0.30 ft. That meant that the force value at the inflection point of the slope occured first at 34.182 kips and a second inflection point at 85.073 kips. Figure 2.32 shows the results obtained for the node where the load was applied at *402.896 ft*. The results in Figure 2.32 show the effect of exceeding the first yield point in the spring model. The purple values are offset from their original position by approximately 0.09 ft after the spring force reached its yield point. The red curve indicates the behavior for a linear elastic spring model where yielding does not occur. Figure 2.33 shows the plastic behavior of the spring at *402.896 ft*, where the normal impact load had its initial point of contact. After 3.63 sec, the linear response oscillates around zero displacement and the plastic response oscillates around 0.098 ft. These behaviors can be observed in Figure 2.33 where the plastic response was reached (second slope in the force-displacement diagram), ending with a permanent displacement of around 0.098 ft.

Figure 2.32 Dynamic response of the transverse spring located at *x = 402.896 ft.*

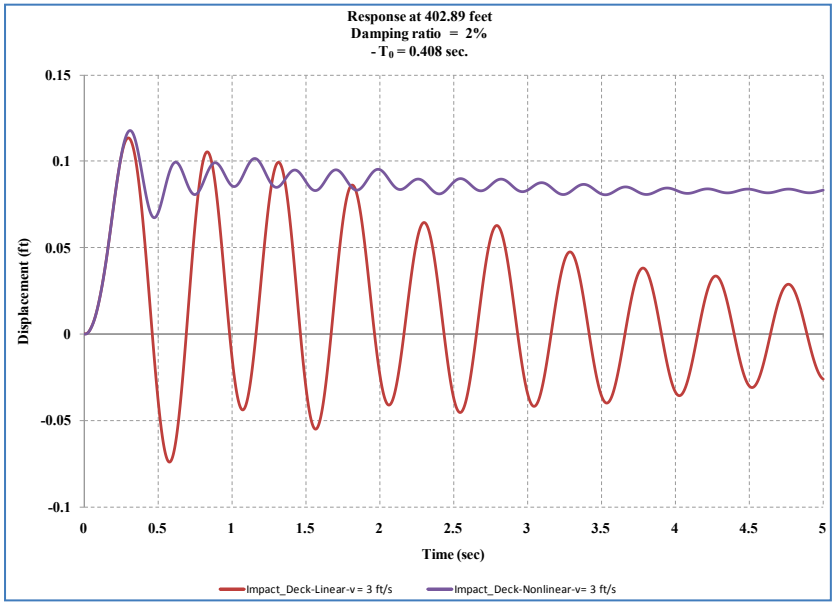
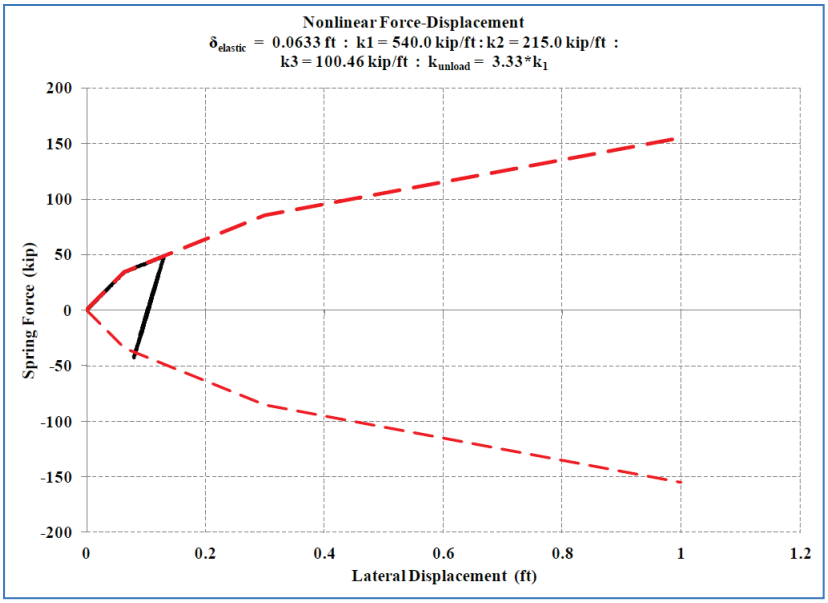


Figure 2.33 Dynamic response of the transverse spring located at *x* = *402.896 ft.*

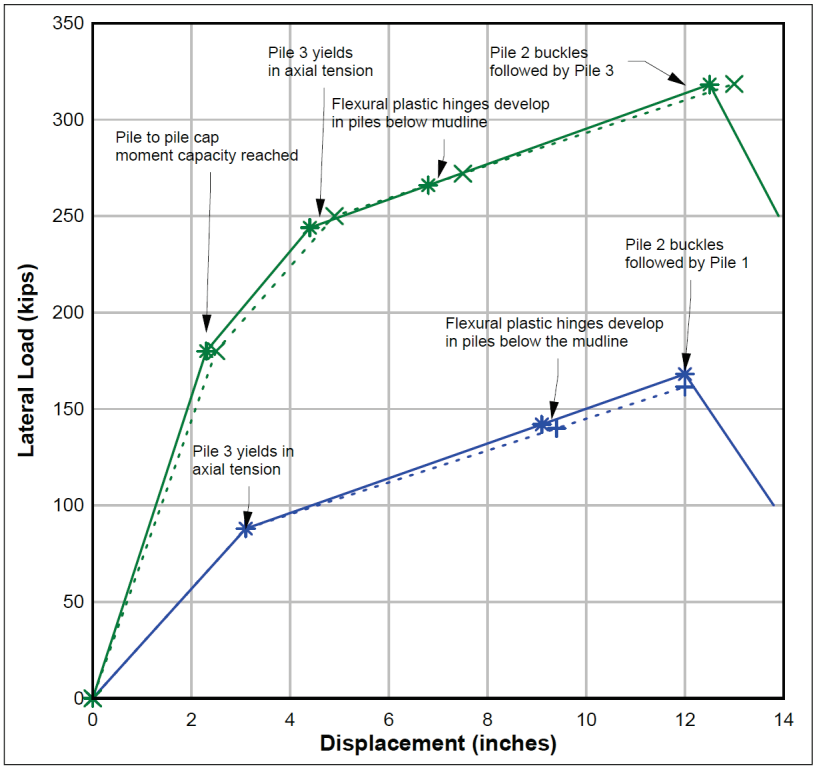


2.9 Impact_Deck GUI results

In section 5, the visualization of data using the Impact_Deck GUI post-processing capabilities will be discussed, but these capabilities are being introduced here to give an idea of the output results from the Impact_Deck processing code, which used the formulation for impact deck structures discussed in section 2.8. The results are from the Lock and Dam 3 example problem in section 5. The impact deck geometry and its material properties were the same as in section 2.8, with the exception of the load parameters (starting position and velocity along the approach wall) and the transverse non-linear spring properties of the individual pile cluster sub-system. The load still used the Winfield Test # 10 impact-force time history, but the starting position was moved to 501.188 ft from the beginning of the wall and had a velocity of 1.0 ft/sec (along the wall).

The calculation of pile group stiffness was determined through push-over analyses performed on a single pile group. The Lock and Dam 3 impact-deck pile group consisted of a fixed head system of one vertical and two batter piles, all with a diameter of 24 in. In this case, the push-over analysis took all the piles into account, including the effects of batter (Figure 2.34).

Figure 2.34 Reprint of the Figure 4-4 transverse direction of loading push-over analyses from Ebeling et al. (2012); fixed head results in green and pinned head results in blue.



The push-over analysis for a transverse load on the fixed head, wet site analysis (dashed green curve shown in Figures 4-4 and B-8 on pages 81 and 153, respectively, of Ebeling et al. 2012) was defined by the points listed in Table 2.1. These values were used to define the transverse spring model for an individual group of 3 piles.

For the longitudinal spring model, the longitudinal forces acting on the impact deck when the two plastic hinge points occured were 1850 kips and 2970 kips, respectively. These forces were much greater than and likely from a barge train impact event; thus no yielding of any pile groups in the longitudinal direction was anticipated. The data contained in Table 2.2 were developed using the push-over analysis procedure outlined in section 3 or Appendix A of Ebeling et al. (2012) for loading applied in the transverse direction.

Table 2.1 Primary loading curve for the transverse spring model of a single pile group with a leading vertical pile followed by two batter piles (Lock and Dam 3).

Force	Deflection		Notes on Flexural Plastic Hinging Conditions
(kips)	(inches)	(feet)	From Ebeling et al. (2012)
0.0	0.0	0.0	
180.0	2.462	0.20517	Pile to pile cap moment capacity reached
250.0	4.899	0.40825	Pile 3 yields in axial tension
272.0	7.544	0.62867	Flexural plastic hinges develop in piles below mudline
317.75	13.044	1.087	Pile 2 buckles

Table 2.2 Primary loading curve for the longitudinal spring model of a single pile group with a leading vertical pile followed by two batter piles (Lock and Dam 3).

Force	Deflection		Notes on Flexural Plastic Hinging Conditions
(kips)	(inches)	(feet)	
0.0	0.0	0.0	
123.0	4.18	0.34833	Pile to pile cap moment capacity reached
149.7	7.62	0.635	Flexural plastic hinges develop in piles below mudline

According to Figure B-3 of Ebeling et al. (2012), yielding occurred for a pile when the moment exceeded 8544 kip-inch with no significant axial loading (i.e., pure bending).

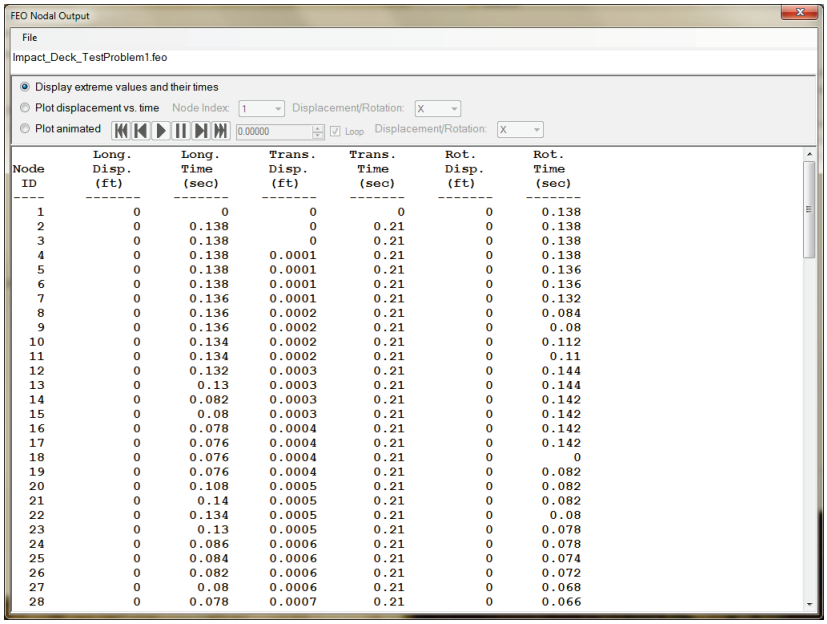
These Table 2.2 values come from the push-over analysis of the 3 pile system with 2 batter piles that were solved as a system, and therefore, the transverse and longitudinal push-over analyses must be performed using CPGA.

The transverse force-displacement relationship (backbone curve) was therefore assumed to have the following slopes (stiffness), $k_1 = 877.32$ *kip/ft,* $k_2 = 344.69$ *kip/ft,* $k_3 = 99.81$ *kip/ft*, and the stiffness when it is in the plastic unload path of $k_{unload} = 1.0 * k_1$. The limit for the elastic displacement was assumed as $\delta_{elastic} = 0.20517$ *ft*. This backbone curve is shown in Figure 2.28a. This section does not provide an engineering analysis, but gives an idea of the information provided so that an engineering analysis might be made.

Nodal outputs provided from the FEO[1] analysis of an impact deck were the longitudinal displacement, transverse displacement, and rotational displacement (in radians) for each node at each time step of the simulation. A Table was also provided that gives the maximum displacements (longitudinal, transverse, and rotational) for each node and the time that the maximum displacement occurred.

Figure 2.35 shows the GUI table of maximums for the example problem in this section. From this GUI table, it is possible to tell the time step and the node with the maximum displacement for transverse, longitudinal, and rotational displacements (as shown in Table 2.3).

Figure 2.35 Impact_Deck GUI Table of maximum nodal displacements for the L&D3 example impact deck.



Node ID	Long. Disp. (ft)	Long. Time (sec)	Trans. Disp. (ft)	Trans. Time (sec)	Rot. Disp. (ft)	Rot. Time (sec)
1	0	0	0	0	0	0.138
2	0	0.138	0	0.21	0	0.138
3	0	0.138	0	0.21	0	0.138
4	0	0.138	0.0001	0.21	0	0.138
5	0	0.138	0.0001	0.21	0	0.136
6	0	0.138	0.0001	0.21	0	0.136
7	0	0.136	0.0001	0.21	0	0.132
8	0	0.136	0.0002	0.21	0	0.084
9	0	0.136	0.0002	0.21	0	0.08
10	0	0.134	0.0002	0.21	0	0.112
11	0	0.134	0.0002	0.21	0	0.11
12	0	0.132	0.0003	0.21	0	0.144
13	0	0.13	0.0003	0.21	0	0.144
14	0	0.082	0.0003	0.21	0	0.142
15	0	0.08	0.0003	0.21	0	0.142
16	0	0.078	0.0004	0.21	0	0.142
17	0	0.076	0.0004	0.21	0	0.142
18	0	0.076	0.0004	0.21	0	0
19	0	0.076	0.0004	0.21	0	0.082
20	0	0.108	0.0005	0.21	0	0.082
21	0	0.14	0.0005	0.21	0	0.082
22	0	0.134	0.0005	0.21	0	0.08
23	0	0.13	0.0005	0.21	0	0.078
24	0	0.086	0.0006	0.21	0	0.078
25	0	0.084	0.0006	0.21	0	0.074
26	0	0.082	0.0006	0.21	0	0.072
27	0	0.08	0.0006	0.21	0	0.068
28	0	0.078	0.0007	0.21	0	0.066

Table 2.3 Maximum nodal displacements for the Impact_Deck example problem.

	Node number	Value	Time (seconds)
Transverse	86	0.0663 feet	0.26
Longitudinal	137	0.002 feet	0.212
Rotational	93	0.0008 radians	0.26

[1] FEO is the Finite Element Output format for the Impact_Deck program.

Figures 2.36, 2.37, and 2.38 show the time histories for displacements at nodes 86, 137, and 93, respectively. Because some of these displacements were very small, and the data were stored with limited precision, some of these plots developed 'jaggies', where the data seems to form stair steps.

Figure 2.36 Transverse nodal displacement time histories for node 86.

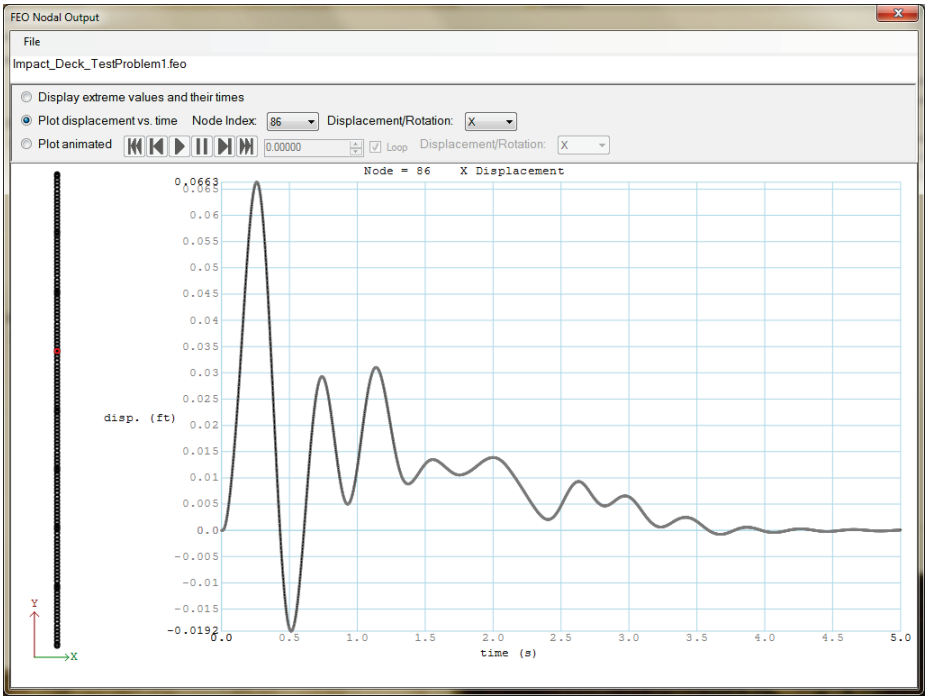


Figure 2.37 Longitudinal nodal displacement time histories for node 137.

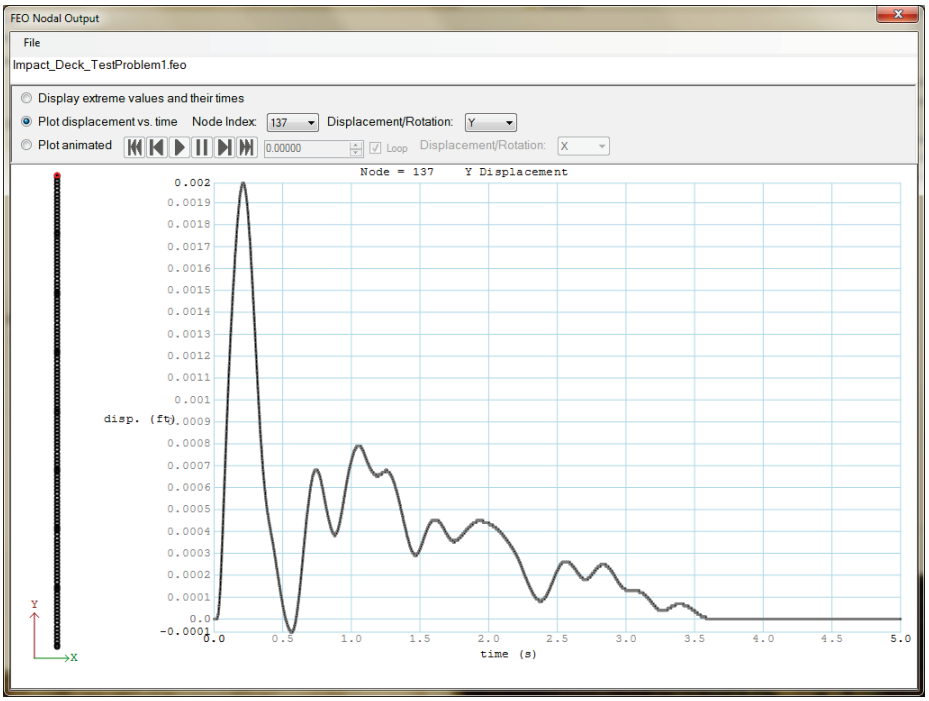
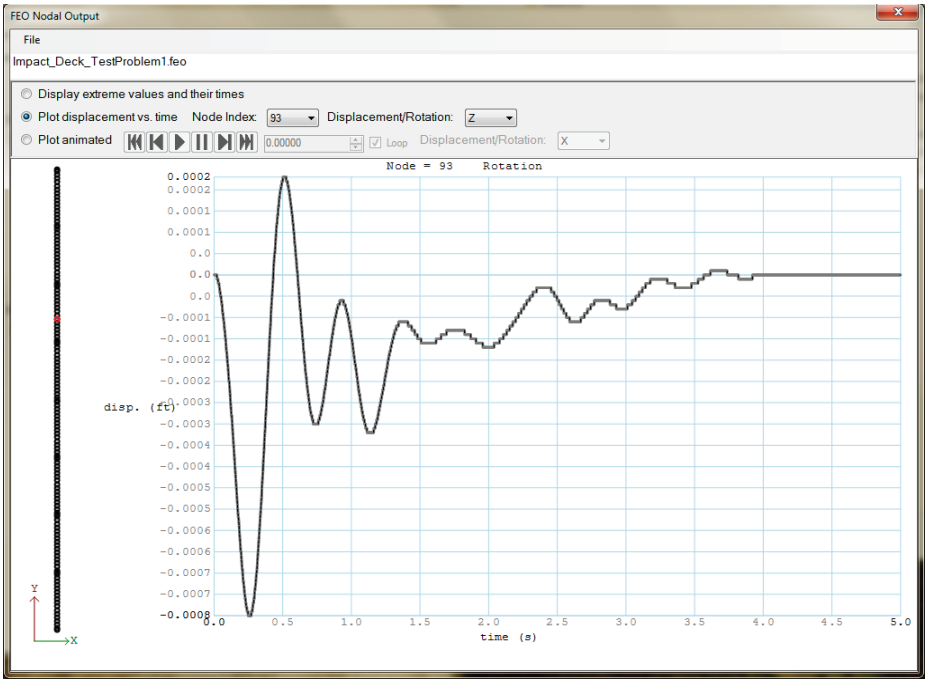


Figure 2.38 Rotational nodal displacement time histories for node 93.



The Impact_Deck GUI also allowed the user to visualize the entire beam in motion using an exaggerated plot of displacements transversely, longitudinally, and rotationally. Figures 2.39, 2.40, and 2.41 show the displacements of the wall from these animated plots at the moment where the maximum displacement occurred, 0.26 sec for longitudinal displacements, 0.21 sec for transverse displacements, and 0.26 sec for rotational displacements. These data were also subject to the jaggies because of the precision of the stored data. The data were scaled to fit the plot.

Element outputs provided from the FEO analysis of an impact deck were the axial force, shear force, and moment for each element at each time step of the simulation. A table was also provided that gives the minimum and maximum forces and moments for each element and the times that the minimum and maximum force/moment occured.

Figures 2.42 – 2.44 show GUI tables of extreme values for the example problem in this section. From this GUI table, it is possible to tell the time step and the element with the extreme axial force, shear force, and moment (as shown in Table 2.4).

Figure 2.39 Transverse wall displacements at 0.26 sec.

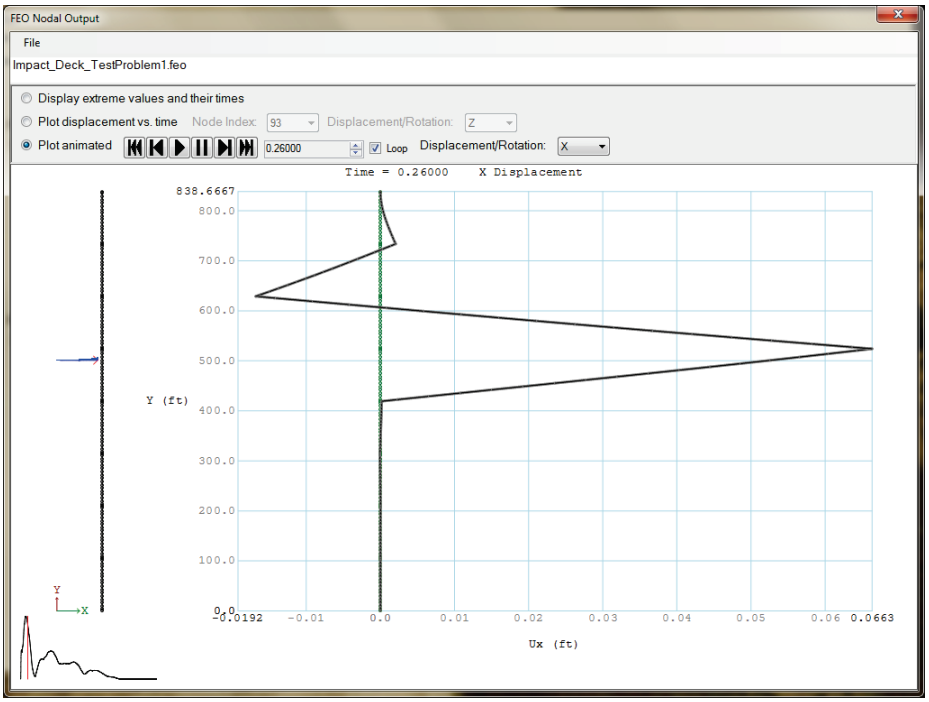


Figure 2.40 Longitudinal wall displacements at 0.21 sec.

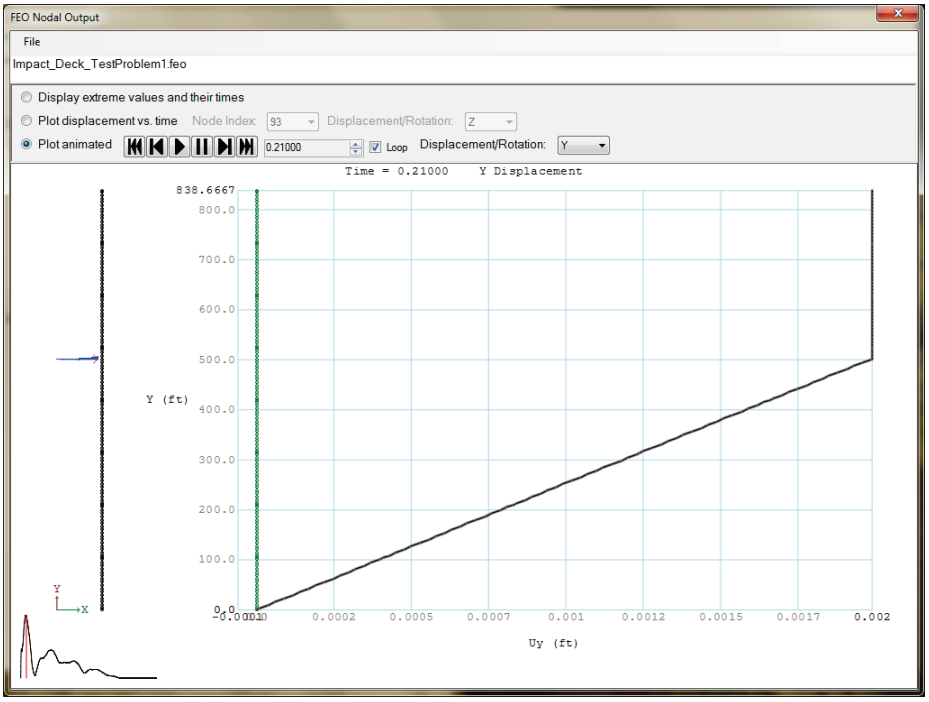


Figure 2.41 Rotational wall displacements at 0.26 sec.

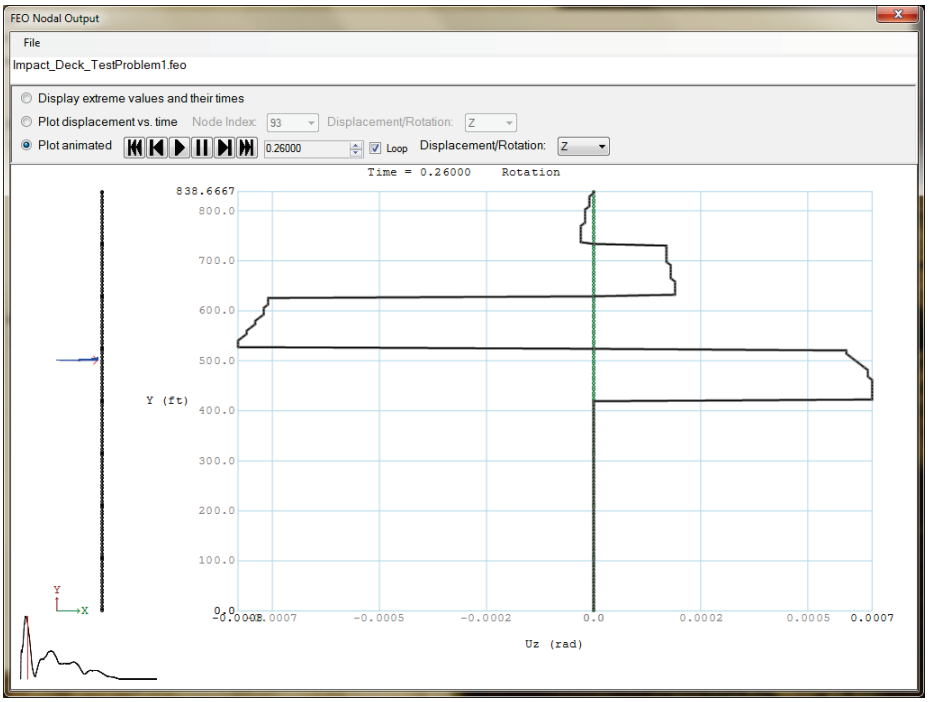
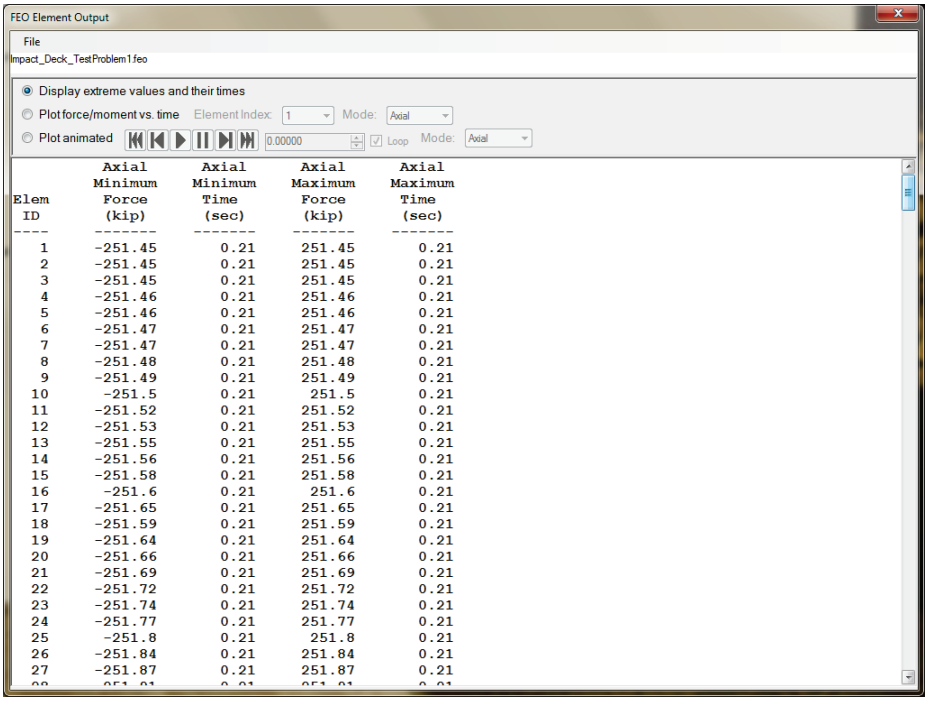
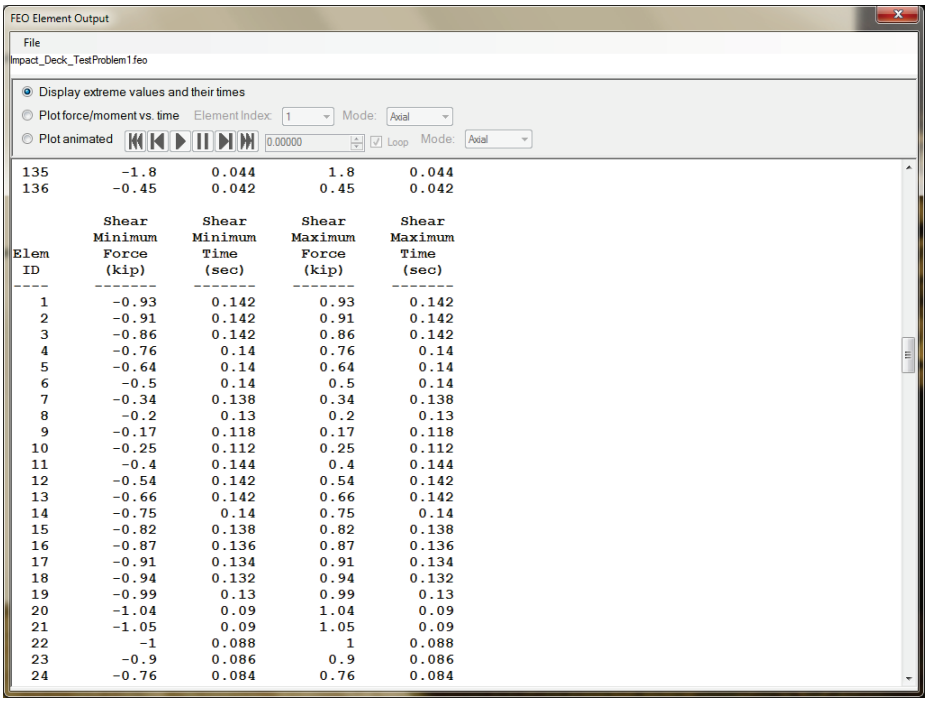


Figure 2.42 Impact_Deck GUI table of element minimum and maximum axial forces for the L&D3 example impact deck.



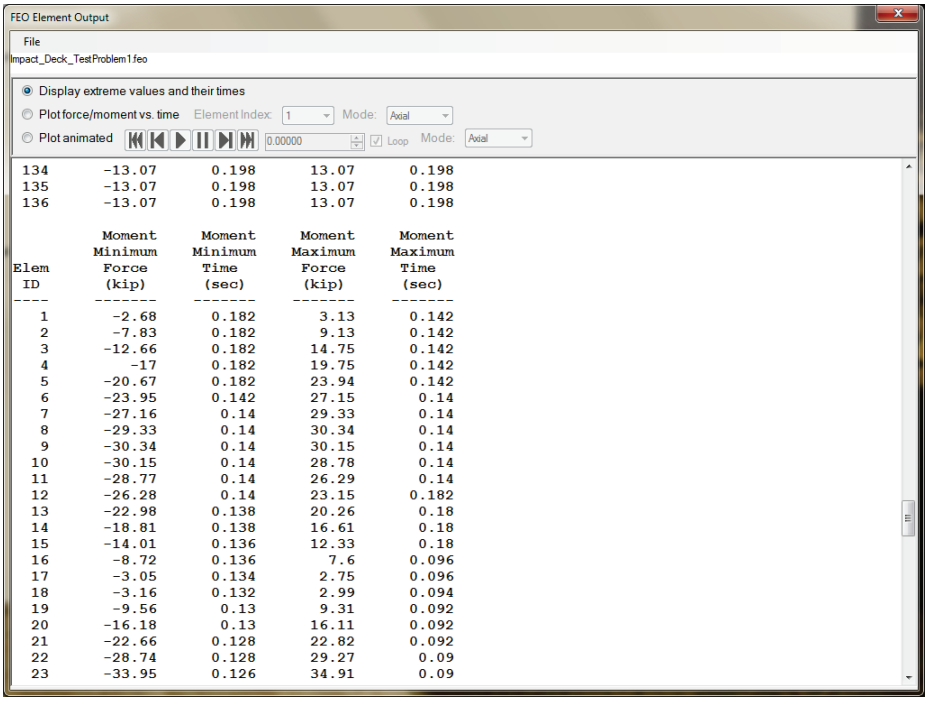
Elem ID	Axial Minimum Force (kip)	Axial Minimum Time (sec)	Axial Maximum Force (kip)	Axial Maximum Time (sec)
1	-251.45	0.21	251.45	0.21
2	-251.45	0.21	251.45	0.21
3	-251.45	0.21	251.45	0.21
4	-251.46	0.21	251.46	0.21
5	-251.46	0.21	251.46	0.21
6	-251.47	0.21	251.47	0.21
7	-251.47	0.21	251.47	0.21
8	-251.48	0.21	251.48	0.21
9	-251.49	0.21	251.49	0.21
10	-251.5	0.21	251.5	0.21
11	-251.52	0.21	251.52	0.21
12	-251.53	0.21	251.53	0.21
13	-251.55	0.21	251.55	0.21
14	-251.56	0.21	251.56	0.21
15	-251.58	0.21	251.58	0.21
16	-251.6	0.21	251.6	0.21
17	-251.65	0.21	251.65	0.21
18	-251.59	0.21	251.59	0.21
19	-251.64	0.21	251.64	0.21
20	-251.66	0.21	251.66	0.21
21	-251.69	0.21	251.69	0.21
22	-251.72	0.21	251.72	0.21
23	-251.74	0.21	251.74	0.21
24	-251.77	0.21	251.77	0.21
25	-251.8	0.21	251.8	0.21
26	-251.84	0.21	251.84	0.21
27	-251.87	0.21	251.87	0.21

Figure 2.43 Impact_Deck GUI table of element minimum and maximum shear forces for the L&D3 example impact deck.



Elem ID	Shear Minimum Force (kip)	Shear Minimum Time (sec)	Shear Maximum Force (kip)	Shear Maximum Time (sec)
135	-1.8	0.044	1.8	0.044
136	-0.45	0.042	0.45	0.042
1	-0.93	0.142	0.93	0.142
2	-0.91	0.142	0.91	0.142
3	-0.86	0.142	0.86	0.142
4	-0.76	0.14	0.76	0.14
5	-0.64	0.14	0.64	0.14
6	-0.5	0.14	0.5	0.14
7	-0.34	0.138	0.34	0.138
8	-0.2	0.13	0.2	0.13
9	-0.17	0.118	0.17	0.118
10	-0.25	0.112	0.25	0.112
11	-0.4	0.144	0.4	0.144
12	-0.54	0.142	0.54	0.142
13	-0.66	0.142	0.66	0.142
14	-0.75	0.14	0.75	0.14
15	-0.82	0.138	0.82	0.138
16	-0.87	0.136	0.87	0.136
17	-0.91	0.134	0.91	0.134
18	-0.94	0.132	0.94	0.132
19	-0.99	0.13	0.99	0.13
20	-1.04	0.09	1.04	0.09
21	-1.05	0.09	1.05	0.09
22	-1	0.088	1	0.088
23	-0.9	0.086	0.9	0.086
24	-0.76	0.084	0.76	0.084

Figure 2.44 Impact_Deck GUI table of element minimum and maximum moments for the L&D3 example impact deck.



Elem ID	Moment Minimum Force (kip)	Moment Minimum Time (sec)	Moment Maximum Force (kip)	Moment Maximum Time (sec)
134	-13.07	0.198	13.07	0.198
135	-13.07	0.198	13.07	0.198
136	-13.07	0.198	13.07	0.198
1	-2.68	0.182	3.13	0.142
2	-7.83	0.182	9.13	0.142
3	-12.66	0.182	14.75	0.142
4	-17	0.182	19.75	0.142
5	-20.67	0.182	23.94	0.142
6	-23.95	0.142	27.15	0.14
7	-27.16	0.14	29.33	0.14
8	-29.33	0.14	30.34	0.14
9	-30.34	0.14	30.15	0.14
10	-30.15	0.14	28.78	0.14
11	-28.77	0.14	26.29	0.14
12	-26.28	0.14	23.15	0.182
13	-22.98	0.138	20.26	0.18
14	-18.81	0.138	16.61	0.18
15	-14.01	0.136	12.33	0.18
16	-8.72	0.136	7.6	0.096
17	-3.05	0.134	2.75	0.096
18	-3.16	0.132	2.99	0.094
19	-9.56	0.13	9.31	0.092
20	-16.18	0.13	16.11	0.092
21	-22.66	0.128	22.82	0.092
22	-28.74	0.128	29.27	0.09
23	-33.95	0.126	34.91	0.09

Table 2.4 Extreme forces/moments for the Impact_Deck example problem.

		Element number	Value	Time (seconds)
Axial	min.	82	-271.67 kips	0.208
	max	81	528.44 kips	0.200
Shear	min.	82	-293.15 kips	0.202
	max	81	702.41 kips	0.200
Moment	min.	81	-5,468.09 kip-feet	0.180
	max	82	5,662.18 kip-feet	0.202

Because the simulated barge train impact occured between nodes shared by elements 81 and 82, the extreme forces were found in those elements. Figures 2.45 - 2.50 show the time histories for the axial force, shear force, and moments for the elements with the minimum and maximum values, respectively.

Figures 2.51 – 2.53 show the axial force, shear force, and moment at 0.200, 0.200, and at 0.180 sec, respectively, for the entire wall. These forces and moments were collected for animated visualization in the Impact_Deck GUI.

Figure 2.45 Axial-force time histories for element 82.

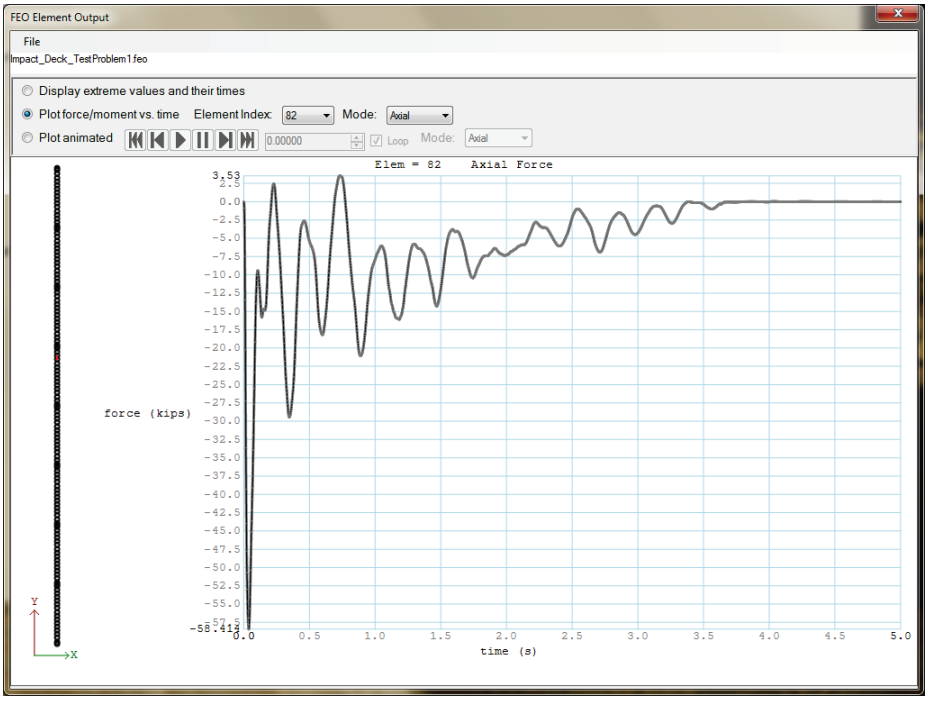


Figure 2.46 Axial-force time histories for element 81.

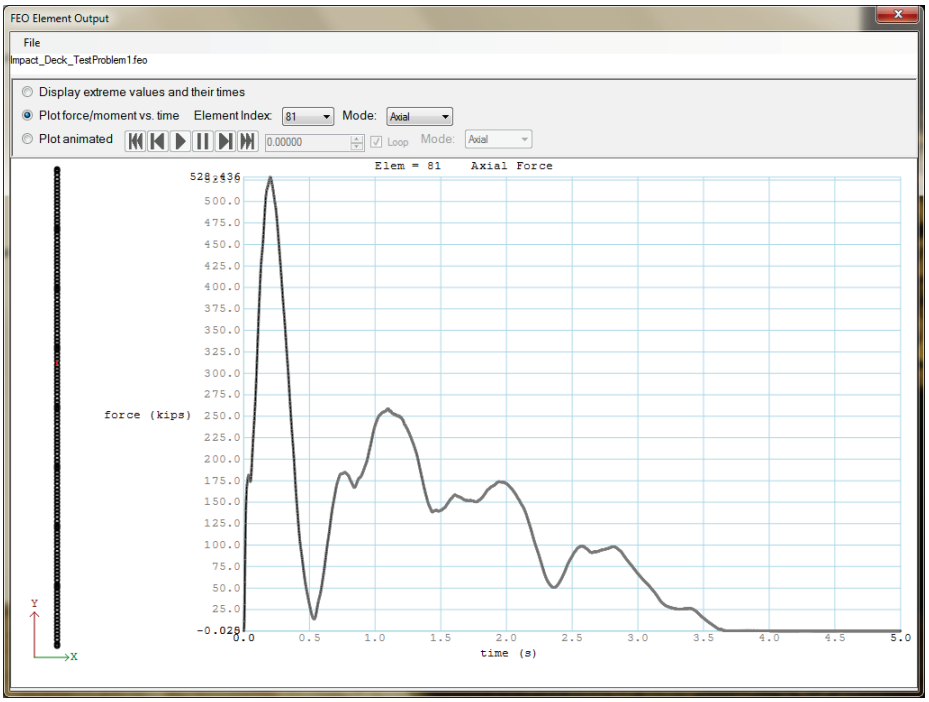


Figure 2.47 Shear-force time histories for element 82.

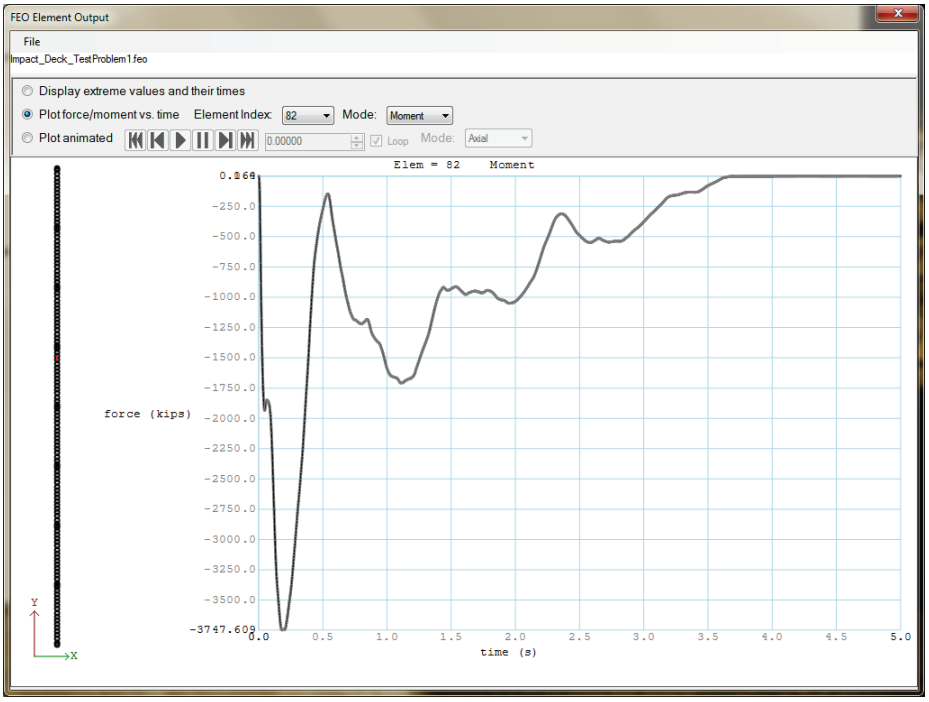


Figure 2.48 Shear-force time histories for element 81.

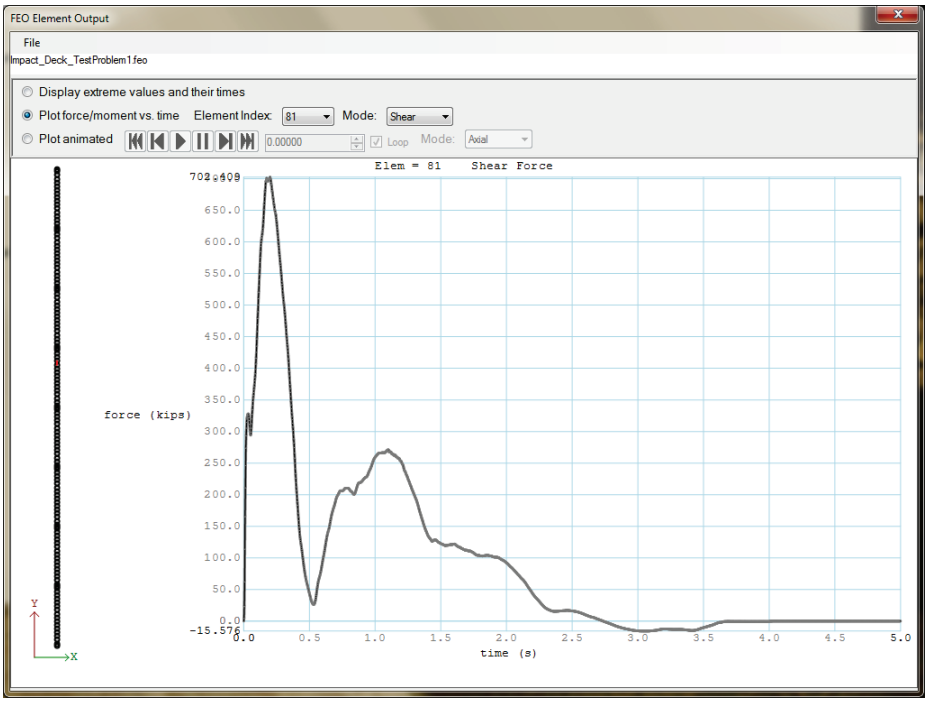


Figure 2.49 Moment time histories for element 81.

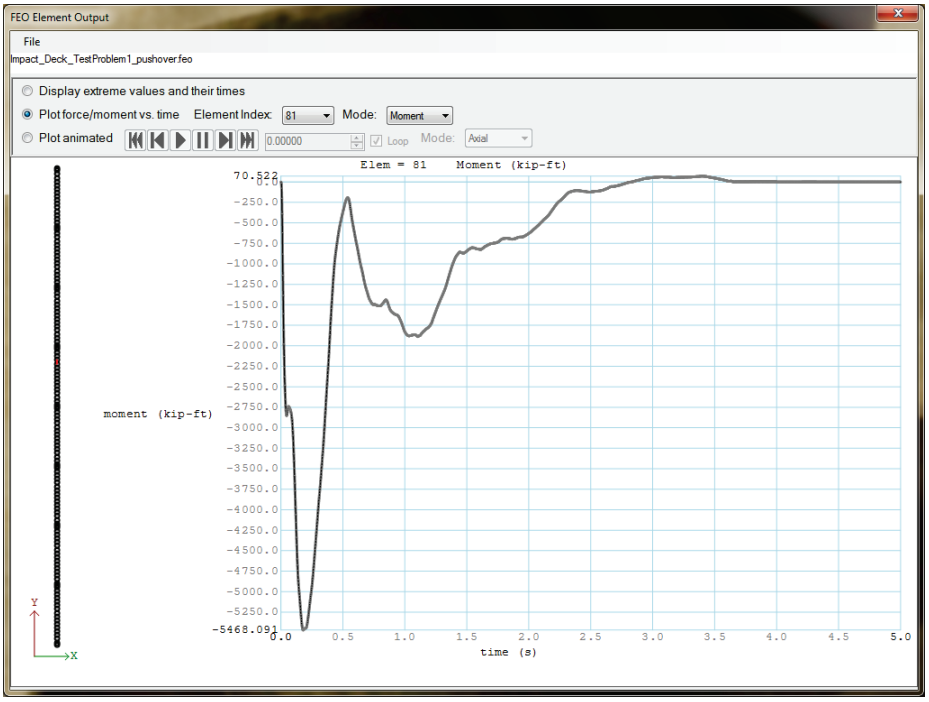


Figure 2.50 Moment time histories for element 82.

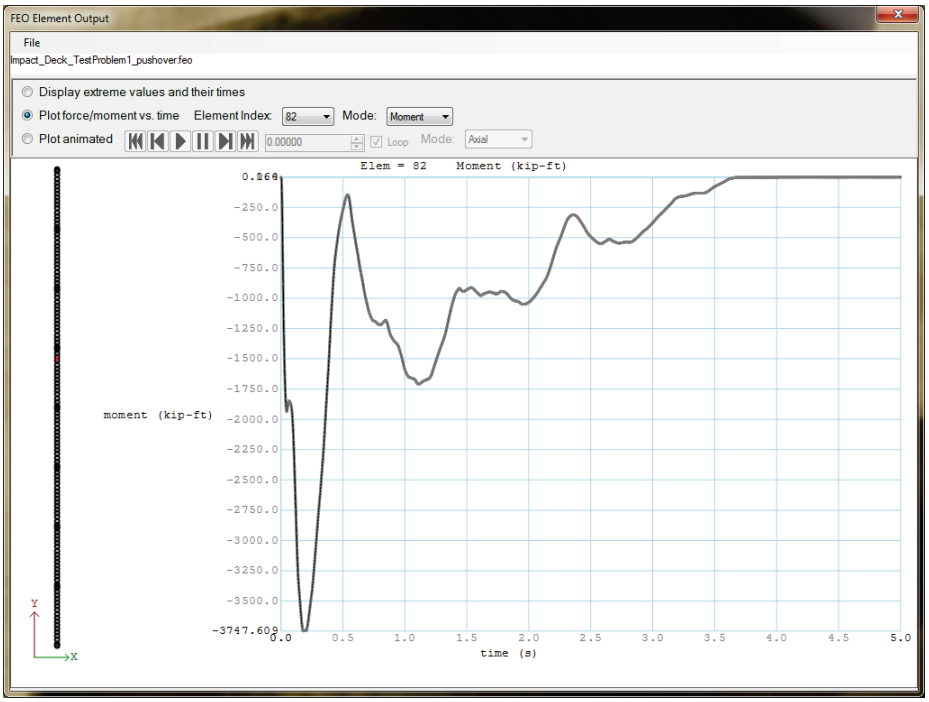


Figure 2.51 Wall axial forces at 0.2 sec.

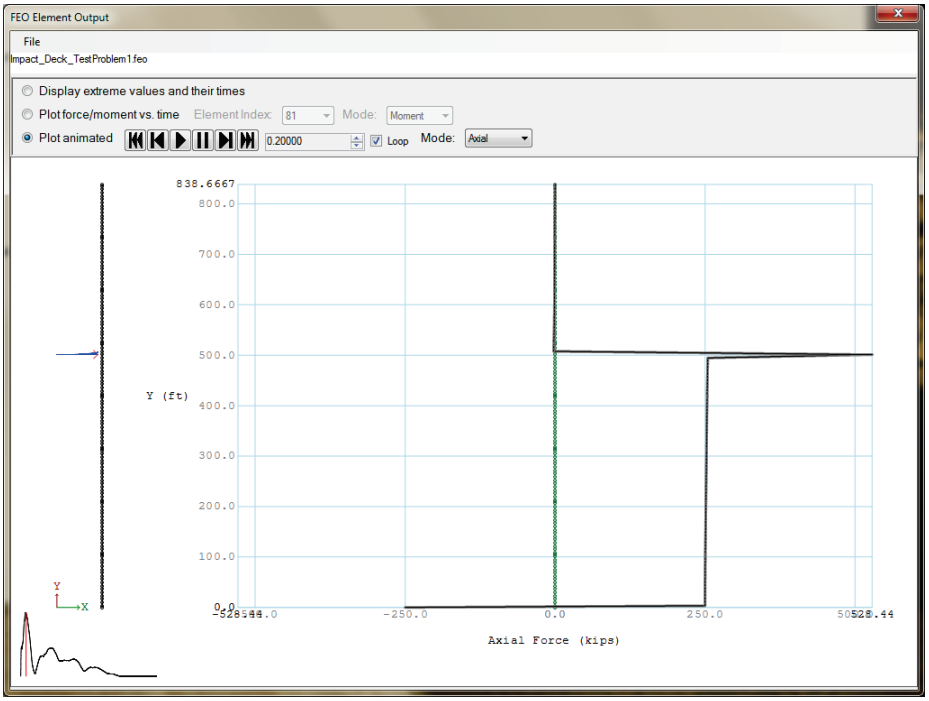


Figure 2.52 Wall shear forces at 0.2 sec.

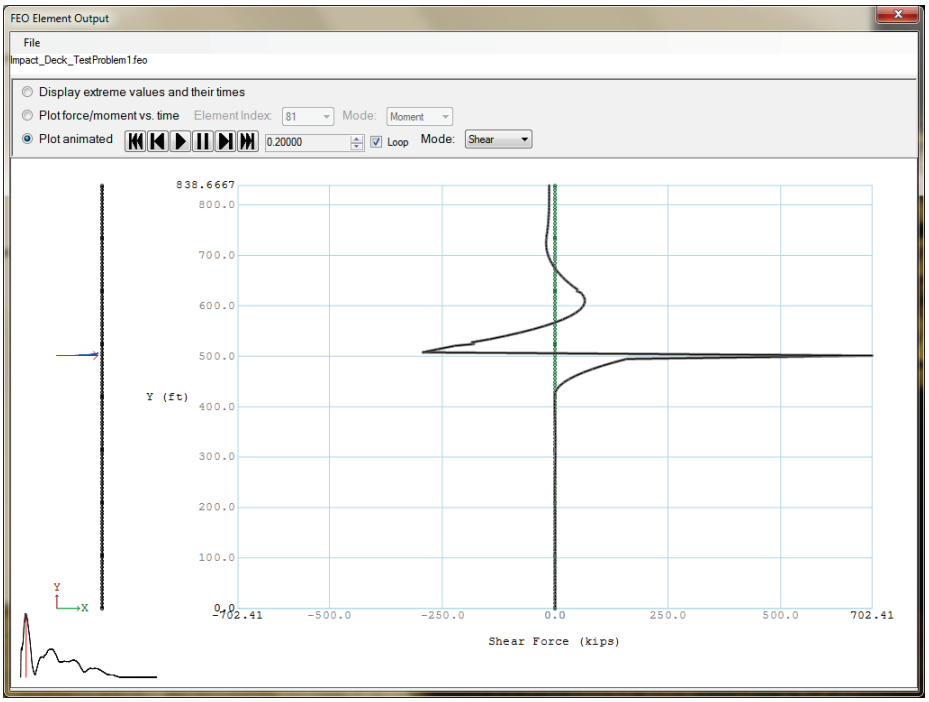
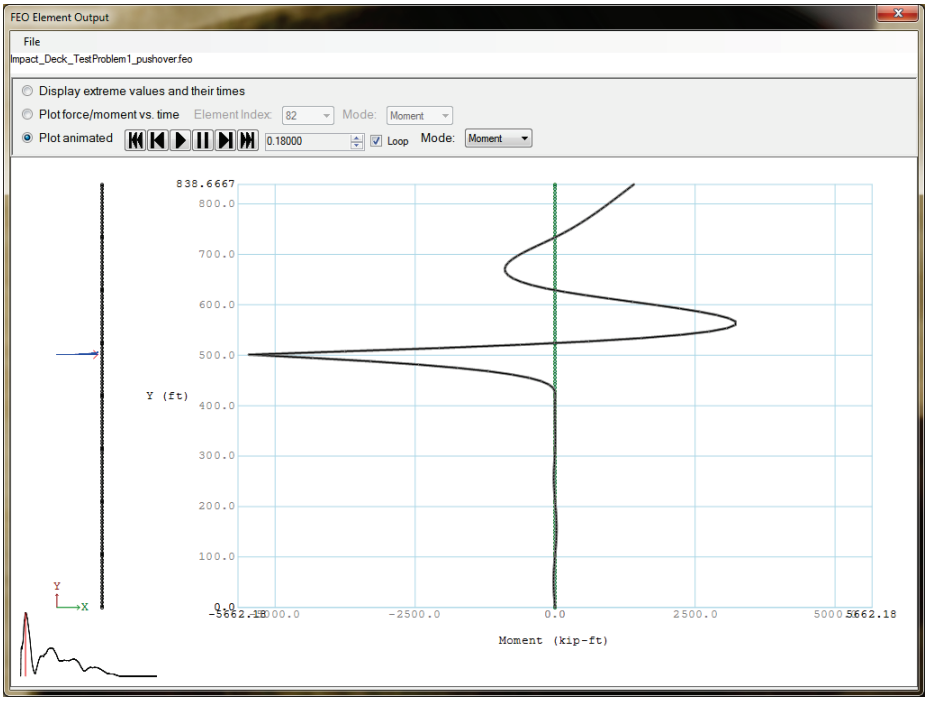


Figure 2.53 Wall moments at 0.18 sec.



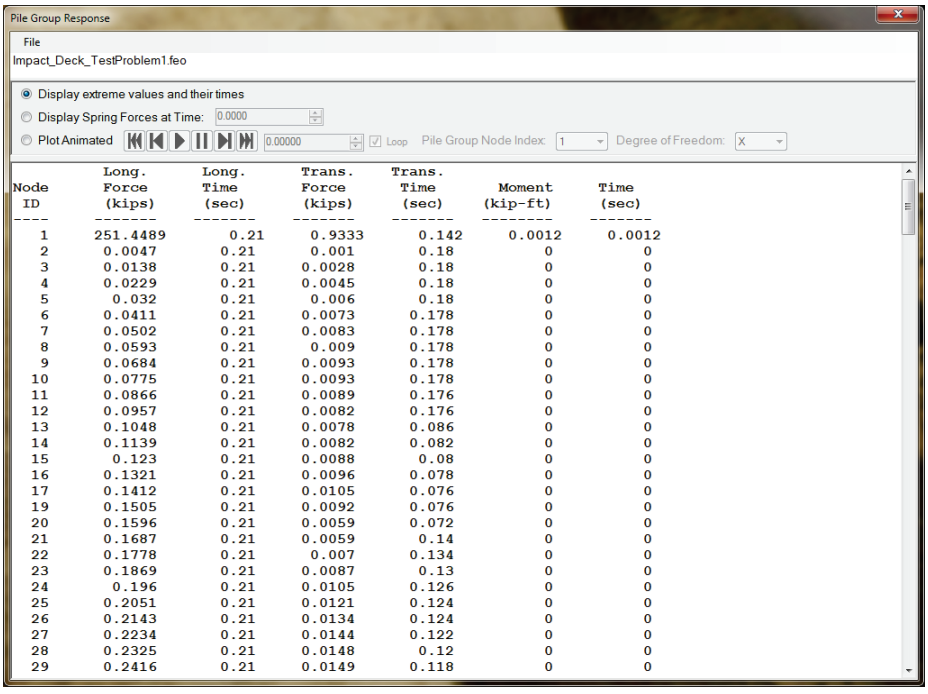
Of primary importance for doing a pile group founded flexible wall analysis, is being able to see exactly how much force each pile group will be able to resist during an impact event. This is measured by finding the resisting force from the spring model used for the pile group for the pile group's

displacement. Figure 2.54 shows the table of maximum forces/moments resisted at the nodes representing a pile group in the impact deck example model. Looking through this table gives the information that the maximum individual pile group response force is in the transverse direction at node 85 and at time 0.26 sec. This peak response force is 54.465 kips. Figure 2.55 is the same window scrolled down to reveal the maximum displacements of these pile group nodes, and when these displacements occurred.

A second table in the program reveals the response forces of each pile group node at a specified time. Figure 2.56 shows this table for time 0.26 sec. At the bottom of this table, the individual responses are summed to reveal the total force in each direction. Information about the impulse calculations over all time is also given at the end of this table. For time 0.26 sec, the total force from the 96 pile groups acting in the transverse direction is 722.776 kips. For the entire run, the transverse impulse was 454.31 kip-sec.

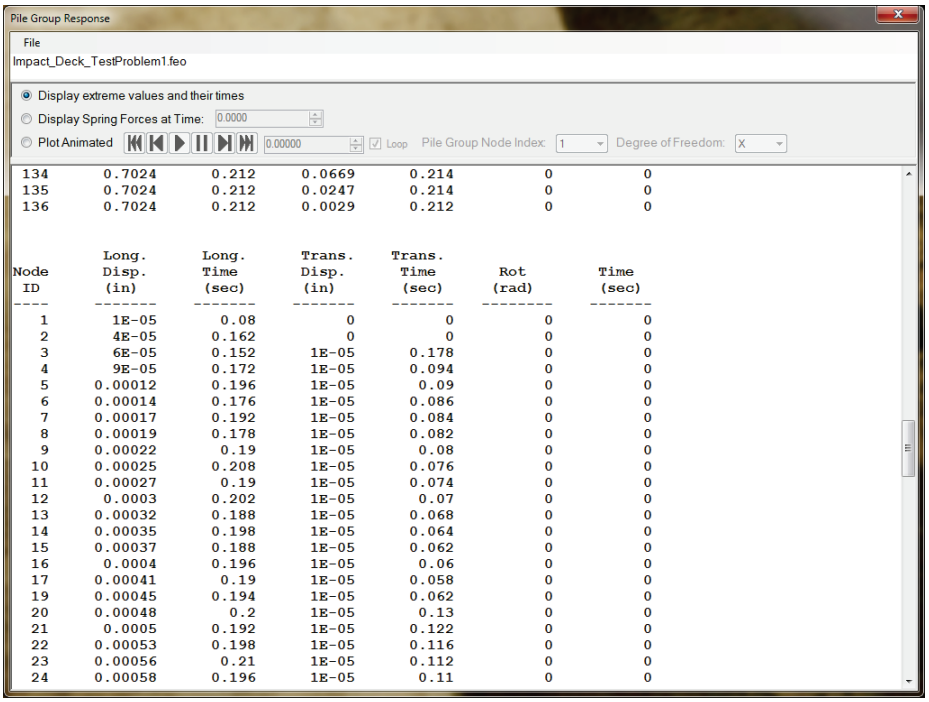
Figure 2.57 shows the response of the pile group at node 85 at time 0.260 sec as a force-versus-displacement plot, and as force and displacement time histories. This is the time when the displacement for the pile group at node 85 is at its maximum location in the transverse direction. In this example, the longitudinal and rotational displacement created small resisting forces (Figures 2.58 and 2.59).

Figure 2.54 Table of pile group response maximum forces and moments and their time.



Node ID	Long. Force (kips)	Long. Time (sec)	Trans. Force (kips)	Trans. Time (sec)	Moment (kip-ft)	Time (sec)
1	251.4489	0.21	0.9333	0.142	0.0012	0.0012
2	0.0047	0.21	0.001	0.18	0	0
3	0.0138	0.21	0.0028	0.18	0	0
4	0.0229	0.21	0.0045	0.18	0	0
5	0.032	0.21	0.006	0.18	0	0
6	0.0411	0.21	0.0073	0.178	0	0
7	0.0502	0.21	0.0083	0.178	0	0
8	0.0593	0.21	0.009	0.178	0	0
9	0.0684	0.21	0.0093	0.178	0	0
10	0.0775	0.21	0.0093	0.178	0	0
11	0.0866	0.21	0.0089	0.176	0	0
12	0.0957	0.21	0.0082	0.176	0	0
13	0.1048	0.21	0.0078	0.086	0	0
14	0.1139	0.21	0.0082	0.082	0	0
15	0.123	0.21	0.0088	0.08	0	0
16	0.1321	0.21	0.0096	0.078	0	0
17	0.1412	0.21	0.0105	0.076	0	0
19	0.1505	0.21	0.0092	0.076	0	0
20	0.1596	0.21	0.0059	0.072	0	0
21	0.1687	0.21	0.0059	0.14	0	0
22	0.1778	0.21	0.007	0.134	0	0
23	0.1869	0.21	0.0087	0.13	0	0
24	0.196	0.21	0.0105	0.126	0	0
25	0.2051	0.21	0.0121	0.124	0	0
26	0.2143	0.21	0.0134	0.124	0	0
27	0.2234	0.21	0.0144	0.122	0	0
28	0.2325	0.21	0.0148	0.12	0	0
29	0.2416	0.21	0.0149	0.118	0	0

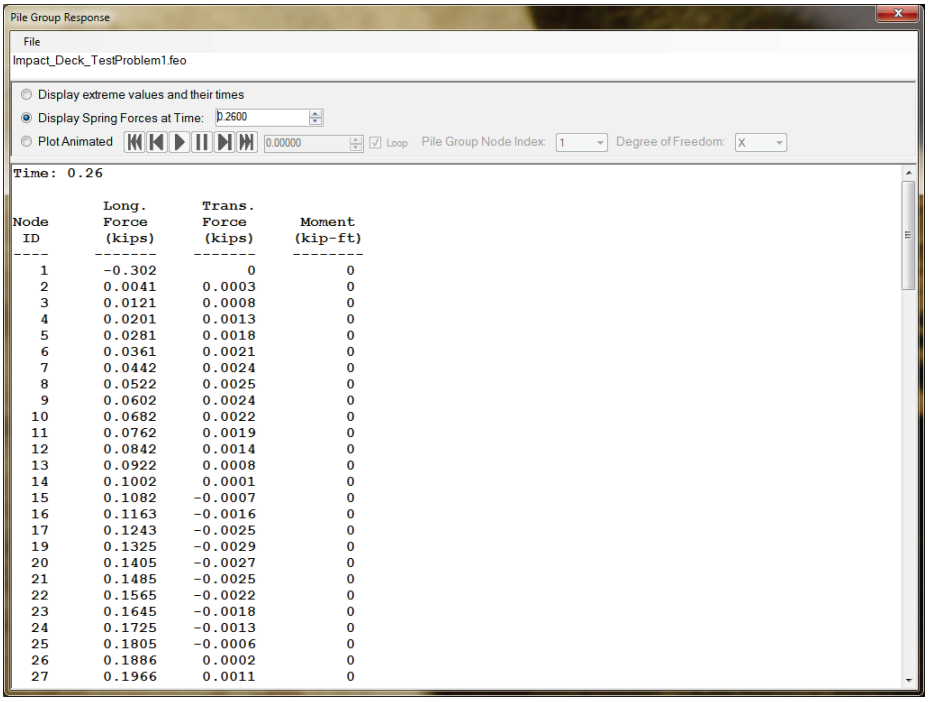
Figure 2.55 Table of pile group response maximum displacements and their time.



134	0.7024	0.212	0.0669	0.214	0	0
135	0.7024	0.212	0.0247	0.214	0	0
136	0.7024	0.212	0.0029	0.212	0	0

Node ID	Long. Disp. (in)	Long. Time (sec)	Trans. Disp. (in)	Trans. Time (sec)	Rot (rad)	Time (sec)
1	1E-05	0.08	0	0	0	0
2	4E-05	0.162	0	0	0	0
3	6E-05	0.152	1E-05	0.178	0	0
4	9E-05	0.172	1E-05	0.094	0	0
5	0.00012	0.196	1E-05	0.09	0	0
6	0.00014	0.176	1E-05	0.086	0	0
7	0.00017	0.192	1E-05	0.084	0	0
8	0.00019	0.178	1E-05	0.082	0	0
9	0.00022	0.19	1E-05	0.08	0	0
10	0.00025	0.208	1E-05	0.076	0	0
11	0.00027	0.19	1E-05	0.074	0	0
12	0.0003	0.202	1E-05	0.07	0	0
13	0.00032	0.188	1E-05	0.068	0	0
14	0.00035	0.198	1E-05	0.064	0	0
15	0.00037	0.188	1E-05	0.062	0	0
16	0.0004	0.196	1E-05	0.06	0	0
17	0.00041	0.19	1E-05	0.058	0	0
19	0.00045	0.194	1E-05	0.062	0	0
20	0.00048	0.2	1E-05	0.13	0	0
21	0.0005	0.192	1E-05	0.122	0	0
22	0.00053	0.198	1E-05	0.116	0	0
23	0.00056	0.21	1E-05	0.112	0	0
24	0.00058	0.196	1E-05	0.11	0	0

Figure 2.56 Table of pile group responses for each pile group individually and summed (not shown) at time 0.26 sec.



Time: 0.26

Node ID	Long. Force (kips)	Trans. Force (kips)	Moment (kip-ft)
1	-0.302	0	0
2	0.0041	0.0003	0
3	0.0121	0.0008	0
4	0.0201	0.0013	0
5	0.0281	0.0018	0
6	0.0361	0.0021	0
7	0.0442	0.0024	0
8	0.0522	0.0025	0
9	0.0602	0.0024	0
10	0.0682	0.0022	0
11	0.0762	0.0019	0
12	0.0842	0.0014	0
13	0.0922	0.0008	0
14	0.1002	0.0001	0
15	0.1082	-0.0007	0
16	0.1163	-0.0016	0
17	0.1243	-0.0025	0
19	0.1325	-0.0029	0
20	0.1405	-0.0027	0
21	0.1485	-0.0025	0
22	0.1565	-0.0022	0
23	0.1645	-0.0018	0
24	0.1725	-0.0013	0
25	0.1805	-0.0006	0
26	0.1886	0.0002	0
27	0.1966	0.0011	0

Figure 2.57 Transverse pile group responses for the pile group at node 85 and at time 0.24 sec.

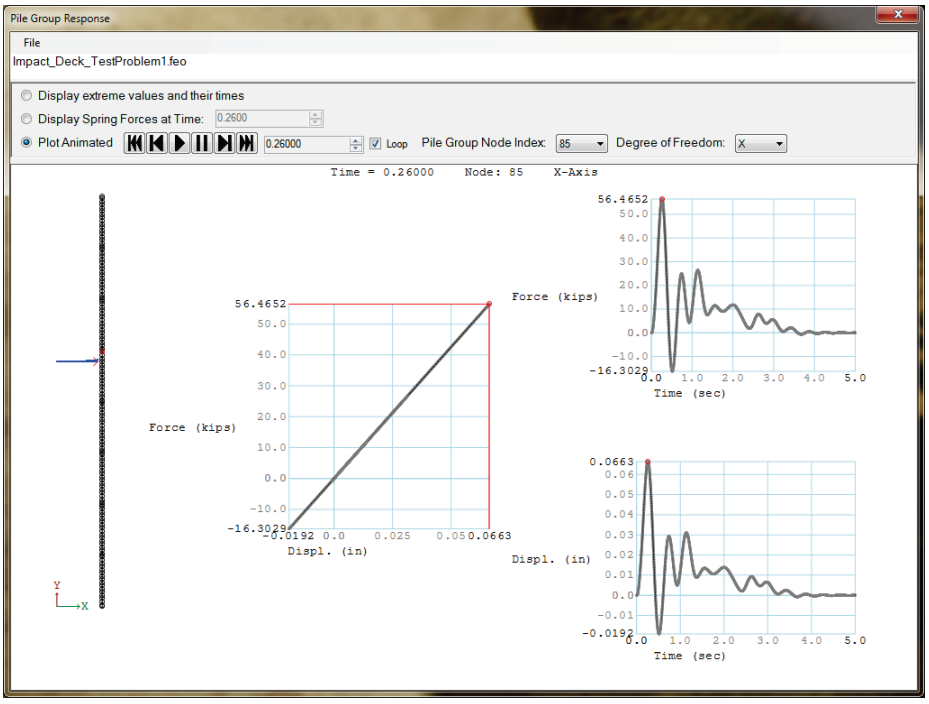


Figure 2.58 Longitudinal pile group responses for the pile group at node 85 and at time 0.24 sec.

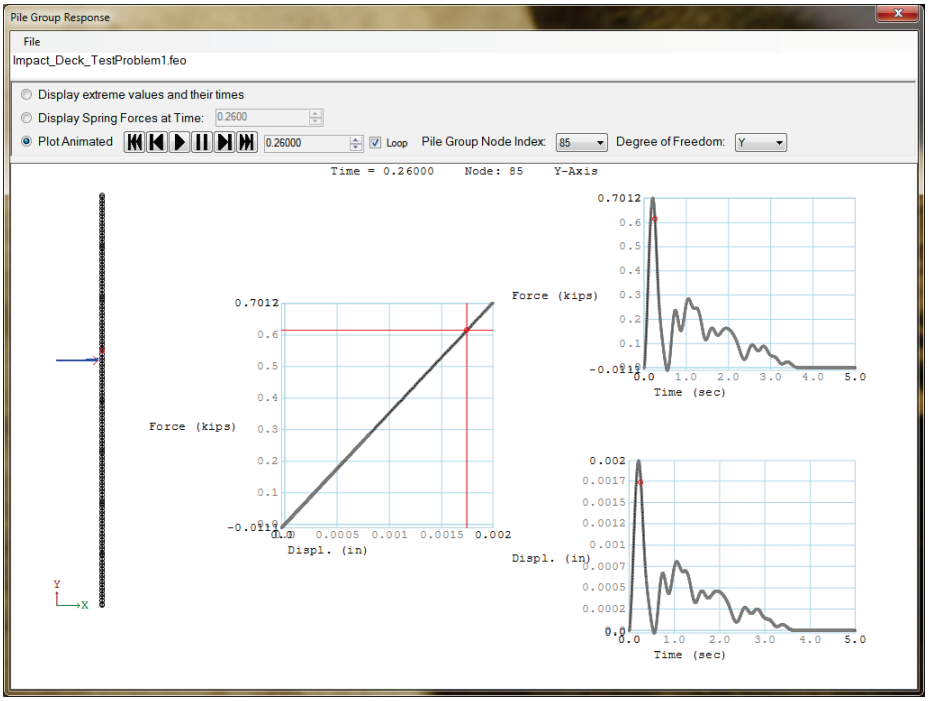
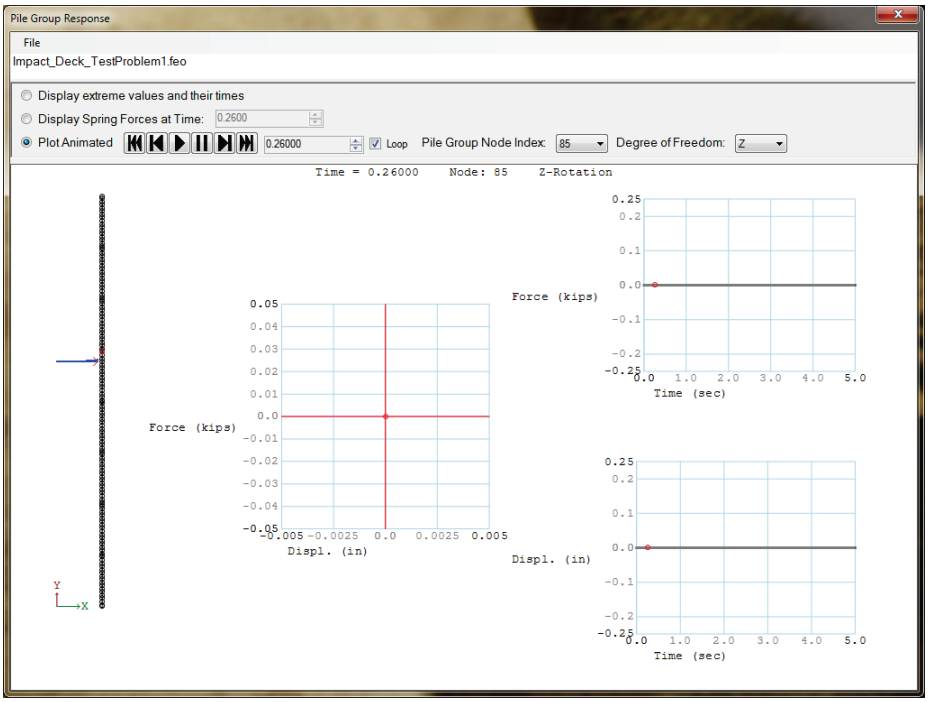


Figure 2.59 Rotational pile group response for the pile group at node 85 and at time 0.24 sec.



The Case for Dynamic Analysis:

This example problem demonstrated the need to perform a dynamic analysis of these pile founded walls. This example used an impact time history that was the result of the Winfield Test # 10. This impact time history was applied transverse to the approach wall at a position starting at 501.187 ft along the wall (at the same location as node 82) and moved at 1 ft/sec along the approach wall. The peak force for the impact time history was 516.4 kips at time 0.174 sec.

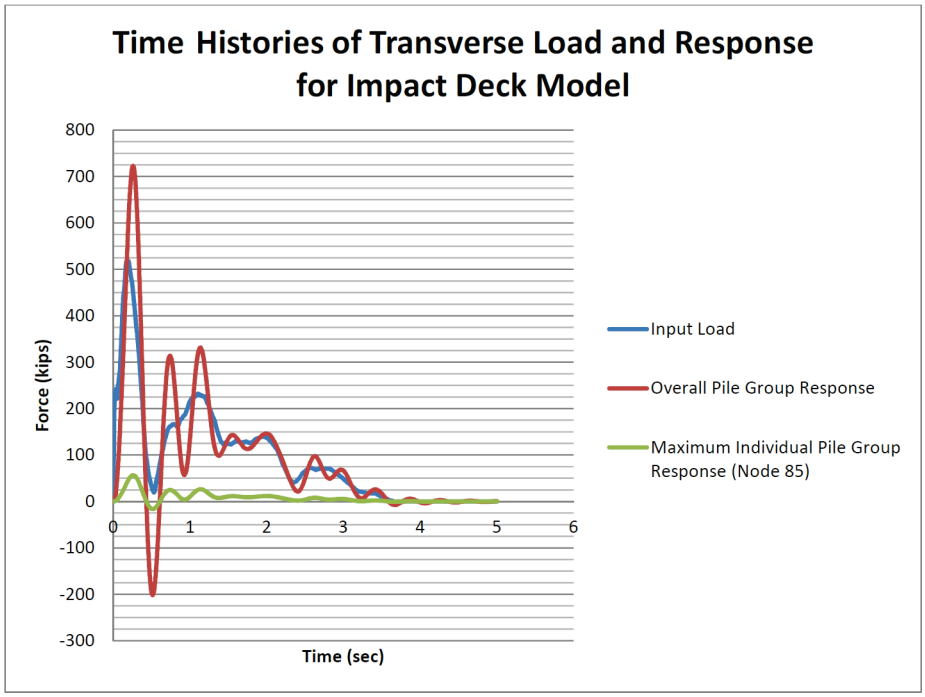
Node 85 (as discussed above) had a maximum transverse force of 56.4652 kips, which occurred at 0.26 sec. This was the last pile group node along a monolith, so its transverse displacement was affected by the moment induced (to the monolith it is connected) by the impact load. The total pile group response for the whole impact deck structure (96 pile group nodes) at time 0.26 sec was 722.775 kips, which was greater than the peak input force. It was also the peak overall response.

At time 0.174, the impact load reached its first peak with a force of 516.2 kips. Data was also collected at this time. Table 2.5 shows the values generated by this data collection. Figure 2.60 takes this information a step further by displaying the time histories for the three forces.

Table 2.5 Transverse forces with respect to time.

Time (s)	Node 85 Force (kips)	Impact Load Force (kips)	Total Pile Group Response (kips)
0.174	39.131	516.200	324.254
0.200	47.277	**516.400**	611.247
0.260	**56.465**	446.358	**722.776**

Figure 2.60 Time-history plot of transverse input forces, total force response for all the pile groups, and an individual pile group response forces.



From Table 2.5 and Figure 2.60, it can be seen that the overall pile group response is dynamic because it does not track with the input force. Instead, the pile groups respond to the input force overtime due to inertial effects. Because of this, the overall pile group response can have higher peak forces. For example, at a time of peak response of 0.2 sec, a maximum impact force of 516.4 kips is applied to the approach wall. The total transverse-force response of 96 nodes represents all of the pile group and totals 611.25 kips. This 18 % larger force response is due to the contribution of the first two terms of the equation of motion (also seen in Appendix A) for the dynamic structural response:

$$[M]\{\ddot{u}(t)\}+[C]\{\dot{u}(t)\}+[K]\{u(t)\}=\{F(t)\} \quad (2.1)$$

At time 0.26 sec, when a peak response force is recorded at node 85 for an individual pile group, the contribution of the first two terms of the equation of motion for the dynamic structural response is even larger resulting in an overall response force of 722.776 kips. This is nearly 40% greater than the peak input force of 516.4 kips. And an overall peak response force of 722.776 kips is 55% larger than the 446.358 kips input force imposed at 0.26 sec. These observations demonstrate the importance of applying the equation of motion for calculating pile group structural response forces (and displacements). These differences explain why a dynamic analysis is required versus a static analysis, which the user provided impact load is applied as a single peak value (e.g., determined to be the input peak force from the time history).

Load Sharing in Dynamic Analysis:

Another point to note is the individual pile group response has much lower peak forces than the input load. This is because the load is being shared with other pile groups along the 96 groups that support the eight impact deck monoliths, which sum up to the overall pile group response. The peak response of node 85, at 56.465 kips, is only 11% of the peak input force of 516.4 kips and 8% (1/12) of the overall peak response force of 722.776 kips. Because there are 16 pile group nodes per monolith, it may be surmised that the peak individual response force would be $1/16^{th}$ instead of $1/12^{th}$ of the overall response. Note the fact that this peak force is obtained only at node 85 and includes transverse displacement due to rotational moment and inertia, which are difficult to predict without dynamic analysis.

Validation Using Impulse Calculations:

The higher peak values of the overall pile group response seem out of place until an impulse calculation (taking the area beneath the time history curves for input load and overall pile group response in Figure 2.60) is performed. Despite inertial effects, the impulse of the input load must be equivalent to the overall pile group response, if the piles do not fail. When an impulse calculation is performed for the overall pile group response, the result is 454 kip-sec. The impulse for the input force is 463 kip-sec. The difference is minimal (<2%) and easily explained by the fact that these are only transverse forces and do not include moment arm effects that are induced by the impact load on the impacted monolith.

2.10 Final Remarks

In this section, the Lock and Dam 3 physical model was presented and the mathematical model to calculate the dynamic response was also developed. Impact_Deck, a computer program, was used to calculate the dynamic response of an elastic beam supported over linear elastic or plastic spring supports. The mathematical formulation featured a method to calculate the end release at the inter-monolith connection. The impact normal and parallel concentrated external load was located at a specified location or assumed to have motion at a specified constant velocity. The damping effect was considered by means of the Rayleigh damping model, which depended on the natural frequencies of the system. These natural frequencies were calculated in an approximate way by using the linear stiffness of the springs and the mass per unit length of the beam. The results of Impact_Deck proved to be valid when compared to the results obtained with SAP2000. An example was presented to show the plastic behavior of the springs and how these results compared to the linear elastic response.

3 An Approach Wall with Impact Beams on Nontraditional Pile Supported Bents – McAlpine Example

3.1 Introduction

This chapter summarizes an engineering methodology and corresponding software feature contained within the Impact_Deck software for performing a dynamic structural response analysis of a flexible impact beam supported over groups of clustered vertical piles configured in a triangle pattern and subjected to a barge impact event. This example is based on an alternative approach wall design proposed for the McAlpine Locks and Dam on the Ohio River in Kentucky.

This example models a glancing blow impact event of a barge train impacting an approach wall as it aligns itself with a lock is an event of short duration; the contact time between the impact corner of the barge train and the approach wall can be as short as a second or as long as several seconds. The next generation of Corps approach walls is more flexible than the massive, stiff-to-rigid structures constructed in the past in order to reduce construction costs as well as to reduce damage to barges during glancing blow impacts with lock approach walls. A flexible approach wall or flexible approach wall system is one in which the wall has the capacity to absorb impact energy by deflecting or "flexing" during impact, thereby affecting the dynamic impact forces that develop during the impact event.

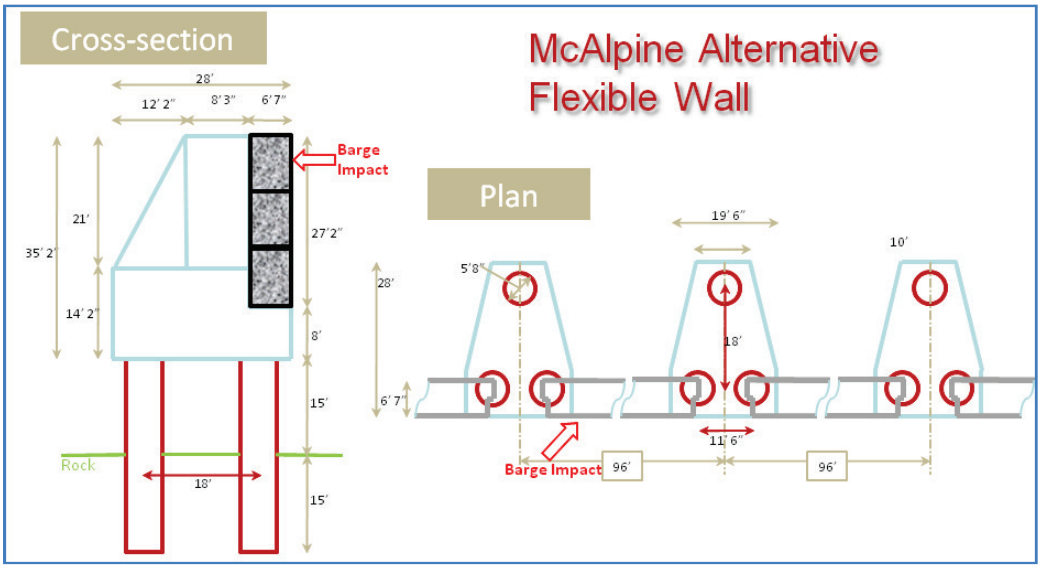
3.2 Alternative Flexible Approach Wall – Physical Model

McAlpine alternative flexible approach wall is located in Louisville, Kentucky, at the Falls of the Ohio. McAlpine Locks and Dam are located at mile point 606.8 and control a 72.9-mile-long (117.3 km) navigation pool. The McAlpine locks underwent a 10-year expansion project that was completed in early 2009. The flexible approach wall system discussed in this section was an alternative flexible approach wall design.

An artist rendering of the McAlpine alternative flexible approach wall (plan and cross-sectional views) is shown in Figure 3.1. The structure consists of continuous, flexible concrete beams with a span of approximately 96 ft per segment. Each end of the beam rests on a pile cap that is supported by a

group of three piles. The supporting piles provide a flexible resistance to the barge train impact forces that are applied to the beam. The continuity of the impact beam with the pile cap impact feature is achieved by means of shear key at each pile group support. That means that the ends of each beam transfers the longitudinal and transverse forces with no moment transfer to each pile group support (i.e., a pinned support). The axial and transverse forces at the end of the beams are transferred to the pile cap by means of a shear key. The shear key portion of the pile cap structural feature has a length of 11.5 ft. The length of the shear key is the distance between two consecutive concrete beams in this figure. The massive pile cap rests over a clustered group of three vertical piles. Each pile is 5 ft 8 in. in diameter. They are arranged in a triangular pattern so as to absorb the torsion generated at the pile group due to the eccentricity between the center of the pile group and the location of the end of each of the flexible impact beams that are supported by a clustered pile group.

Figure 3.1 McAlpine alternative flexible approach wall.

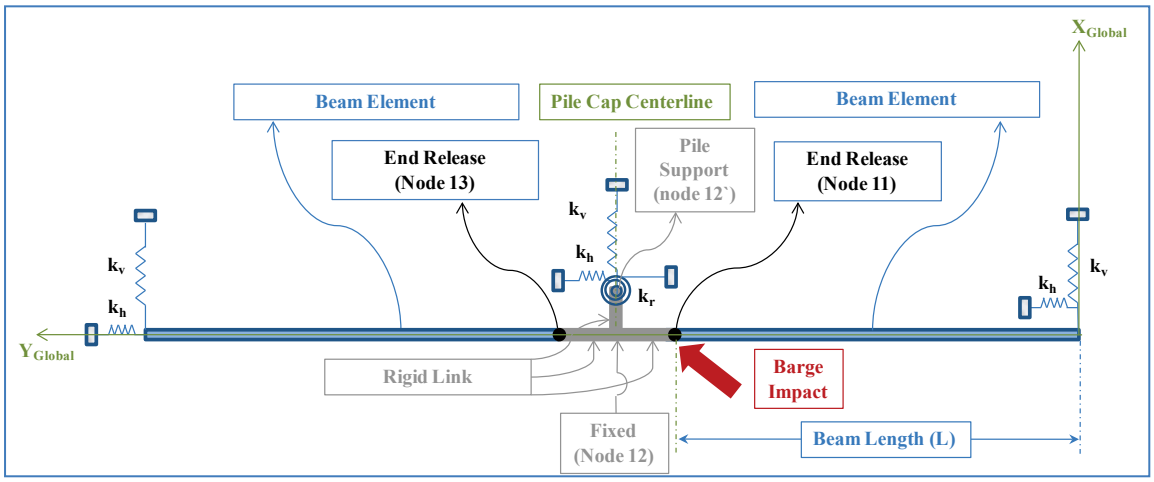


3.3 McAlpine Alternative Flexible Approach Wall – Mathematical Model

The McAlpine alternative flexible approach wall can be modeled using beam elements because its length is much greater than its other two dimensions. The length of each flexible impact beam segment is approximately 96 ft and the width and height are 6 ft 7 in. and 9 ft, respectively. The mathematical model can be seen in Figure 3.2. In the analysis, the model consists of two consecutive beams with longitudinal and transverse elastic-plastic spring

supports at the start and end of the system. These two set of springs model the pile group at the start and end of the two consecutive beams. The transverse non-linear spring represents the effect of the clustered group of three vertical piles. The longitudinal end spring represents the effect of the response of the end support pile group and that of the other groups of piles beyond this location. At the center pile group, three rigid links are used to model the high stiffness and mass of the pile cap. The nodes that connect the impact beams to the pile cap do not transfer moment between these impact beams and the center pile cap. The center pile group is modeled with three springs (two translational and one rotational). The translational spring stiffness is calculated by means of a push-over analysis (section 3 or Appendix A in Ebeling et al. 2012) and the rotational spring stiffness is calculated and seen in Appendix E.

Figure 3.2 McAlpine flexible approach wall mathematical model.



The mathematical model is formulated using 3-D beam elements. A 3-D beam element has 6 degrees of freedom per node, producing 12 degrees of freedom per element. The degrees of freedom per node are 3 translations and 3 rotations as shown in Figure 3.3. The force $F_x(t)$ applied normal to the flexible beams is the impact-force time history developed using the PC-based software Impact_Force (Ebeling et al. 2010). The force $F_y(t)$ is applied parallel to the wall and is a fraction of the normal force calculated using the dynamic coefficient of friction between the barge and the flexible beam contact surface in the Impact_Deck software.

The model used to describe the beam is developed in the plane so the beam element has 3 degrees of freedom per node and 6 degrees of freedom per element. The degrees of freedom per node are 2 translations and 1

rotation (Figure 3.4). Based on the notation of Figure 3.3, the force and moment conditions for *node i* are $F_{i,x} = V_i$, $M_{i,x} = 0$, $F_{i,y} = F_i$, $M_{i,y} = 0$, $F_{i,z} = 0$, and $M_{i,z} = M_i$, and for *node f* are $F_{f,x} = V_f$, $M_{f,x} = 0$, $F_{f,y} = F_f$, $M_{f,y} = 0$, $F_{f,z} = 0$, and $M_{f,z} = M_f$. To transform a 3-D beam element to a 2-D (plane element), the moment about the "x" axis, the moment about the "y" axis, and the force in the "z" directions are equal to zero.

Figure 3.3 (a) Typical 3-D segment of the Impact Deck beam element, (b) Impact force applied to the Impact Deck, (c) Typical 3-D beam element.

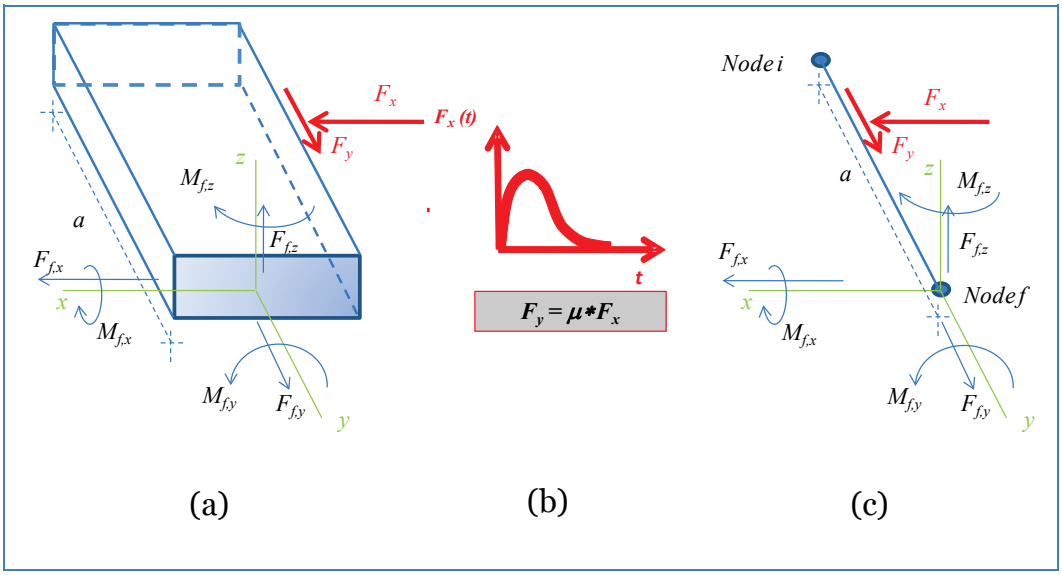
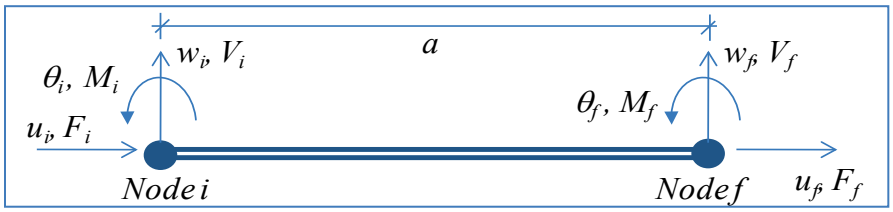


Figure 3.4 Typical 2-D beam element used in Impact_Deck.



A push-over type of analysis was conducted to characterize the force-versus-displacement behavior of a cluster of three vertical piles under static lateral loading and thus define the stiffness coefficient of the two translational springs and one rotational spring. Appendix E summarizes the three-spring stiffness for the McAlpine alternative flexible wall.

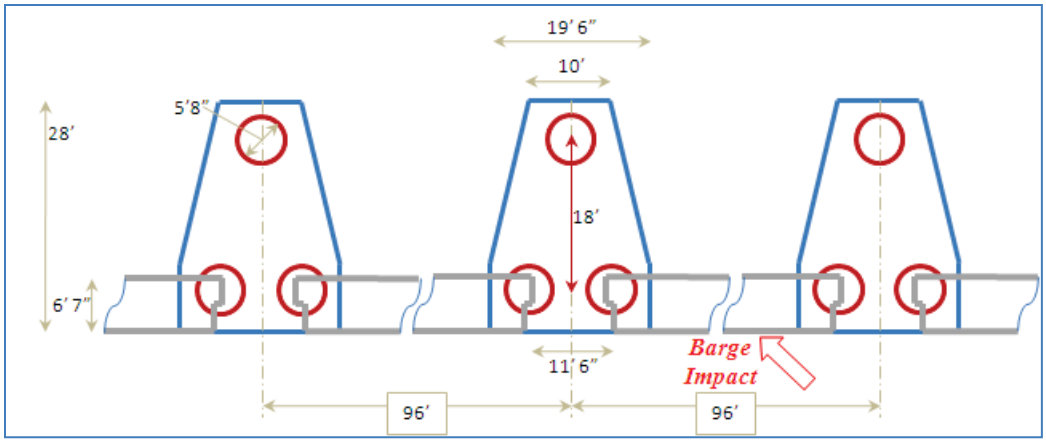
3.4 Nonlinear force-deflection relationship for the springs supports

Section 2.5 discussed how the nonlinear spring response force-displacement backbone curve was used to model plastic deformation in the pile substructure for dynamically loaded structures. Push-over

calculations were similarly performed for the pile layout for the McAlpine alternative flexible wall supports.

The McAlpine alternative flexible wall bent was different from the other bents, in that its piles were not in a straight line. Its drilled-in-place (DIP) piles were placed in a triangle (per the following figure), and it was assumed that a push-over analysis would yield different results than for a traditional pile bent.

Figure 3.5 Plan view of the flexible wall pile layout.



After a push-over analysis in CPGA was performed, it was found that this was not the case, other than the fact that due to the size of the beams and the method of anchoring the beams to the pile cap superstructure the bents actually developed bending failure at the cap and mudline simultaneously.

The transverse and longitudinal push-over, force-versus-displacement curves were effectively the same as taking an individual pile curve and multiplying the force by three. Tables 3.1 and 3.2 summarize the primary loading curves used to define the transverse and longitudinal spring models, respectively.

Appendix E provides a method for calculating the rotational force-versus-displacement curve from the force-displacement curve for a single pile. The single pile curve is provided in Table 3.3.

Table 3.1 Primary loading curve for the transverse spring model for a McAlpine alternative flexible wall bent (3 piles).

Force	Deflection		Notes
(kips)	(inches)	(feet)	Adapted from Appendix A of Ebeling et al. (2012)
0.0	0.0	0.0	
2141.5	1.8	0.15	Pile to pile cap moment capacity reached at the same time hinge develops at equivalent depth of fixity
2141.5	4.0	0.33	Plastic hinge rotation

Table 3.2 Primary loading curve for the longitudinal spring model for a McAlpine alternative flexible wall bent (3 piles).

Force	Deflection		Notes
(kips)	(inches)	(feet)	Adapted from Appendix A of Ebeling et al. (2012)
0.0	0.0	0.0	
2141.5	1.8	0.15	Pile to pile cap moment capacity reached at the same time hinge develops at equivalent depth of fixity
2141.5	4.0	0.33	Plastic hinge rotation

Table 3.3 Primary loading curve for a spring model for a single 6-ft diameter DIP pile.

Force	Deflection		Notes
(kips)	(inches)	(feet)	Adapted from Appendix A of Ebeling et al. (2012)
0.0	0.0	0.0	
713.8	1.8	0.15	Pile-to-pile cap moment capacity reached at the same time hinge develops at equivalent depth of fixity
713.8	4.0	0.33	Plastic hinge rotation

3.5 Solving for the motion of the structure

The equations of motion for a flexible approach wall structure comprised of decks supported on clustered pile groups and their end-release computations for the McAlpine alternative flexible approach wall model and other similar structural systems are given in Appendix B. Appendix I discusses the Rayleigh damping feature of the structural model, with section I.3 giving information specific to the McAlpine alternative flexible approach wall model. The numerical methods to be used in the solution of the equations of motion are either HHT-α or Wilson-θ, which are discussed in Appendix F and G, respectively.

3.6 Validation of Impact_Deck Computer Program

The validation of Impact_Deck computer program for the McAlpine alternative flexible approach wall model was made against the results obtained from the computer program SAP2000. The beam had a total length of 180.5 ft long. In the validation procedure, the beam was modeled with 24 nodes and 24 beam elements. The three rigid elements that model the pile cap support were included in the model. A set of linear elastic springs was located at node 1 and 23 where the start and end pile supports were placed.[1] The strength of the concrete was assumed as $f'c = 5{,}000\ psi$ with a corresponding modulus of elasticity for the concrete of $E = 580{,}393.25\ ksf$. The beam cross-sectional area and the beam second moment of area (moment of inertia) were 54.668 ft^2 and 517.2 ft^4, respectively. The mass per linear foot of beam was calculated as $\bar{m}$ = 0.25486 kip *sec^2/ft. A damping factor of 0.02 (i.e., 2% of the critical damping) was used in both computer program models. Figure 3.6, impact-force time history was the Winfield test # 10 (generated using Impact_ Force, Ebeling et al. 2010) and applied at node 11 (i.e., $x = 84.5$ ft). The tangential-force time history was set equal to the transverse time history multiplied by a dynamic coefficient of friction of 0.5. The impact load was kept stationary at node 11 due to restrictions in loading for SAP2000. A pile group rotational spring stiffness value of 12,426,909 kip*ft/rad was computed as outlined in the Appendix E calculation steps. This calculation used a stiffness value of 132,189.5 kip/ft as the initial segment of the push-over curve which was applied to each of the two translational springs for each pile of the three-pile groups. The stiffness of the three (two translational and one rotational) representing the central pile group was assigned to node 12', located 7.708 ft in the transverse direction behind node 12. This position was located at the center of rotation of the pile group. Figures 3.7 to 3.10 show the dynamic response time histories of nodes 1, 12', and 23. With the exception of a few minor differences, both computer programs resulted in the computation of essentially the same system response values. At nodes 1 and 23, some differences in the magnitude of the computed transverse displacement values were apparent. However, the magnitudes of these values were very small, which was associated with numerical approximations. Figure 3.10 shows the rotation time histories computed at nodes 12 and 12'. These two nodes defined the rigid beam element of the pile cap, which was perpendicular to the impact beam model. The rotations were the same for both nodes and indicated a rigid element behavior.

[1] The SAP2000 analysis is restricted to a linear spring model for each group of clustered piles.

Figure 3.6 Force time history of Winfield Test # 10.

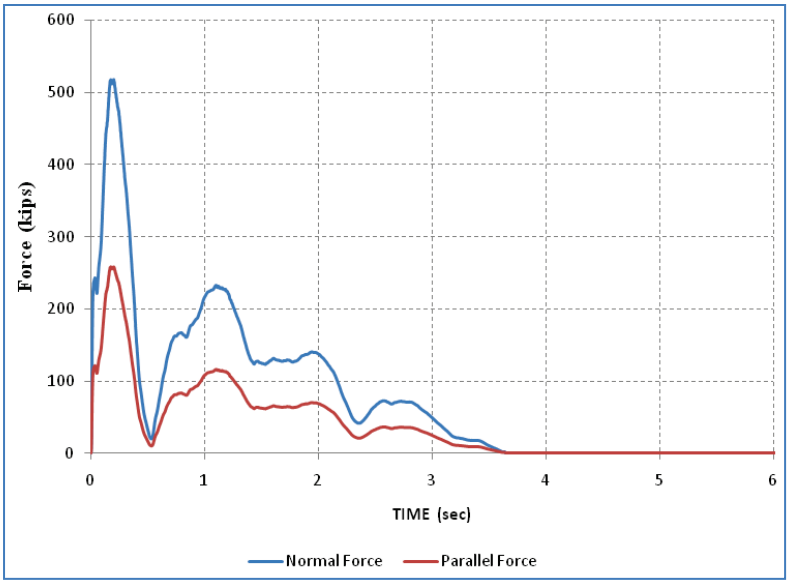


Figure 3.7 Validation of Impact_Deck against SAP2000 – Transverse displacement at node 1.

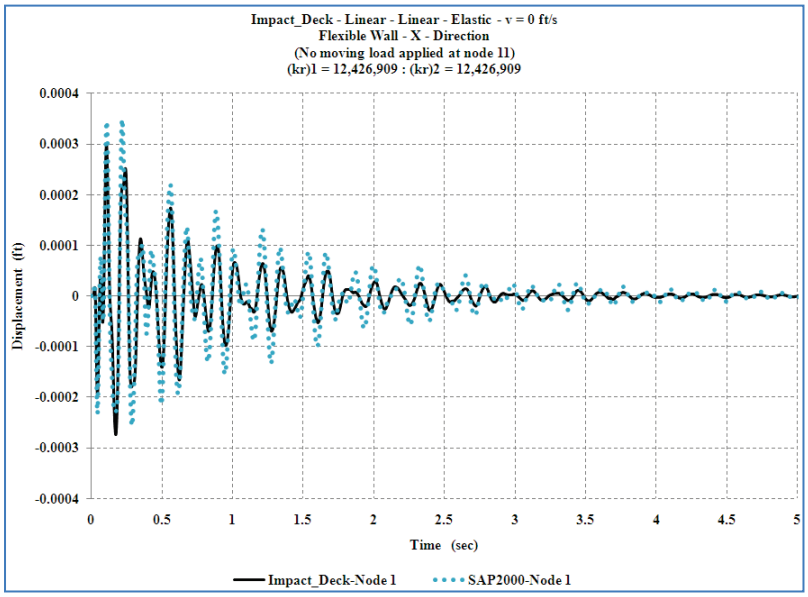


Figure 3.8 Validation of Impact_Deck against SAP2000 – Transverse displacement at node 23.

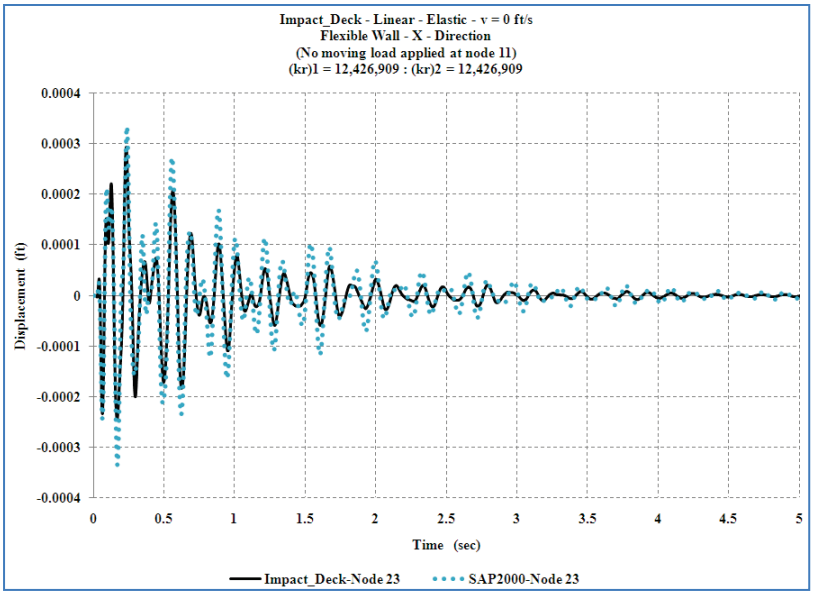


Figure 3.9 Validation of Impact_Deck against SAP2000 – Transverse displacement at node 12'.

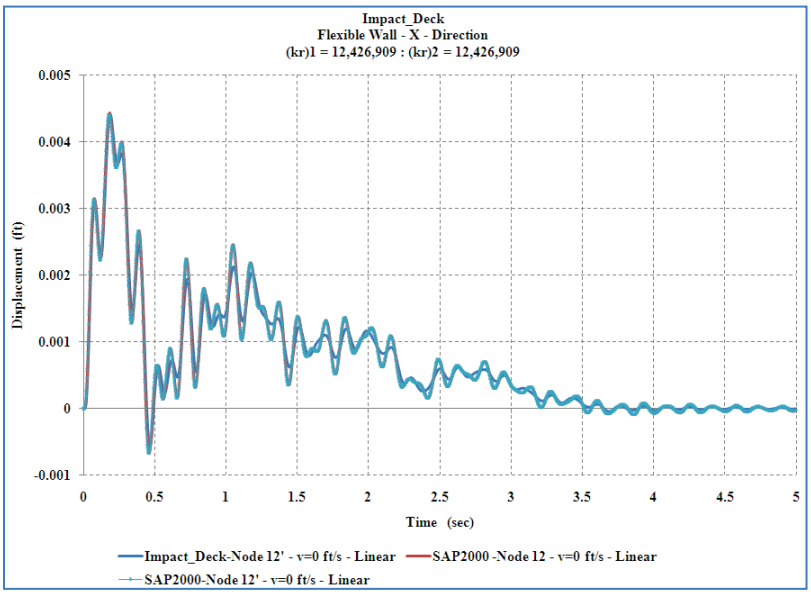
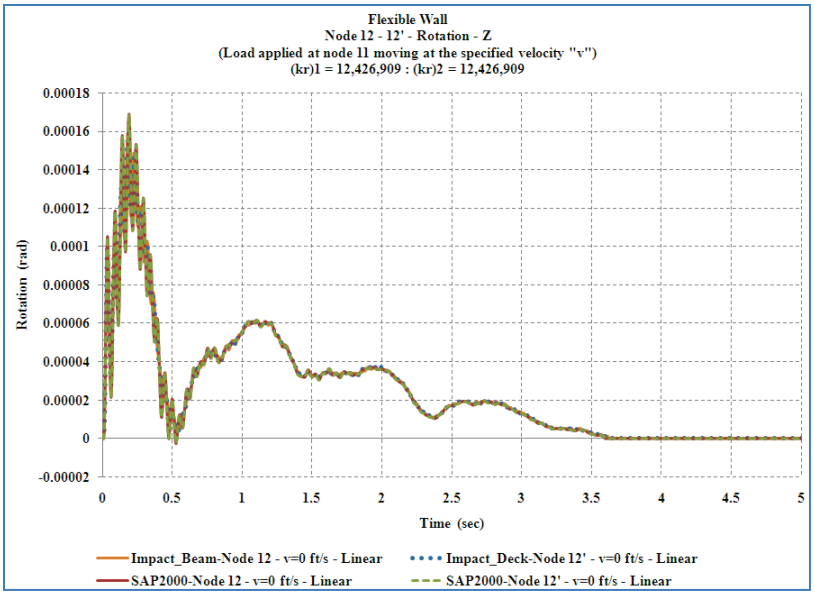


Figure 3.10 Validation of Impact_Deck against SAP2000 – Rotation at node 12 and 12'.



3.7 Numerical Example of the Elastic-Plastic Response Using Impact_Deck

This section presents the results of a numerical example that demonstrates the plastic behavior capability of the nonlinear impact-deck clustered pile springs. Plastic response can develop if the limiting elastic displacement specified by the user (i.e., Point 1 in Figure 3.5) is low enough to force the springs to enter into the zone of plastic response. The input data for the Impact_Deck computer program for McAlpine alternative flexible approach wall were as follows: The beam has a total length of 180.5 ft long with 24 nodes and 24 beam elements. The three rigid elements that model the pile cap support was included in the model. A set of linear elastic springs were located at node 1 and 23 where the start and end pile supports were placed. The strength of the concrete was assumed as $f'c = 5{,}000\ psi$ producing a modulus of elasticity for the concrete of $E = 580{,}393.25\ ksf$. The beam cross-sectional area and the beam second moment of area (moment of inertia) were 54.668 ft^2 and 517.2 ft^4, respectively. The mass per linear foot of beam was calculated as $\bar{m}$ = 0.25486 kip *sec^2 / ft. A damping factor of 0.02 (i.e., 2% of the critical damping) was used. The force time history was the Winfield test # 10 and shown in Figure 3.6. The tangential-force time history was set equal to the transverse force time history but multiplied by a dynamic coefficient of friction of 0.5. In this example, the load was assumed to be in motion along the impact beam at a velocity of $v = 3\ ft/sec$ starting at the node located at $x = 84.5\ ft$ in one set of calculations and applied at $x = 84.5\ ft$ along the beam for the entire duration of the impact event in the

second set of calculations (i.e., with at $v = 0$ *ft/sec*). In order to ensure plastic deformations, the spring models obtained by the push-over analysis were not used. Instead, the initial slopes for the stiffness of the two translational springs were assigned values equal to $k_1 = 132{,}189.5$ *kip/ft* and $k_2 = 66{,}094.75$ *kip/ft* with a stiffness for unload after the elastic displacement equal to $k_{unload} = k_1$. The elastic displacement that defines the point of demarcation for elastic and plastic zone behavior was $\delta_{elastic} = 0.003$ *ft*. The rotational spring stiffness was set equal to k_{1r} = 12,426,909.0 *kip*ft/rad* and k_{2r} = 6,213,454.5 *kip*ft/rad* with a stiffness for unload after the elastic displacement was equal to $(k_{unload})_r = k_{1r}$. The elastic rotation that defines the point of demarcation for elastic and plastic zone behavior was $\theta_{elastic} = 0.25$ *rad*. The stiffness of the three (two translational and one rotational) representing the central pile group was assigned to node 12', located 7.708 ft in the transverse direction behind node 12. Figure 3.11 shows the dynamic response time history obtained for node 12 and 12' (i.e., center of rigidity of the three pile group). The green nodal displacement trace in this figure shows a permanent lateral displacement of approximately 0.0011 ft after the transverse pile group spring develops plastic behavior. Figure 3.12 shows the rotational behavior of node 12 and 12'. If the impact load is moving, the response shows a change in sign for the rotation indicating that the load moves from one rigid element to the next rigid element, that is, the load moves from the right element from the centerline of the pile cap to the left element. After 3.63 sec, the linear response oscillates around zero displacement and the plastic response oscillates around 0.0011 ft. The explanation for the noted behaviors is explained by the fact that Figure 3.13 shows that plastic response is reached (i.e., response along the second slope of the force-displacement diagram) ending with a permanent displacement of around 0.0011 ft.

3.8 Impact_Deck GUI results

The Impact_Deck GUI was also used to run the McAlpine flexible wall problem in this section. This section does not provide an engineering analysis, but gives an idea of what information is provided so that an engineering analysis might be made.

The inputs are the same as those used for validating the model, with the minor exception that the longitudinal velocity of the barge train was 1 ft/sec, and that the push-over analysis spring models for the pile groups were used. These changes did not allow the pile groups to go into plastic deformation during loading.

Figure 3.11 Dynamic transverse response of node 12 and 12'.

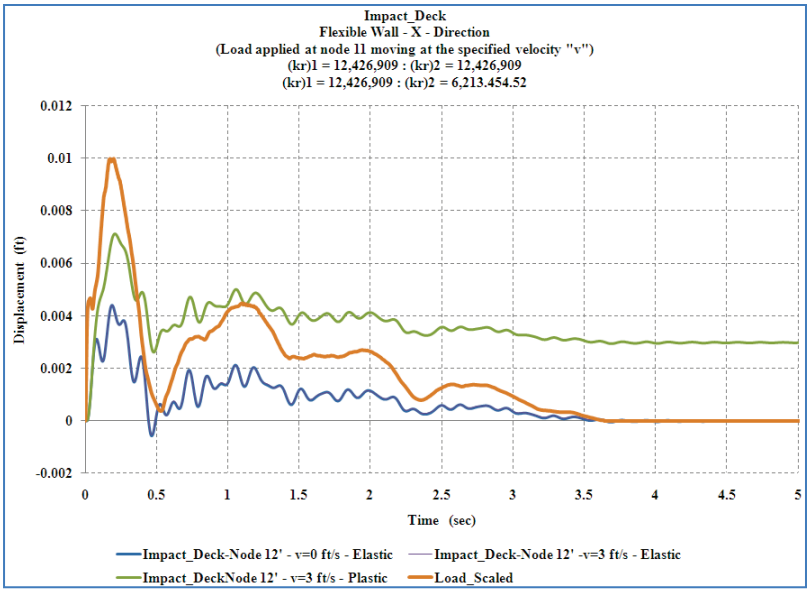


Figure 3.12 Dynamic response of the rotational spring at node 12 and 12'.

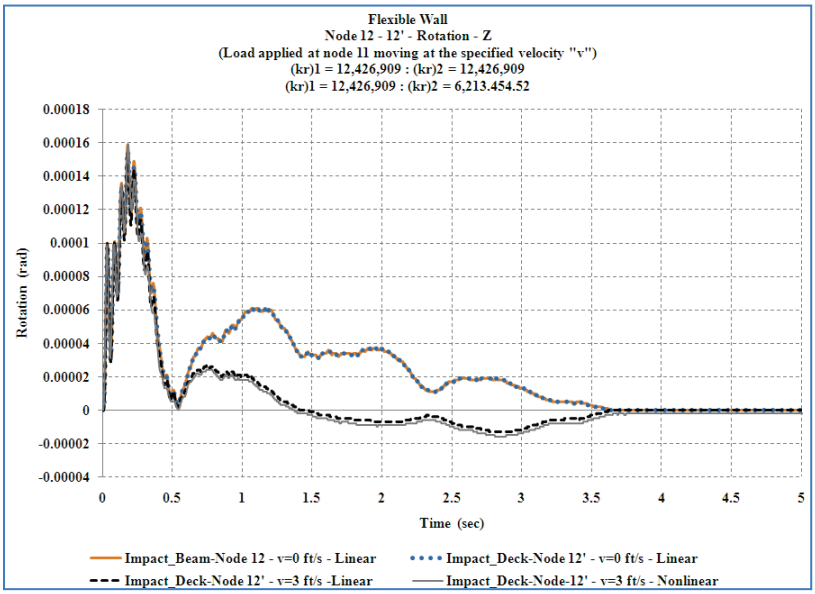
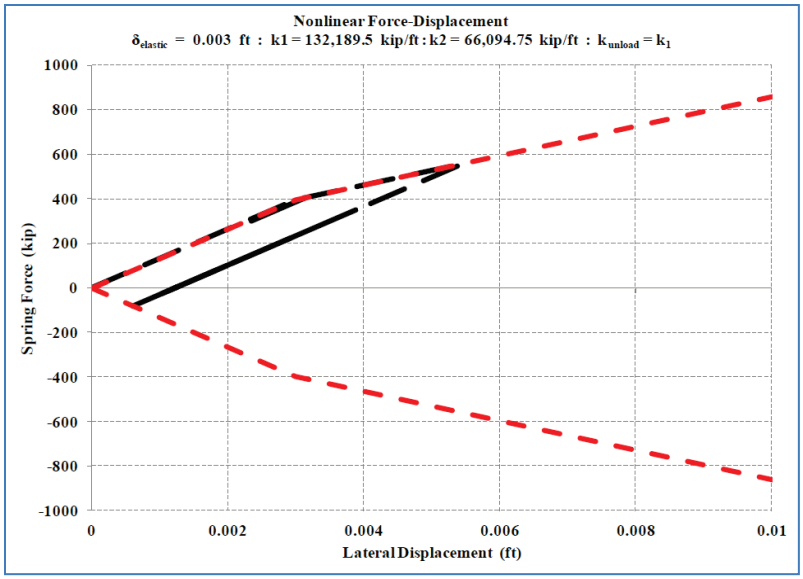


Figure 3.13 Dynamic response of the transverse spring located at *x* = *84.5 ft.*



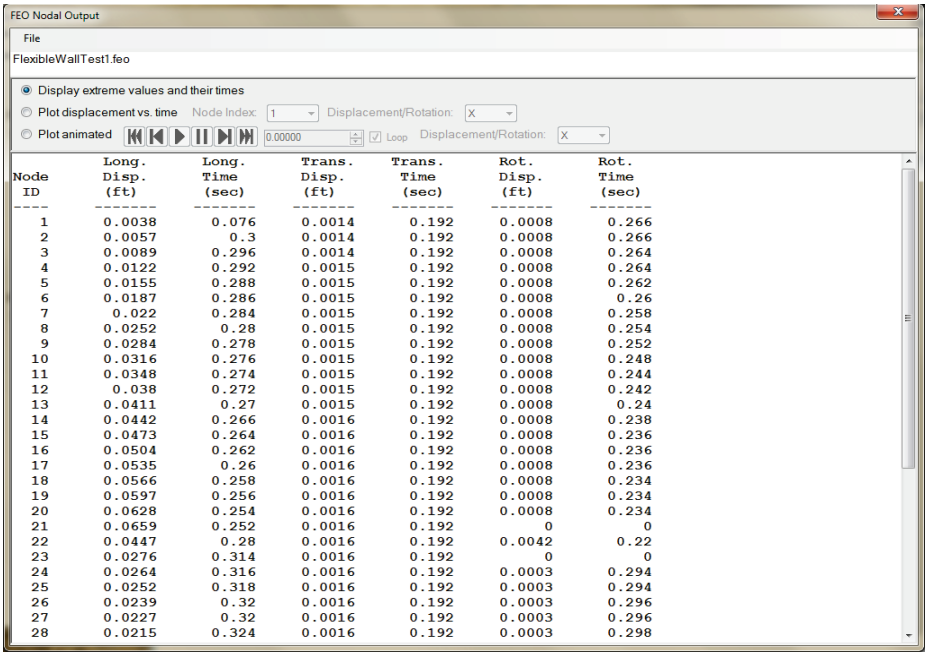
Nodal outputs provided from the FEO analysis of a flexible wall are the longitudinal displacement, transverse displacement, and rotational displacement (in radians) for each node at each time step of the simulation. A table is also provided that gives the maximum displacements (longitudinal, transverse, and rotational) for each node and the time that the maximum displacement occurs.

Figure 3.14 shows the GUI table of maximums for the example problem in this section. From this GUI table, it is possible to tell the time step and the node with the maximum displacement for transverse, longitudinal, and rotational displacements (as shown in Table 3.4).

Figures 3.15, 3.16, and 3.17 show the time histories for displacements at nodes 21 and 22 (longitudinal and rotational). Because some of these displacements are very small, and the data were stored with limited precision, some of these plots develop jaggies, where the data seems to form stair steps.

The Impact_Deck GUI also allows the user to visualize the entire beam in motion using an exaggerated plot of displacements transversely, longitudinally, and rotationally. Figures 3.18, 3.19, and 3.20 show the displacements of the wall from these animated plots at the moment where the maximum displacement occurred: 0.252 sec for transverse displacements, 0.192 sec for longitudinal displacements, and 0.22 sec for rotational displacements. These data were also subject to the jaggies because of the precision of the stored data. The data were scaled to fit the plot.

Figure 3.14 Impact_Deck GUI table of maximum nodal displacements for the McAlpine flexible wall.



Node ID	Long. Disp. (ft)	Long. Time (sec)	Trans. Disp. (ft)	Trans. Time (sec)	Rot. Disp. (ft)	Rot. Time (sec)
1	0.0038	0.076	0.0014	0.192	0.0008	0.266
2	0.0057	0.3	0.0014	0.192	0.0008	0.266
3	0.0089	0.296	0.0014	0.192	0.0008	0.264
4	0.0122	0.292	0.0015	0.192	0.0008	0.264
5	0.0155	0.288	0.0015	0.192	0.0008	0.262
6	0.0187	0.286	0.0015	0.192	0.0008	0.26
7	0.022	0.284	0.0015	0.192	0.0008	0.258
8	0.0252	0.28	0.0015	0.192	0.0008	0.254
9	0.0284	0.278	0.0015	0.192	0.0008	0.252
10	0.0316	0.276	0.0015	0.192	0.0008	0.248
11	0.0348	0.274	0.0015	0.192	0.0008	0.244
12	0.038	0.272	0.0015	0.192	0.0008	0.242
13	0.0411	0.27	0.0015	0.192	0.0008	0.24
14	0.0442	0.266	0.0016	0.192	0.0008	0.238
15	0.0473	0.264	0.0016	0.192	0.0008	0.236
16	0.0504	0.262	0.0016	0.192	0.0008	0.236
17	0.0535	0.26	0.0016	0.192	0.0008	0.236
18	0.0566	0.258	0.0016	0.192	0.0008	0.234
19	0.0597	0.256	0.0016	0.192	0.0008	0.234
20	0.0628	0.254	0.0016	0.192	0.0008	0.234
21	0.0659	0.252	0.0016	0.192	0	0
22	0.0447	0.28	0.0016	0.192	0.0042	0.22
23	0.0276	0.314	0.0016	0.192	0	0
24	0.0264	0.316	0.0016	0.192	0.0003	0.294
25	0.0252	0.318	0.0016	0.192	0.0003	0.294
26	0.0239	0.32	0.0016	0.192	0.0003	0.296
27	0.0227	0.32	0.0016	0.192	0.0003	0.296
28	0.0215	0.324	0.0016	0.192	0.0003	0.298

Table 3.4 Maximum nodal displacements for the McAlpine flexible wall example problem.

	Node number	Value	Time (seconds)
transverse	21	0.0659 feet	0.252
longitudinal	22	0.0016 feet	0.192
rotational	22	0.0042 radians	0.220

Figure 3.15 Transverse nodal displacement time histories for node 21.

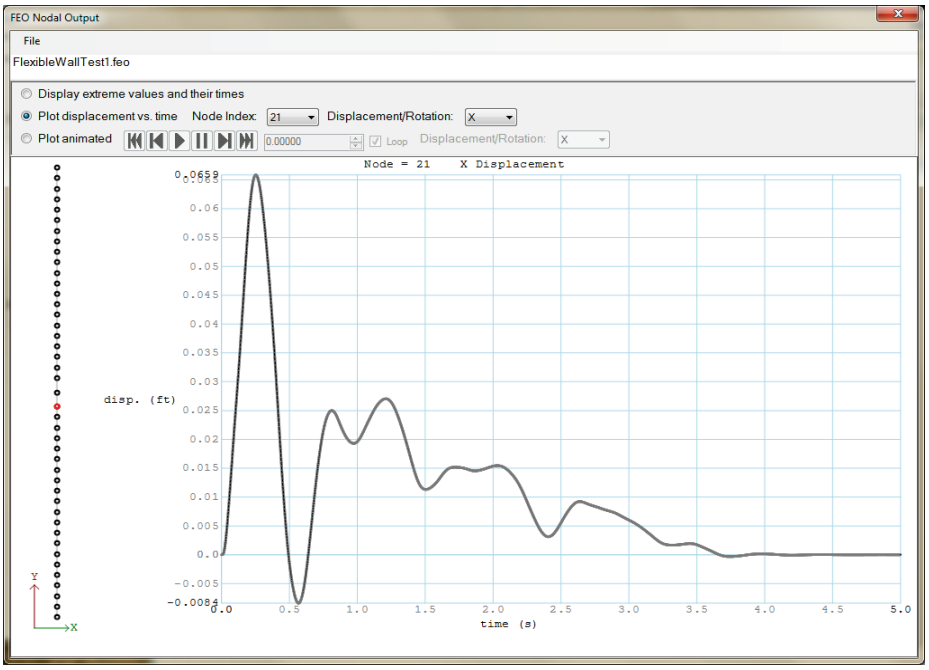


Figure 3.16 Longitudinal nodal displacement time histories for node 22.

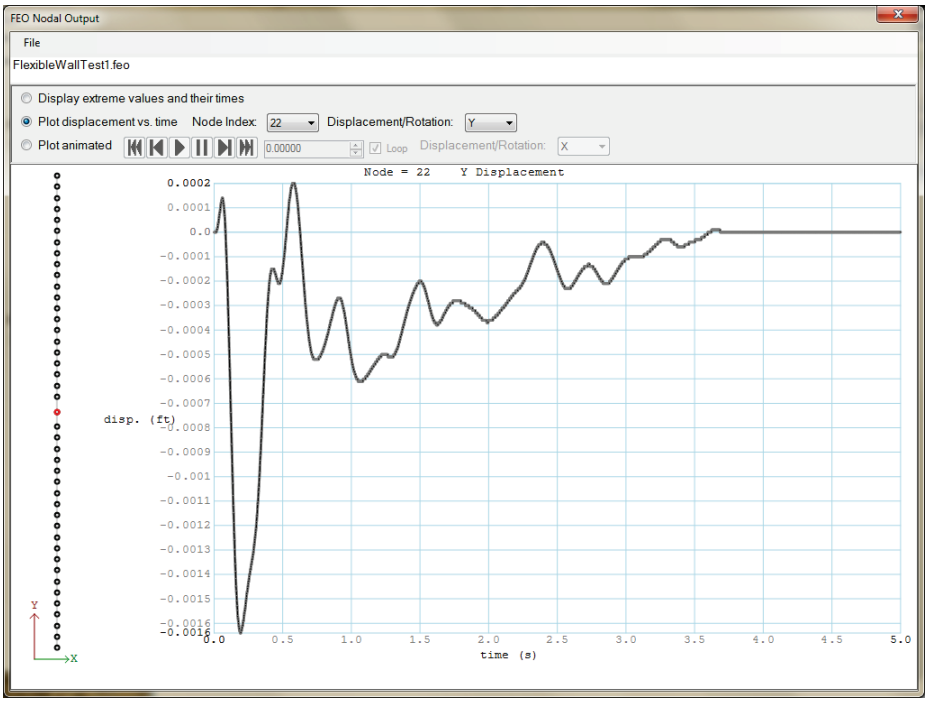


Figure 3.17 Rotational nodal displacement time histories for node 22.

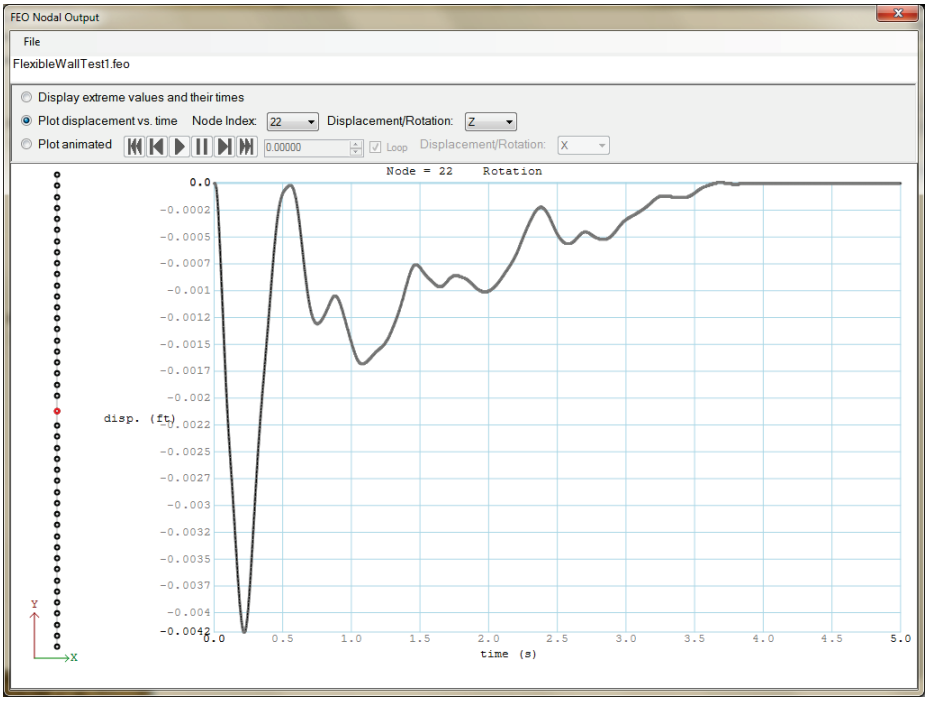


Figure 3.18 Transverse wall displacements at 0.252 sec.

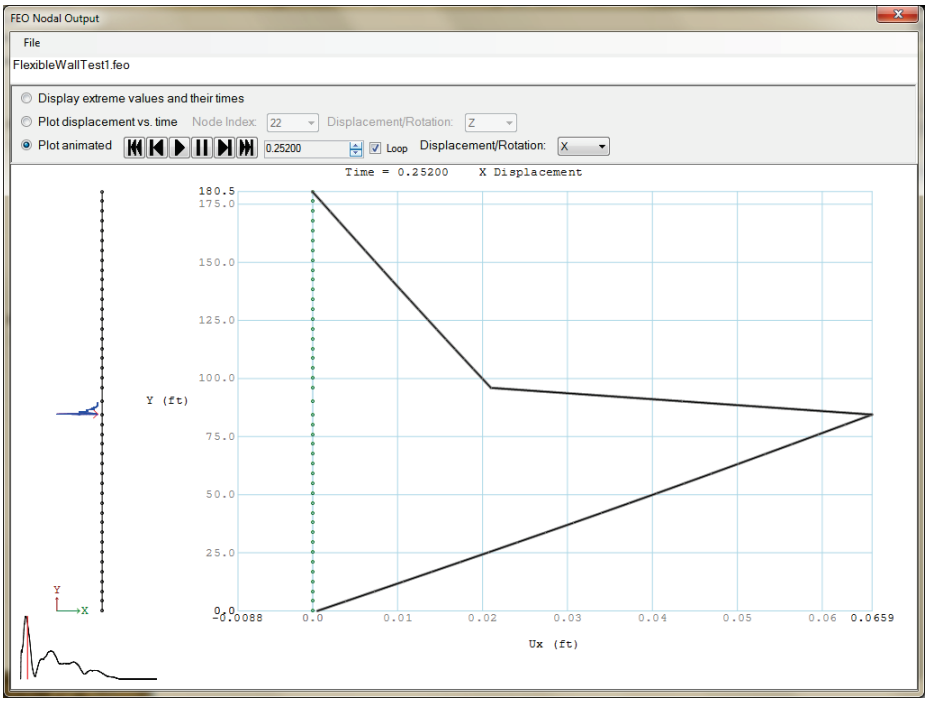


Figure 3.19 Longitudinal wall displacements at 0.192 sec.

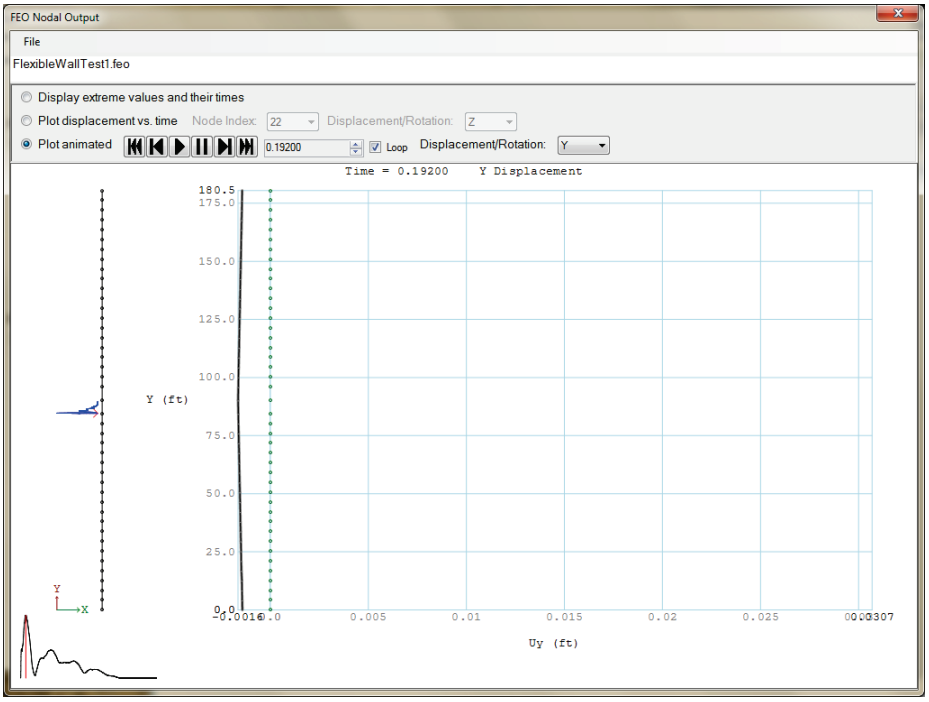
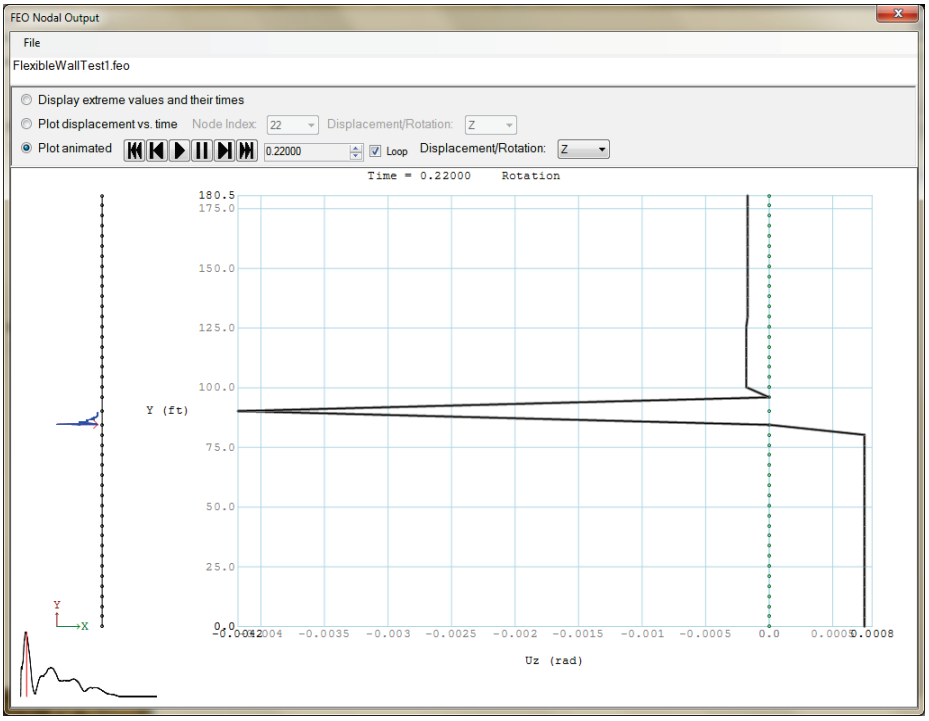


Figure 3.20 Rotational wall displacements at 0.22 sec.



Element outputs provided from the FEO analysis of an impact deck are the axial force, shear force, and moment for each element at each time step of the simulation. A table is also provided that gives the minimum and maximum forces and moments for each element and the times that the minimum and maximum force/moment occur.

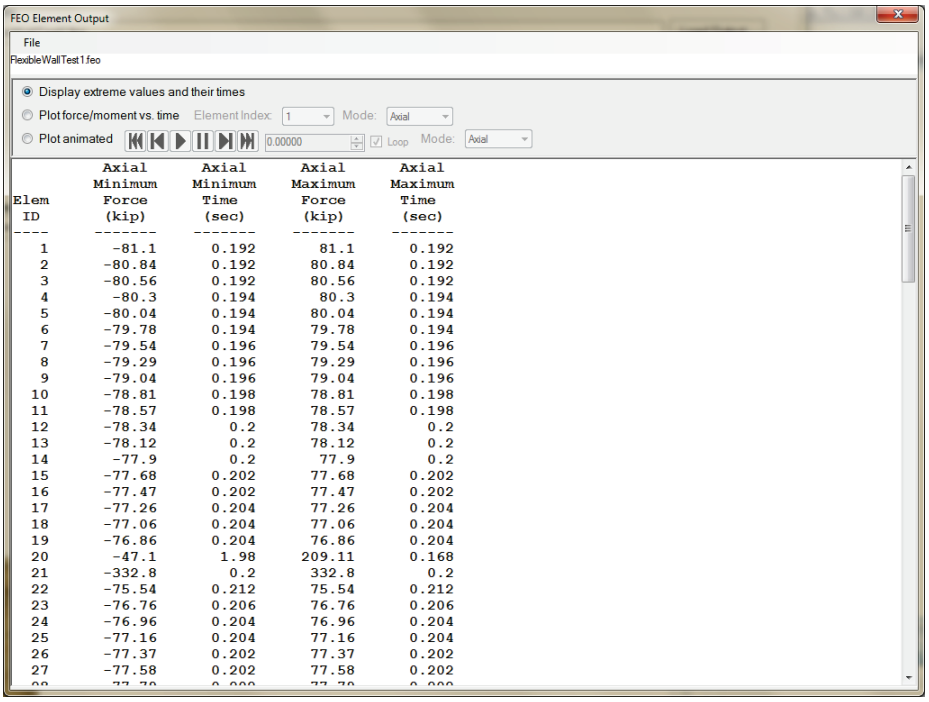
Figure 3.21 shows the GUI tables of extreme values for the example problem in this section. The beginning of the axial force extremes table is shown. The shear force extremes table and moment extremes table are available by scrolling in the interface. From this GUI table, it is possible to tell the time step and the element with the extreme axial force, shear force, and moment (as shown in Table 3.5).

Because the simulated barge train impact occurs between nodes shared by elements 20 and 21, the extreme forces are found primarily in those elements. Figures 2.44 - 2.49 show the time histories for the axial force, shear force, and moments for the elements with the minimum and maximum values, respectively.

Figures 3.28 - 3.30 show the axial force at 0.2 sec, shear force at 0.22 sec, and moment at 0.220 sec for the entire wall. These are created from the Impact_Deck GUI feature to view the animated forces.

Of primary importance for doing the pile group founded flexible wall analysis, is being able to see exactly how much force each pile group will be able to resist during an impact event. This is measured by finding the resisting force from the spring model used for the pile group for the pile group's displacement. Figure 3.31 shows the table of forces/moments resisted at the nodes representing a pile group in the Impact-Deck example model.

Figure 3.21 Impact_Deck GUI table of element minimum and maximum axial forces for the McAlpine flexible wall example.



Elem ID	Axial Minimum Force (kip)	Axial Minimum Time (sec)	Axial Maximum Force (kip)	Axial Maximum Time (sec)
1	-81.1	0.192	81.1	0.192
2	-80.84	0.192	80.84	0.192
3	-80.56	0.192	80.56	0.192
4	-80.3	0.194	80.3	0.194
5	-80.04	0.194	80.04	0.194
6	-79.78	0.194	79.78	0.194
7	-79.54	0.196	79.54	0.196
8	-79.29	0.196	79.29	0.196
9	-79.04	0.196	79.04	0.196
10	-78.81	0.198	78.81	0.198
11	-78.57	0.198	78.57	0.198
12	-78.34	0.2	78.34	0.2
13	-78.12	0.2	78.12	0.2
14	-77.9	0.2	77.9	0.2
15	-77.68	0.202	77.68	0.202
16	-77.47	0.202	77.47	0.202
17	-77.26	0.204	77.26	0.204
18	-77.06	0.204	77.06	0.204
19	-76.86	0.204	76.86	0.204
20	-47.1	1.98	209.11	0.168
21	-332.8	0.2	332.8	0.2
22	-75.54	0.212	75.54	0.212
23	-76.76	0.206	76.76	0.206
24	-76.96	0.204	76.96	0.204
25	-77.16	0.204	77.16	0.204
26	-77.37	0.202	77.37	0.202
27	-77.58	0.202	77.58	0.202

Table 3.5 Extreme forces/moments for the Impact_Deck example problem.

		Element number	Value	Time (seconds)
Axial	min	21	-332.80 kips	0.200
	max	20	332.80 kips	0.200
Shear	min	21	-541.18 kips	0.220
	max	20	541.18 kips	0.220
Moment	min	31	-1,036.58 kip-feet	0.198
	max	21	3,111.78 kip-feet	0.220

Figure 3.22 Axial-force time histories for element 21.

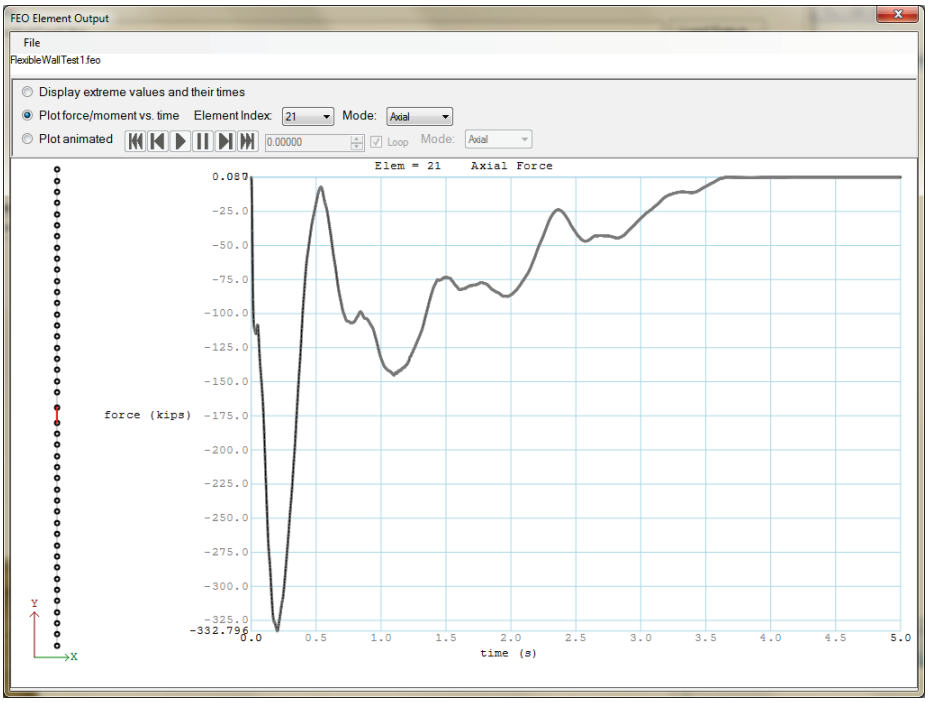


Figure 3.23 Axial-force time histories for element 20.

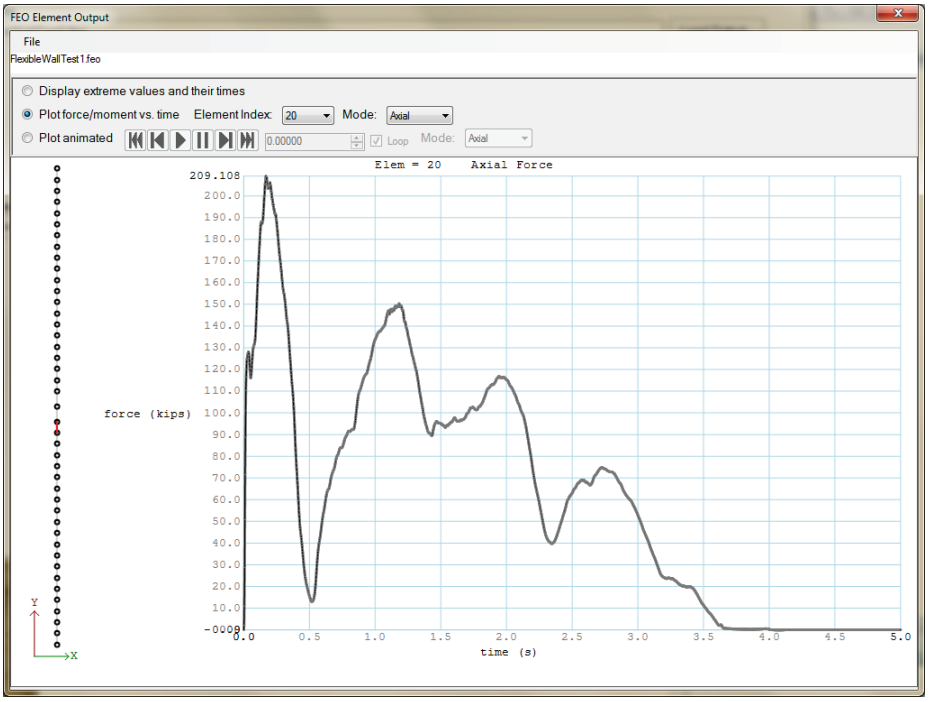


Figure 3.24 Shear-force time histories for element 21.

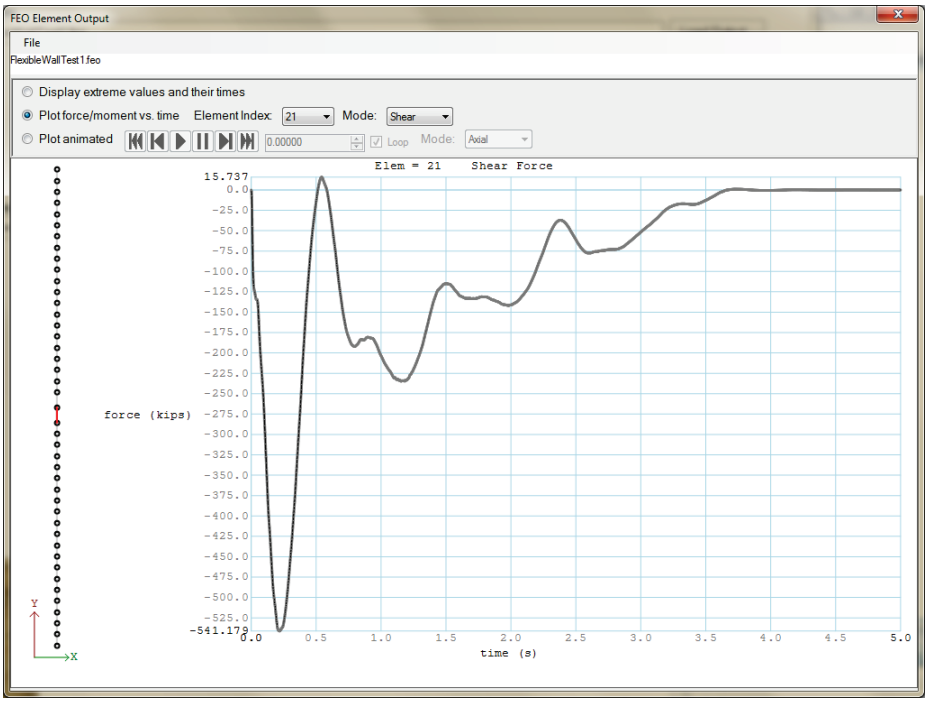


Figure 3.25 Shear-force time histories for element 20.

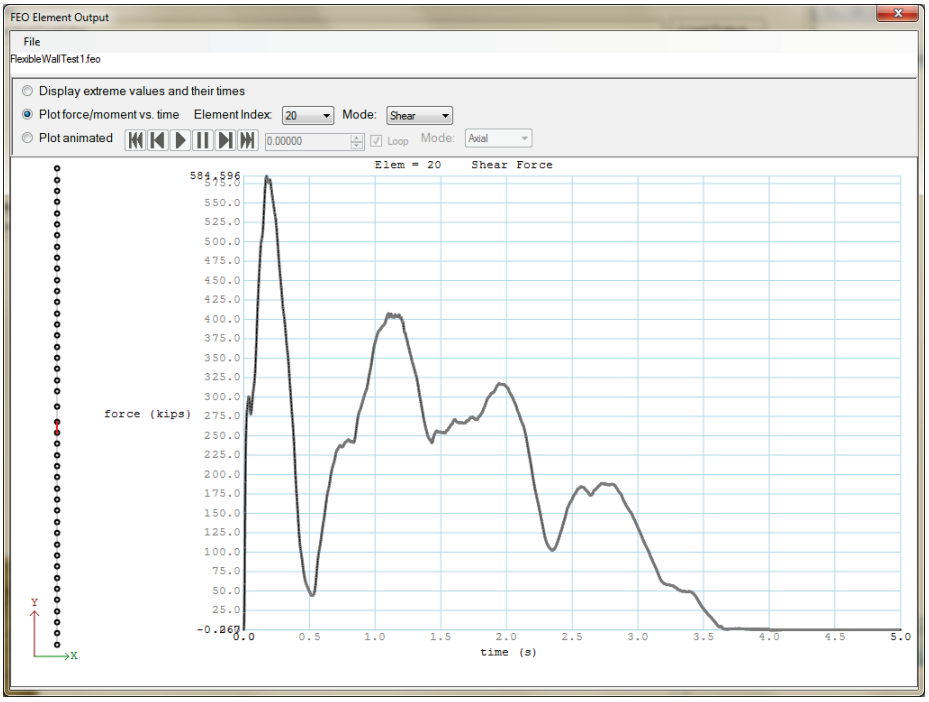


Figure 3.26 Moment time histories for element 31.

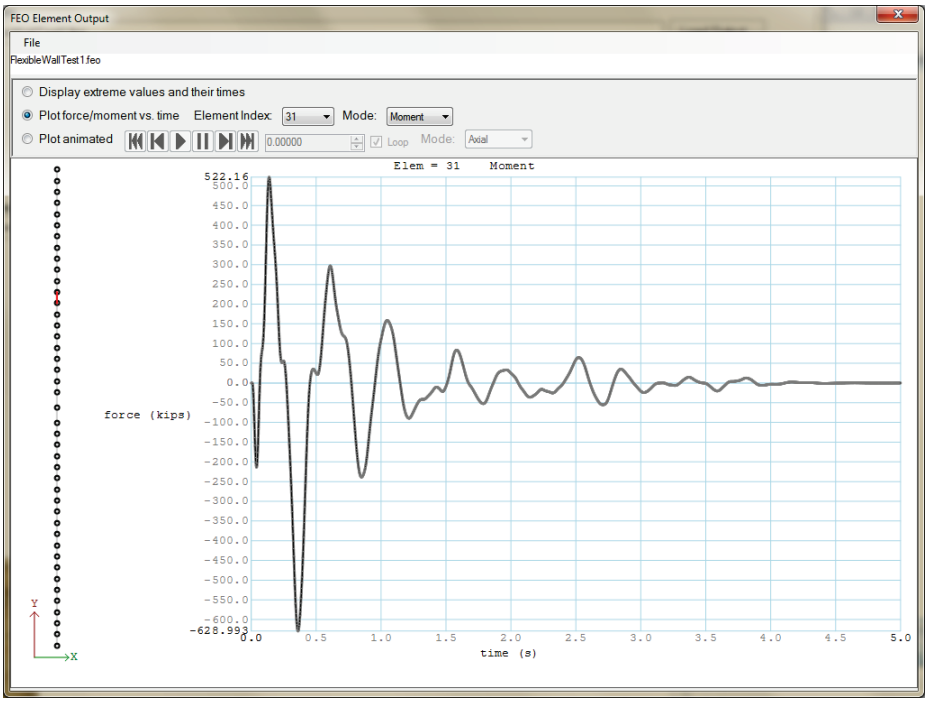


Figure 3.27 Moment time histories for element 21.

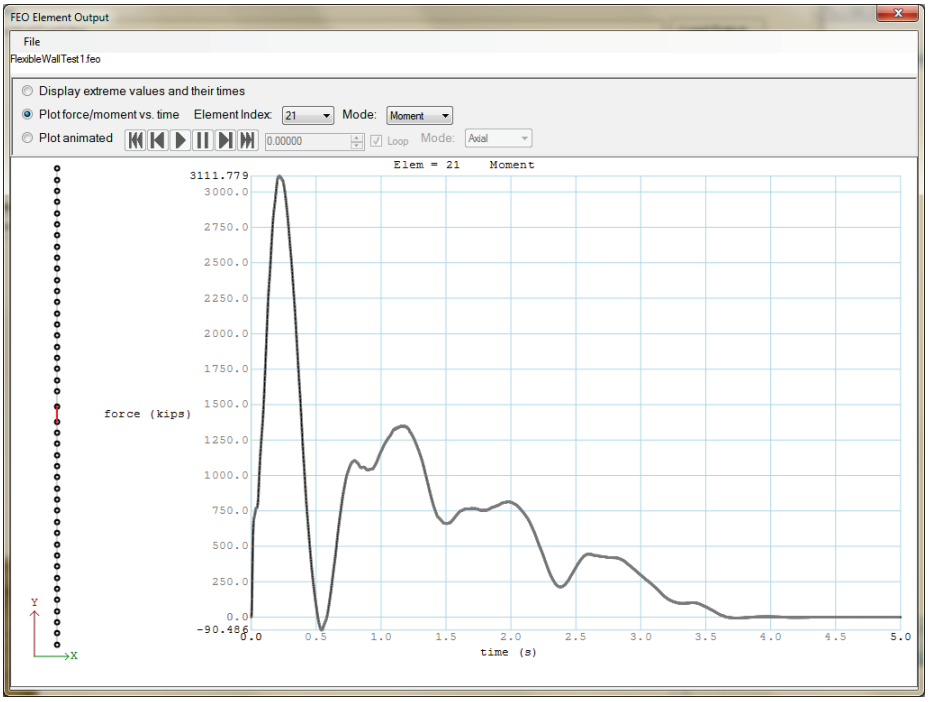


Figure 3.28 Wall axial forces at 0.2 sec.

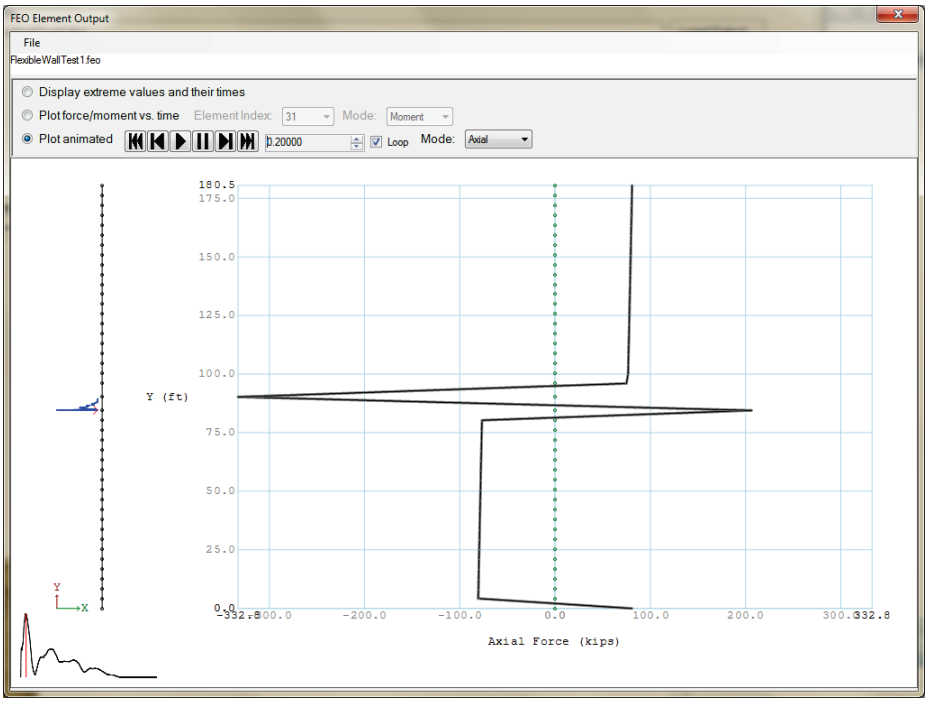


Figure 3.29 Wall shear forces at 0.220 sec.

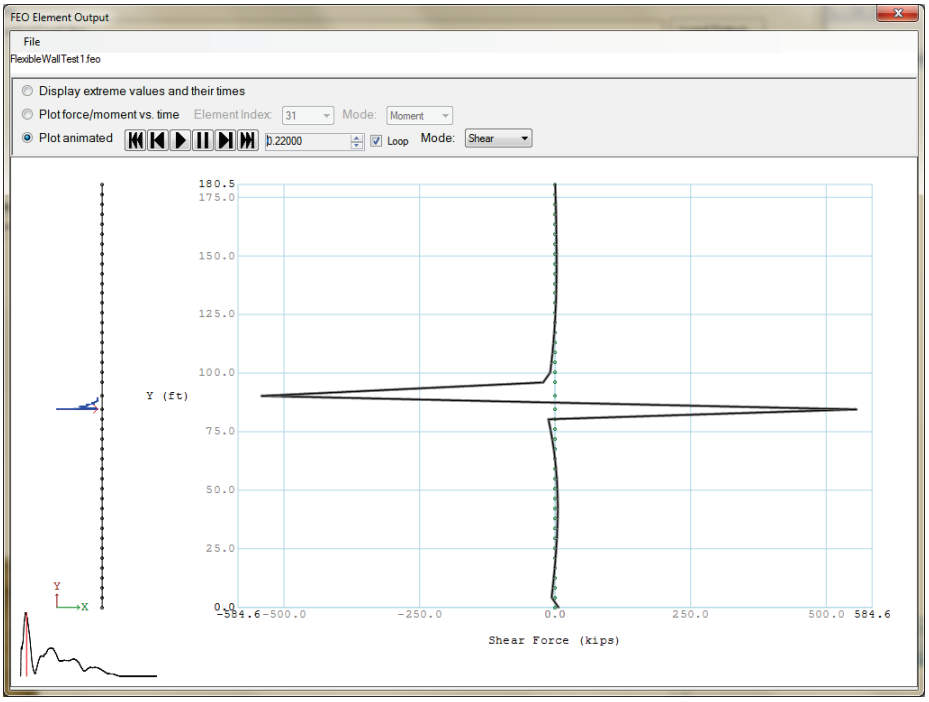


Figure 3.30 Wall moments at 0.220 sec.

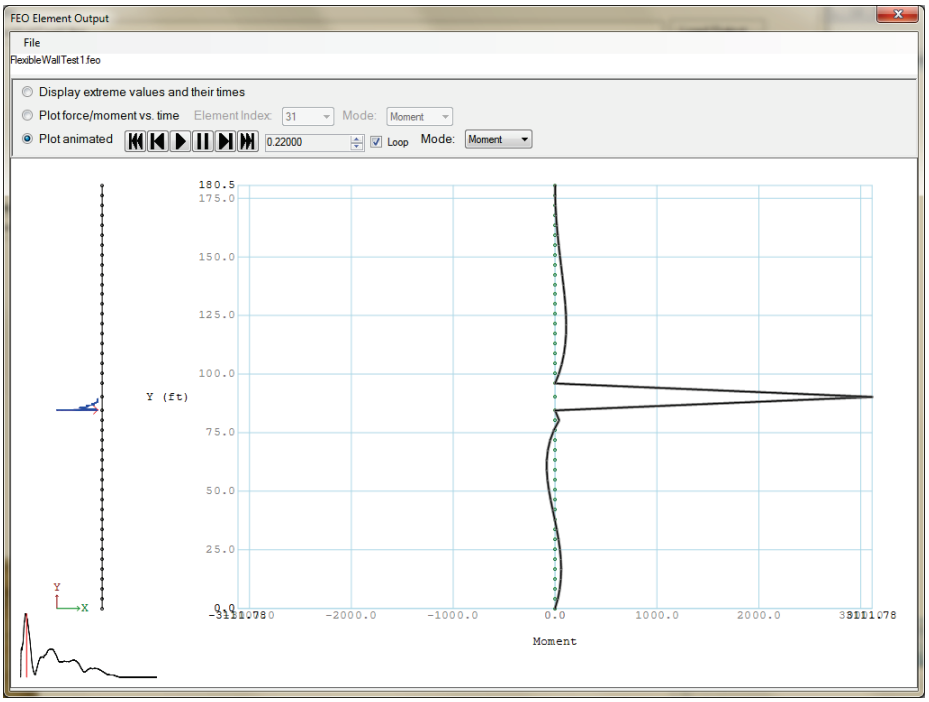
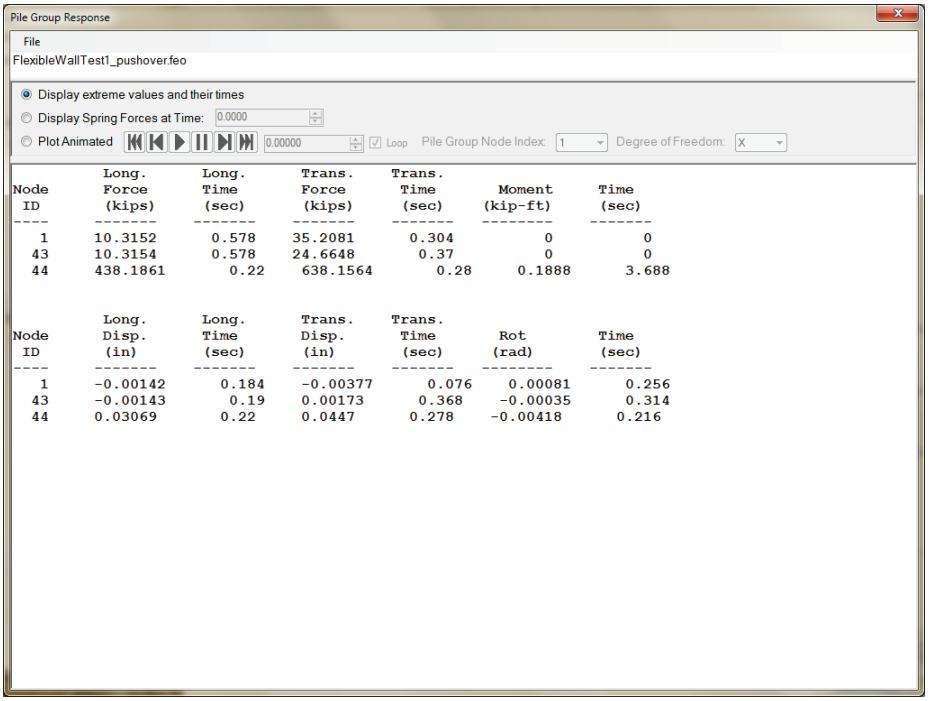


Figure 3.31 Table of pile group response maximum displacements.



Node ID	Long. Force (kips)	Long. Time (sec)	Trans. Force (kips)	Trans. Time (sec)	Moment (kip-ft)	Time (sec)
1	10.3152	0.578	35.2081	0.304	0	0
43	10.3154	0.578	24.6648	0.37	0	0
44	438.1861	0.22	638.1564	0.28	0.1888	3.688

Node ID	Long. Disp. (in)	Long. Time (sec)	Trans. Disp. (in)	Trans. Time (sec)	Rot (rad)	Time (sec)
1	-0.00142	0.184	-0.00377	0.076	0.00081	0.256
43	-0.00143	0.19	0.00173	0.368	-0.00035	0.314
44	0.03069	0.22	0.0447	0.278	-0.00418	0.216

Figure 3.32 Response forces for the pile groups at time 0.2200 sec.

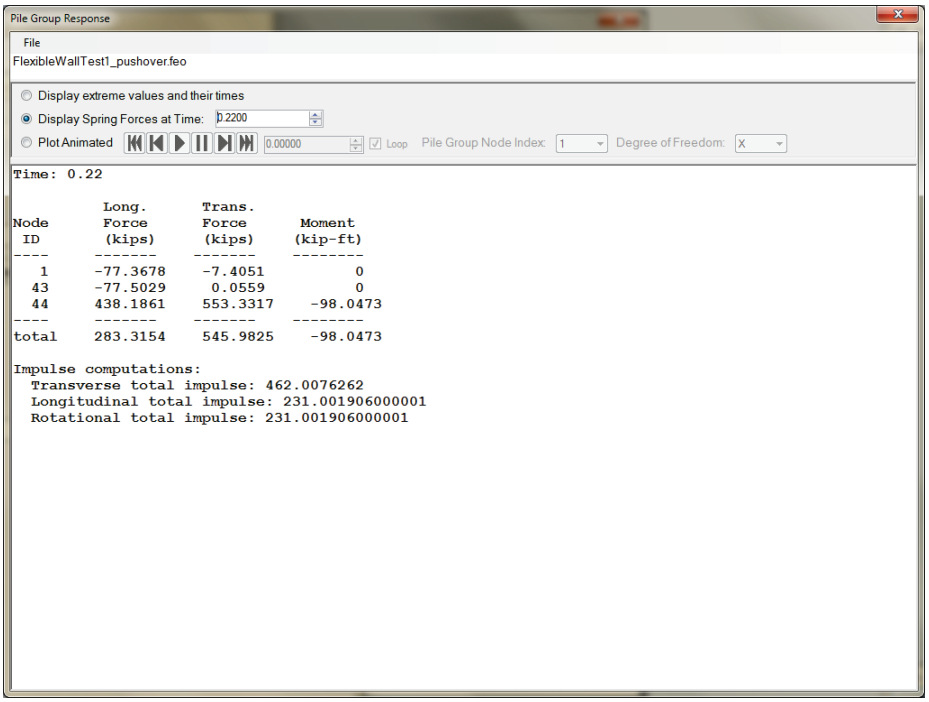


Figure 3.33 Response forces for the pile groups at time 0.2800 sec.

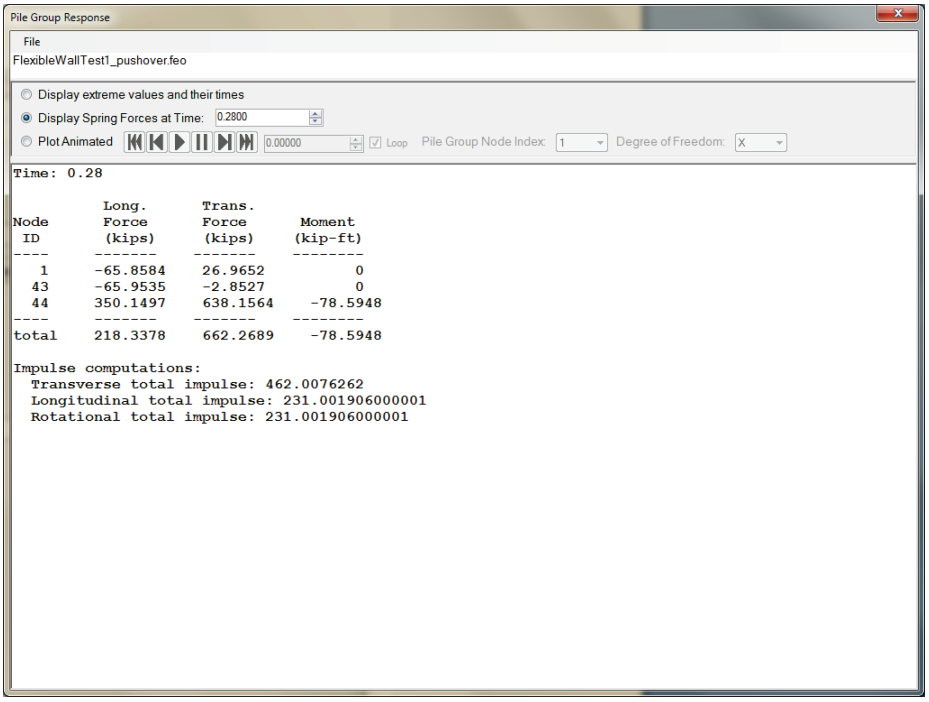
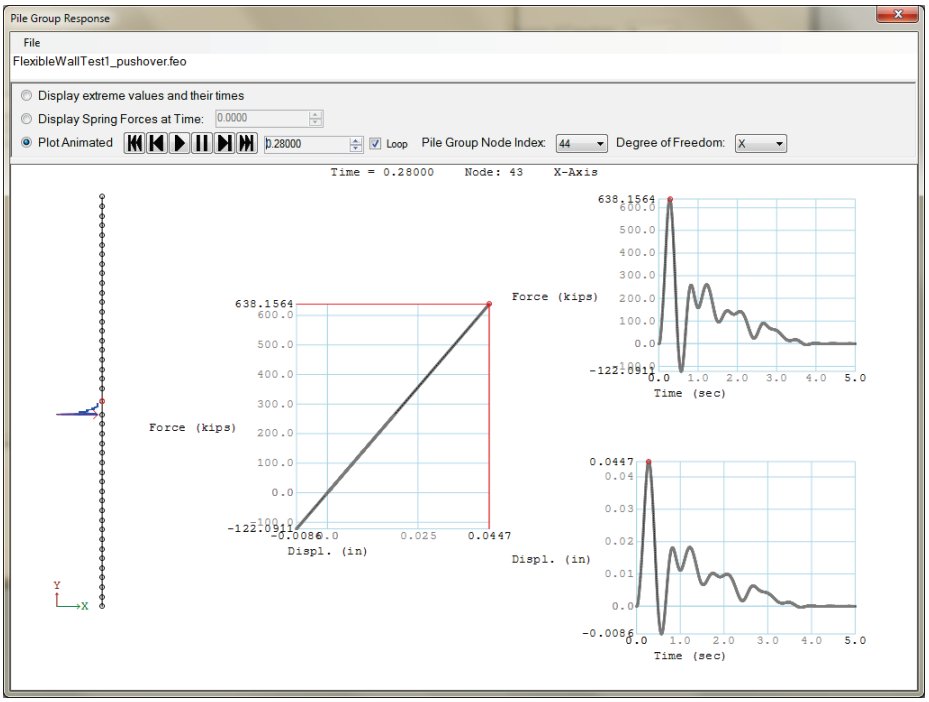


Figure 3.34 Pile group response for the pile group at node 2 and at time 0.298 sec.



Figures 3.32 and 3.33 show the instantaneous response forces at time 0.22 and 0.28 sec, respectively. At time 0.22, the longitudinal and moment forces reach their peak values of 438.186 kips and -98.047 kip-ft for node 44, which was created at the center of rotation for the pile group. At time 0.28, the peak transverse response force is 638.156 kips at node 44.

Figure 3.34 shows the response of the pile group at node 44 at time 0.28 sec as a force-versus-displacement plot, and as force and displacement time histories. This is the time when the displacement for the pile group at node 44 is at its maximum location in the transverse direction.

The Case for Dynamic Analysis:

This example problem demonstrates the necessity of performing a dynamic analysis of these pile founded walls. This example uses an impact time history that is the result of the Winfield Test #10. This impact time history is applied transverse to the approach wall at a position starting at 84.5 ft along this section of wall (close to the longitudinal location of node 44) and moved at 1 ft/sec along the approach wall. The peak force for the impact time history was 516.4 kips at time 0.2 sec.

Node 44 (as discussed above) has a maximum transverse force of 638.156 kips, which occurs at 0.28 sec. This is the pile group node between two flexible walls, so its transverse displacement has been affected by the inertial effects of the walls and the over structure, as well as rotational response. The total pile group response for the section of flexible wall structure (with 3 pile group nodes) at this time (0.28 sec) is 662.269 kips, this total response force is greater than the peak input force. It is also the peak overall response. Table 3.6 shows the values generated by this data collection. Figure 3.35 takes this information a step further by displaying the time histories for the three forces.

Table 3.6 Transverse forces with respect to time.

Time (s)	Node 44 Force (kips)	Impact Load Force (kips)	Total Pile Group Response (kips)
0.200	492.3062	**516.400**	483.616
0.280	**638.1564**	446.358	**662.269**

Figure 3.35 Time-history plot of transverse input forces, total force response for all the pile groups, and an individual pile group response forces.

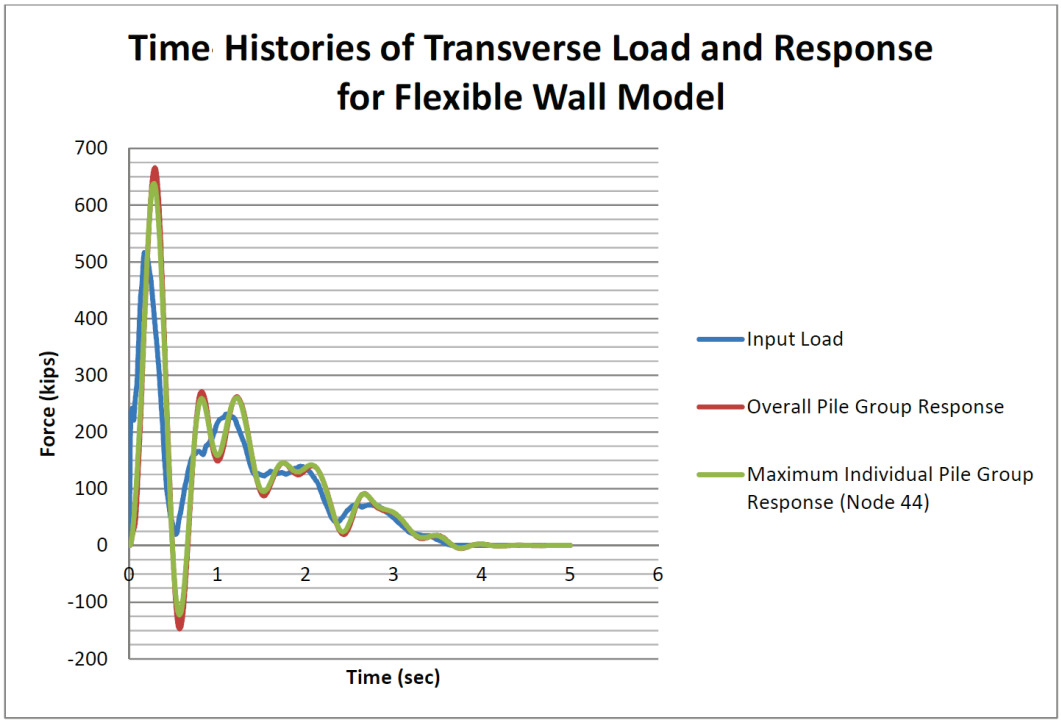


Table 3.6 and Figure 3.35 show that the overall pile group response is dynamic because it does not track with the input force. Instead, the pile groups respond to the input force over time due to inertial effects. Because of this, the overall pile group response can have higher peak forces. For

example, at the time of peak response of 0.2 sec a maximum impact force of 516.4 kips is applied to the approach wall. The total transverse force response of the 3 nodes representing the pile groups at the beam supports is 483.616 kips. This 6.3% smaller summed force response is due to the contribution of the first two terms of the equation of motion (also seen in Appendix A) for the dynamic structural response:

$$[M]\{\ddot{u}(t)\}+[C]\{\dot{u}(t)\}+[K]\{u(t)\}=\{F(t)\} \quad \text{(2.1 bis)}$$

The summed transverse effects are smaller than the peak load because the mass of the beams are accelerated slowly. At time 0.28 sec, when a peak response force is recorded at node 44 for an individual pile group, the contribution of the first two terms of the equation of motion for the dynamic structural response is even larger resulting in an overall response force of 662.269 kips. This is nearly 28.3% greater than the peak input force of 516.4 kips. These observations demonstrate the importance of applying the equation of motion for calculating pile group structural response forces (and displacements). These differences explain why a dynamic analysis is required versus a static analysis in which the user-provided impact load is applied as a single peak value (e.g., determined to be the input peak force from the time history).

For simply supported beams, the effect of load sharing between pile groups is altered by the modal characteristics of the system (Ebeling et al. 2012). Because this system is very stiff, the inertia of the beam and pile cap superstructure cause localized response at the node closest to the impact. This is shown by the fact that the peak response force at node 44 is 638.156 kips, which is within 4% of the total transverse response force (662.269 kips). Notice that the peak transverse response force at node 44 is greater than the peak transverse input force. This implies that dynamic analysis using impulse momentum principles should be performed to determine the greatest forces acting at any pile group.

Validation Using Impulse Calculations:

The higher peak values of the overall pile group response seem out of place until an impulse calculation (taking the area beneath the time history curves for input load and overall pile group response in Figure 3.35) is performed. Despite inertial effects, the impulse of the input load must be equivalent to the overall pile group response, if the piles do not fail. When

an impulse calculation is performed for the overall pile group response, the result is 463 kip-sec. The impulse for the input force is 463 kip-sec. The difference is minimal, less than 1%.

Load Sharing:

For this type of flexible approach wall structural system, there can be load sharing (depending upon the structural detailing) in the longitudinal direction starting with the first pile group beyond the point of impact. There will also be load sharing in the transverse direction among the pair of pile bents supporting the impact beam for an impact anywhere along the simply supported beam. However, this structural configuration does not have the advantage of the significant load sharing among pile groups that the Lock and Dam 3 impact deck configuration possesses. This is exemplified by the observation that the node 44 maximum transverse force of 638.156 kips, which occurs at 0.28 sec, is greater than the peak input force of 516.4 kips occurring at 0.2 sec. The pile group total transverse response force is greater than the peak input force. For Lock and Dam 3, the peak transverse force for the pile group possessing the maximum peak force of any of the 96 pile groups was 56.4652 kips. The Lock and Dam 3 dynamic structural response analysis was subjected to the same input impact force time history specified in this analysis.

3.9 Final Remarks

In this section, the McAlpine flexible wall physical model was presented and the mathematical model to calculate the dynamic response was also developed. Impact_Deck is a computer program that was used to calculate the dynamic response of an elastic beam supported over linear elastic or plastic spring supports. The mathematical formulation modeled the ends of the simply supported beams with no moment transfer. The impact normal and parallel concentrated external load was located at a specified location or assumed to have motion at a specified constant velocity. The damping effect was considered by means of the Rayleigh damping model which depended on the natural frequencies of the system. These natural frequencies were calculated in an approximate way by using the linear stiffness of the pile groups and the mass of the impact beams. The results of Impact_Deck proved to be valid when compared to the results obtained with SAP2000. Finally, an example was presented to show the plastic behavior of the springs and how this result compared to the linear elastic response.

4 Traditional Impact Beam Guard Walls

4.1 Introduction

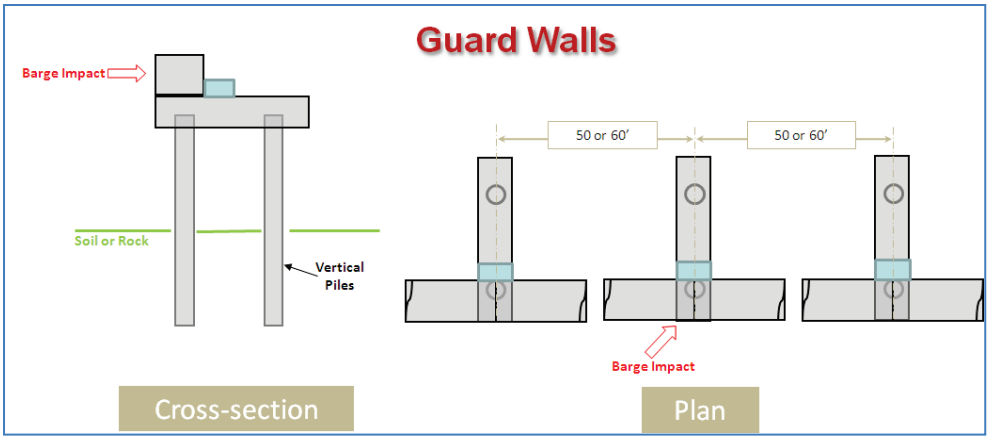
This chapter summarizes an engineering methodology using the Impact_Deck software for performing a dynamic structural response analysis of a flexible impact beam supported over pile groups and subjected to a barge impact event. For this example, a traditional model of impact beams simply supported on bents with in-line pile groups is examined.

This example models a glancing blow impact event of a barge train impacting an approach wall as it aligns itself with a lock is an event of short duration; the contact time between the impact corner of the barge train and the approach wall can be as short as a second or as long as several seconds. The next generation of Corps approach walls is more flexible than the massive, stiff-to-rigid structures constructed in the past in order to reduce construction costs as well as to reduce damage to barges during glancing blow impacts with lock approach walls. A flexible approach wall or flexible approach wall system is one in which the wall has the capacity to absorb impact energy by deflecting or "flexing" during impact, thereby affecting the dynamic impact forces that develop during the impact event.

4.2 Guard Walls – Physical Model

Guard walls are a kind of flexible wall commonly used at locks by the Corps. Each segment of a flexible guard wall structure consists of a continuous elastic concrete beam with a span of approximately 50 or 60 ft long, each segment. The continuity of the beam is achieved by means of shear key at each pile group support. This means the beams transfer the longitudinal and transverse forces with no moment transfer at each pile supports. The axial and transverse forces at the end of the beams are transferred to the pile cap by means of a shear key. The shear key is a concrete block behind the end and start of two consecutive flexible impact beams. The length of the shear key is equal to the width of the pile cap of the pile group. The shear key is part of the massive pile cap that rest over the pile group. The pile group consists of two aligned piles, each with a diameter of 5 ft 8 in. The two piles are arranged in such a way that no torsion transfers to the pile group. A plan view drawing and a cross-section view are presented in Figure 4.1.

Figure 4.1 Guard wall schematic drawing.



4.3 Guard wall – Mathematical Model

The guard wall can be considered as a beam element because its length is much greater than the other two directions. The length of each segment is around 50 or 60 ft, heights and widths of 6 ft 7 in., and 9 ft, respectively, are not untypical. The mathematical model is described in Figure 4.2. The model in the analysis has two consecutive beams with longitudinal and transverse elastic-plastic spring supports at the start, mid span, and end of the system. These three sets of springs model the pile group at the start, mid span, and end of the two consecutive beams. The nodes that connect the beams to the pile cap do not transfer moment between the beams and the center pile cap. The center pile group is modeled with three springs (two translational and one rotational) in the generalized Impact_Deck software formulation. This model is similar to the McAlpine alternative flexible approach wall model but with two differences. First, no rigid link is used in the guard wall model. Second, no rotational elastic-plastic rotational spring is included.

The mathematical model can be done using 3-D beam elements. A 3-D beam element has 6 degrees of freedom per node, producing 12 degrees of freedom per element. The degrees of freedom per node are 3 translations and 3 rotations as shown in Figure 4.3. The applied normal force $F_x(t)$ is the impact-force time history developed using the PC-based software Impact_Force. The applied parallel force $F_y(t)$ is a fraction of the normal force calculated using the dynamic coefficient of friction between the barge and the impact deck surfaces.

Figure 4.2 Guard flexible approach wall mathematical model.

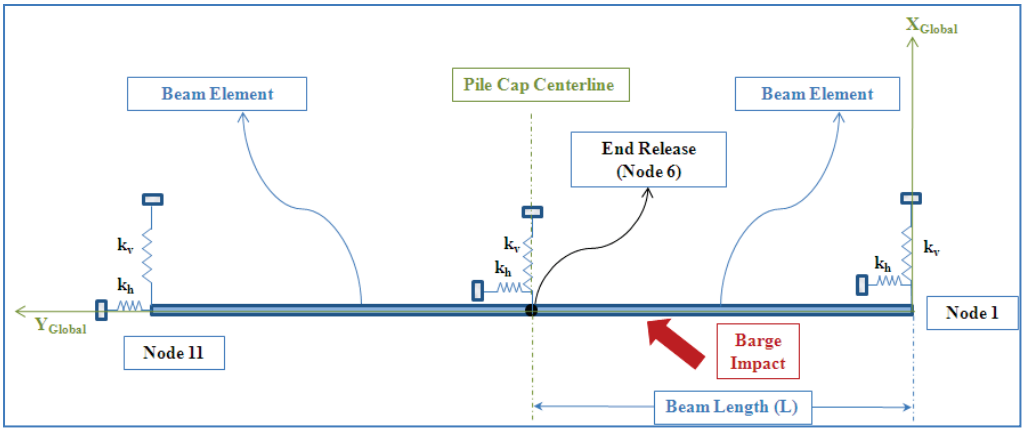
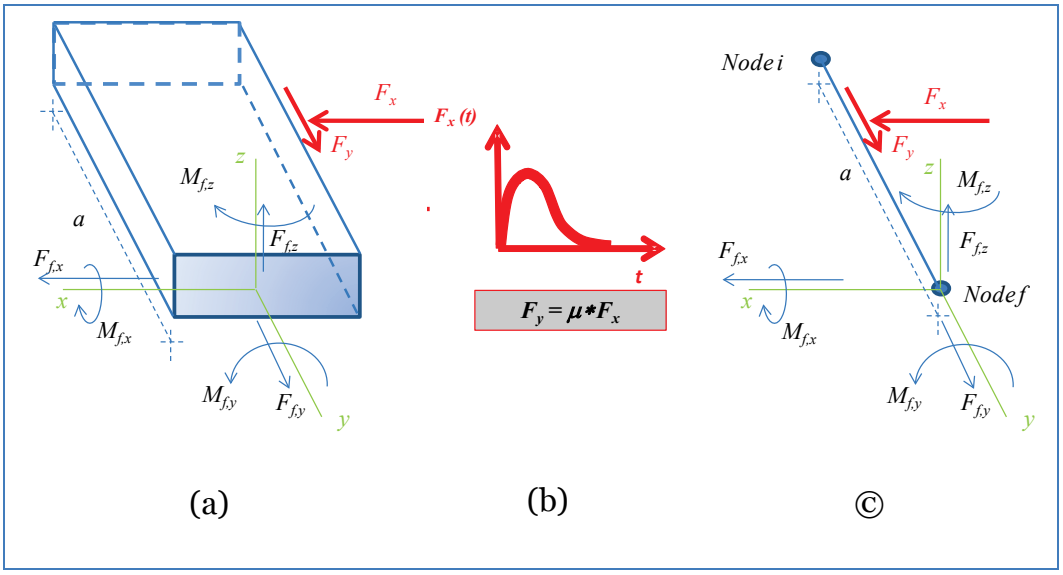
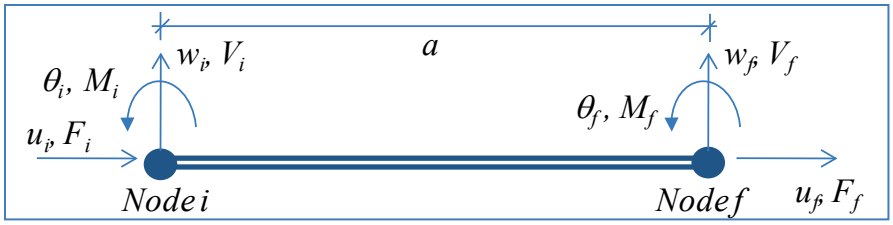


Figure 4.3 (a) Typical 3-D segment of the Impact Deck beam element, (b) Impact force applied to the Impact Deck, (c) Typical 3-D beam element.



If the model used to describe the beam is developed in the plane, the beam element has 3 degrees of freedom per node and 6 degrees of freedom per element. The degrees of freedom per node are 2 translations and 1 rotation, as shown in Figure 4.4. Based on the notation of Figure 4.3, the force and moment conditions for *node i* are $F_{i,x} = V_i$, $M_{i,x} = 0$, $F_{i,y} = F_i$, $M_{i,y} = 0$, $F_{i,z} = 0$, and $M_{i,z} = M_i$, and for *node f* are $F_{f,x} = V_f$, $M_{f,x} = 0$, $F_{f,y} = F_f$, $M_{f,y} = 0$, $F_{f,z} = 0$, and $M_{f,z} = M_f$. Basically, to transform a 3-D beam element to a 2-D (plane element), the moment about the "*x*" axis, the moment about the "*y*" axis, and the force in the "*z*" directions are equal to zero.

Figure 4.4 Typical 2-D beam element used in Impact_Deck.



The behavior of the three piles under static lateral load was done to determine the stiffness coefficient of the springs. To have an idea of the magnitude of the linear translational spring stiffness, refer to the calculation in Appendix E.

4.4 Nonlinear force-deflection relationship for the springs supports

Section 2.5 discussed how the nonlinear spring response force-displacement backbone curve was used to model plastic deformation in the pile substructure for dynamically loaded structures. Push-over calculations were similarly performed for the pile layout for guard wall supports.

Figure 4.5 shows the results for a fixed-head single pile analysis from Figure 3.21 of Ebeling et al. (2012). Notice that these curves have three linear segments with two breakpoints. As the transverse loading at the pile cap increases, the bending moment at the top of pile-to-bent will increase until this moment connection yields and fixity is lost. After this occurs, the top of pile-to-bent behaves as a pinned-head condition with no constraint against rotation being offered within this region. Observe in the push-over curve that the rate of deformation has increased for the same incremental load after this hinge is formed. This results in a "softer" spring stiffness representation in this zone of the push-over curve. The pile bent system continues to resist the increase in lateral loading up until the level of loading that induces a second plastic hinge (shown as the second breakpoint in Figure 4.5). This second breakpoint is reached when the piles start to hinge at or below the mudline. Beyond this point, the push-over curve continues to provide the same resistance for a time until the plastic hinge rotation capacity of the piles are exhausted at this point below the mudline (refer to section A. 10 in Appendix A of Ebeling et al. 2012 for these this capacity computation) and can no longer support the structure.

The resulting curve for the Saul analysis (CPGA) on the wet site for two DIP piles is shown in the force-versus-deflection, push-over curve values listed in Table 4.1.

Figure 4.5 Force-displacement relations from push-over analysis of a single guard wall pile.

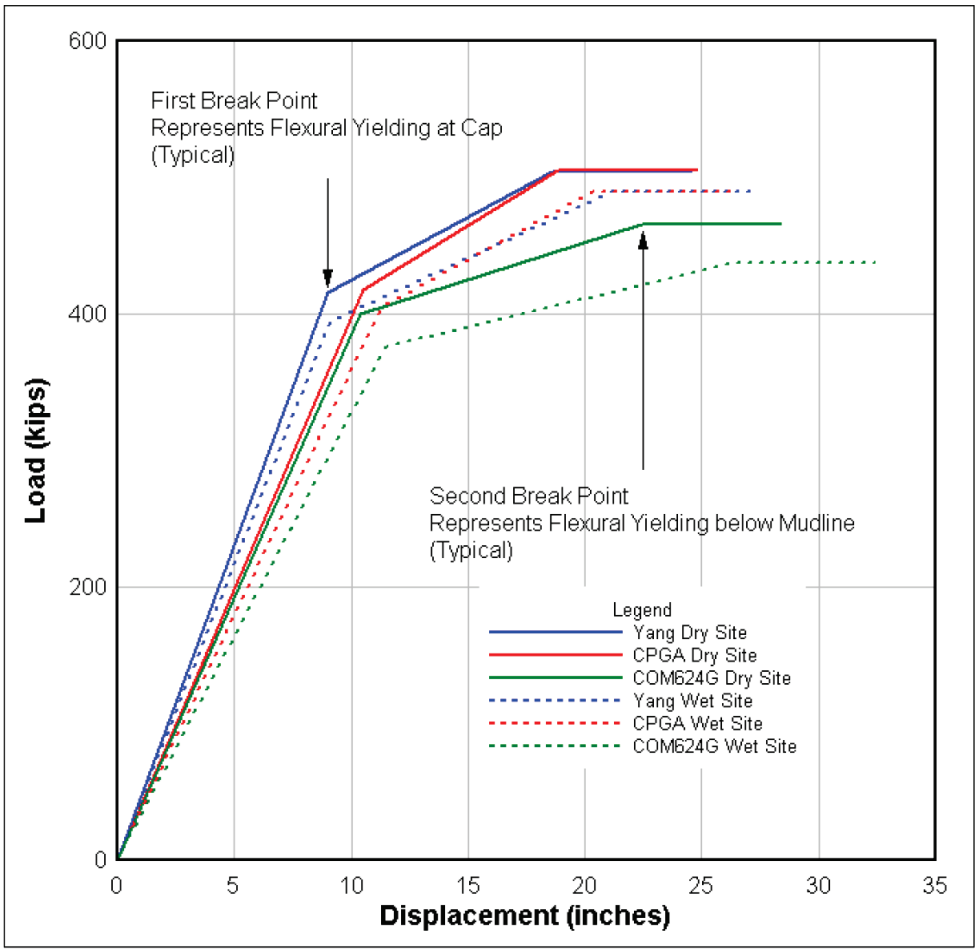


Table 4.1 Primary loading curve for the transverse spring model for a bent with two vertical piles.

Force	Deflection		Notes
(kips)	(inches)	(feet)	Adapted from Appendix A of Ebeling et al. (2012)
0.0	0.0	0.0	
810.0	11.28	0.94	Pile to pile cap moment capacity reached
980.0	20.272	1.68933	Flexural plastic hinges develop in piles below mudline
980.0	26.272	2.18933	Plastic hinge rotation

In the longitudinal direction, a push-over analysis must be performed for the pinned-head single pile condition, since there are no other piles to constrain the bent against rotation in the direction of the longitudinal load. The pile bent will maintain the same relative position with the top of the piles. The pile bent will rotate with the top of piles as the moments increase in the piles and will continue to rotate until the piles begin to

hinge below the mudline. In this case, the push-over analysis was performed with COM624G as a single pile model because the piles were vertical and a pinned-head boundary condition was imposed at the top of the pile. Again, because two piles were used, the force acting due to deflection was doubled.

Table 4.2 Primary loading curve for the longitudinal spring model for a bent with two vertical piles.

Force	Deflection		Notes
(kips)	(inches)	(feet)	Adapted from Appendix A of Ebeling et al. (2012)
0.0	0.0	0.0	
418.0	31.1	2.59167	Flexural plastic hinges develop in piles below mudline
418.0	37.1	3.09167	Plastic hinge rotation

4.5 Solving for the motion of the structure

The equations of motion for a structure comprised of decks supported on groups of piles and their end-release computations similar to the guard wall model is given in Appendix A. Appendix I gives a discussion of Rayleigh damping with section I.3 giving information specific to the guard wall model. The numerical method to be used, either HHT-α or Wilson-θ are discussed in Appendix F and G, respectively.

4.6 Validation of Impact_Deck Computer Program

The validation of the Impact_Deck computer program for the guard wall model was made against the results obtained from the well-known computer program SAP2000. The beam had a total length of 100.0 ft. In that validation, the beam was modeled with 11 nodes and 10 beam elements. A set of linear elastic springs were located at node 1, 6, and 11 where the pile supports were placed. The strength of the concrete was assumed as $f'c = 5000\ psi$ producing a modulus of elasticity for the concrete of $E = 580393.25\ ksf$. The beam cross-sectional area and the beam second moment of area (moment of inertia) were 54.668 ft^2 and 517.2 ft^4, respectively. The mass per linear foot of beam was calculated as $\bar{m}$ = 0.25486 kip *sec^2/ft. A damping factor of 0.02 or 2% of the critical damping was used in both computer programs. The force time history was the Winfield test # 10 (Ebeling et al. 2010), as shown in Figure 4.6 and applied at node 6 with zero translational velocity. The tangential-force time history was the same as the transverse but multiplied by a dynamic coefficient of

friction of 0.5. The translational spring stiffness was constant and equal to 88,125 kip/ft. Figures 4.7 and 4.8 show the dynamic-response time histories for node 1 and node 6 in the transverse direction. Both computer programs presented basically the same response of the system. At node 1, some differences in magnitudes were apparent. However, the magnitudes were very small, which was associated to numerical approximations.

Figure 4.6 Force time history of Winfield Test # 10.

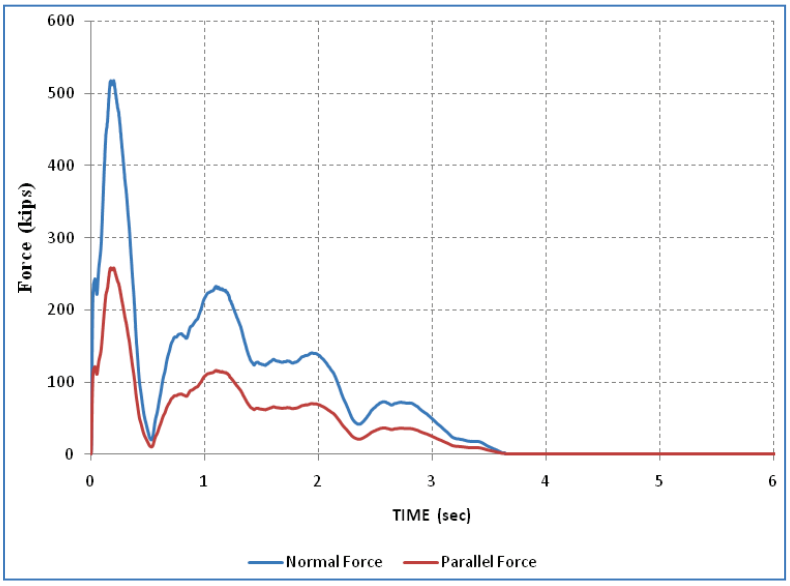


Figure 4.7 Validation of Impact_Deck against SAP2000 – Transverse displacement at node 1.

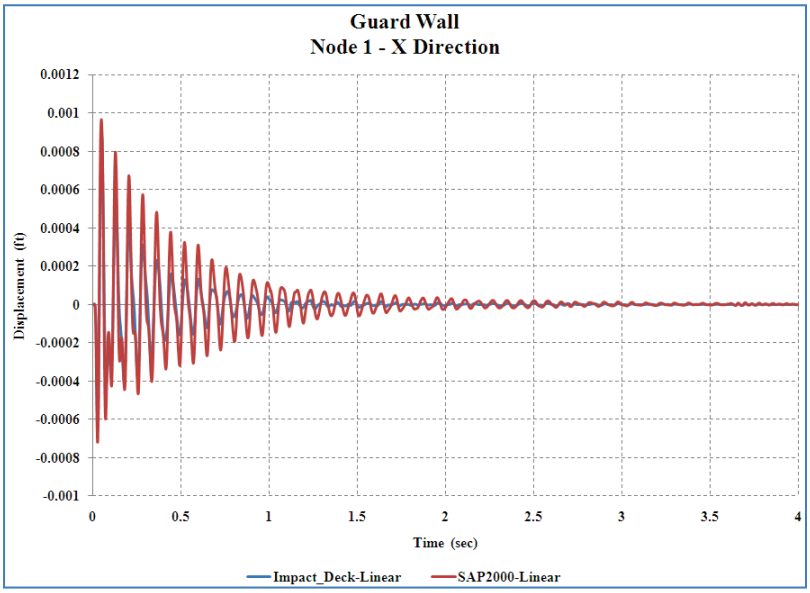
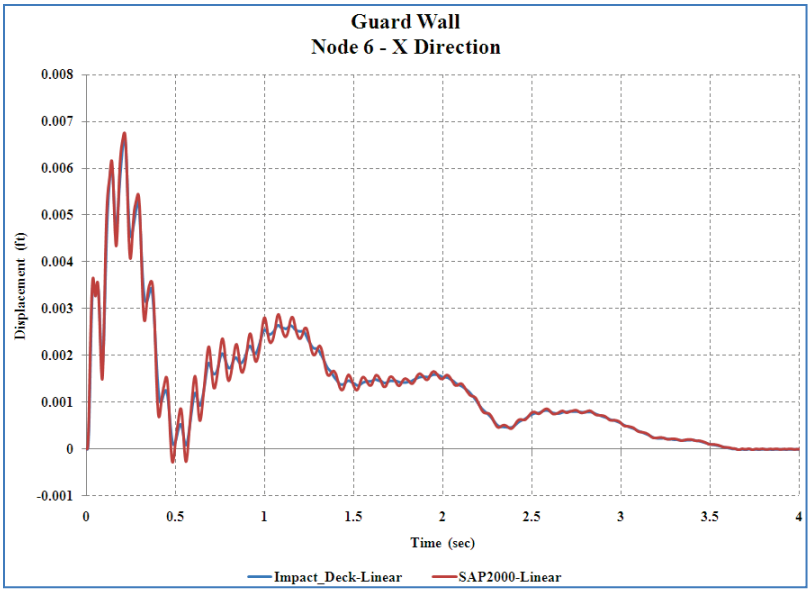


Figure 4.8 Validation of Impact_Deck against SAP2000 – Transverse displacement at node 6.



4.7 Numerical Example of the Elastic-Plastic Nonlinear Response Using Impact_Deck

In this section, a numerical example will be shown that demonstrates the "activation" of the plastic behavior of the pile group springs. This can be possible if the limit elastic displacement specified by the user was low enough to force the springs to enter into the plastic response zone. The input data for the Impact_Deck computer program for the guard wall were as follows. The beam has a total length of 100.0 ft long with 11 nodes and 10 beam elements. A set of linear elastic springs were located at node 1, 6, and 11 where the start, mid span, and end pile supports were placed. The strength of the concrete was assumed as $f'c = 5000\ psi$ producing a modulus of elasticity for the concrete of $E = 580393.25\ ksf$. The beam cross-sectional area and the beam second moment of area (moment of inertia) were 54.668 ft^2 and 517.2 ft^4, respectively. The mass per linear foot of beam was calculated as $\overline{m}$ = 0.25486 kip *sec^2 / ft. A damping factor of 0.02 or 2% of the critical damping was used in both computer programs. The force time history was the Winfield test # 10 as shown in Figure 4.6 and applied at node 6 with zero translational velocity. The tangential-force time history was the same as the transverse but multiplied by a dynamic coefficient of friction of 0.5. The translational springs stiffness were equal to $k_1 = 88{,}126.33\ kip/ft$ and $k_2 = 44{,}063.165\ kip/ft$ with a stiffness for unload after the elastic displacement equal to $k_{unload} = k_1$. The elastic displacement that defines the elastic and plastic zone was $\delta_{elastic} = 0.003\ ft$.

Figure 4.11 shows the dynamic-response time history obtained for node 12 and 12' (i.e., centerline of center pile group). It was observed that the permanent lateral displacement of approximately 0.0035 ft when the pile entered the plastic behavior. Figure 4.9 shows the transverse-displacement time history of node 1 for the elastic and plastic behavior. It was presented that no permanent displacement was reached by the transverse spring at node 1. For the two spring models, it remained in the elastic zone. Figure 4.10 shows the transverse-displacement time history of node 6 for the elastic and plastic behavior. A permanent displacement was reached by the transverse spring at node 6. For the elastic-plastic spring at node 6, permanent displacement of about 0.0035 ft was calculated. These behaviors can be observed in Figure 4.11, where the plastic response was reached (second slope in the force-displacement diagram) ending with a permanent displacement of around 0.0035 ft. It was important to observe the two stages where the spring load and unload in the plastic zone occured. That happened at an approximate time of 0.1 and 0.2 sec.

4.8 Impact_Deck GUI results

The Impact_Deck GUI was also used to run the guard wall problem in this section. This section does not provide an engineering analysis, but gives an idea of what information was provided so that an engineering analysis might be made.

Figure 4.9 Dynamic transverse response of node 1.

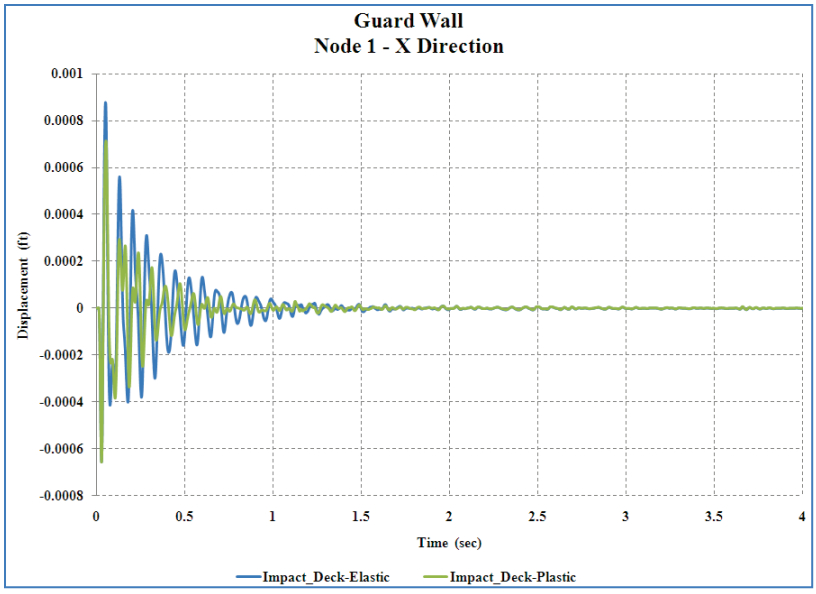


Figure 4.10 Dynamic transverse response of spring at node 6.

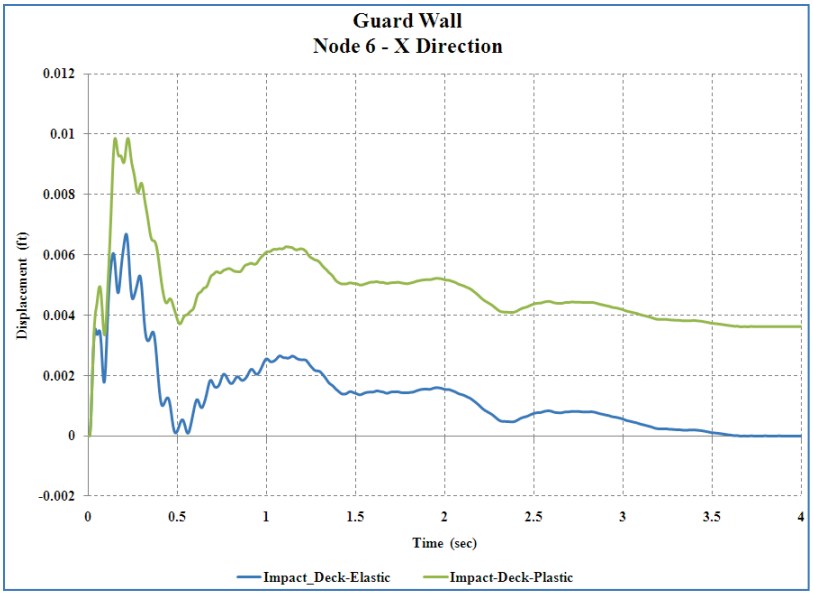
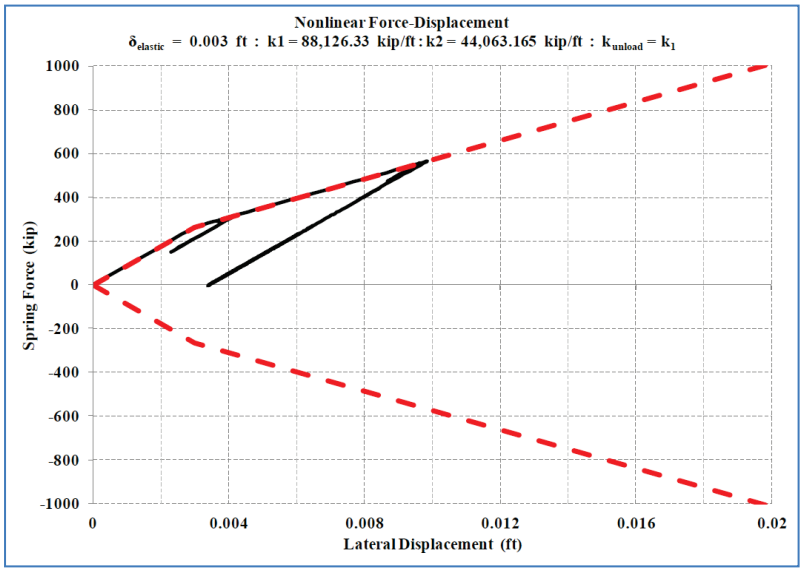


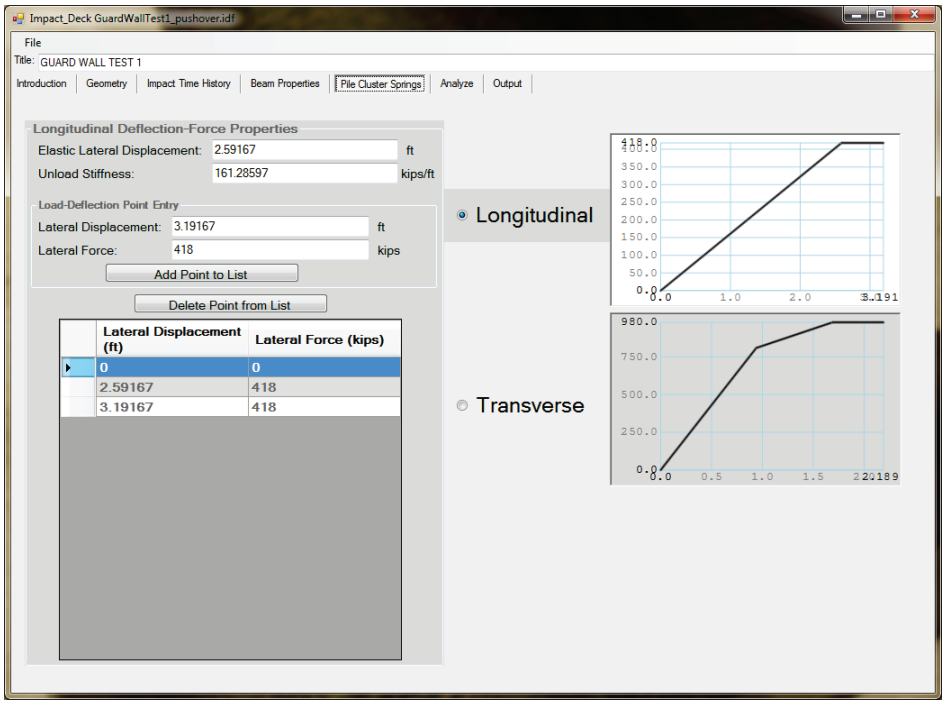
Figure 4.11 Plastic force-displacement of the transverse spring at node 6.



The model input for material properties was essentially the same as entered in section 4.7 with a few exceptions. The spring models (transverse and longitudinal), for each pile group was returned to the values specified in section 4.4 and shown in Figure 4.12.

The geometry for the beams was more highly resolved, with 50 beam elements per wall section and 51 nodes per beam. The pile group nodes were node numbers 1, 51, and 101. In all other respects, the input models were similar.

Figure 4.12 Impact_Deck GUI pile group longitudinal and transverse spring model backbone curves.



Nodal outputs provided from the FEO analysis of a flexible wall were the longitudinal displacement, transverse displacement, and rotational displacement (in radians) for each node at each time step of the simulation. A table was also provided that gives the maximum displacements (longitudinal, transverse, and rotational) for each node and the time that the maximum displacement occured.

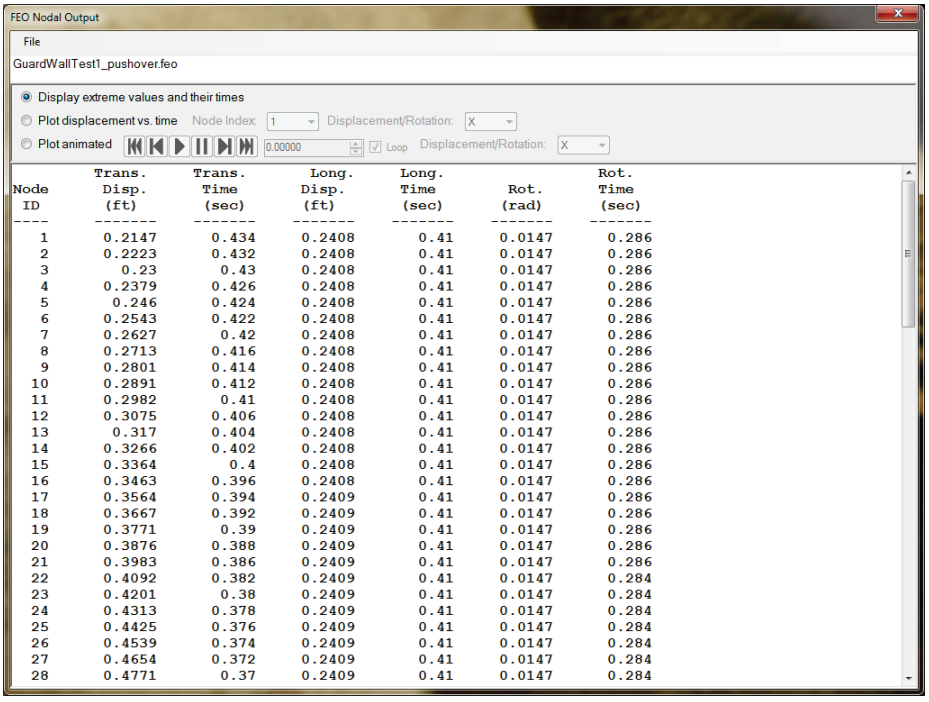
Figure 4.13 shows the GUI table of maximums for the example problem in this section. From this GUI table, it is possible to tell the time step and the node with the maximum displacement for transverse, longitudinal, and rotational displacements (Table 4.3).

Figures 4.14, 4.15, and 4.16 show the time histories for the displacements at nodes 51 and 50. Because some of these displacements were very small, and the data were stored with limited precision, some of these plots developed jaggies.

The Impact_Deck GUI also allowed the user to visualize the entire beam in motion using an exaggerated plot of displacements longitudinally, transverse, and rotationally. Figures 4.17, 4.18, and 4.19 show the displacements of the wall from these animated plots at the moment where the maximum

displacement occurred, 0.332 sec for transverse displacements, 0.41 sec for longitudinal displacements, and 0.286 sec for rotational displacements. These data were also subjected to the jaggies because of the precision of the stored data. The data were scaled to fit the plot.

Figure 4.13 Impact_Deck GUI table of maximum nodal displacements for the guard wall.



Node ID	Trans. Disp. (ft)	Trans. Time (sec)	Long. Disp. (ft)	Long. Time (sec)	Rot. (rad)	Rot. Time (sec)
1	0.2147	0.434	0.2408	0.41	0.0147	0.286
2	0.2223	0.432	0.2408	0.41	0.0147	0.286
3	0.23	0.43	0.2408	0.41	0.0147	0.286
4	0.2379	0.426	0.2408	0.41	0.0147	0.286
5	0.246	0.424	0.2408	0.41	0.0147	0.286
6	0.2543	0.422	0.2408	0.41	0.0147	0.286
7	0.2627	0.42	0.2408	0.41	0.0147	0.286
8	0.2713	0.416	0.2408	0.41	0.0147	0.286
9	0.2801	0.414	0.2408	0.41	0.0147	0.286
10	0.2891	0.412	0.2408	0.41	0.0147	0.286
11	0.2982	0.41	0.2408	0.41	0.0147	0.286
12	0.3075	0.406	0.2408	0.41	0.0147	0.286
13	0.317	0.404	0.2408	0.41	0.0147	0.286
14	0.3266	0.402	0.2408	0.41	0.0147	0.286
15	0.3364	0.4	0.2408	0.41	0.0147	0.286
16	0.3463	0.396	0.2408	0.41	0.0147	0.286
17	0.3564	0.394	0.2409	0.41	0.0147	0.286
18	0.3667	0.392	0.2409	0.41	0.0147	0.286
19	0.3771	0.39	0.2409	0.41	0.0147	0.286
20	0.3876	0.388	0.2409	0.41	0.0147	0.286
21	0.3983	0.386	0.2409	0.41	0.0147	0.286
22	0.4092	0.382	0.2409	0.41	0.0147	0.284
23	0.4201	0.38	0.2409	0.41	0.0147	0.284
24	0.4313	0.378	0.2409	0.41	0.0147	0.284
25	0.4425	0.376	0.2409	0.41	0.0147	0.284
26	0.4539	0.374	0.2409	0.41	0.0147	0.284
27	0.4654	0.372	0.2409	0.41	0.0147	0.284
28	0.4771	0.37	0.2409	0.41	0.0147	0.284

Table 4.3 Maximum nodal displacements for the guard wall example problem.

	Node number	Value	Time (seconds)
Transverse	51	0.7706 feet	0.332
Longitudinal	51	0.2409 feet	0.41
Rotational	50	0.0147 radians	0.286

Figure 4.14 Transverse nodal displacement time histories for node 51.

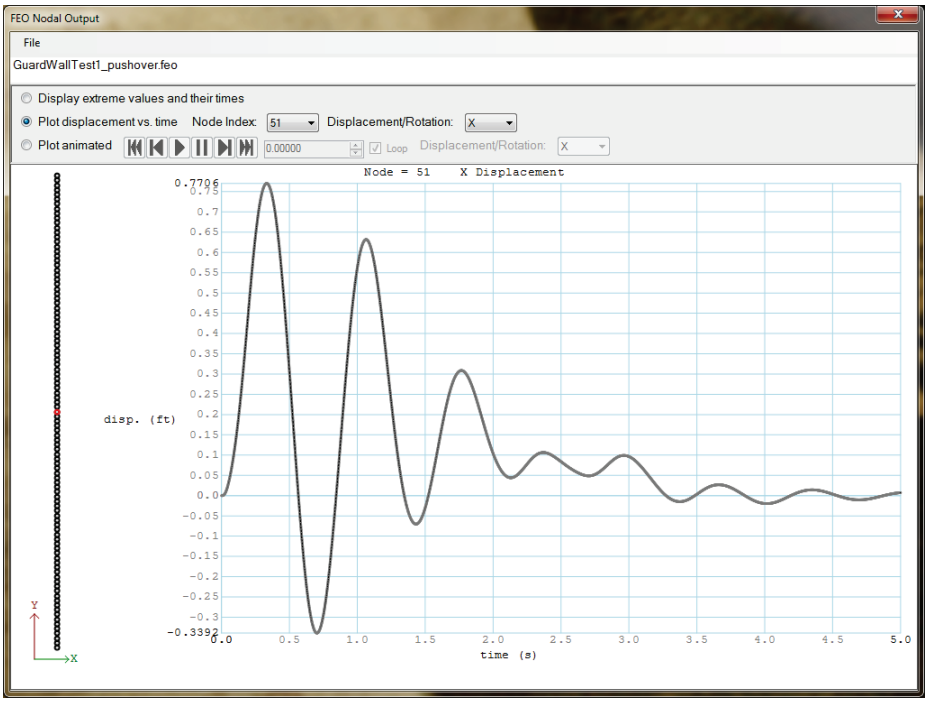


Figure 4.15 Longitudinal nodal displacement time histories for node 51.

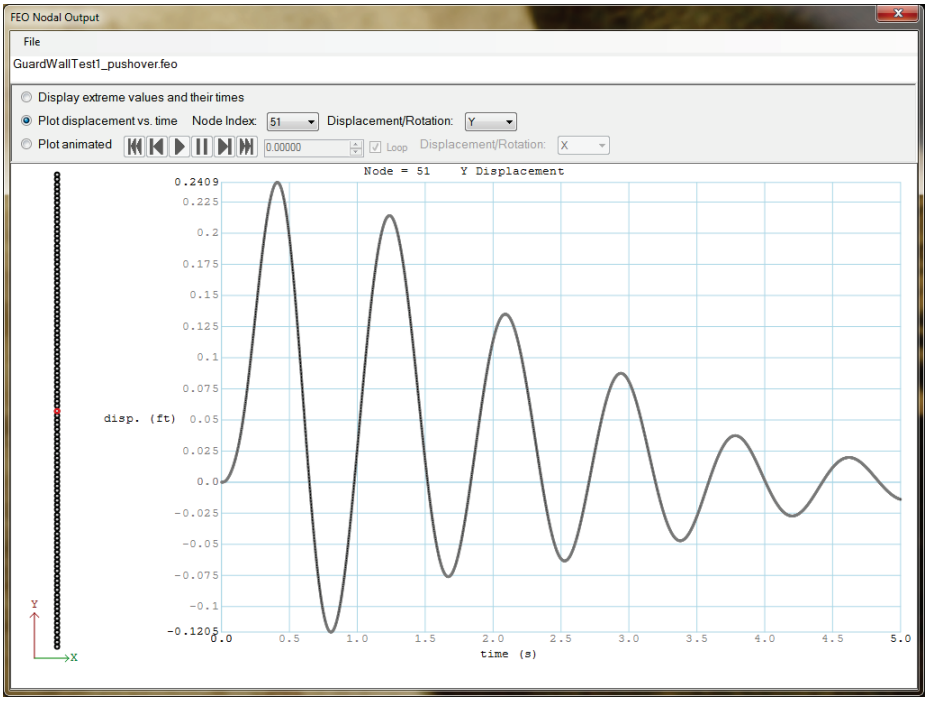


Figure 4.16 Rotational nodal displacement time histories for node 50.

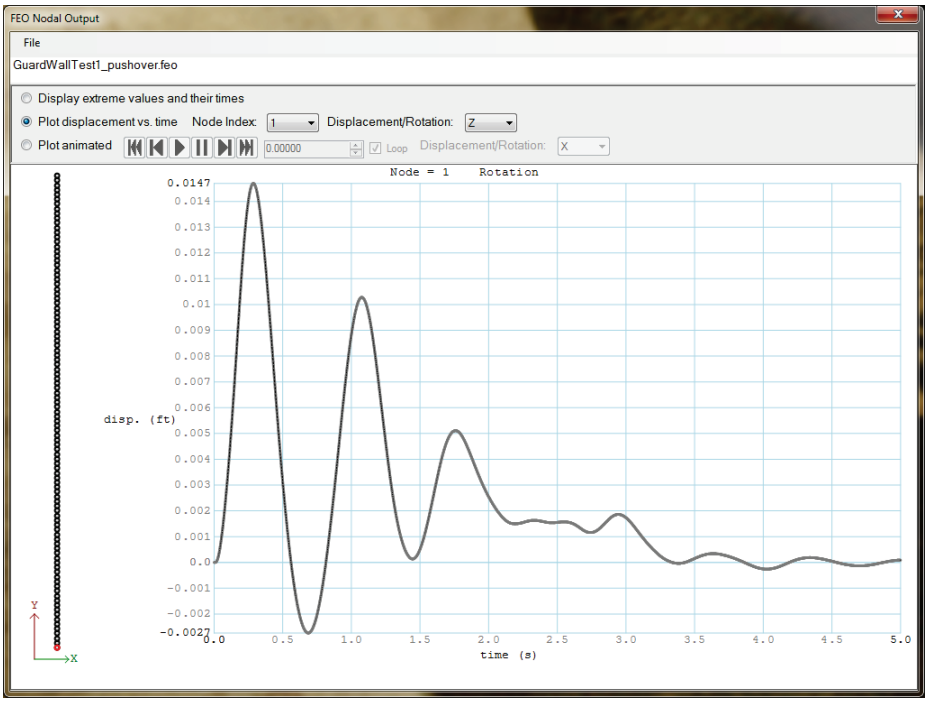


Figure 4.17 Transverse wall displacements at 0.332 sec.

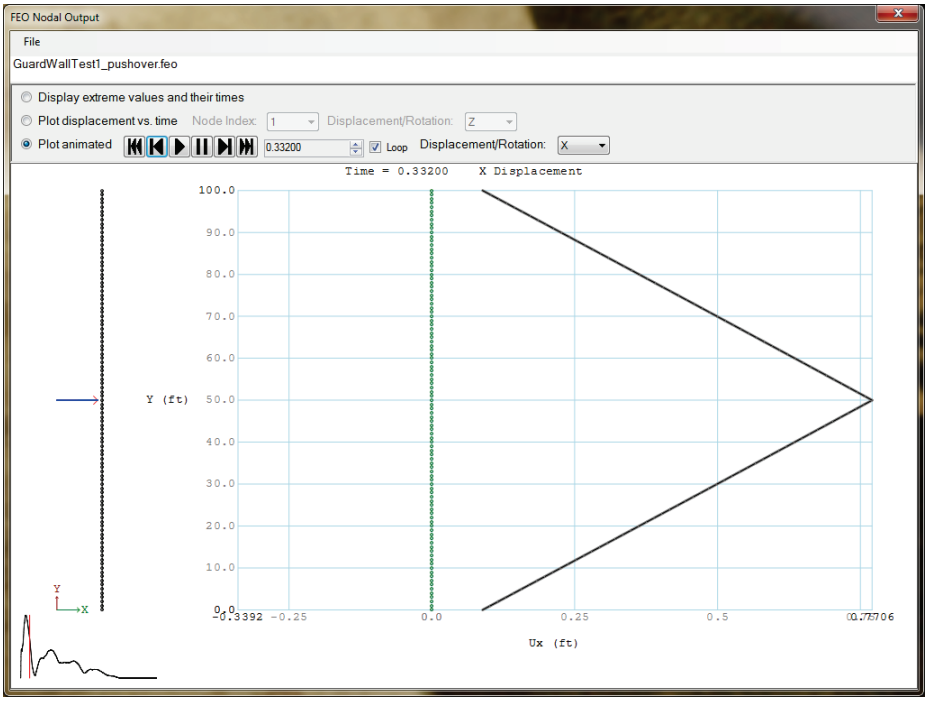


Figure 4.18 Longitudinal wall displacements at 0.41 sec.

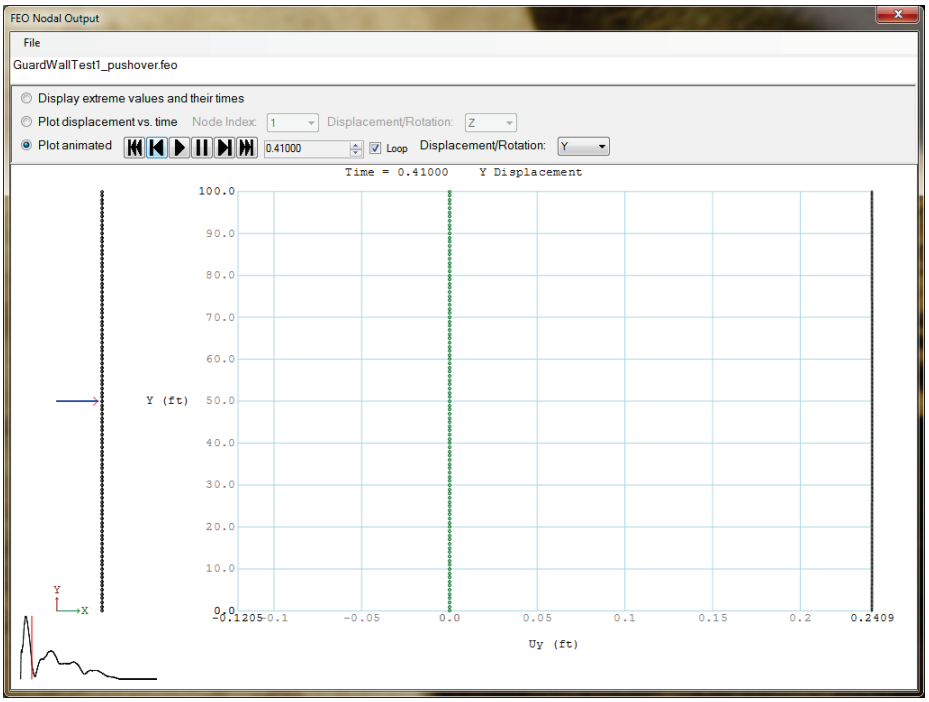
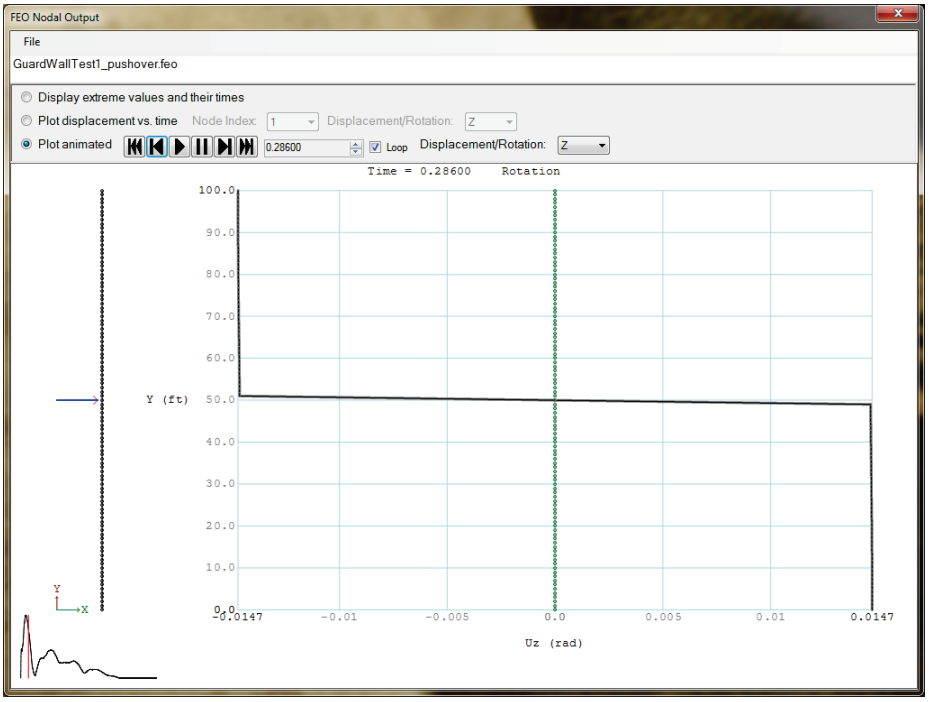


Figure 4.19 Rotational wall displacements at 0.286 sec.

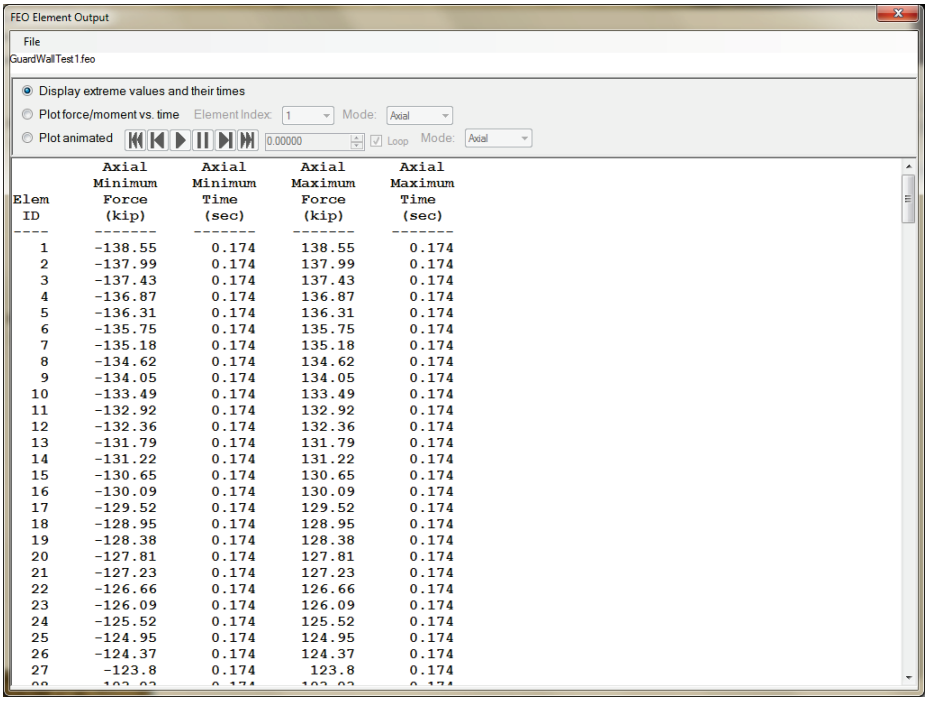


Element outputs provided from the FEO analysis of an impact deck were the axial force, shear force, and moment for each element at each time step of the simulation. A table was also provided that gives the minimum and

maximum forces and moments for each element and the times that the minimum and maximum force/moment occured

Figure 4.20 show GUI tables of extreme values for the example problem in this section. The beginning of the axial force extremes table is shown. The shear force extremes table and moment extremes table are available by scrolling in the interface. From this GUI table, it is possible to tell the time step and the element with the extreme axial force, shear force, and moment (as shown in Table 4.4). Because the impact occurs at the midpoint of the guard wall and doesn't move for this example, the forces are symmetric about the impact point (node 51).

Figure 4.20 Impact_Deck GUI table of element minimum and maximum axial forces for the guard wall Example.



Elem ID	Axial Minimum Force (kip)	Axial Minimum Time (sec)	Axial Maximum Force (kip)	Axial Maximum Time (sec)
1	-138.55	0.174	138.55	0.174
2	-137.99	0.174	137.99	0.174
3	-137.43	0.174	137.43	0.174
4	-136.87	0.174	136.87	0.174
5	-136.31	0.174	136.31	0.174
6	-135.75	0.174	135.75	0.174
7	-135.18	0.174	135.18	0.174
8	-134.62	0.174	134.62	0.174
9	-134.05	0.174	134.05	0.174
10	-133.49	0.174	133.49	0.174
11	-132.92	0.174	132.92	0.174
12	-132.36	0.174	132.36	0.174
13	-131.79	0.174	131.79	0.174
14	-131.22	0.174	131.22	0.174
15	-130.65	0.174	130.65	0.174
16	-130.09	0.174	130.09	0.174
17	-129.52	0.174	129.52	0.174
18	-128.95	0.174	128.95	0.174
19	-128.38	0.174	128.38	0.174
20	-127.81	0.174	127.81	0.174
21	-127.23	0.174	127.23	0.174
22	-126.66	0.174	126.66	0.174
23	-126.09	0.174	126.09	0.174
24	-125.52	0.174	125.52	0.174
25	-124.95	0.174	124.95	0.174
26	-124.37	0.174	124.37	0.174
27	-123.8	0.174	123.8	0.174

Table 4.4 Extreme Forces/Moments for the Impact Deck Example Problem.

		Element number	Value	Time (seconds)
Axial	Min.	1&100	-153.99 kips	0.410
	Max.	1&100	153.99 kips	0.410
Shear	Min.	51	-214.86 kips	0.714
	Max.	50	214.86 kips	0.714
Moment	Min.	27&75	-2532.67 kip-feet	0.716
	Max.	26&74	2532.67 kip-feet	0.716

Figures 4.21 – 4.26 show the time histories for the axial force, shear force, and moments for the elements 50 and 51, respectively. This shows the symmetry of the solution.

Figure 4.21 Axial force time histories for element 51.

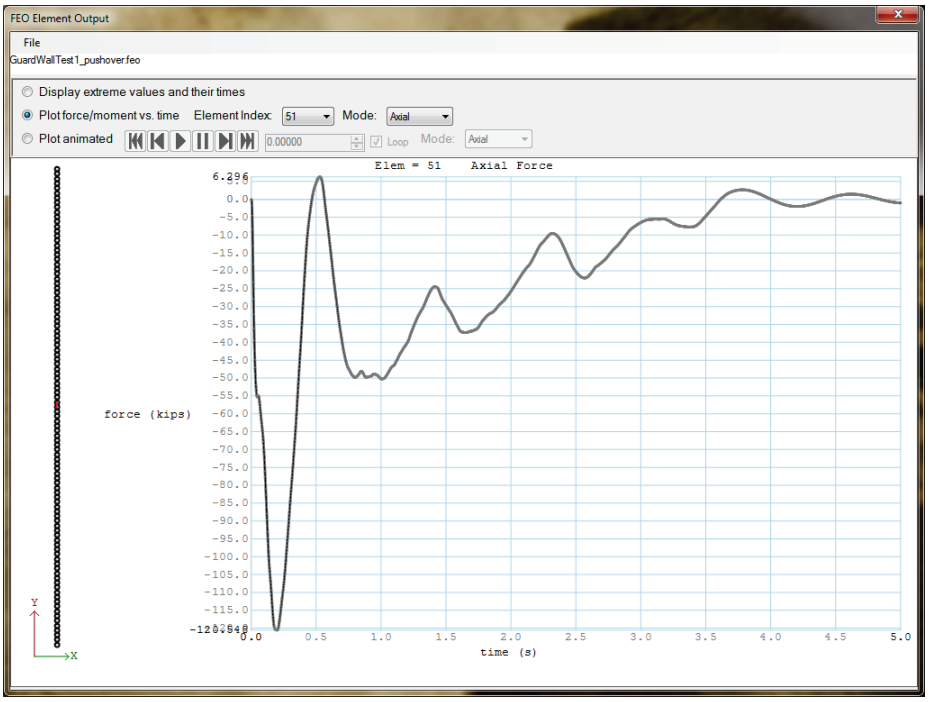


Figure 4.22 Axial force time histories for element 50.

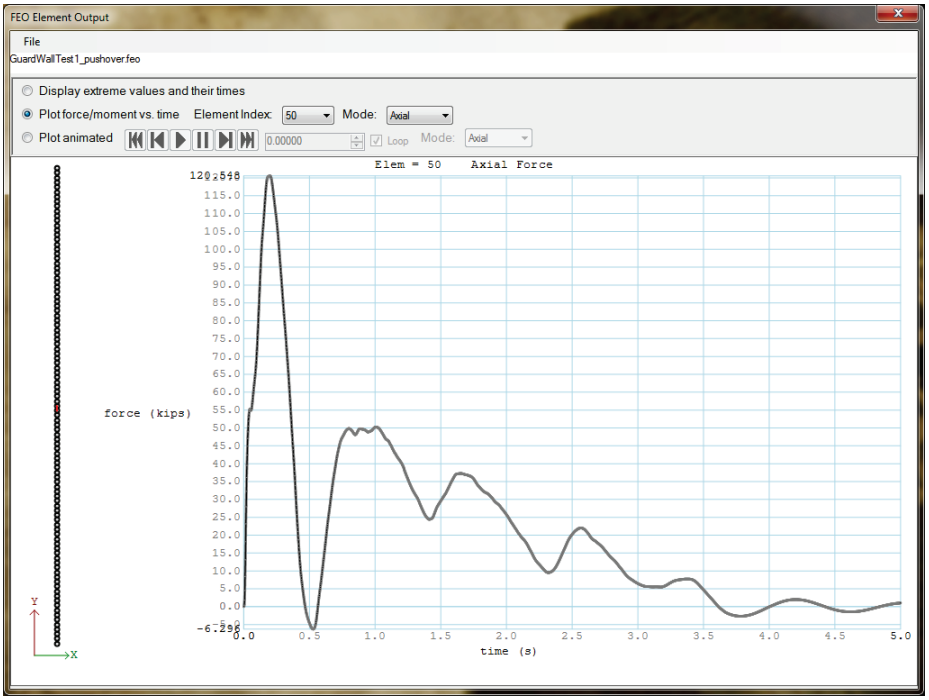


Figure 4.23 Shear force time histories for element 51.

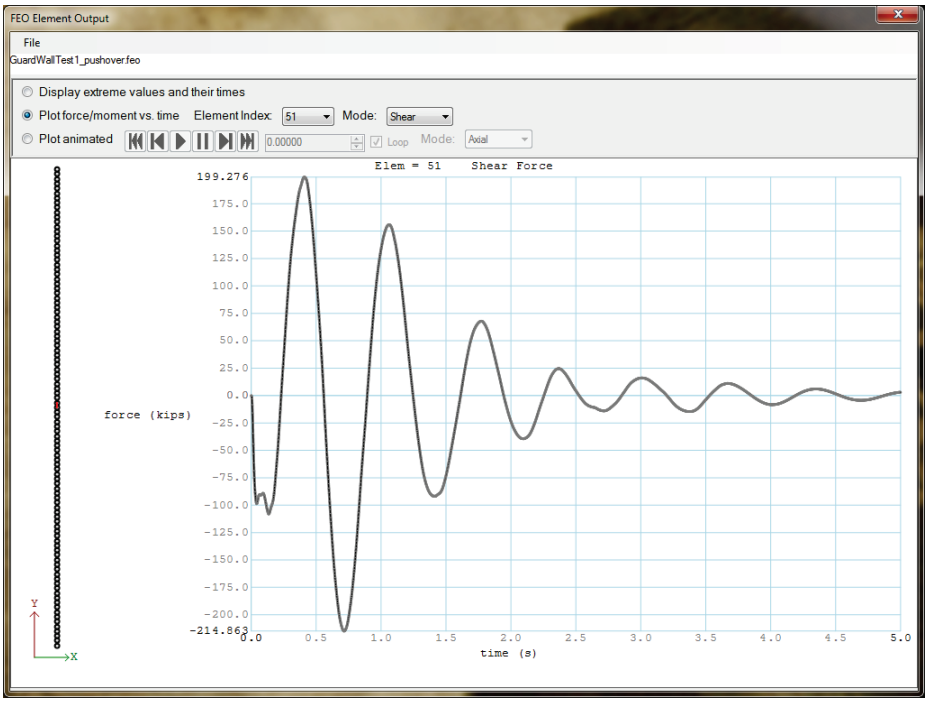


Figure 4.24 Shear force time histories for element 50.

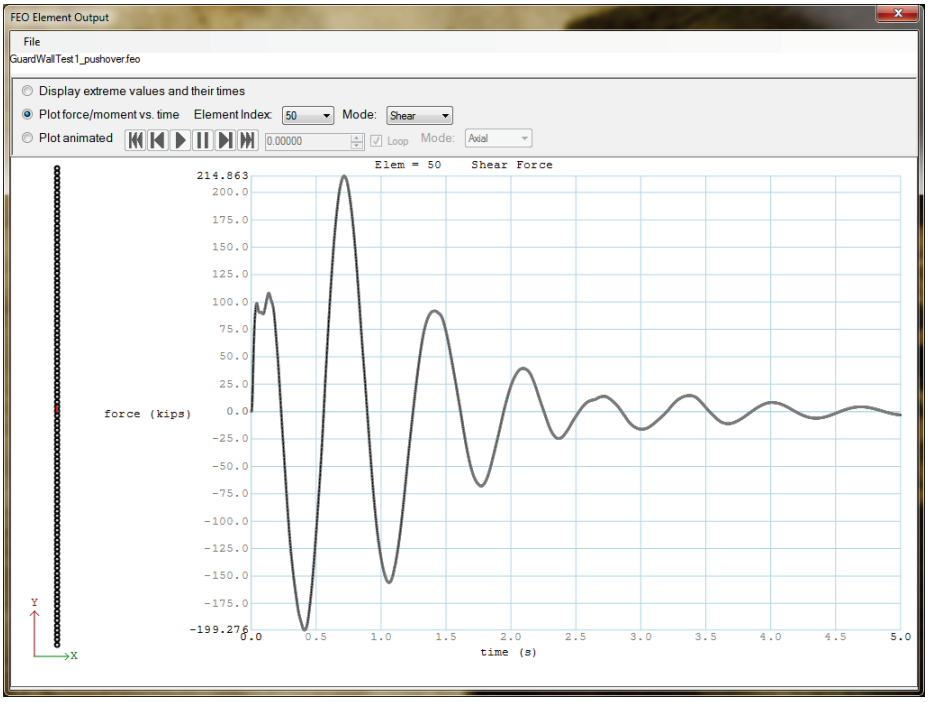


Figure 4.25 Moment time histories for element 51.

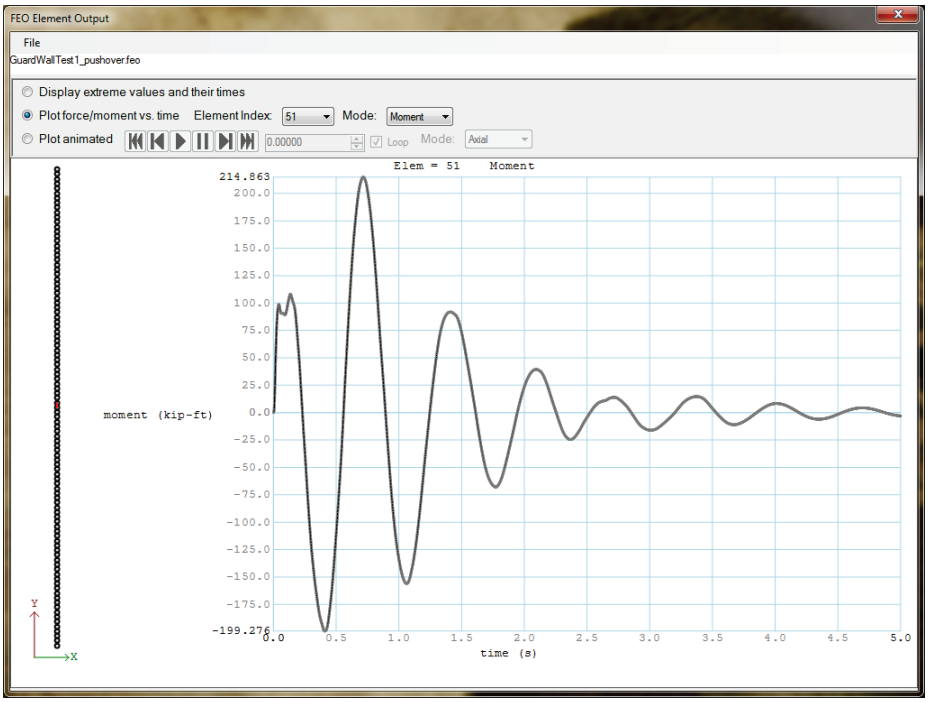
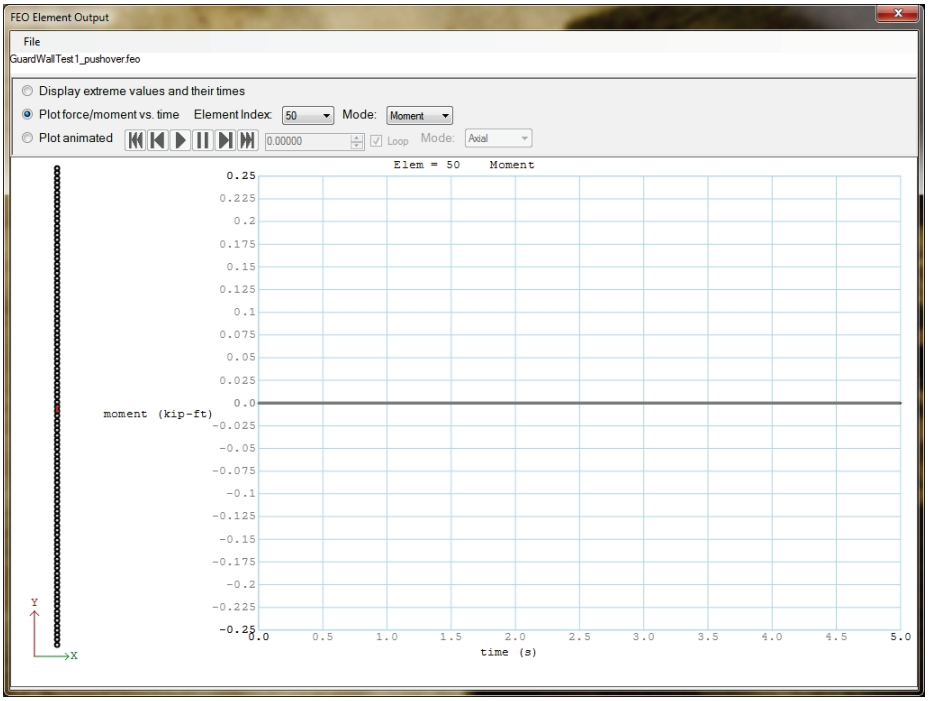


Figure 4.26 Moment time histories for element 50.



Figures 4.27 – 4.29 show the axial force, shear force, and moment at 0.410, 0.714, and at 0.716 sec, respectively, for the entire wall. These are created to view the animated forces in the Impact_Beam GUI.

Figure 4.27 Wall axial forces at 0.410 sec.

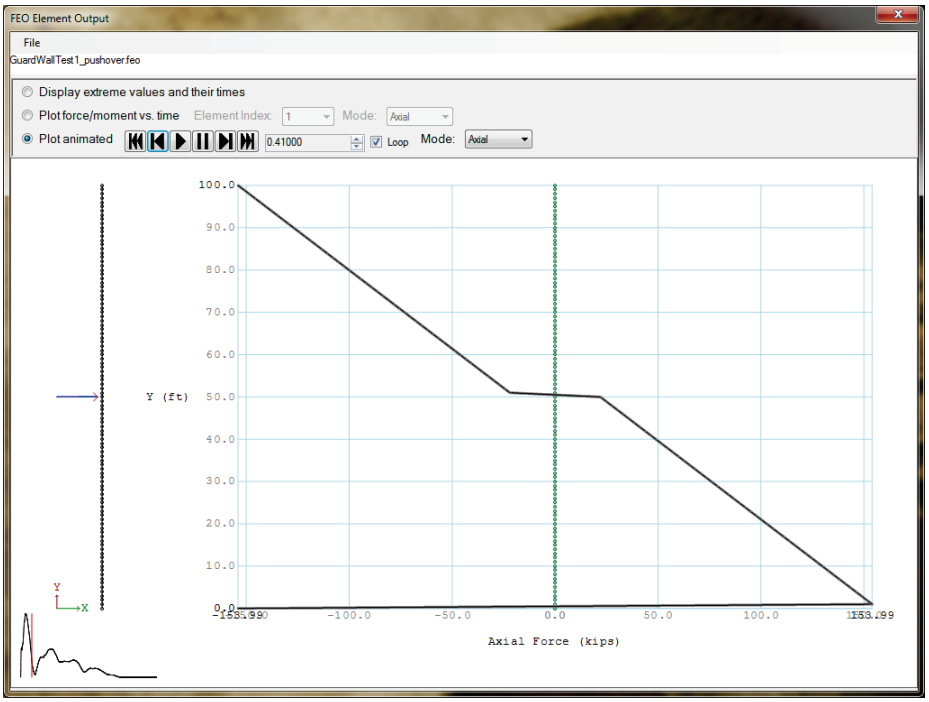


Figure 4.28 Wall shear forces at 0.714 sec.

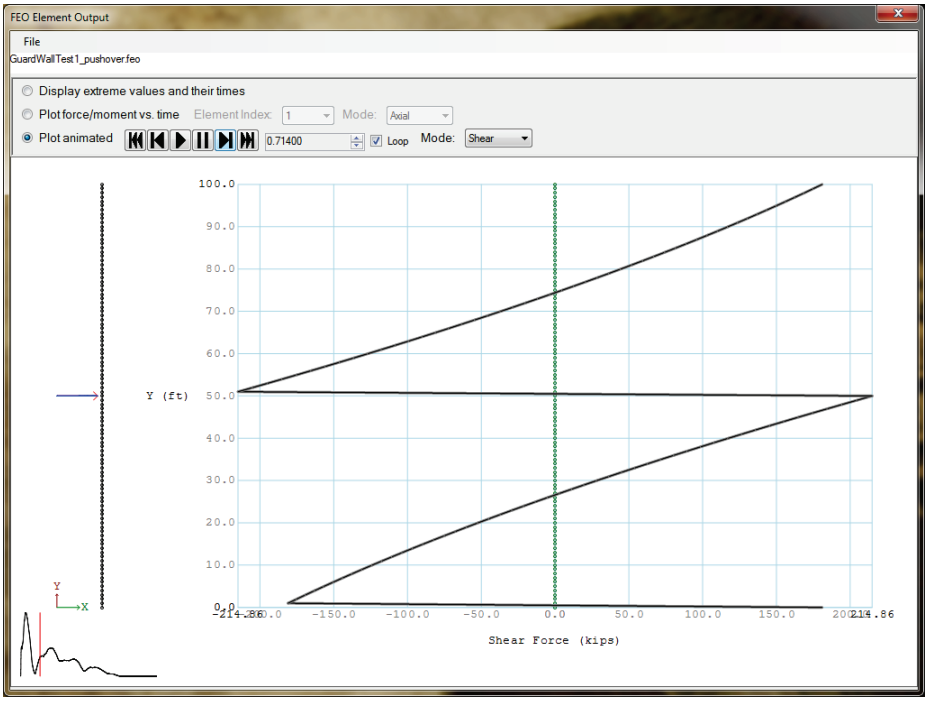
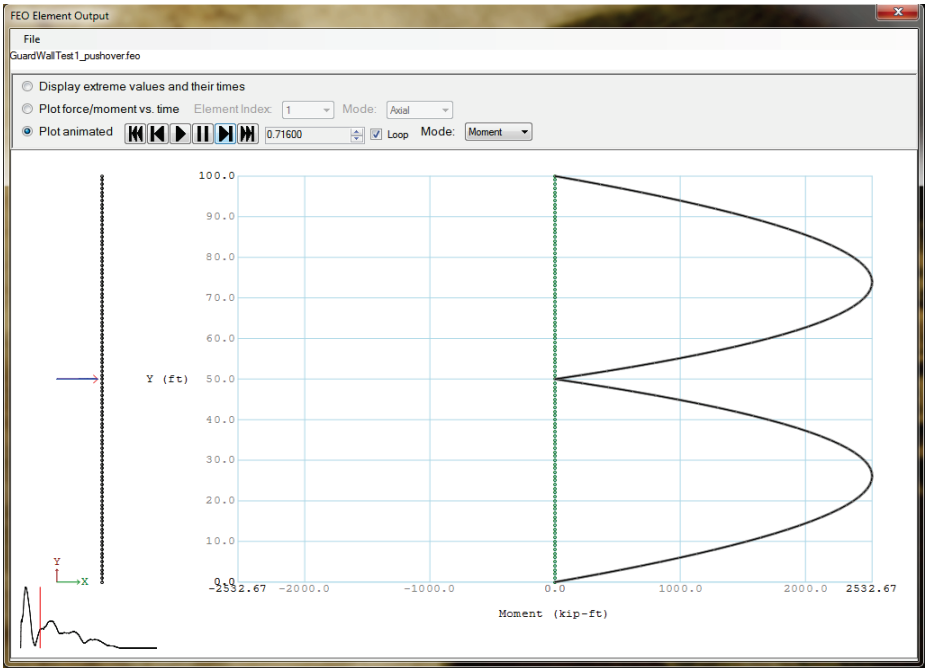
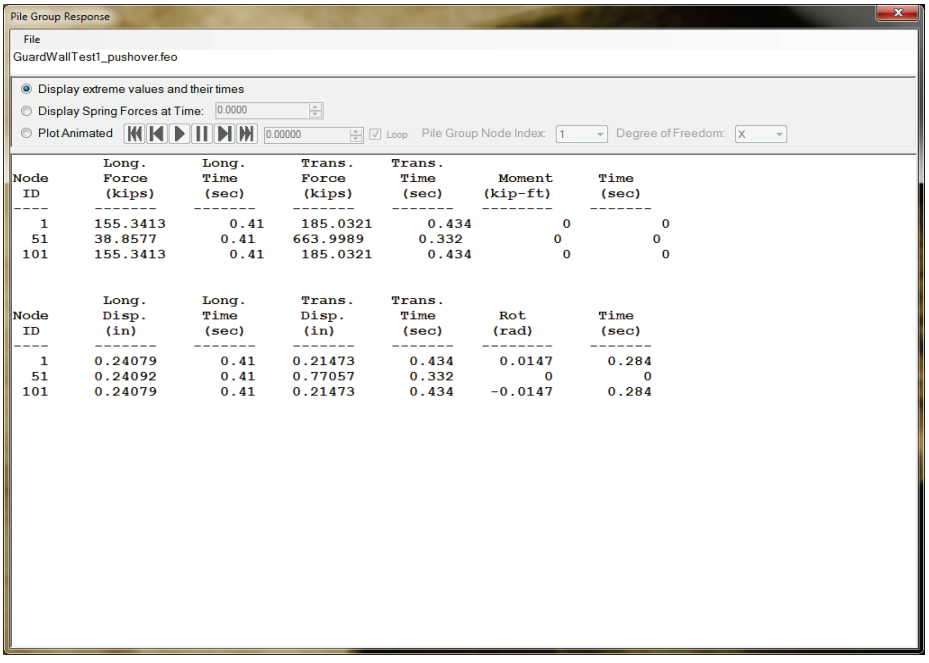


Figure 4.29 Wall moments at 0.716 sec.



Of primary importance for doing a pile-group founded flexible wall analysis is being able to see exactly how much force each pile group will be able to resist during an impact event. This is measured by finding the resisting force from the spring model used for the pile group for the pile group's displacement. Figure 4.30 shows the table of forces/moments resisted at the nodes representing a pile group in the Impact_Deck example model.

Figure 4.30 Table of pile group response maximum displacements.



Node ID	Long. Force (kips)	Long. Time (sec)	Trans. Force (kips)	Trans. Time (sec)	Moment (kip-ft)	Time (sec)
1	155.3413	0.41	185.0321	0.434	0	0
51	38.8577	0.41	663.9989	0.332	0	0
101	155.3413	0.41	185.0321	0.434	0	0

Node ID	Long. Disp. (in)	Long. Time (sec)	Trans. Disp. (in)	Trans. Time (sec)	Rot (rad)	Time (sec)
1	0.24079	0.41	0.21473	0.434	0.0147	0.284
51	0.24092	0.41	0.77057	0.332	0	0
101	0.24079	0.41	0.21473	0.434	-0.0147	0.284

Figure 4.31 Forces at the three pile group nodes at time 0.332 sec.

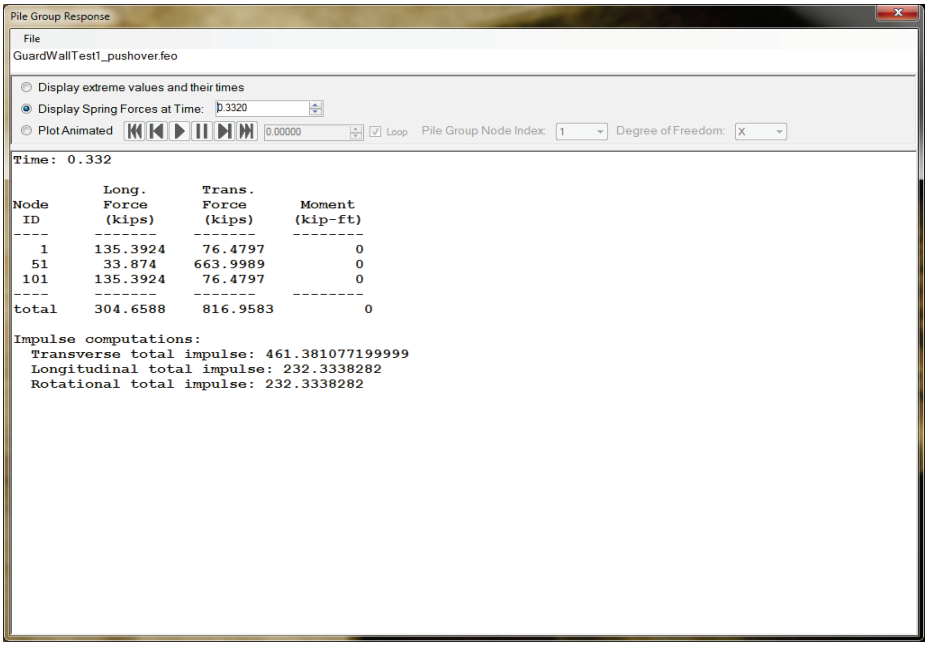
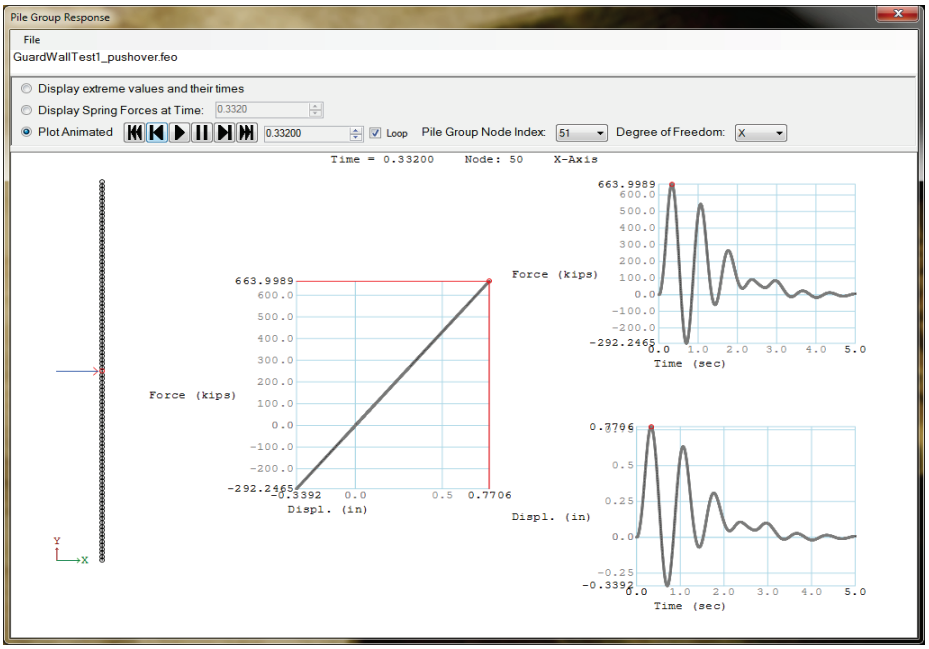


Figure 4.31 displays the values for the forces and displacements for the pile group at node 51 at time 0.332 sec. Figure 4.32 shows the response of the pile group at node 51 at time 0.332 sec as a force-versus-displacement plot, and as force and displacement time histories. This is the time when the displacement for the pile group at node 51 is at its maximum location in the transverse direction.

Figure 4.32 Transverse pile group response for the pile group at node 51 and at time 0.332 sec.



The Case for Dynamic Analysis:

This example problem demonstrates the necessity of performing a dynamic analysis of these pile founded walls. This example uses an impact time history that is the result of the Winfield Test #10 (Ebeling et al. 2010). This impact time history is applied transverse to the approach wall at a position starting at 50.0 ft along this section of wall (at the longitudinal location of node 51) and moved at 0 ft /sec along the approach wall. The peak force for the impact time history was 516.4 kips at time 0.200 sec. Table 4.5 provides a summary of transverse forces and the times at which they occur as well as the magnitude of the impact force occurring at this same point in time. Peak forces at the three times of interest are shown in bold in this table.

Table 4.5 Transverse forces with respect to time.

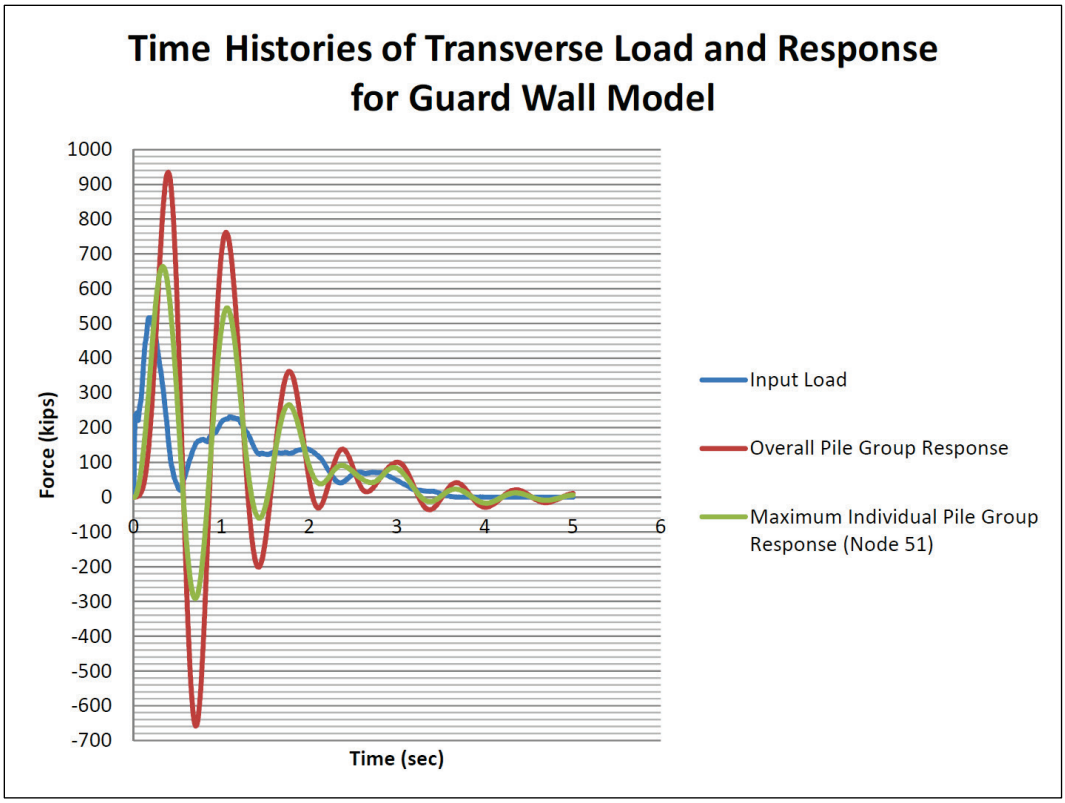
Time (s)	Node 51 Force (kips)	Impact Load Force (kips)	Total Pile Group Response (kips)
0.200	398.9343	**516.400**	232.6187
0.332	**663.9989**	320.2922	816.9583
0.392	606.7369	174.0544	**934.5545**

Node 51 (as discussed above) has a maximum transverse force of 663.999 kips, which occurs at 0.332 sec. This is the pile group node between two flexible approach wall impact beams, so its transverse displacement has been affected by the inertial effects of the walls and the over structure, as well as rotational response. The total pile group response for the section of flexible approach wall structural model (with 3 pile group nodes) at this time (0.332 sec) is 816.958 kips.

The peak overall force occurs at a later time for the guard wall bents (at 0.392 sec) than in the input force time history (0.2 sec). This may be due to the natural frequency of the system with less stiff supporting piles but more analysis (e.g., considering modal analysis of the piles as discussed in Appendix E of Ebeling et al. 2012) will be required. The peak overall force occurs at 0.392 sec and have a value of 934.555 kips, exceeding the peak input force of 516.4 kips by a good margin.

Figure 4.33 takes this information a step further by displaying the time histories for the three forces.

Figure 4.33 Time-history plot of transverse input forces, total force response for all the pile groups, and an individual pile group response forces.



From Table 4.5 and Figure 4.33, it can be seen that the overall pile group response is dynamic because it does not track with the input force. Instead, the pile groups respond to the input force over time due to inertial effects. Because of this, the overall pile group response can have higher peak forces. For example, at the time of peak response of 0.2 sec a maximum impact force of 516.4 kips is applied to the approach wall. The total transverse force response of the three nodes representing the pile groups at the beam supports is 232.619 kips. This 55% smaller summed force response is due to the contribution of the first two terms of the equation of motion (Equation 2.1, also seen in Appendix A) for the dynamic structural response:

$$[M]\{\ddot{u}(t)\}+[C]\{\dot{u}(t)\}+[K]\{u(t)\}=\{F(t)\} \qquad \text{(2.1 bis)}$$

The summed transverse effects are thought to be smaller than the peak input force because the mass of the beams is accelerated slowly. At time 0.332 sec, when a peak response force is recorded at node 51 for an individual pile group, the contribution of the first two terms of the equation

of motion for the dynamic structural response is even larger, resulting in an overall response force of 663.999 kips. This is nearly 28.6% greater than the peak input force of 516.4 kips (occurring at 0.2 sec). Additionally, the overall response does not reach a peak until 0.392 sec with an even larger value of 934.555 kips. This greater overall force results from the pile groups all developing a positive deformation at the same time. These observations demonstrate the importance of applying the equation of motion for calculating pile group structural response forces (and displacements). These differences explain why a dynamic analysis is required versus a static analysis in which the user-provided impact load is applied as a single peak value (e.g., determined to be the input peak force from the time history).

For this type of simply supported impact beam structural system with two beams, the modal contribution characteristics of the substructure system (Ebeling et al. 2012) may be important. Because this pile substructure system is relatively flexible, the inertia of the impact beams and pile cap superstructure may cause vibrations to be more in sync with the impact event. Expansion of the current dynamic Impact_Deck model would be required to account for this feature.

Validation Using Impulse Calculations:

The higher peak values of the overall pile group response seem out of place until an impulse calculation (taking the area beneath the time history curves for input load and overall pile group response in Figure 3.35) is performed. Despite inertial effects, the impulse of the input load must be equivalent to the overall pile group response, if the piles do not fail. When an impulse calculation is performed for the overall pile group response, the result is 461 kip-sec. The impulse for the input force is 463 kip-sec. The difference is minimal, less than 1%.

Load Sharing:

For this type of flexible approach wall structural system, there can be load sharing (depending upon the structural detailing) in the longitudinal direction starting with the first pile group beyond the point of impact. There will also be load sharing in the transverse direction among the pair of pile bents supporting the impact beam for an impact anywhere along the simply supported beam. However, this structural configuration does not have the advantage of the significant load sharing among pile groups

that the Lock and Dam 3 impact deck configuration possesses. This is exemplified by the observation that the node 51 maximum transverse force of 663.999 kips, which occurs at 0.392 sec, is greater than the peak input force of 516.4 kips occurring at 0.2 sec. The pile group total transverse response force is greater than the peak input force. For Lock and Dam 3, the peak transverse force for the pile group possessing the maximum peak force of any of the 96 pile groups, was 56.4652 kips. The Lock and Dam 3 dynamic structural response analysis was subjected to the same input impact-force time history specified in this analysis.

4.9 Final Remarks

In this section, the flexible guard wall physical model was presented and the mathematical model to calculate the dynamic response was also developed. Impact_Deck calculated the dynamic response of an elastic beam supported over linear elastic or plastic spring supports. The mathematical formulation also modeled the center pile group connection to the ends of the simply supported impact beams with zero moment transfer. The impact normal and parallel concentrated external load can be located at a specified location or can be assumed to have motion at a specified constant velocity. The damping effect was considered by means of the Rayleigh damping model which depended on the natural frequencies of the system. These natural frequencies were calculated in an approximate way by using the linear stiffness of the pile groups and the mass of the impact beams. The results of Impact_Deck proved to be valid when compared to the results obtained with SAP2000. Finally, an example was presented to show the plastic behavior of the springs and how this result compared to the linear elastic response.

5 Impact_Deck Graphical User Interface (GUI)

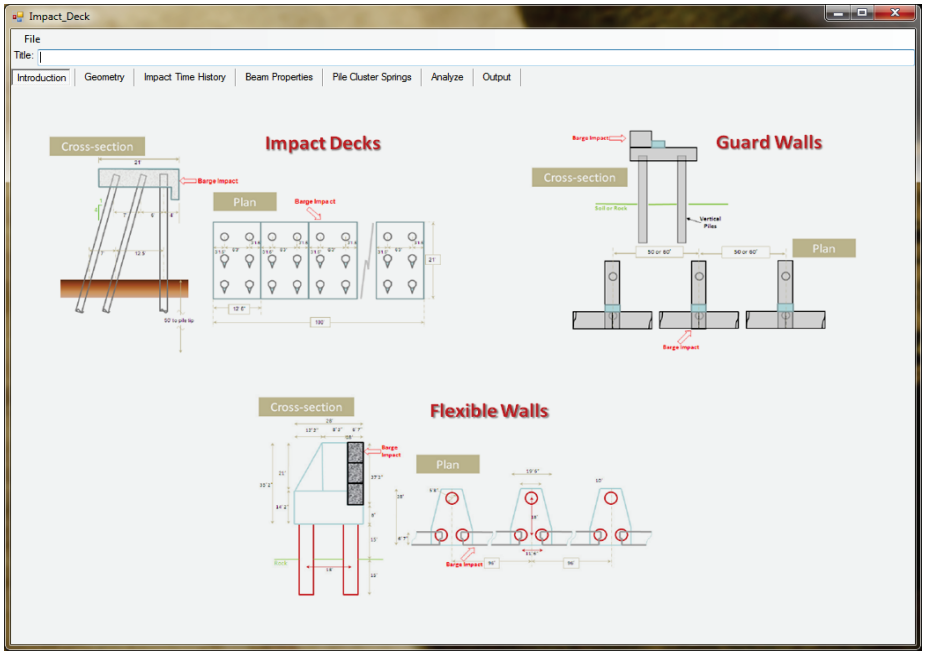
5.1 Introduction

This section introduces the Impact_Deck GUI, which provides pre-processing and post-processing capabilities to the Impact_Deck engineering code. The purpose of the GUI is to provide the user a way to specify the input model types, input model parameters, analyze the input, and visualize the output.

The program has a simple menu that allows the user to create a new data input set, open an existing set of input data, save the current input data in an existing or new input file, and exit the program. On the line below the menu, enter the title of the project; this will provide a reference for the user.

Beneath the title bar, the Impact_Deck GUI uses a tabbed data input scheme where input data were grouped by related data and functionality. The Introduction Tab shows cross-section and plan views of examples of the different types of structures that can be analyzed with the Impact_Deck software (Figure 5.1).

Figure 5.1 Introducing Impact_Deck.



The following sections discuss the other tabs in the Impact_Deck program.

5.2 Geometry Tab

The Geometry Tab is made up of subsections of data that specify the positions and velocities associated with the wall model and the source of the impact (typically, a barge train). These positions and velocities are entered in feet and feet/second, respectively. The rest of the program assumes English units for version 1.0. The geometry information assumes a right-handed coordinate system, with the lock approach wall lying along the Y-axis (i.e., the longitudinal direction) and the X-axis proceeds into the wall (i.e., the transverse direction).

The first section, at the upper left corner of the tab, is the selection of the type of wall to analyze. The choices reflect the three types of walls discussed previously; flexible approach walls, guard walls, and impact decks. Selecting any of these options changes the inputs available for the rest of the program. Figures 5.2 through 5.4 show the Geometry Tab when each of the options is selected.

Figure 5.2 Geometry for a flexible wall.

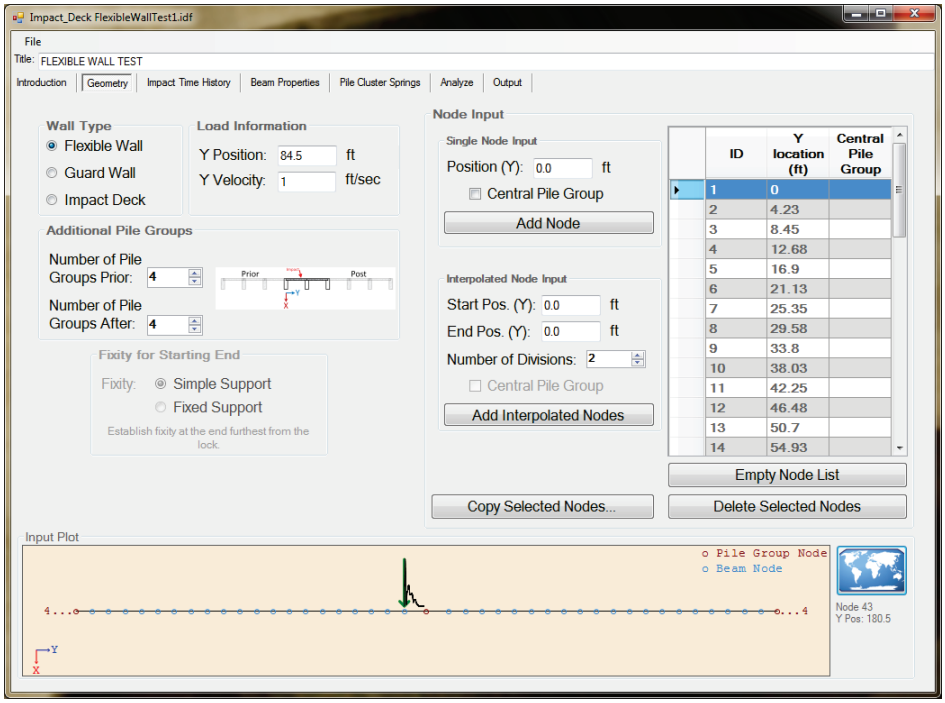


Figure 5.3 Geometry for a guard wall.

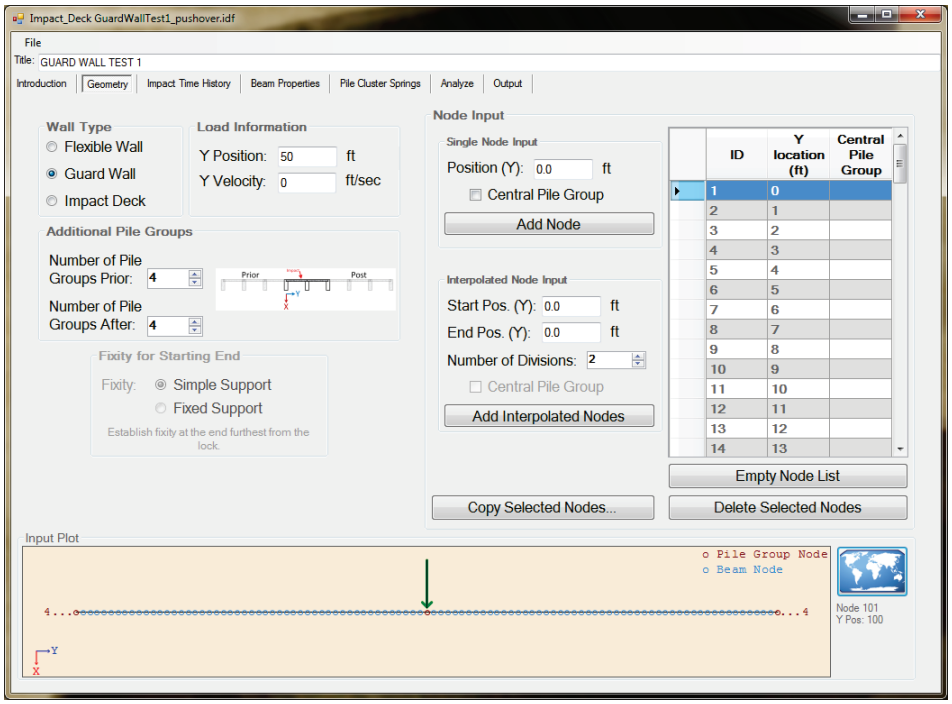
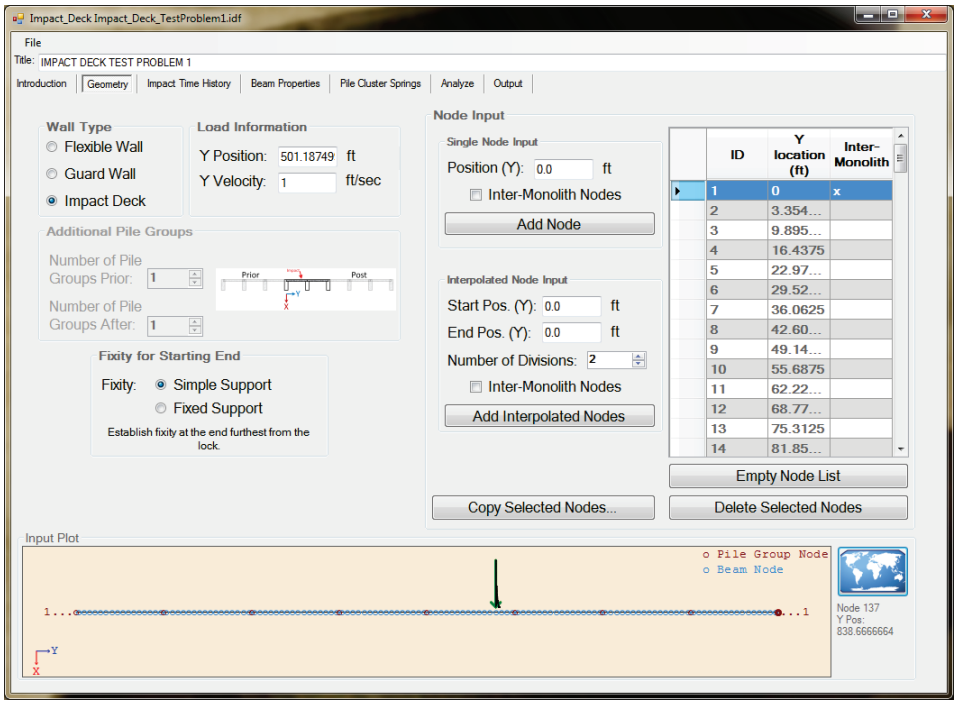


Figure 5.4 Geometry for an Impact_Deck.



The second subsection is unaffected by the approach wall type. This is the load information subsection. In this subsection are the inputs for the Y-position for the start of the impact and the velocity at which the impact

travels along the wall. The impact time history, which is input on the next tab, determines the duration of the analysis.

For flexible approach walls and guard walls, only two simply supported impact beams on three pile groups are included in the model. The Additional Pile Groups section allows the user to specify the number of pile groups that exist prior to and after the modeled section, so that those pile groups can contribute to the response.

An impact deck consists of a series of impact monoliths with each monolith supported by clustered groups of piles. The impact deck structure is modeled as an entire set of beams spanning between multiple pile supports. Each pile support is modeled as a pair of transverse and longitudinal nonlinear springs (established through a push-over analysis as outlined in Ebeling et al. 2012). The fixity for the Starting End subsection allows the user to specify how the starting end of the approach wall, at the end away from the lock, is affixed. The fixed support constrains the end point in translation and rotation. The simple support has the end of the wall section resting on the connection to the end cell.

At the right of the tab is the nodal input section for the wall. Because the wall always proceeds along the Y-axis, all of the nodes specified by the user can be entered with only a Y-coordinate. This approach wall has its origin at the point along the approach wall that is furthest from the lock chamber.

For the flexible approach wall and guard wall models, the first and last nodes in the wall are automatically assigned to be pile group nodes, but the user must flag one of the internal nodes as associated with the central pile group. The pile group nodes are the nodes where the spring models for the piles resist the impact on the wall. The process for creating the central pile group will be discussed further in this section.

For the Impact_Deck model, most of the nodes are connected to a pile group, but some nodes represent only the connectivity between the sections of impact deck monoliths. These nodes are called inter-monolith nodes. The inter-monolith nodes are not connected to a pile group and have different end-release properties. The process for creating the inter-monolith nodes is similar to the method used to create the central pile group for the flexible wall and guard wall models.

Before discussing the creation and deletion of nodes, the visualization of nodes must be discussed. In the node input section to the right of the tab, there is a list containing the node information. The list will provide the position of the node and if the node is a central pile group/inter-monolith node or not. This list is given to provide the user with specific nodal data.

At the bottom of the tab is the Input Plot area. This plot shows the existing nodes, their connectivity, load conditions on the wall, and the number of pile groups prior and after the displayed wall segment (for flexible wall and guard wall models). The position of the starting point of the barge train impact is shown with an arrow pointing at the wall. The direction of the barge train velocity (parallel to the approach wall) is input prior to specifying an impact-force time history. After an impact-force time history has been selected, the time history is displayed from the starting point until the end of the time history due to the velocity of the impact.

Nodes are displayed with different colors depending on whether the pile is a pile group/inter-monolith node. Blue nodes represent unsupported nodes (no pile group) for the flexible approach wall and guard wall models and regular pile group nodes for the Impact_Deck model. The red nodes represent the pile group nodes for the flexible approach wall and guard wall models and inter-monolith connection nodes for the Impact_Deck model.

When the mouse is moved across the Input Plot window with no mouse button pressed, the node that the cursor is closest to will be highlighted, and information about that node will be presented to the right of the Input Plot window. This is shown in Figure 5.3 and Figure 5.4.

The view in the Input Plot window can be zoomed by click-dragging with the right mouse button (Figure 5.5). The view will be changed to display everything in the selected region with the aspect ratio maintained (Figure 5.6). The button to the right of the Input Plot window with a global map on it is the Zoom Extents button. Clicking this button reveals the entire wall as it is currently defined.

Nodes can be selected by click-dragging with the left mouse button. Nodes that are surrounded by the dragged bounding box will all be selected. Multiple selection regions are not permitted at this time. Selected nodes are drawn with a line through them to differentiate them from the unselected nodes (Figure 5.7). Selected nodes may be copied or deleted, as discussed below.

Figure 5.5 Zooming in the input plot section.

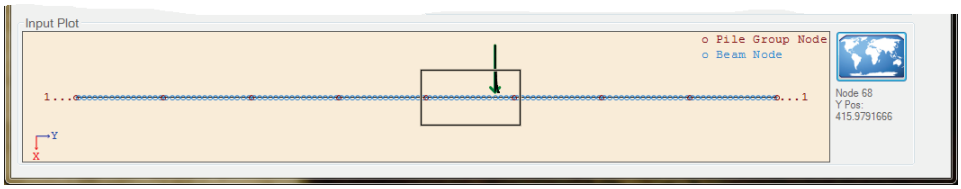


Figure 5.6 The zoomed view.

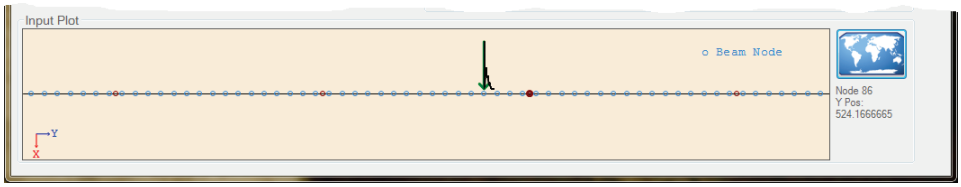
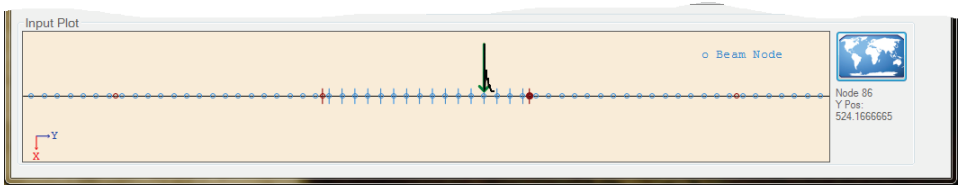


Figure 5.7 Selected nodes are highlighted.



There are three ways to create nodes in the node list. These three methods allow the user to input individual nodes, multiple nodes using interpolation, and copying and pasting nodes.

The Single Node Input subsection allows the user to specify a location along the wall as a Y-axis position. Recall that the wall lies along the Y-axis and that the X-axis is into the wall with a right-handed coordinate system. A checkbox permits the user to specify whether this node is a central pile group node for the flexible wall and guard wall models and an inter-monolith node for the Impact_Deck model. Clicking the Add Node button in this subsection adds the node to the node list and plots it in the Input Plot area. Adding a node at the location where a node already exists will not create a new node, but can change the status of the node to or from a central pile group/inter-monolith node.

Multiple nodes can be input using the Interpolated Node Input subsection. When a start and end position are entered with a number of divisions between nodes in that distance, nodes will be linearly distributed in that distance. The number of nodes placed will be equal to the number of divisions plus one; a node is placed at the start position and then the following nodes are placed at the total length divided by the number divisions away from the previous node, until the end point is reached.

Because there can be only one central pile group, interpolated nodes are not allowed to set that status. However, each node could be an inter-monolith node, so setting that status is allowed. Again, nodes that will be placed at the same location as existing nodes will not create a new node, but can change the status of the existing node.

If there are nodes selected, then nodes can be created by clicking the Copy Selected Nodes button. When the button is selected, the Copy Selected Nodes dialog will appear that asks for an offset for the selected nodes (Figure 5.8). Clicking the Cancel button will terminate the copy event, but clicking Accept will cause the Copy Selected Nodes with Offset dialog box to open (Figure 5.9). Clicking the Accept button in this dialog creates a copy of the selected nodes with their attributes at the offset location relative to the original nodal positions (Figure 5.10). The original nodes are then deselected so they will not be copied again, because the Copy Selected Nodes with an Offset dialog box stays open in case multiple copies of the nodes needs to be made at the same relative distance. Clicking the Cancel button does not copy the last set of selected nodes, and terminates the operation.

There are two methods for removing nodes. The Empty Node List button removes every node in the model. The Delete Selected Nodes button removes only the selected nodes, as shown in the Input Plot window.

Figure 5.8 Entering an offset to copy selected nodes.

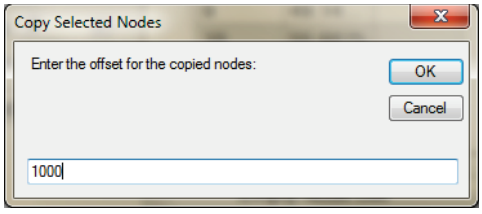


Figure 5.9 Confirming the offset copy (which can be performed multiple times).

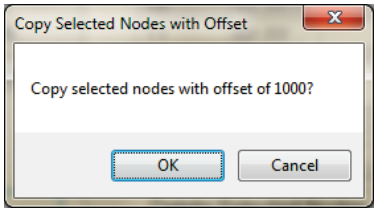
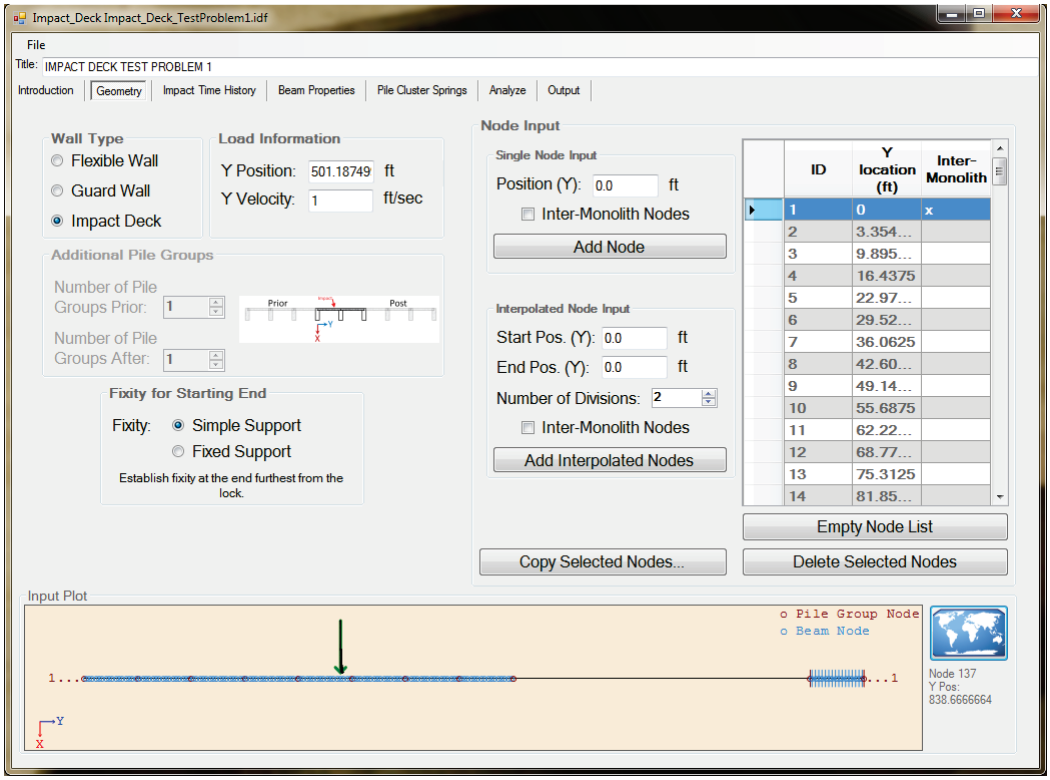


Figure 5.10 Selected nodes are copied at the offset position.



5.3 Impact Time History Tab

The Impact Time History Tab is very simple. There is a method to browse for a time-history file and there is a button to adjust the time history to allow time for the pile-founded impact deck or flexible approach wall to reach a state where little-to-no displacements occur.

The Browse button permits the user to bring in an impact time history file. Currently, the only format supported is the ".ETH" format output by Impact_Force. When an impact time history has been chosen the path for the file selected, relevant comments about the time history and actual values are displayed per Figure 5.11.

The time history can be altered to add samples of zero force at the end to allow time for the dynamic structural response to settle after the deformations have completed. Clicking the Extend Force Time History button brings up the Extend Force Time History dialog. The user can specify a new length for the time history and the time history will be extended to the new length (Figure 5.12).

Figure 5.11 Input for an impact time history.

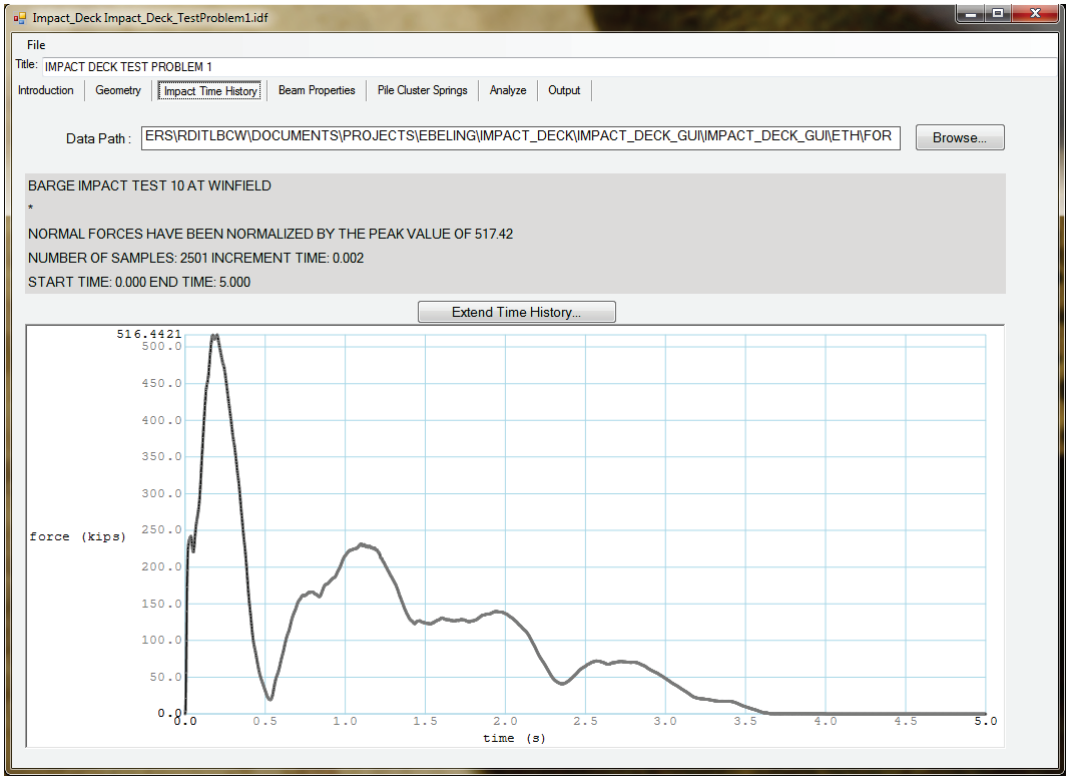
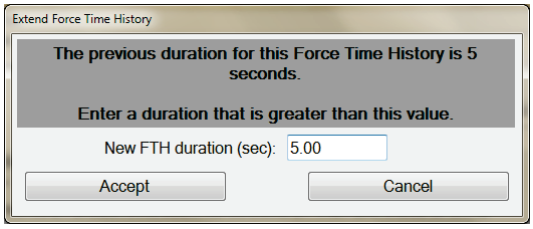


Figure 5.12 Extending a time history with 0.0 value.



5.4 Beam Properties Tab

The beam properties are different depending on whether a flexible approach wall model is chosen or if the guard wall or Impact_Deck model is chosen. For the flexible approach wall model, the beam properties also include the ability of the beam to flex and rotate differently than the guard wall beam or impact deck's deck (Figures 5.13 and 5.14).

The primary beam input, which is shared between the three models, are the Modulus of Elasticity, Cross-sectional Area, Moment of Inertia, Mass per Unit Length, Damping Ratio, and the Coefficient of Friction Between the Barge and the Beam/Deck.

Figure 5.13 Beam properties tab as it appears for a flexible wall.

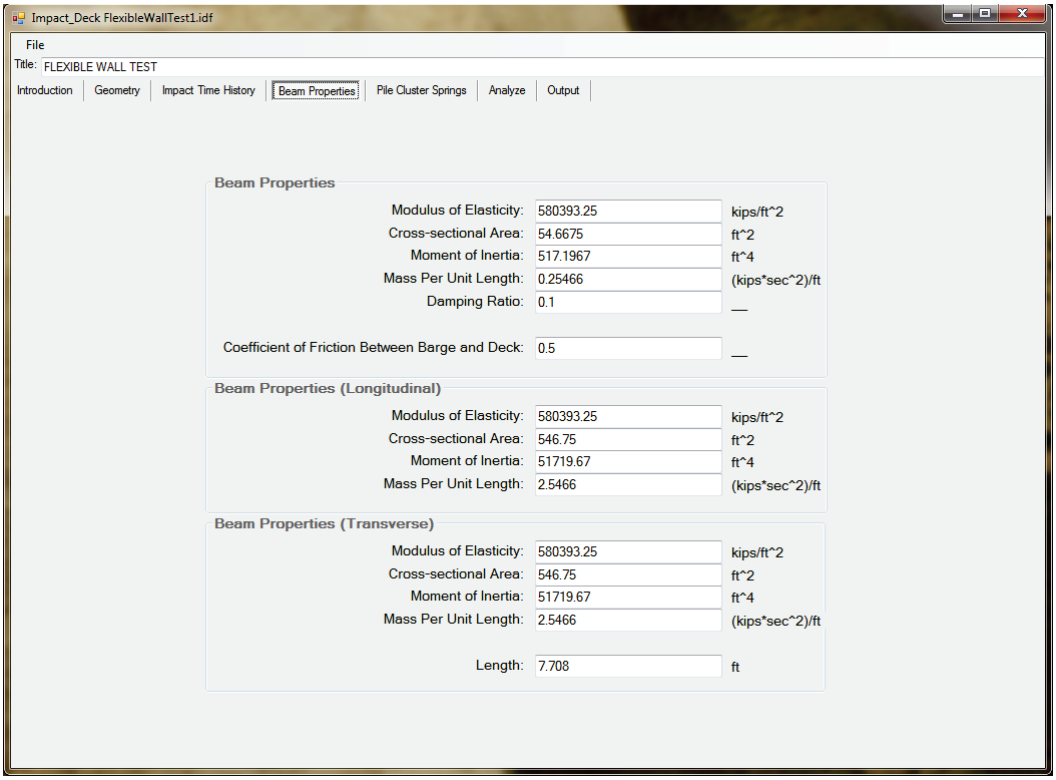
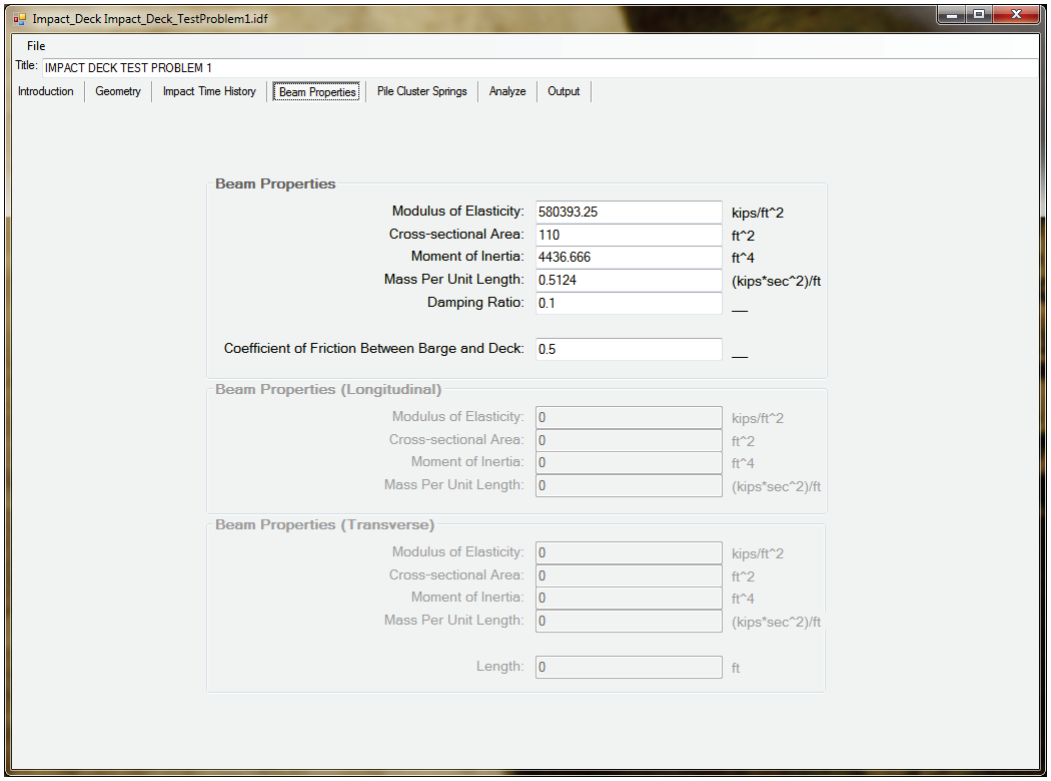


Figure 5.14 Beam properties tab as it appears for an impact deck or guard wall.



Flexible walls have input for properties acting along the beam and transverse to the beam. The longitudinal properties are the Modulus of Elasticity, Cross-sectional Area, Moment of Inertia, and Mass per Unit Length for the length of the wall. The transverse properties are the Modulus of Elasticity, Cross-sectional Area, Moment of Inertia, Mass per Unit Length, and the Length of the wall beam.

5.5 Pile Cluster Spring Tab

For the Impact_Deck software, pile clusters are modeled as non-linear springs. In the Pile Cluster Spring Tab, these non-linear pile cluster springs are defined.

Again, there is a difference based on the wall model being used. Because the flexible approach wall model has pile groups that can rotate, entry of a rotational spring model is allowed (Figure 5.15). Figure 3.1 shows an example of a clustered three-pile group providing rotational resistance, with Appendix E summarizing the computations leading to the value assigned to its rotational spring stiffness. Because the guard wall and the impact deck wall models do not allow the pile caps to rotate, rotational springs are not defined (Figure 5.16).

Figure 5.15 Beam properties tab as it appears for a flexible wall.

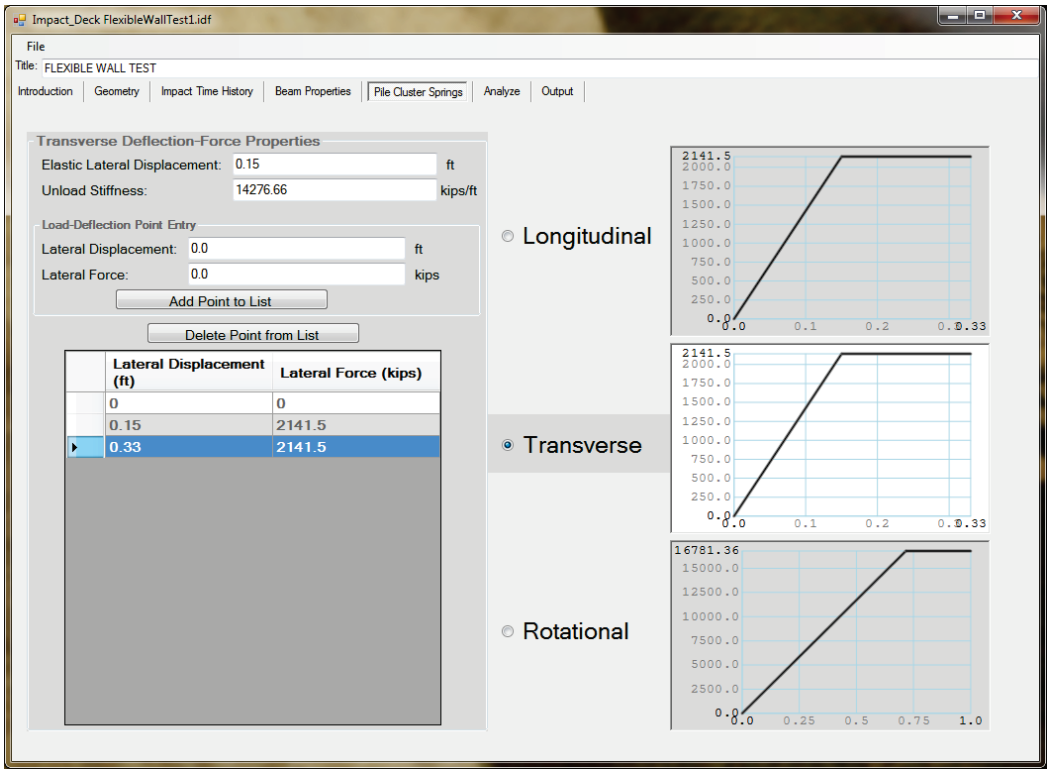
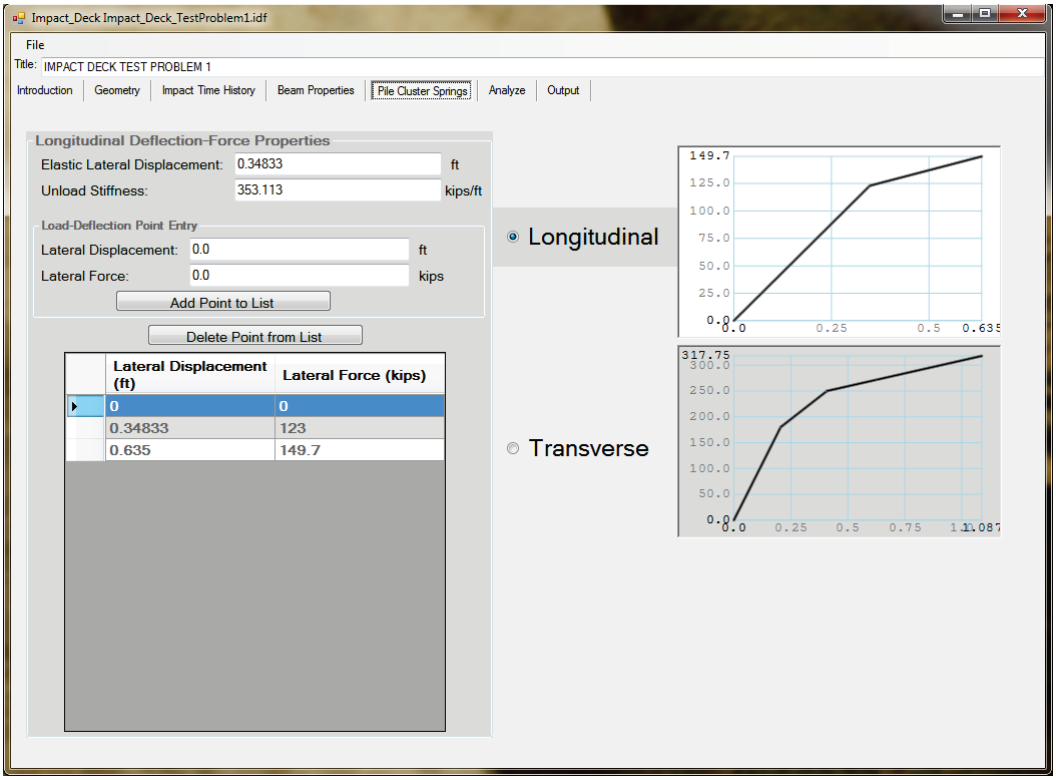


Figure 5.16 Beam properties tab as it appears for an Impact_Deck.



To the right of this tab, there is a graph of the currently defined springs (longitudinal, transverse, and possibly rotational). Radio buttons next to these graphs allow the user to choose the spring definition currently being edited. The currently edited spring definition has a graph with a white background, and its values are displayed in the Edit subsection to the left.

In the Edit subsection, there are three changes the user can apply to the current spring

- Change the Unload/Reload characteristics of the curve
- Add a force-displacement point to the curve
- Delete a force displacement point from the curve

There are two values that can be entered to adjust the Unload/Reload characteristics of the spring model. The first value is the amount of elastic lateral displacement allowed before plastic deformation occurs. The second value is the unload/reload stiffness, which is the force-versus-displacement slope that will be followed from the peak displacement and its force after a plastic deformation has occurred. These values will typically be the point where the first point on the curve is and the slope the

first linear segment makes on the curve, but entry of these values lends more flexibility.

Adding a point to the curve requires that the user enter a displacement and the force at that displacement, and then press the Add Point to List button. The points in the list (which are shown below the Point Entry subsection) are sorted by displacement. The points in the list are plotted in the current graph. Multiple forces may not be entered at the same displacement. When a new displacement/force pair is at the same displacement as an existing point, the new point overrides the previous point.

To delete a point in the current spring model, the user can click on the row in the list for the point. That point is highlighted in blue. Pressing the Delete Point from List button removes the point from the list.

These operations work for each of the spring model types.

5.6 Analyze Tab

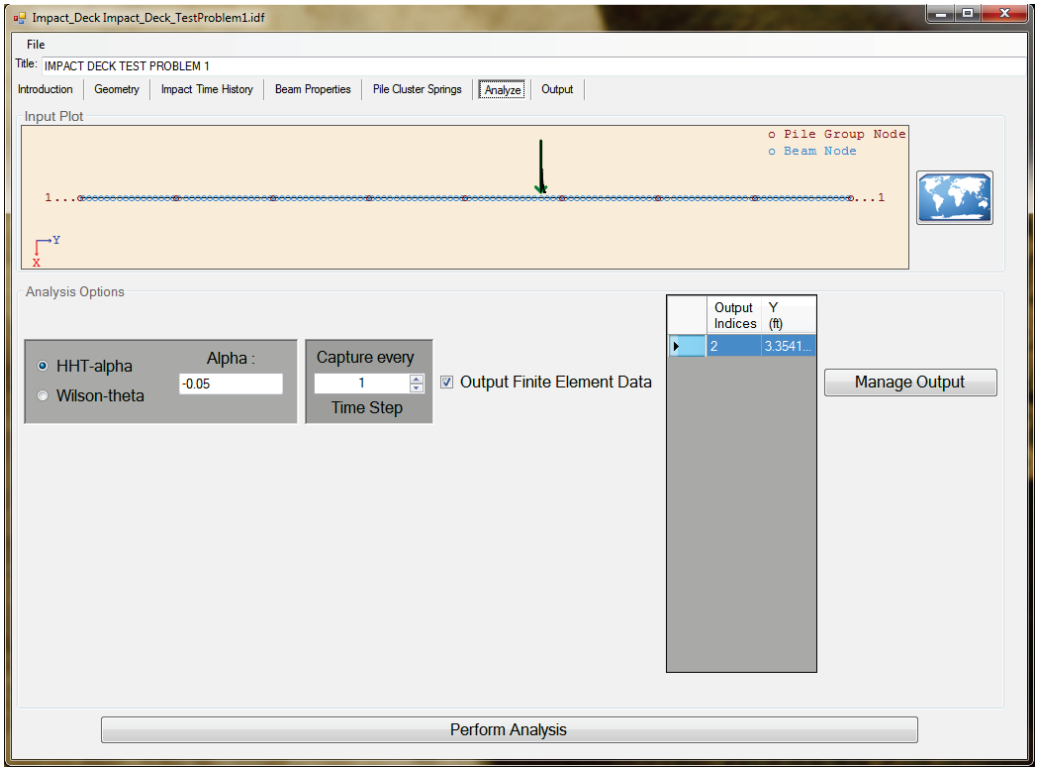
The Analyze Tab (Figure 5.17) allows the user to:

- View his wall model,
- Choose a solution method,
- Set the capture rate for data,
- Select specific elements for more direct Finite Element Data, and
- Perform an analysis.

The input plot display mirrors the input plot display on the Geometry Tab, but does not allow the user to select nodes. In this way, a wall model can be quickly verified.

There are two solution methods that can be applied to compute the dynamic structural response for the approach wall model: the HHT-α method and the Wilson-θ method. Each method has a different tolerance for the solution to be met. For the HHT-α method an alpha tolerance can be specified that must be met to finish the simulation. Similarly, for the Wilson-θ method, a value for Theta can be specified such that the method will converge.

Figure 5.17 Analyze tab input for analysis method and specified output.



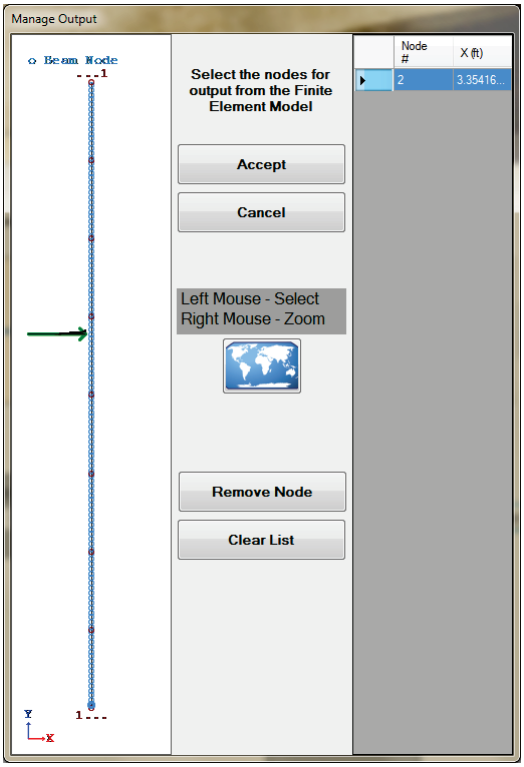
Time-history response analysis of a MDOF structural system model can result in large files of computed time histories for the various output variables. In order to reduce the size of the output files, the following feature has been added: each time step in the computed simulation results can be captured or the user can skip past a designated number of time steps. Entering 1 in the Capture every Time Step subsection guarantees that every time step is captured; entering 2 in the subsection means that every other time step is captured; and entering 3 in the subsection means that every third time step is captured and is repeated thusly.

If the checkbox labeled Output Finite Element Data is checked, then the user can select specific finite element nodes that he/she would like to have text output for. The list next to the checkbox shows the nodes that will currently be output. To change the list, press the Manage Output button.

Pressing the Manage Output button brings up a dialog box that gives the user the power to select output nodes (Figure 5.18). A diagram similar to the Input Plot of the Geometry tab is on the left of the Manage Output dialog. This diagram can be zoomed in much the same manner and a Zoom Extents button is provided. The node selection process works in a

different fashion in the Manage Output dialog. When the user left click-drags an area in the diagram, the nodes are toggled between being selected and not selected. In other words, if a node was selected when the mouse was left click-dragged over it, it will be deselected. This allows the user to select multiple groups of nodes by selecting a group and then deselecting a subgroup. Selected nodes are shown highlighted.

Figure 5.18 Selecting finite element nodes where data will be captured.



A current list of selected nodes is displayed at the right of the dialog. There are also options to delete a node by selecting it from the list and then pressing the Remove Node button, and to clear the entire list by pressing the Clear List button. In order to use the list chosen in the Manage Output dialog, press the Accept button. Pressing the Cancel button keeps the original list.

At the bottom of the Analyze Tab is the button labeled Perform Analysis. When this button is pressed, the processor is started with the current input data.

5.7 Output Tab

In the Output tab, output data files can be selected by the users for visualization of results. There are two main files that are output for each Impact_Deck processor run. There is the .FEO (Finite Element Output) file which contains the node and element results in a time domain solution, and there is the Run File output in .OUT format that explains how the run proceeded and provides only the requested node input from the Analysis Tab, so the user does not have to look for specific information in a very large file.

The Output tab is therefore broken into two sections (Figure 5.19). Each section has a Load Output button, which is used to browse for the specific file. These files are automatically populated with the output from the current input file when the Perform Analysis button is pressed on the Analyze tab. When a file is selected for either section, that section's buttons become enabled, and that file's data is available to be visualized (Figure 5.20).

Figure 5.19 Output tab for selecting and viewing select data.

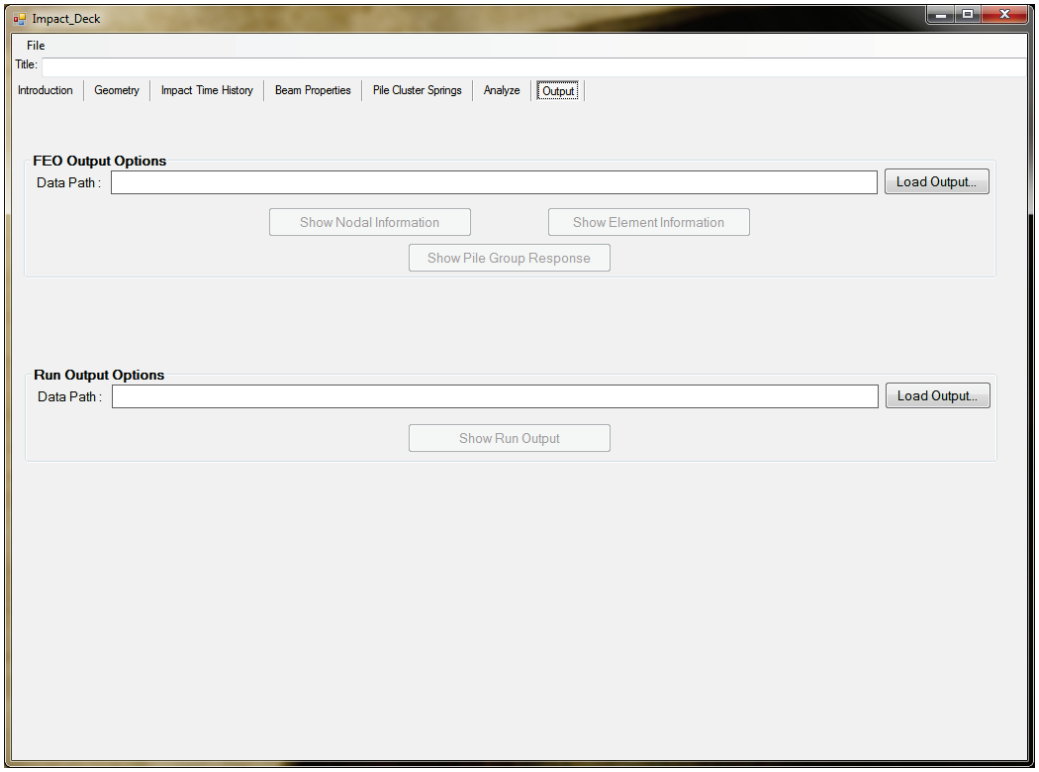
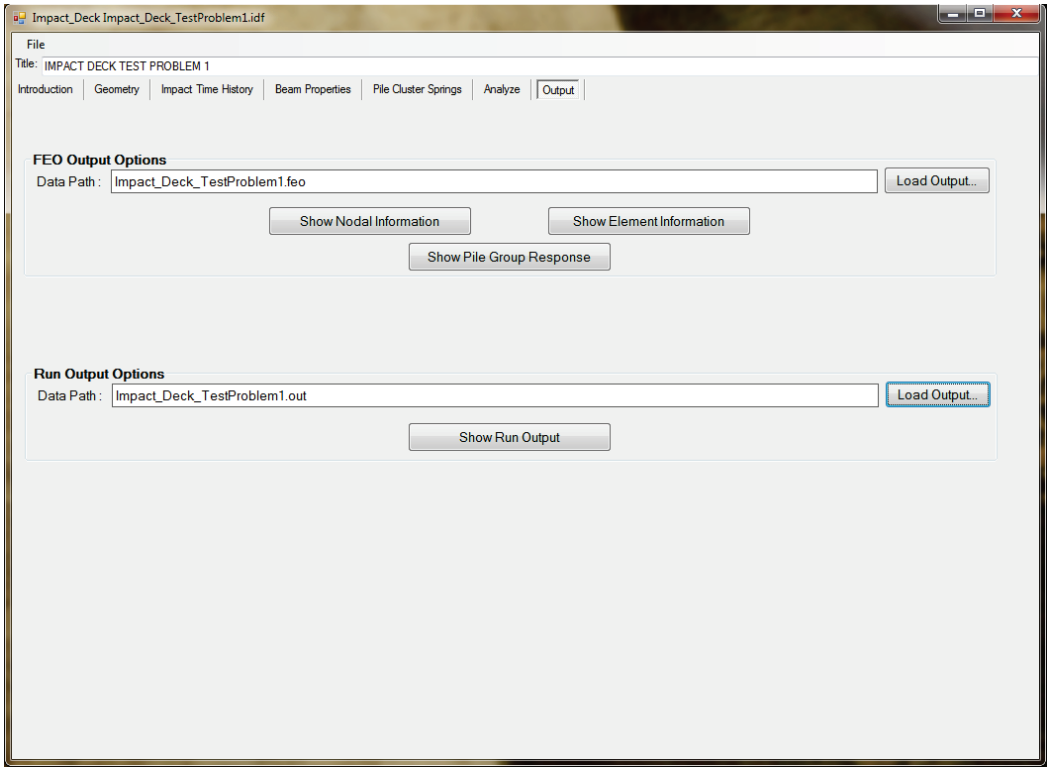


Figure 5.20 Output tab with selected data.



For the FEO output file, there are three data to visualize: the Nodal Information, the Element Information, and the Pile Group Response. For the Run file output, the user can see the text file detailing how the program ran, and the specific finite element information selected on the Analyze Tab. These options are discussed below.

5.7.1 FEO Nodal Output

Pressing the Show Nodal Information button from the Output Tab brings up the FEO Nodal Output window. The window has a minimal menu, with only options to save the currently displayed information (either as text or as a .PNG bitmap graphic file for graphical data) and to close the window. The currently selected file name is displayed immediately below the menu. Beneath the menu are radio buttons that allow the user to present different information from the .FEO file.

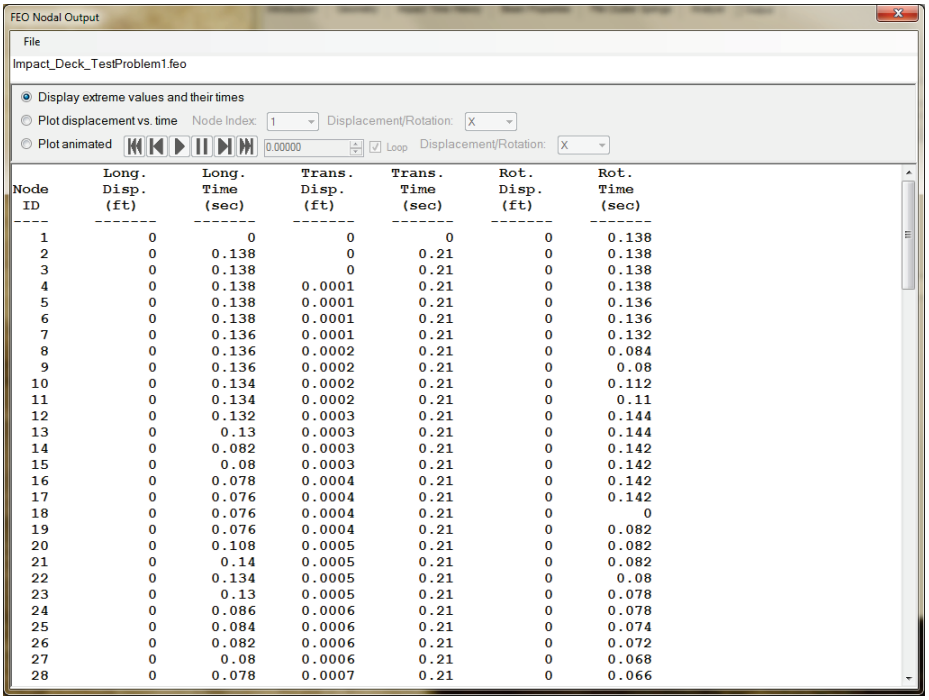
The FEO Nodal Output window presents nodal information in three ways

1. The maximum values of all the nodes are presented as text
2. Individual nodal properties are shown as a 2-D plot of displacement versus time

3. The entire structure is shown as a 2-D animated plot with the structure along the Y-axis, and the displacement along the X-axis.

When the "Display extreme values and their times" radio button is selected, a list of nodes with each node's maximum values of displacement (longitudinal, transverse, and rotation) and the times when those maximums occurred is displayed (Figure 5.21). The longitudinal displacements occur along the wall beam, transverse displacements occur into the wall beam, and rotations occur about the node in the beam.

Figure 5.21 FEO nodal output window showing maximum nodal values for all the nodes.



Node ID	Long. Disp. (ft)	Long. Time (sec)	Trans. Disp. (ft)	Trans. Time (sec)	Rot. Disp. (ft)	Rot. Time (sec)
1	0	0	0	0	0	0.138
2	0	0.138	0	0.21	0	0.138
3	0	0.138	0	0.21	0	0.138
4	0	0.138	0.0001	0.21	0	0.138
5	0	0.138	0.0001	0.21	0	0.136
6	0	0.138	0.0001	0.21	0	0.136
7	0	0.136	0.0001	0.21	0	0.132
8	0	0.136	0.0002	0.21	0	0.084
9	0	0.136	0.0002	0.21	0	0.08
10	0	0.134	0.0002	0.21	0	0.112
11	0	0.134	0.0002	0.21	0	0.11
12	0	0.132	0.0003	0.21	0	0.144
13	0	0.13	0.0003	0.21	0	0.144
14	0	0.082	0.0003	0.21	0	0.142
15	0	0.08	0.0003	0.21	0	0.142
16	0	0.078	0.0004	0.21	0	0.142
17	0	0.076	0.0004	0.21	0	0.142
18	0	0.076	0.0004	0.21	0	0
19	0	0.076	0.0004	0.21	0	0.082
20	0	0.108	0.0005	0.21	0	0.082
21	0	0.14	0.0005	0.21	0	0.082
22	0	0.134	0.0005	0.21	0	0.08
23	0	0.13	0.0005	0.21	0	0.078
24	0	0.086	0.0006	0.21	0	0.078
25	0	0.084	0.0006	0.21	0	0.074
26	0	0.082	0.0006	0.21	0	0.072
27	0	0.08	0.0006	0.21	0	0.068
28	0	0.078	0.0007	0.21	0	0.066

When the "Plot displacement vs. time" radio button is selected, the user can select a node to view using the "Node Index" combo box. When a node has been selected, the user can select whether to plot the node's X-displacement, Y-displacement, or Rotation versus Time in the plot below by selecting from the "Displacement/Rotation" combo box.

When these options have been selected, the graphic window below shows the relevant plot (Figures 5.22 through 5.24). At the top of the display is the selected node number and selected displacement. To the left of the plot is a display of the coordinate system and the wall with nodes and connectivity. The selected node is displayed in red to highlight where the node is in

Figure 5.22 Graph of node 70 X-displacement vs time.

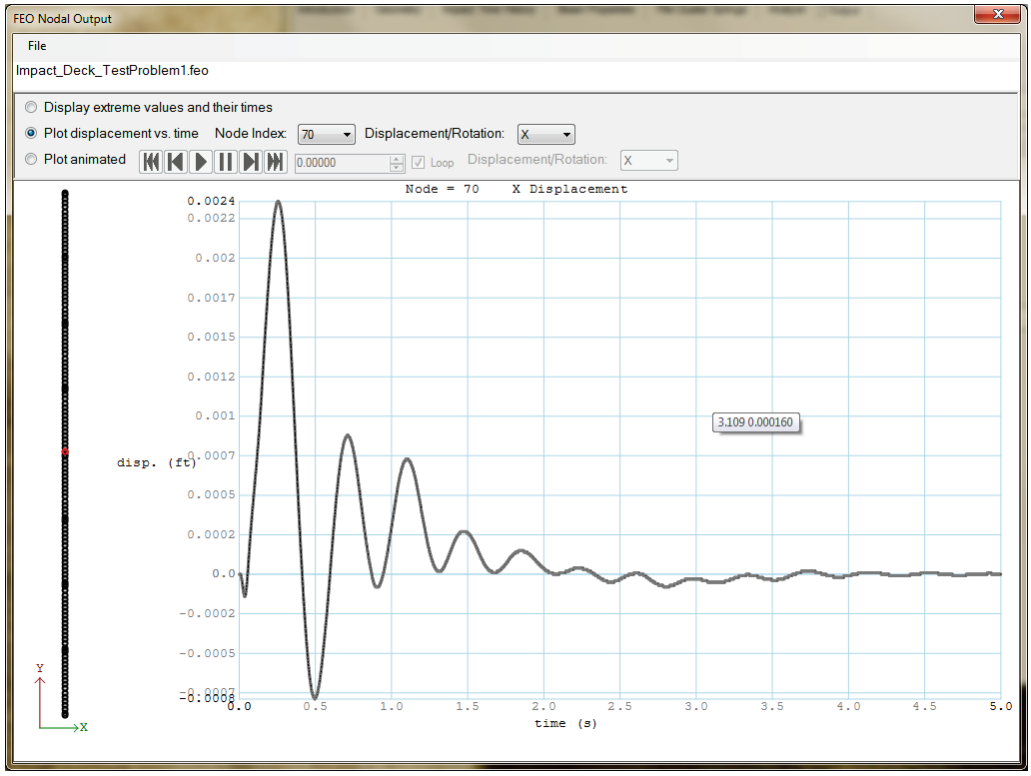


Figure 5.23 Graph of node 70 Y-displacement vs time.

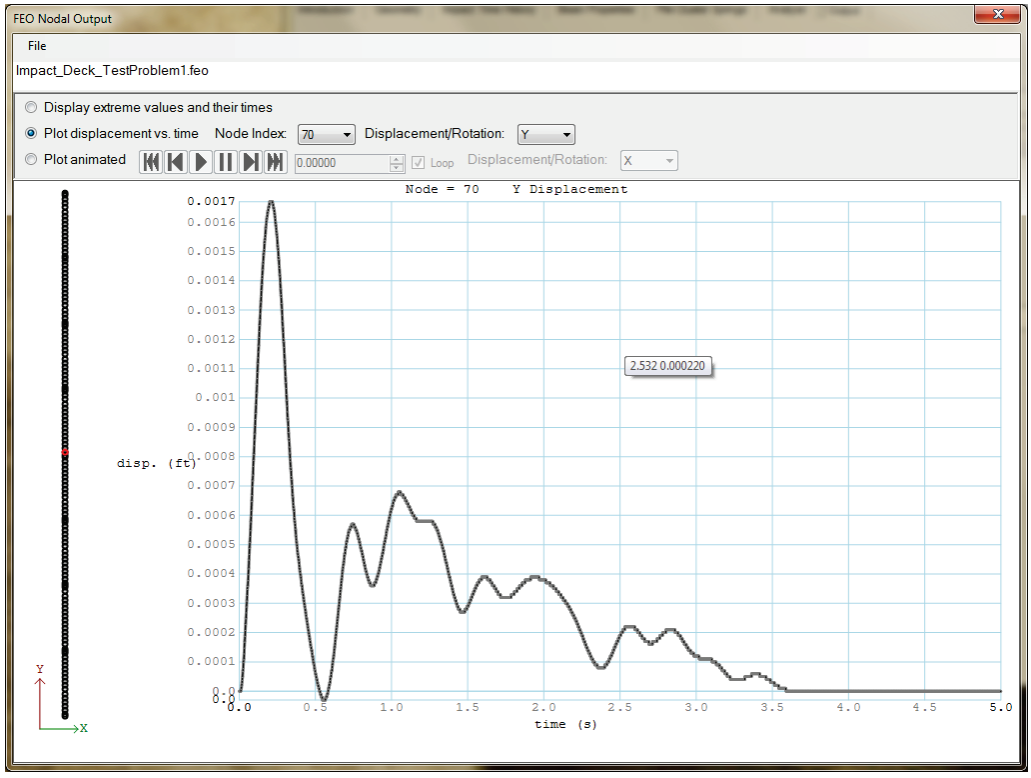
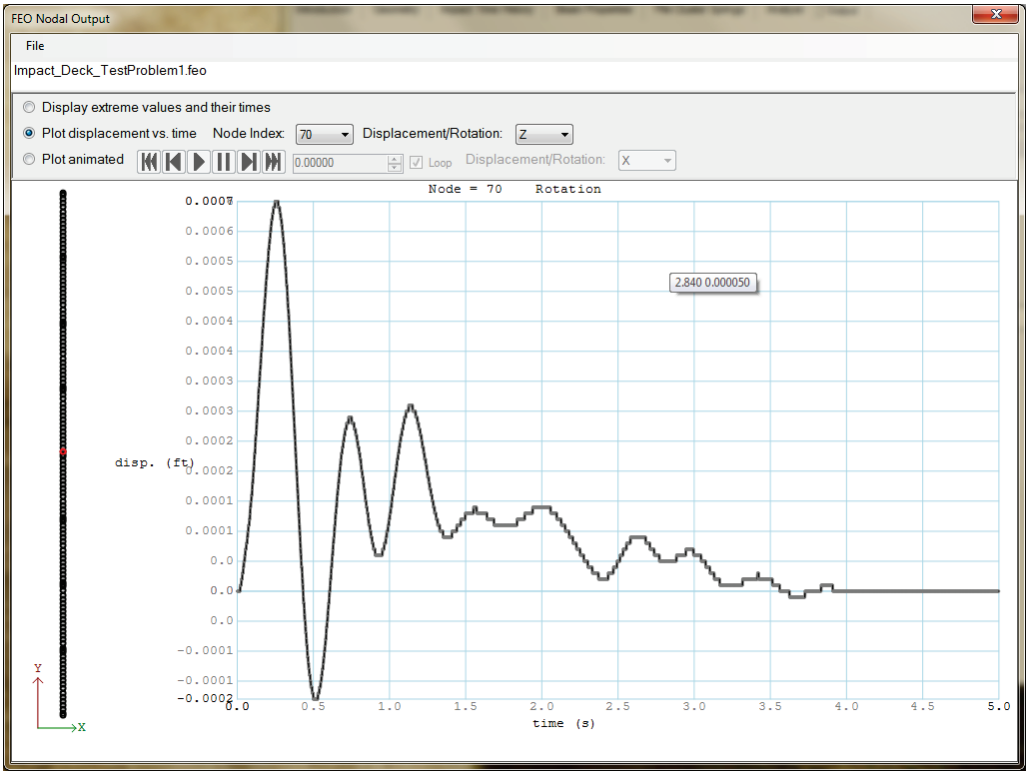


Figure 5.24 Graph of node 70 Z-displacement vs time.



relation to the wall. The rest of the area is the 2-D plot of the displacement versus time for the selected node and displacement. When the mouse is placed over this plot, a tooltip is shown revealing the displacement for the time that the cursor is over.

It should be noticed that some displacements have some artifacts in their plots, typically shown as “staircase steps”. The “staircase steps” occur when the resolution of the data, with small numbers, outstrips the precision of the floating point variables used to represent the data. Aggregating this data leads to discontinuities in the curve which appear as “steps”. These steps occur in the low amplitude region of the curve which is inconsequential to the design. Notice in Figure 5.24 that the image depicts the vertical displacement of a node of the impact model and that the vertical displacement only varies by 0.0009 inches at the extremes, which will have an inconsequential bearing on the response forces of the structure.

When the “Plot animated” radio button is selected, the user can select whether to plot the wall’s X-displacement, Y-displacement, or Rotation versus Time in the plot below by selecting from the “Displacement/

Rotation" combo box. The displacements/rotations at each node are linearly interpolated from node to node.

Immediately next to the radio button is the animation control. This control has typical buttons that

- Return the animation to the beginning time step,
- Step to the previous time step,
- Play the animation,
- Pause the animation,
- Step to the next time step, and
- Take the animation to the last time step.

Next to the buttons in the animation control is the current time display. The time display can be stepped up or down using the arrows next to the display. A checkbox next to the current time display allows the user to select if the animation will loop to the beginning or stop when the last time step has been reached.

When these options have been selected, the graphic window below shows the relevant plot (Figures 5.25 through 5.27). At the top of the display is the current time and selected displacement. To the left of the plot is a display of the coordinate system and the wall with nodes and connectivity. The plot of the impact-load time history from the starting position of the impact to the ending impact location, based on the velocity of the impacting barge train, is displayed along the wall. The current location of the load is displayed as a red line along the time history.

Because the impact can have a very low velocity, it can sometimes be hard to see the full impact in the wall view. For that reason, the time history display with a red line showing the current time is shown at the bottom left of the plot for the input impact-force time history.

The rest of the area is the 2-D plot of the displacements of each node relative to the wall. The scaled displacements are shown in the scale along the X-dimension. The nodal displacements are connected with line segments, effectively linearly interpolating the displacements between nodes.

Figure 5.25 Animated graph of wall X-displacement.

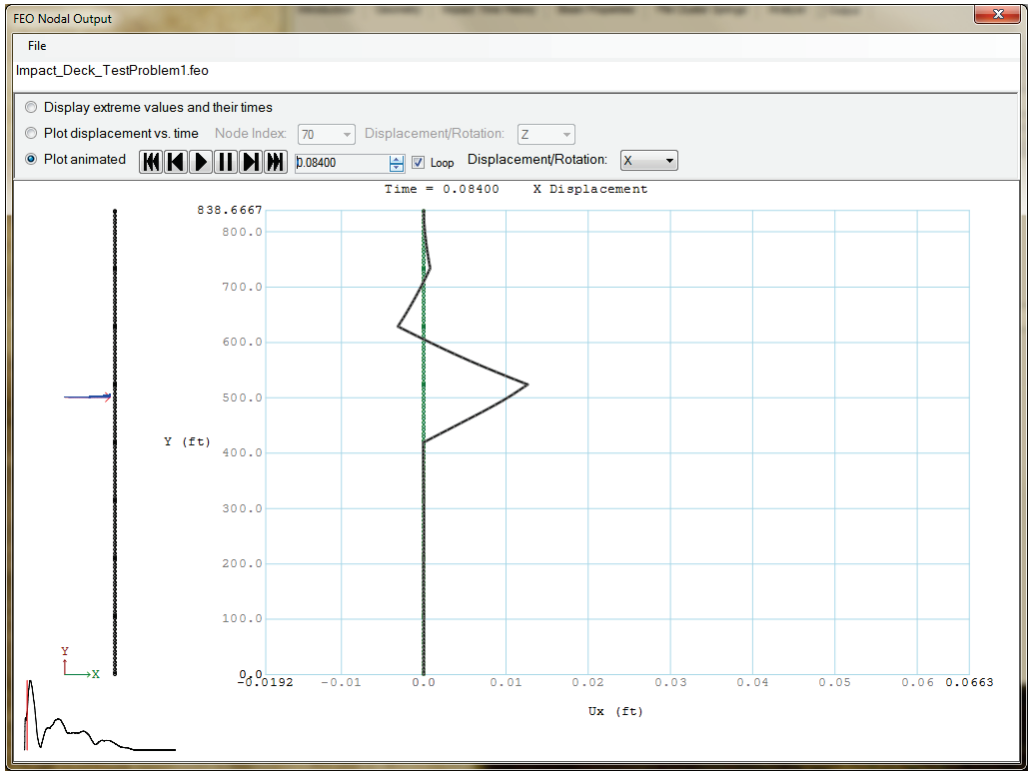


Figure 5.26 Animated graph of wall Y-displacement.

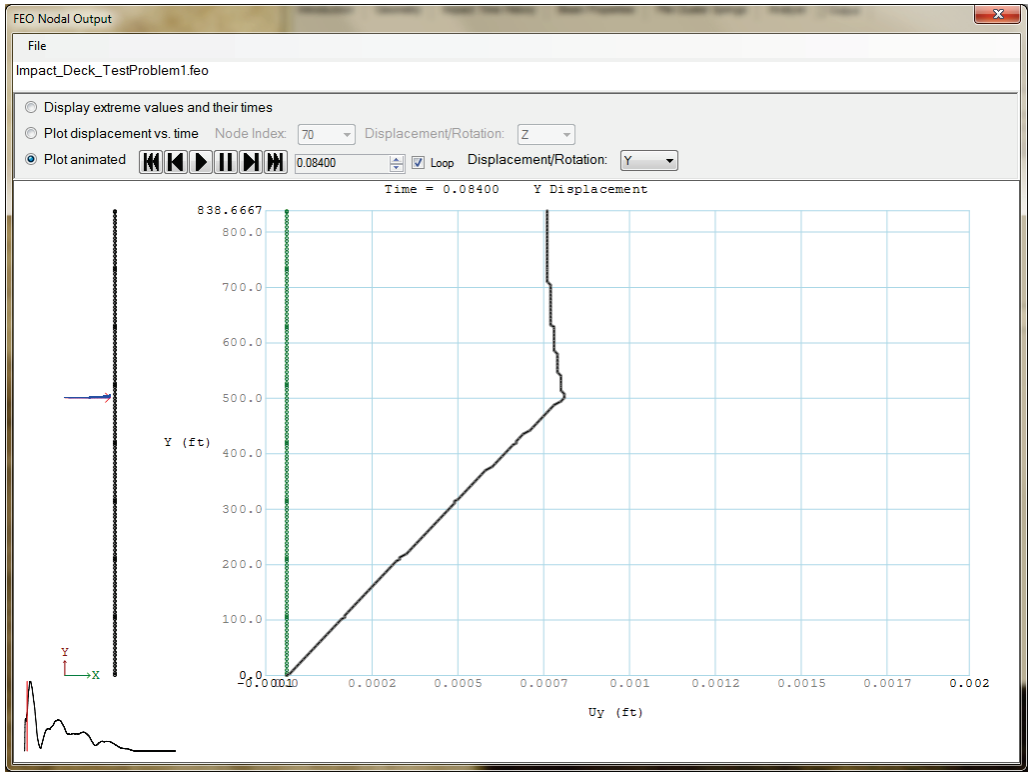
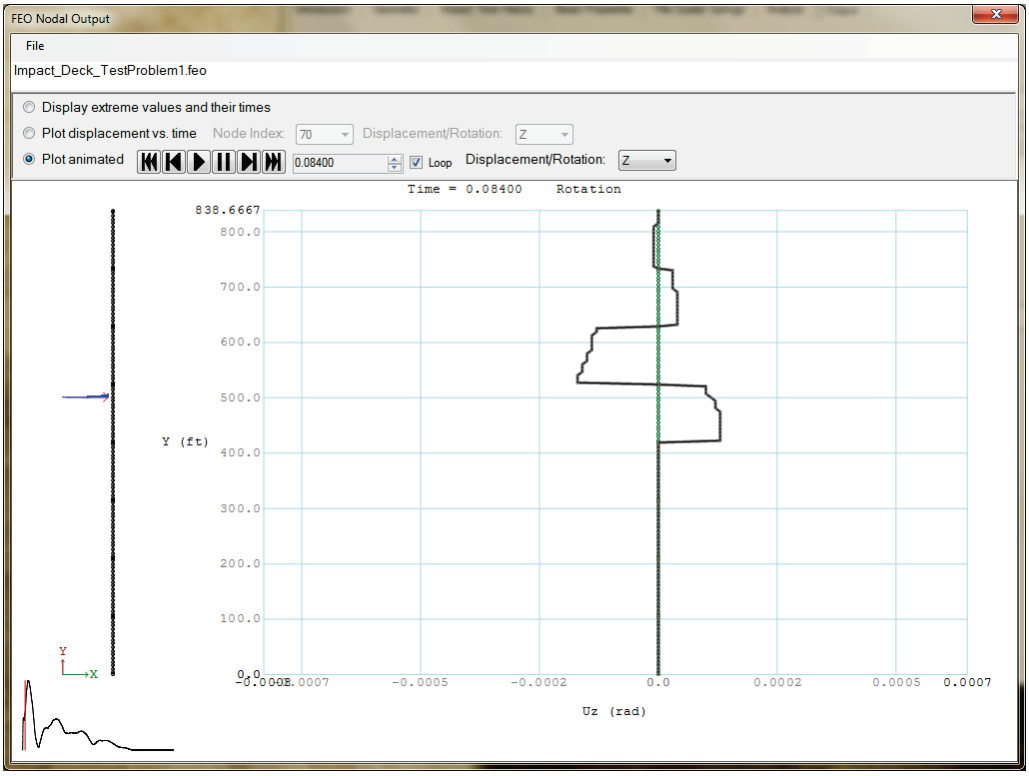


Figure 5.27 Animated graph of wall Z-displacement.



5.7.2 FEO Element Output

Pressing the Show Element Information button from the Output tab brings up the FEO Element Output window. The window has a minimal menu, with only options to save the currently displayed information (either as text or as a .PNG bitmap graphic file for graphical data) and to close the window. The currently selected file name is displayed immediately below the menu. Beneath the menu are radio buttons that allow the user to present different information from the .FEO file.

The FEO Nodal Output window presents element information in three ways

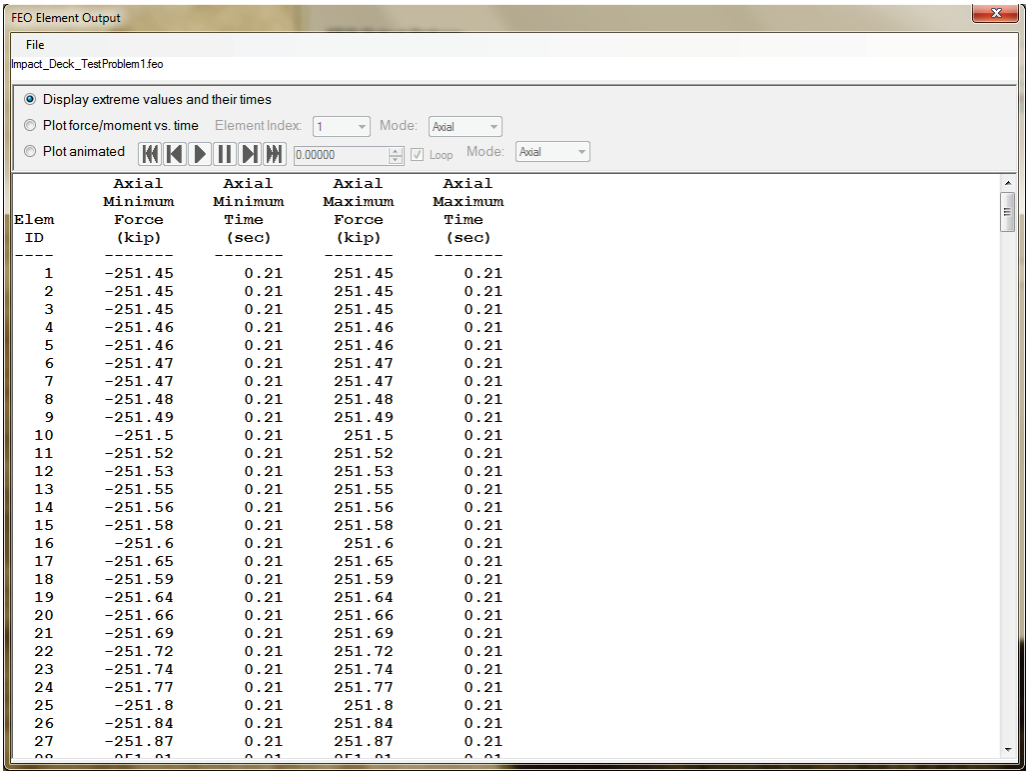
1. The minimum and maximum values of all the elements are presented as text
2. Individual elements are shown as a 2-D plot of force/moment versus time
3. The entire structure is shown as a 2-D animated plot with the structure along the Y-axis, and the force/moment along the X-axis.

When the “Display extreme values and their times” radio button is selected, a set of lists containing each element’s minimum and maximum

force/moment (axial force, shear force, and moment) and the time that those extreme values occurred is displayed (Figure 5.28).

When the "Plot force/moment vs. time" radio button is selected, the user can select an element to view using the "Element Index" combo box. When an element has been selected, the user can decide whether to plot the element's Axial force, Shear force, or Moment versus Time in the plot below by selecting from the "Mode" combo box.

Figure 5.28 FEO element output window showing maximum and minimum force and moments acting on all the elements.



Elem ID	Axial Minimum Force (kip)	Axial Minimum Time (sec)	Axial Maximum Force (kip)	Axial Maximum Time (sec)
1	-251.45	0.21	251.45	0.21
2	-251.45	0.21	251.45	0.21
3	-251.45	0.21	251.45	0.21
4	-251.46	0.21	251.46	0.21
5	-251.46	0.21	251.46	0.21
6	-251.47	0.21	251.47	0.21
7	-251.47	0.21	251.47	0.21
8	-251.48	0.21	251.48	0.21
9	-251.49	0.21	251.49	0.21
10	-251.5	0.21	251.5	0.21
11	-251.52	0.21	251.52	0.21
12	-251.53	0.21	251.53	0.21
13	-251.55	0.21	251.55	0.21
14	-251.56	0.21	251.56	0.21
15	-251.58	0.21	251.58	0.21
16	-251.6	0.21	251.6	0.21
17	-251.65	0.21	251.65	0.21
18	-251.59	0.21	251.59	0.21
19	-251.64	0.21	251.64	0.21
20	-251.66	0.21	251.66	0.21
21	-251.69	0.21	251.69	0.21
22	-251.72	0.21	251.72	0.21
23	-251.74	0.21	251.74	0.21
24	-251.77	0.21	251.77	0.21
25	-251.8	0.21	251.8	0.21
26	-251.84	0.21	251.84	0.21
27	-251.87	0.21	251.87	0.21

When these options have been selected, the graphic window below shows the relevant plot (Figures 5.29 through 5.31). At the top of the display is the selected element number and selected force/moment. To the left of the plot is a display of the coordinate system and the wall with nodes and element connectivity. The selected element is displayed in red to highlight where the element is in relation to the wall. The rest of the area is the 2-D plot of the force/moment versus time for the selected element and force/moment. When the mouse is placed over this plot, a tooltip is shown revealing the force/moment for the time that the cursor is over.

Figure 5.29 Graph showing element 60 axial force vs time.

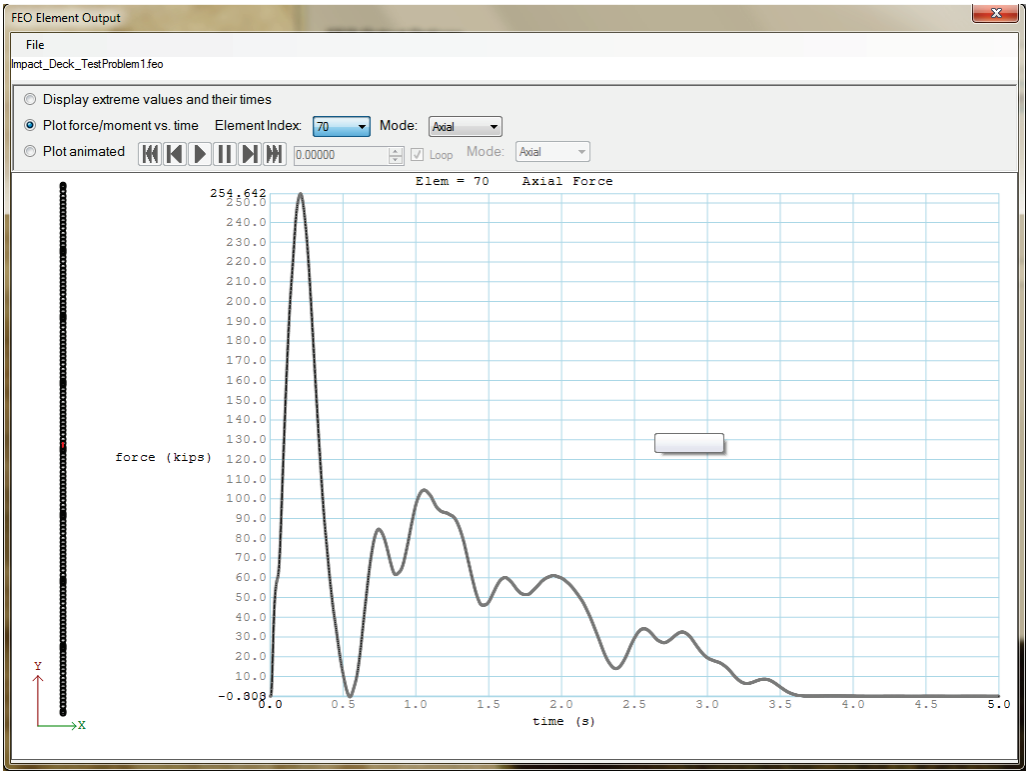


Figure 5.30 Graph showing element 60 moment force-length vs time.

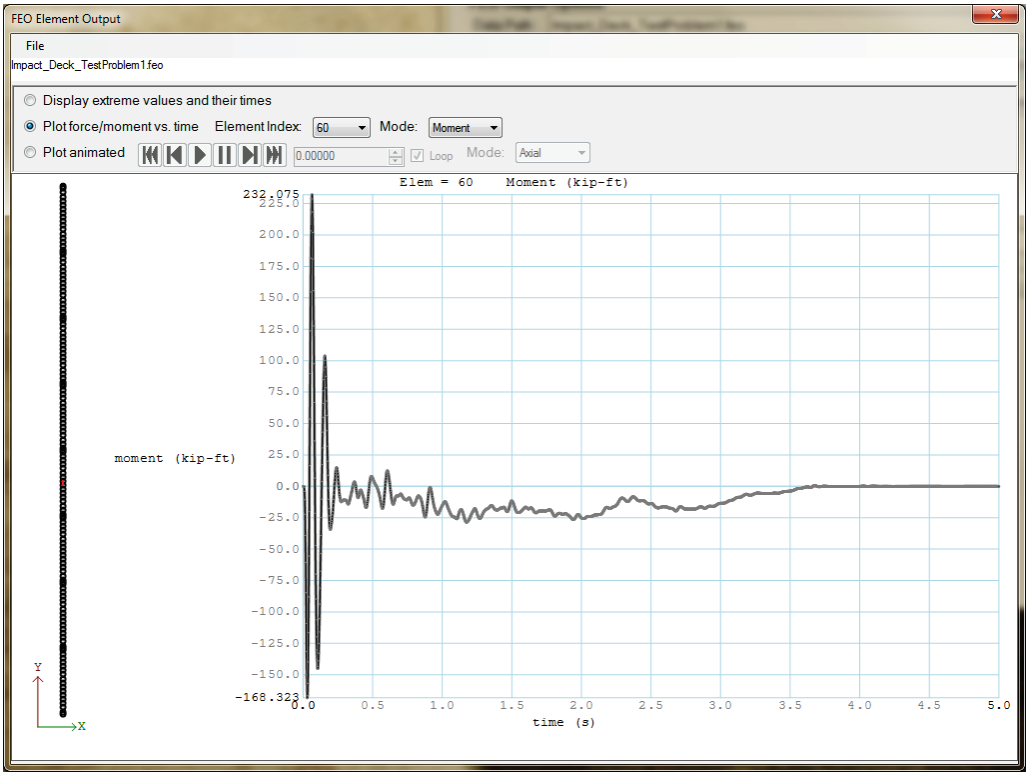
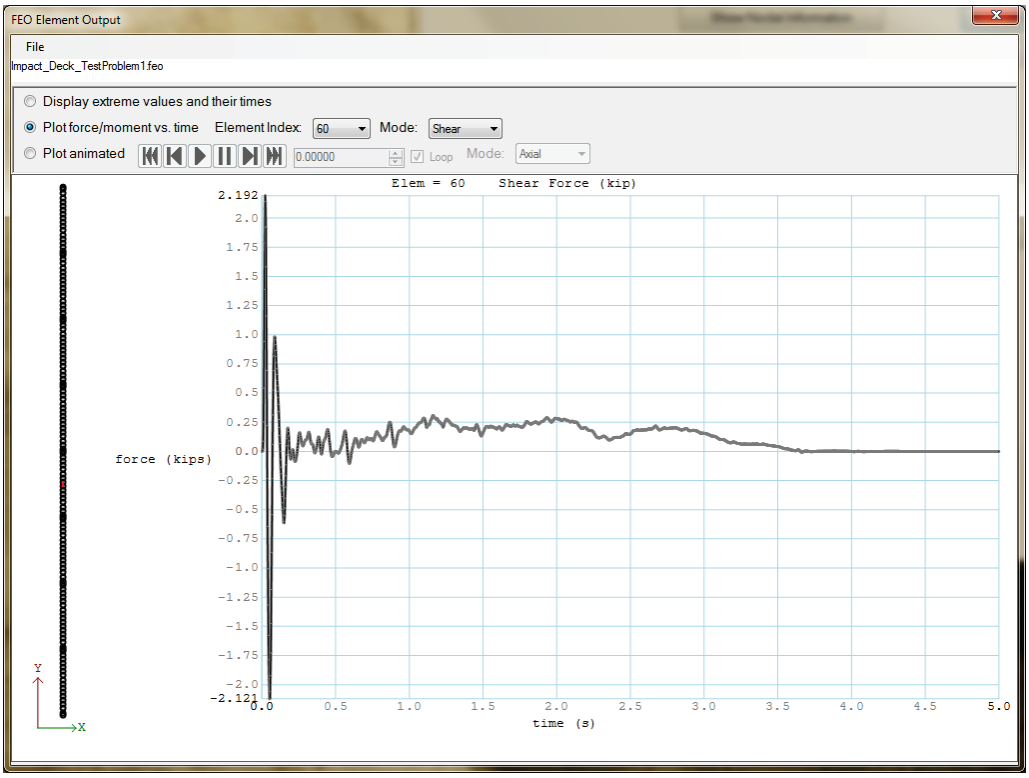


Figure 5.31 Graph showing element 60 shear force vs time.



When the “Plot animated” radio button is selected, the user can select whether to plot the wall’s Axial force, Shear force, or Moment versus Time in the plot below by selecting from the “Mode” combo box. The force/moment at each element is linearly interpolated from element to element. The animation control behaves in the same manner as it did for the FEO Nodal Output window.

When these options have been selected, the graphic window below shows the relevant plot (Figures 5.32 through 5.34). At the top of the display is the current time and selected force/moment mode. To the left of the plot is a display of the coordinate system and the wall with nodes and element connectivity. The plot of the impact-load time history from the starting position of the impact to the ending impact location, based on the velocity of the impacting barge train, is displayed along the wall. The current location of the load is displayed as a red line along the time history.

Because the impact can have a very low velocity, it can sometimes be hard to see the full impact in the wall view. For that reason, the time history display with a red line showing the current time is shown at the bottom left of the plot for the input impact-force time history.

Figure 5.32 Animated graph of axial forces acting on the wall.

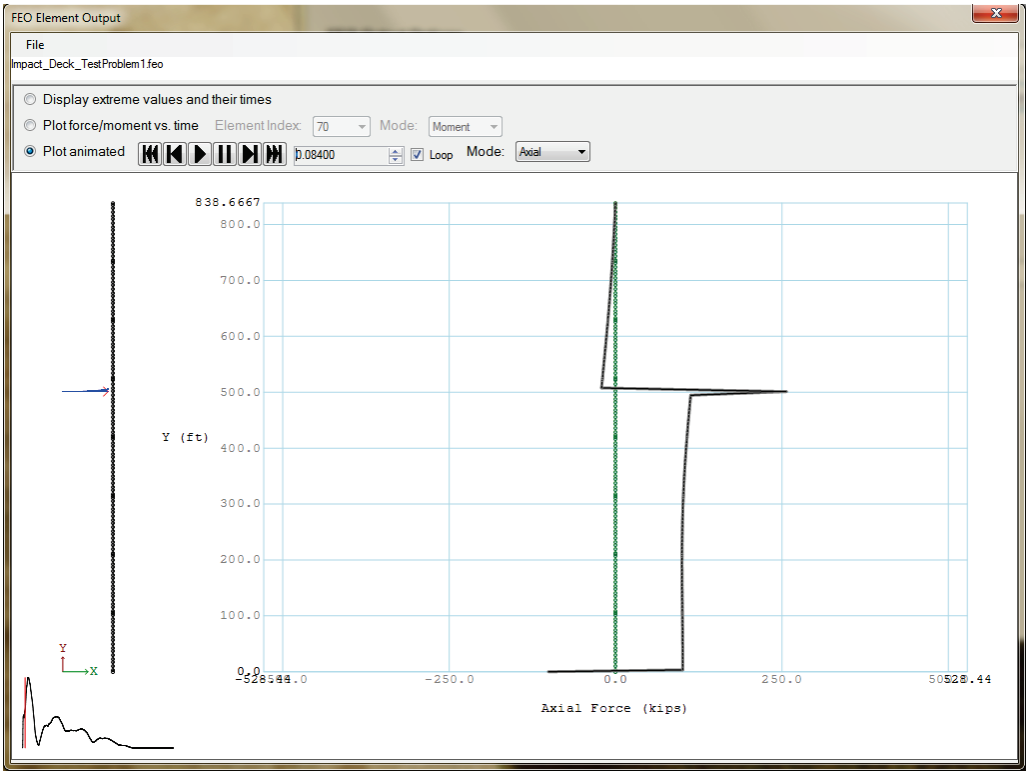


Figure 5.33 Animated graph of moments acting on the wall.

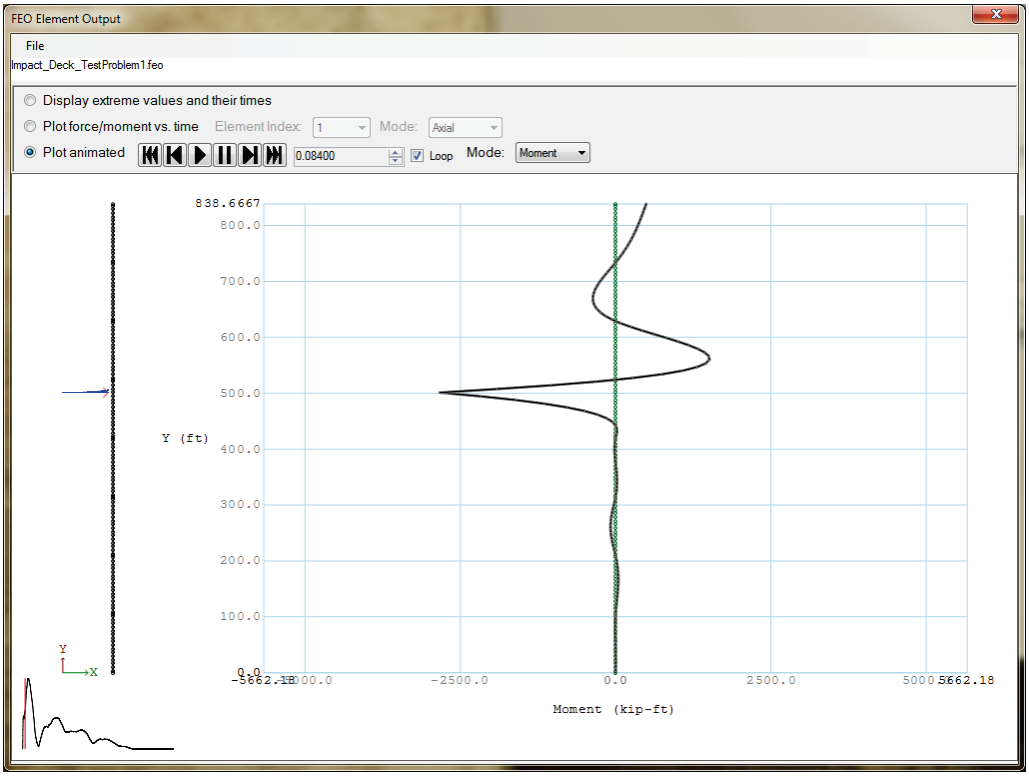
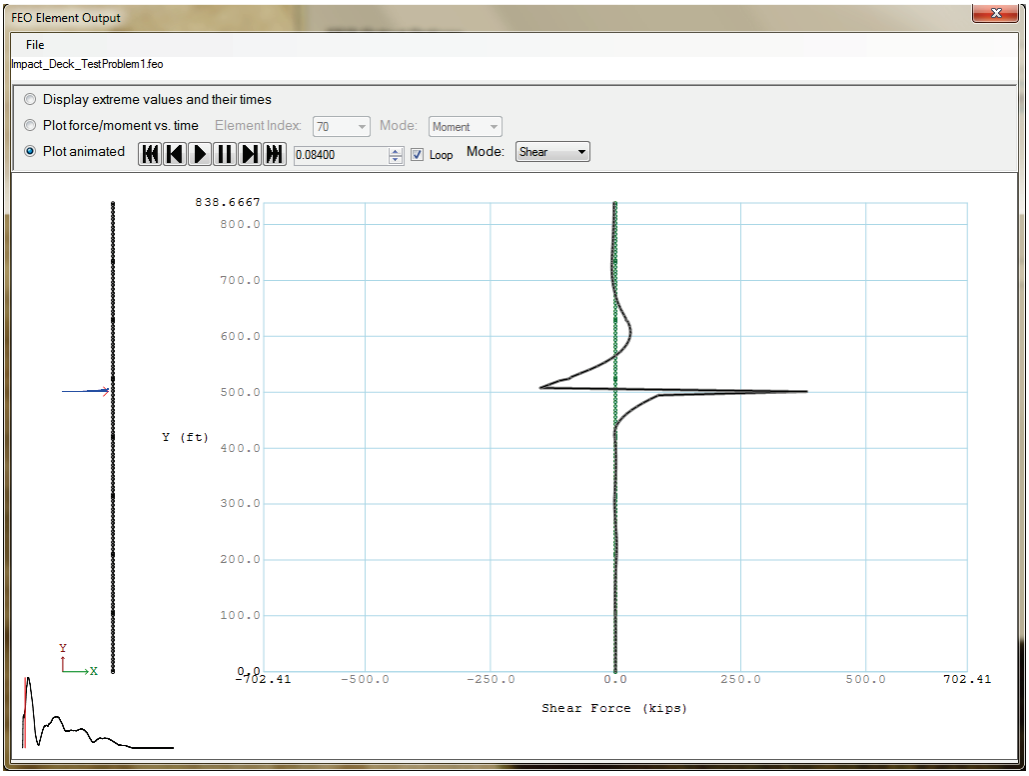


Figure 5.34 Animated graph of shears acting on the wall.



The rest of the area is the 2-D plot of the force/moment of each element relative to the wall. The scaled force/moment is shown in the scale along the X-dimension. The element force/moment is projected to the nodes and the values connected with line segments, effectively linearly interpolating the force/moments between elements.

5.7.3 FEO Pile Group Response

Pressing the Show Pile Group Response button from the Output tab brings up the Pile Group Response window. The window has a minimal menu, with only options to save the currently displayed information (either as text or as a .PNG bitmap graphic file for graphical data) and to close the window. The currently selected file name is displayed immediately below the menu. Beneath the menu are radio buttons that allow the user to present different information from the .FEO file.

The Pile Group Response window presents element information in three ways:

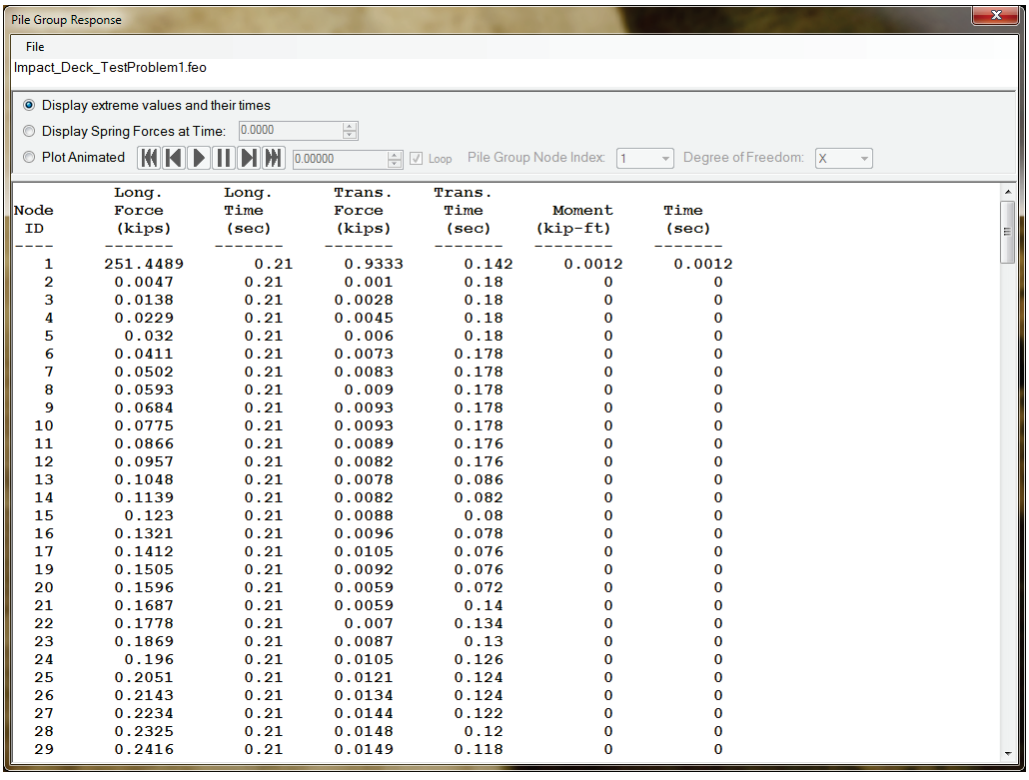
1. The minimum and maximum values of all the pile group nodes are presented as text

2. The force and moment values at any selected time during the analysis are presented as text
3. The entire structure is shown as a 2-D animated plot with the structure along the Y-axis, and the pile group force/moment along the X-axis.

When the "Display extreme values and their times" radio button is selected, a list containing each pile group nodes's minimum and maximum group response force/moment (longitudinal force, transverse force, and moment) and the time that those extreme values occurred (Figure 5.35) and peak displacements and when they occurred (Figure 5.36) are displayed.

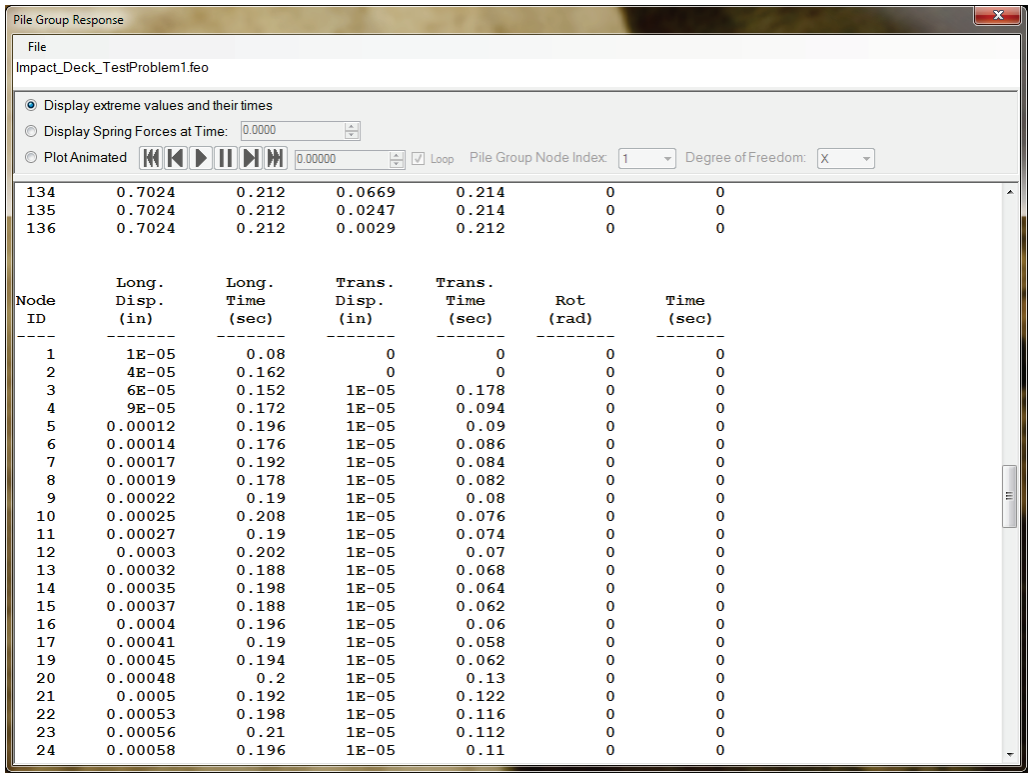
When the "Display Spring Forces at Time" radio button is selected, the user can enter a time in the simulation and get a snapshot of the forces acting at each pile group node at that time (Figure 5.37). At the base of the list, the forces are totaled to give an overall force acting at all of the pile group nodes. Additionally, the total impulse calculations for longitudinal and transverse forces and the moments are presented at the end of the list.

Figure 5.35 Pile Group Response Maximum and Minimum Forces and Moments.



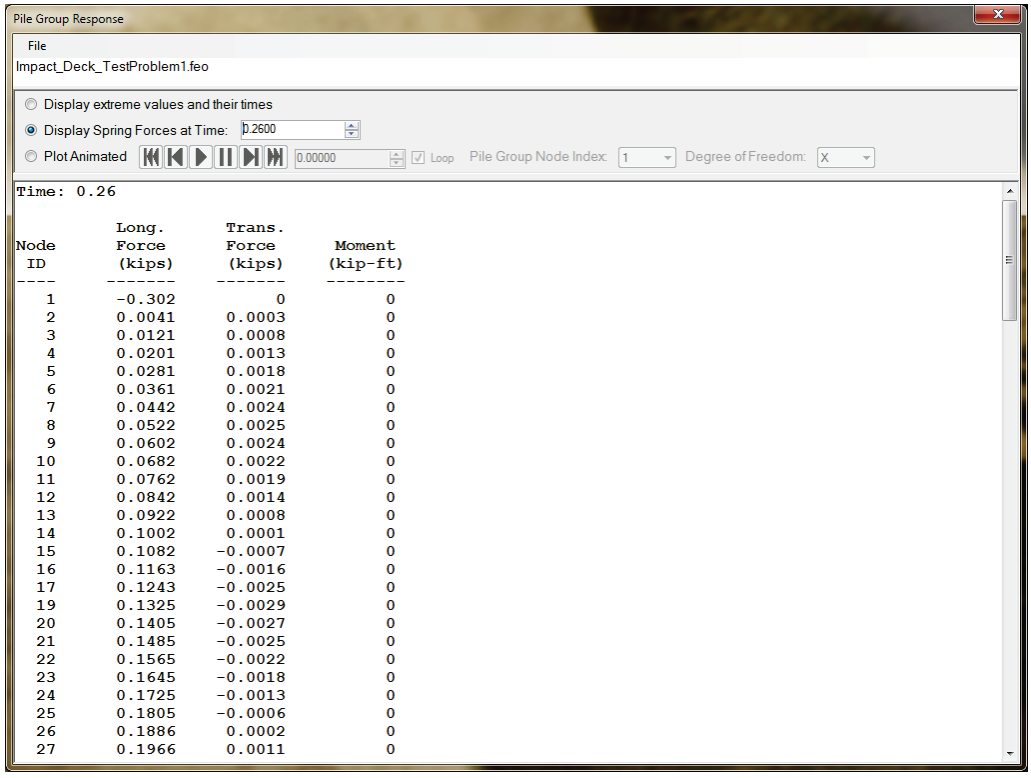
Node ID	Long. Force (kips)	Long. Time (sec)	Trans. Force (kips)	Trans. Time (sec)	Moment (kip-ft)	Time (sec)
1	251.4489	0.21	0.9333	0.142	0.0012	0.0012
2	0.0047	0.21	0.001	0.18	0	0
3	0.0138	0.21	0.0028	0.18	0	0
4	0.0229	0.21	0.0045	0.18	0	0
5	0.032	0.21	0.006	0.18	0	0
6	0.0411	0.21	0.0073	0.178	0	0
7	0.0502	0.21	0.0083	0.178	0	0
8	0.0593	0.21	0.009	0.178	0	0
9	0.0684	0.21	0.0093	0.178	0	0
10	0.0775	0.21	0.0093	0.178	0	0
11	0.0866	0.21	0.0089	0.176	0	0
12	0.0957	0.21	0.0082	0.176	0	0
13	0.1048	0.21	0.0078	0.086	0	0
14	0.1139	0.21	0.0082	0.082	0	0
15	0.123	0.21	0.0088	0.08	0	0
16	0.1321	0.21	0.0096	0.078	0	0
17	0.1412	0.21	0.0105	0.076	0	0
19	0.1505	0.21	0.0092	0.076	0	0
20	0.1596	0.21	0.0059	0.072	0	0
21	0.1687	0.21	0.0059	0.14	0	0
22	0.1778	0.21	0.007	0.134	0	0
23	0.1869	0.21	0.0087	0.13	0	0
24	0.196	0.21	0.0105	0.126	0	0
25	0.2051	0.21	0.0121	0.124	0	0
26	0.2143	0.21	0.0134	0.124	0	0
27	0.2234	0.21	0.0144	0.122	0	0
28	0.2325	0.21	0.0148	0.12	0	0
29	0.2416	0.21	0.0149	0.118	0	0

Figure 5.36 Pile Group Response Peak Deflections.



Node ID	Long. Disp. (in)	Long. Time (sec)	Trans. Disp. (in)	Trans. Time (sec)	Rot (rad)	Time (sec)
134	0.7024	0.212	0.0669	0.214	0	0
135	0.7024	0.212	0.0247	0.214	0	0
136	0.7024	0.212	0.0029	0.212	0	0
1	1E-05	0.08	0	0	0	0
2	4E-05	0.162	0	0	0	0
3	6E-05	0.152	1E-05	0.178	0	0
4	9E-05	0.172	1E-05	0.094	0	0
5	0.00012	0.196	1E-05	0.09	0	0
6	0.00014	0.176	1E-05	0.086	0	0
7	0.00017	0.192	1E-05	0.084	0	0
8	0.00019	0.178	1E-05	0.082	0	0
9	0.00022	0.19	1E-05	0.08	0	0
10	0.00025	0.208	1E-05	0.076	0	0
11	0.00027	0.19	1E-05	0.074	0	0
12	0.0003	0.202	1E-05	0.07	0	0
13	0.00032	0.188	1E-05	0.068	0	0
14	0.00035	0.198	1E-05	0.064	0	0
15	0.00037	0.188	1E-05	0.062	0	0
16	0.0004	0.196	1E-05	0.06	0	0
17	0.00041	0.19	1E-05	0.058	0	0
19	0.00045	0.194	1E-05	0.062	0	0
20	0.00048	0.2	1E-05	0.13	0	0
21	0.0005	0.192	1E-05	0.122	0	0
22	0.00053	0.198	1E-05	0.116	0	0
23	0.00056	0.21	1E-05	0.112	0	0
24	0.00058	0.196	1E-05	0.11	0	0

Figure 5.37 Pile Group Response Maximum and Minimum Forces and Moments.



Time: 0.26

Node ID	Long. Force (kips)	Trans. Force (kips)	Moment (kip-ft)
1	-0.302	0	0
2	0.0041	0.0003	0
3	0.0121	0.0008	0
4	0.0201	0.0013	0
5	0.0281	0.0018	0
6	0.0361	0.0021	0
7	0.0442	0.0024	0
8	0.0522	0.0025	0
9	0.0602	0.0024	0
10	0.0682	0.0022	0
11	0.0762	0.0019	0
12	0.0842	0.0014	0
13	0.0922	0.0008	0
14	0.1002	0.0001	0
15	0.1082	-0.0007	0
16	0.1163	-0.0016	0
17	0.1243	-0.0025	0
19	0.1325	-0.0029	0
20	0.1405	-0.0027	0
21	0.1485	-0.0025	0
22	0.1565	-0.0022	0
23	0.1645	-0.0018	0
24	0.1725	-0.0013	0
25	0.1805	-0.0006	0
26	0.1886	0.0002	0
27	0.1966	0.0011	0

When the “Plot Animated” radio button is selected, the user can plot an individual pile group node’s force-versus-displacement over time. Using the “Pile Group Node Index” combo box, the user can select a pile group node for display. The “degree of freedom” combo box provides the axis that the resulting force is applied. The animation control behaves in the same manner as it did for the FEO Nodal Output window.

When these options have been selected, the graphic window below shows the relevant plot (Figures 5.38 through 5.40). At the top of the display is the current time, the selected pile group node, and selected force axis. To the left of the plot is a display of the coordinate system and the wall with nodes and element connectivity. The selected pile group node is highlighted in red to show the pile group node position relative to the structure. The plot of the impact-load time history from the starting position of the impact to the ending impact location, based on the velocity of the impacting barge train, is displayed along the wall. The current location of the load is displayed as a red line along the time history.

Figure 5.38 Animated plot of node 85 X-force and displacement vs time.

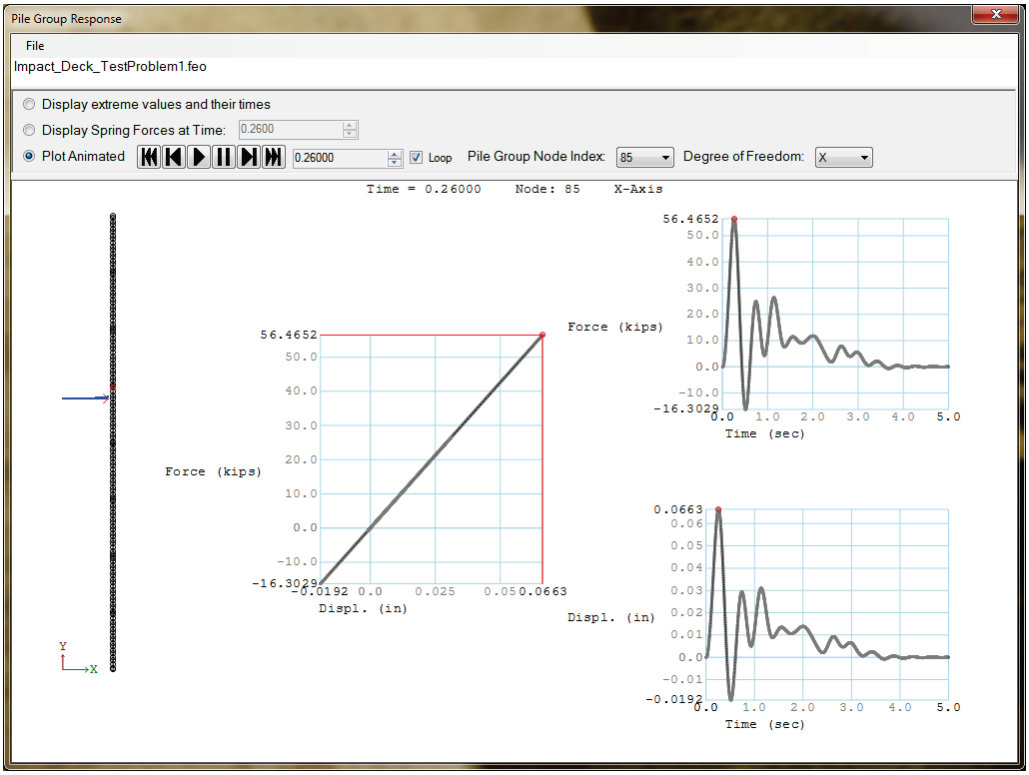


Figure 5.39 Animated plot of node 85 Y-force and displacement vs time.

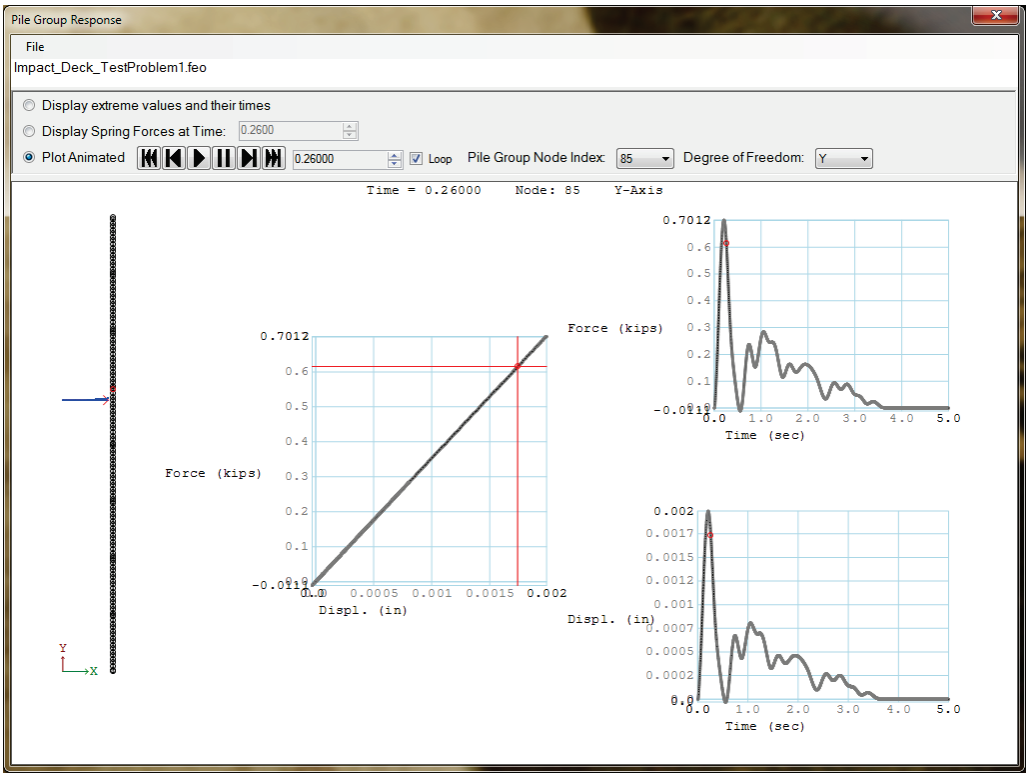
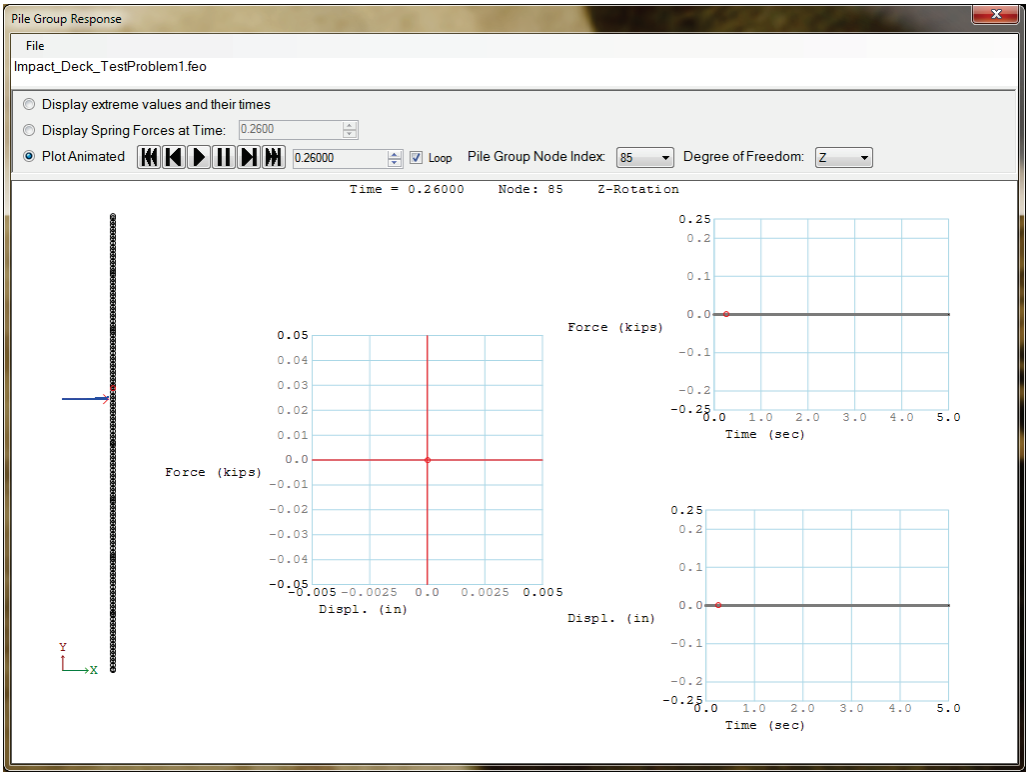


Figure 5.40 Animated plot of node 85 Z-force and displacement vs time.



Besides the wall plot, there are three additional plots. The plot in the upper left is the resultant force-versus-time plot. This force results from spring deformation along the selected axis. A red point shows the current time and its force for the selected pile group node.

The plot in the lower left is the displacement versus time plot. A red point shows the current time and its displacement for the selected pile group node.

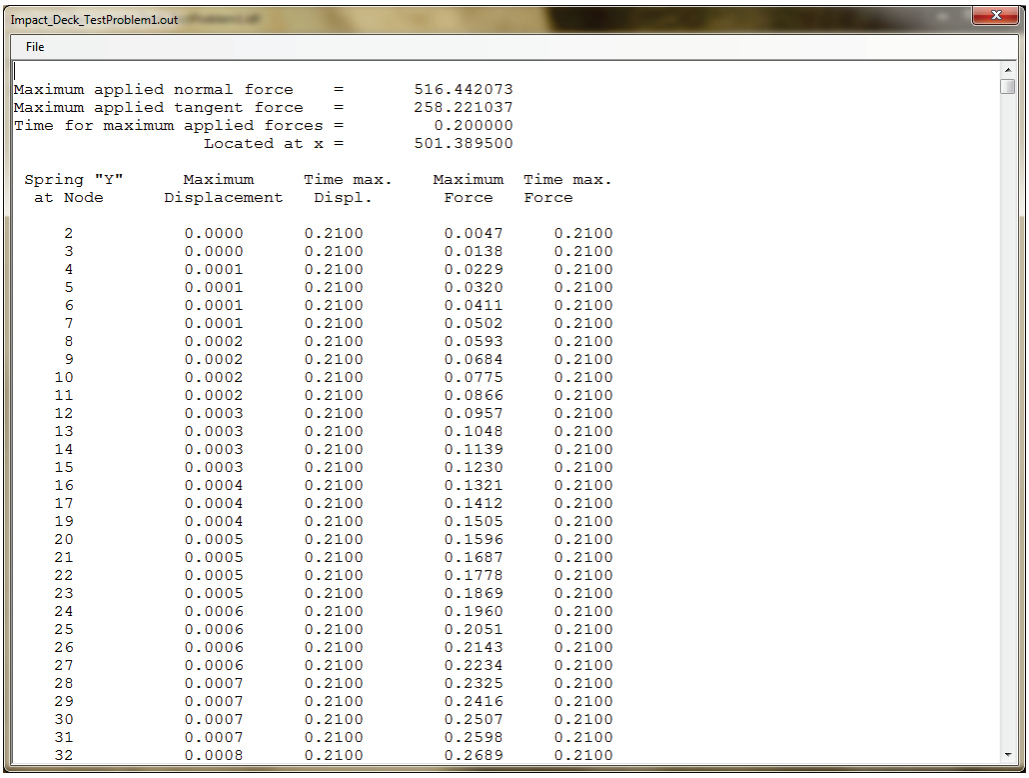
The center plot shows the force-versus-displacement plot. This plot shows how force varies with displacement at the pile group node. Because this graph has axis with values that may be repeated (and therefore is not a mathematical function), the current force and time are located with cross-hairs for the current time.

Note that the Z-axis DOF is not a 3-D axis but a rotational axis at the pile. For pile group nodes that are not connected due to a moment release between deck sections, the force versus the rotational displacement will give a zero value.

5.7.4 Run Information

Pressing the Show Run Output button from the Output Tab brings up a text window with the results of the program run (Figure 5.41). The menu allows the user to save the file to a new location or exit the Run Output window. How the program worked is displayed in this window, as well as any specific finite element data requested in the Analyze Tab.

Figure 5.41 Output run information with selected FEO node output.



Impact_Deck_TestProblem1.out

File

```
Maximum applied normal force    =       516.442073
Maximum applied tangent force   =       258.221037
Time for maximum applied forces =         0.200000
                  Located at x =       501.389500

 Spring "Y"      Maximum     Time max.    Maximum  Time max.
  at Node      Displacement   Displ.       Force   Force

     2           0.0000      0.2100        0.0047     0.2100
     3           0.0000      0.2100        0.0138     0.2100
     4           0.0001      0.2100        0.0229     0.2100
     5           0.0001      0.2100        0.0320     0.2100
     6           0.0001      0.2100        0.0411     0.2100
     7           0.0001      0.2100        0.0502     0.2100
     8           0.0002      0.2100        0.0593     0.2100
     9           0.0002      0.2100        0.0684     0.2100
    10           0.0002      0.2100        0.0775     0.2100
    11           0.0002      0.2100        0.0866     0.2100
    12           0.0003      0.2100        0.0957     0.2100
    13           0.0003      0.2100        0.1048     0.2100
    14           0.0003      0.2100        0.1139     0.2100
    15           0.0003      0.2100        0.1230     0.2100
    16           0.0004      0.2100        0.1321     0.2100
    17           0.0004      0.2100        0.1412     0.2100
    19           0.0004      0.2100        0.1505     0.2100
    20           0.0005      0.2100        0.1596     0.2100
    21           0.0005      0.2100        0.1687     0.2100
    22           0.0005      0.2100        0.1778     0.2100
    23           0.0005      0.2100        0.1869     0.2100
    24           0.0006      0.2100        0.1960     0.2100
    25           0.0006      0.2100        0.2051     0.2100
    26           0.0006      0.2100        0.2143     0.2100
    27           0.0006      0.2100        0.2234     0.2100
    28           0.0007      0.2100        0.2325     0.2100
    29           0.0007      0.2100        0.2416     0.2100
    30           0.0007      0.2100        0.2507     0.2100
    31           0.0007      0.2100        0.2598     0.2100
    32           0.0008      0.2100        0.2689     0.2100
```

5.8 Example: Geometry Input for the Impact Deck at Lock and Dam 3

The example problem for the Lock and Dam 3 impact deck that was input in section 2 present the most complex geometry for GUI input. In this case, the approach wall structure had 8 reinforced concrete monoliths. These monoliths were connected to each other and with the single end cell at the start of the approach wall with a pinned connection, and to the neighboring monoliths through a connection that transfer shear and axial forces but not moments.

The monoliths themselves were to be constructed by connecting together 8 concrete segments that were 12 ft 6 in. in length. Each segment was supported by two pile groups. Each pile group cluster consisted of 3 piles – a vertical pile at the front of the group, closest to where an impact would occur, and two batter piles with a batter of 1:4. The spacing between the pile groups was to be 6 ft 3 in., which resulted in monoliths with a length of 100 ft. These plans changed, as engineering plans often do, due to wall length requirements. The new monolith length ended up becoming 104 ft 10 in. The distance between pile groups grew to 6 ft 3.5 in. The distance from the ends of the monolith to the first and last pile group was 3 ft 4.25 in.

In this case, it was natural to model each monolith as a set of nodes in the Impact_Deck GUI, and then copy the monolith nodes 7 times (for 8 monoliths). The end nodes of the first monolith were the connecting nodes. These nodes were at 0 ft 0 in. and 104 ft 10 in., which translated to decimal feet of 0.0 ft and 104.833 ft. Because inches did not convert to nice decimal feet, the user must determine his or her personal level of precision. Because that last node was coincident with the first node of the next monolith, the last node does not needed to be entered as it will be created in the copy and offset command. Therefore, the user only needs to place a node at position 0.0 ft. Because it was an inter-monolith node, the check-box was checked to flag the node (Figure 5.42).

The rest of the nodes in the monolith represented each pile group location in the monolith. These monolith groups started 3 ft 4.25 in. from the start of the monolith (at 0 ft 0 in.) and ended at 3 ft 4.25 in. from the end of the monolith (at 104 ft 10 in.). These coordinates in decimal feet were 3.354 ft and 101.479 ft, respectively. There were 16 pile groups in the monolith with 15 divisions between them. Entering these values into the "Interpolated Node Input" box (with the inter-monolith nodes check-box unchecked) created the nodes for the pile groups (Figure 5.43).

Figure 5.42 Add node at position 0.0 ft as an inter-monolith node.

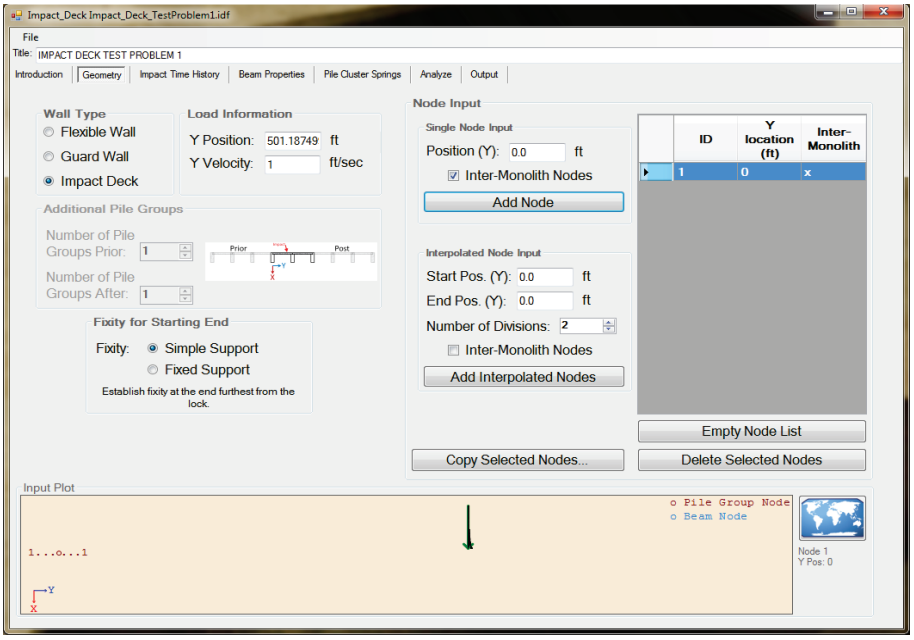
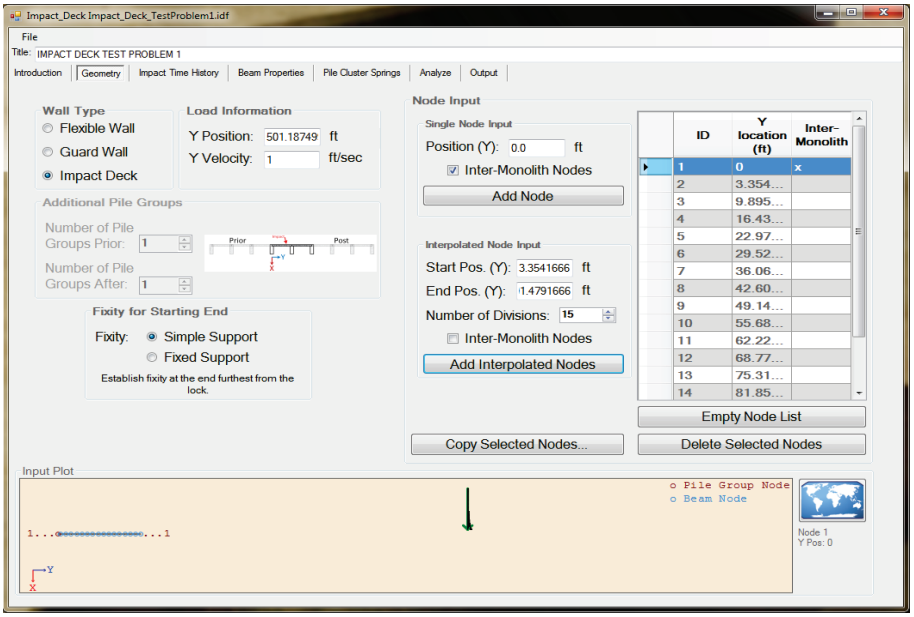


Figure 5.43 Add interpolated nodes from 3.3541666 ft to 101.4791666 ft.



When the set of nodes for the monolith were created (without the ending inter-monolith nodes), all of the nodes for the monolith were selected using a left-mouse, click-drag operation (Figures 5.44 and 5.45). Clicking the "Copy Selected Nodes…" button allowed the user to create copies of this monolith node set multiple times (Figure 5.46). Enter in the offset of the monolith as 104 ft 10 in. (104.833 decimal feet- Figure 5.47), then click the OK button in the "Copy Selected Nodes with Offset" window seven times (Figure 5.48).

Figure 5.44 Selecting nodes with a left-mouse, click-drag.

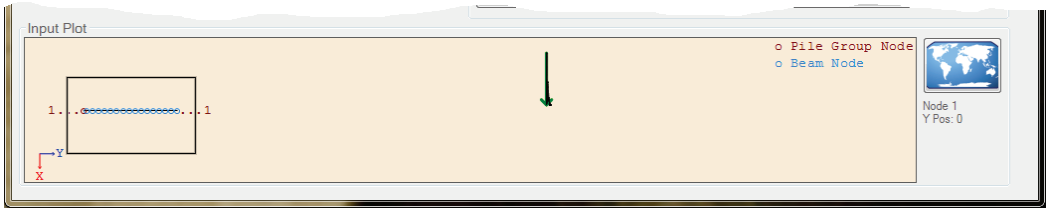


Figure 5.45 Selected nodes are shown with vertical lines.



Figure 5.46 Selected nodes can be copied multiple times with the copy selected nodes button.

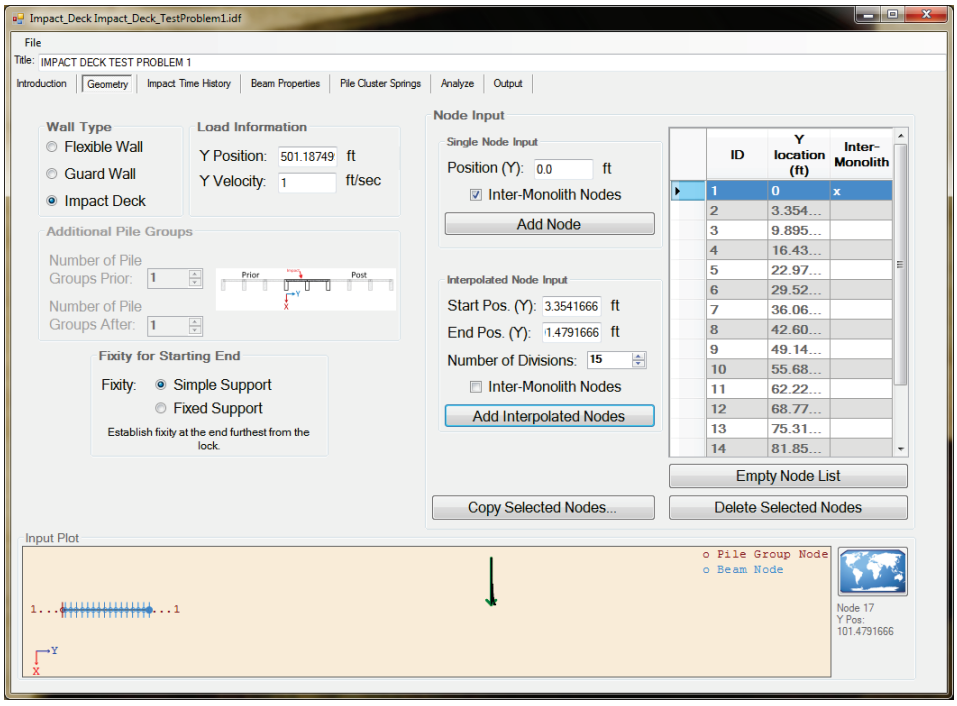


Figure 5.47 The copy selected nodes dialog lets the user specify an offset.

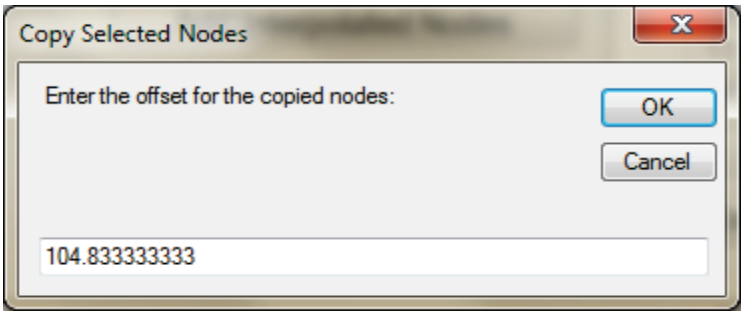
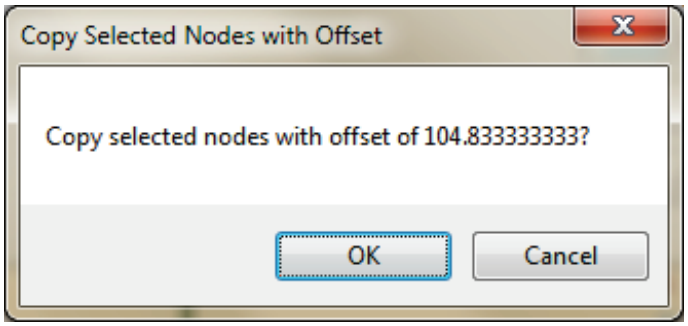
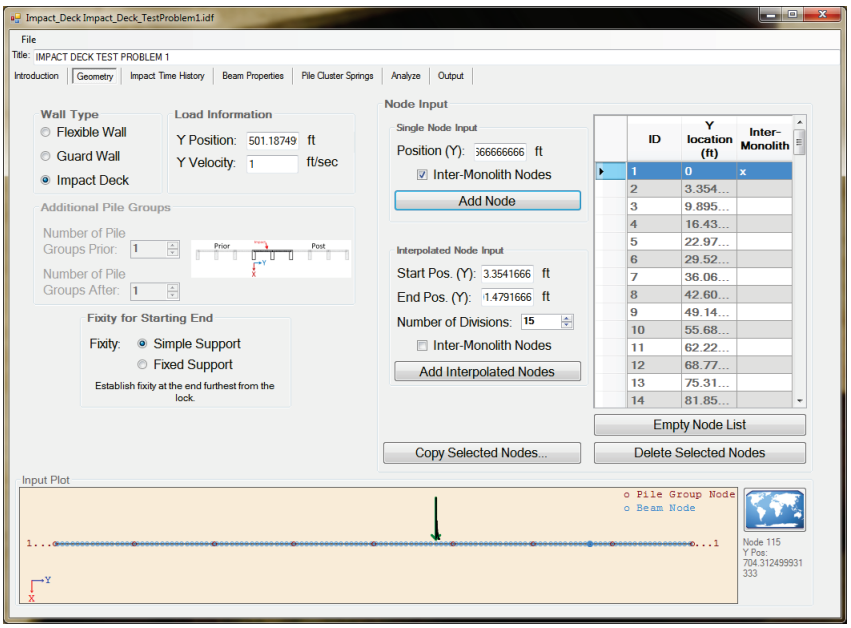


Figure 5.48 Select OK the number of times that the selected nodes need to be copied.



Because the monolith was modeled without the ending inter-monolith connection, the last connection was added using the “Single Node Input” box. Its position was at 838’-8” (838.666 decimal feet). This node was created as an inter-monolith node (Figure 5.49).

Figure 5.49 Finally, Add the Final Node.



Hopefully, this subsection has revealed the usefulness of the Impact_Deck GUI methods for modeling geometry using interpolation and copying of repetitive structures that might otherwise require a good amount of calculation for the user.

5.9 Final Remarks

In this section, the user was presented with the GUI specifications. From this information, the user should be able to define the geometry, select a force time history for an impact, give beam and pile group properties, and perform an analysis from this input model. After the analysis was performed, methods for varying visualization of results were presented, either as static or dynamic plots with information for nodes, elements, and resultant forces at pile groups. The user was also presented with examples that show input for the various structures, and the GUI output (impact decks, flexible approach walls, and guard walls).

6 Conclusions and Recommendations

In this research project, an involved dynamic time-domain analysis was performed to determine the displacement and response forces of flexible pile groups supporting a concrete beam or deck used for the absorption of energy from a barge train impact. An impact force time history was used to represent an impact event (Ebeling et al. 2010). Three different types of pile-founded, flexible approach walls were studied: an impact deck, an alternative flexible approach wall, and a guard wall.

The first case was the Lock and Dam 3 impact deck structure consisting of eight concrete monoliths. These monoliths were supported over a series of equally spaced rows of three cluster pile groups. An internal pin (i.e., with no bending moment transfer) formed the connection between adjacent monoliths. At one end of the structural system, the impact deck monolith was pin-connected to a massive concrete circular cell and at the other end of the structural system the impact deck monolith was free. This structural system was modeled by means of typical beam elements between each pile-group row or between the last pile group row of the monolith to the inter-monolith pin connection. Each pile-group was modeled by using a pair of elastic-plastic translational springs. The definitions of the spring stiffness was determined by doing a push-over analysis of a single pile-group cluster. The dynamic-impact load had a specified starting point and was stationary or moving along the wall. A damping effect was included using the Rayleigh damping theory, which depends on the natural frequency of the system. The two natural frequencies of the structural system (to be used for Rayleigh damping) were calculated in an approximate form by using the spring stiffness and the mass of the impact beam or deck. After the global mass, damping, and stiffness matrices and the load vector were assembled, the dynamic time-history response of the system was calculated.

The second case was the McAlpine alternative flexible approach wall. A section of the approach wall consisted of two consecutive concrete beams supported over three pile groups was modeled with the software. The effect of non-impacted beams was modeled simplistically and the user specifies how many beams before and after the area of interest exist (i.e., where the impact event occurs). The connection of the first beam to the second beam at the center pile cap was accomplished by using a shear key (i.e., no bending moment transfer). In fact, due to the distance between

the end of one beam and the start of the second beam, the shear key had to be modeled also as two rigid beam elements, which connected at a node centered between the two beam end nodes. From there, a rigid beam element was perpendicularly connected back to a node at the center of rigidity of the pile group and its cap. This established the position of the two translational springs and one rotational spring support. In this way, the force-translational and moment-rotational effects of the central pile group were modeled. This structural system was modeled by means of typical beam elements between each pile group and the three rigid beam elements of the central pile cap. The pile groups at the start and end of the structural system were modeled by using elastic-plastic translational springs. The central pile group was modeled by using two elastic-plastic translational springs and one elastic-plastic rotational spring. The definitions of the translational spring stiffness was determined by doing a push-over analysis of a typical pile group. The rotational spring properties were defined by using the translational spring properties of the pile group as shown in Appendix E. The dynamic impact-force time history had a specified starting point and was stationary or moving along the beam. A damping effect was included using the Rayleigh damping theory, which depended on the natural frequency of the system. The two natural frequencies of the structural system (to be used for Rayleigh damping) were calculated in an approximate form by using the spring stiffness and the mass of the beam. After the global mass, damping, and stiffness matrices and the load vector were assembled, the dynamic time-history response of the system was calculated.

The third case was a typical guard wall. A section of the approach wall consisted of two consecutive concrete beams supported over three pile groups was modeled with the software. The connection of the first beam to the second beam in the center pile cap was achieved by using a shear key (i.e., no bending moment transfer). This structural system was modeled by means of typical beam elements between each pile row. The beam elements that connect at the central pile row were modeled with end releases (i.e., no moment transfer). The start, central, and end pile rows of the structural system were modeled by using a pair of elastic-plastic springs. The definitions of the stiffness for the translational and longitudinal springs were determined by doing a push-over analysis of a typical pile group. The dynamic impact load had a specified starting point and was stationary or moving along the beam. A damping effect was included using the Rayleigh damping theory, which depended on the

natural frequency of the system. The two natural frequencies of the structural system (to be used for Rayleigh damping) were calculated in an approximate form by using the spring stiffness and the mass of the impact beam or deck. After the global mass, damping, and stiffness matrices and the load vector were assembled, the dynamic response of the system was calculated.

The general input data for these three models were the nodes and their positions along the wall, modulus of elasticity of the beam, cross-sectional area of the beam, moment of inertia of the beam, mass per unit length of the beam, damping ratio, dynamic coefficient of friction between the lead impact barge and the wall, the initial point of contact, velocity of the moving load, springs properties, and force time history description. The accuracy of the solution depended on the appropriateness of these variables.

To demonstrate the effectiveness of the methodology developed in the Impact_Deck computer program, a validation against SAP2000 and several examples were presented. The validation produced outstanding results. In the examples when the plastic behavior was reached, the time history results were in agreement with the developed elastic-plastic, force-displacement relationship of the springs. It was recognized that SAP2000 will not handle a moving dynamic load nor the nonlinear springs used to model the unique clustered pile groups responses. These are two unique capabilities of the Impact_Deck software.

An important conclusion from the Impact_Deck analyses was that inertial effects of the wall superstructure and substructure during dynamic loading were important to the computed results and should not be ignored. A dynamic analysis must be performed because the resulting overall peak response force was much greater than the peak input impact force and the overall peak response force happened much later in time than when the peak input impact force occured. For every structure analyzed, the overall peak response force had a greater value than the peak input impact force value and the time to the overall peak response force was greater than the time to the peak input impact force. For the simply supported beam guard wall model (in section 4) the overall response force was 181% of the peak input impact force. The overall peak response time was 0.392 sec, or 0.192 sec after the peak input impact force time of 0.2 sec.

The peak response force for any single pile-group node as a substructure for a simply supported beam, in situations where load sharing was minimal (in the McAlpine alternative flexible approach wall and guard wall examples), also exceeded the peak input load force and, due to inertial effects, happened at a later time than the peak input impact force. For the McAlpine alternative flexible approach wall and the guard wall examples, the peak response force for the single pile group node with the greatest force was and 123% and 128% of the peak input load force, respectively. These peaks occurred 0.08 and 0.132 sec after the time to peak input impact force. These were important considerations for the design of pile supported approach wall structures subjected to barge train impact loading.

The peak response force for any single pile-group node with a fixed connection to a deck, and where multiple pile groups support the monolith deck, benefited from the effect of load sharing. In this case, the motion of the impact deck generated a response from all of the pile groups (16, in our example). Because of the shear key connection between monoliths, the pile groups of all 8 monoliths responded similarly to the impact deck motion. However, despite load sharing at 0.04 sec after the peak input load, the peak response force for any pile group reached its peak value of 56.456 kips. This was 11% of the peak input load force, or 7.8% of the peak overall pile-group response force. While it was reasonable to assume a force reduction of greater than 16 times could occur, the real reduction was only slightly more than 9 times less for the peak input load and nearly 13 times less for the peak overall pile group response. Load sharing occured, but its effects were not as pronounced, due to the inertia of the impact deck under a dynamic barge train time history load. These results demonstrated the advantage of using this moment resistant impact deck monolith supported on a large number of smaller piles versus using a simply supported impact beam with larger piles and longer spans: the design forces for each individual pile group was much less. Site conditions and the use of clever, cost-effective, in-the-wet and above-the-wet construction practices (including the use of precast structural features) will dictate which design type will ultimately possess the greater advantage (in cost and effort) for an approach wall project.

References

Bathe, K. 1996. *Finite element procedures*, Englewood Cliffs, New Jersey: Prentice Hall.

Chopra, Anil K. 1995. Dynamics of structures; theory and applications to earthquake engineering, Englewood Cliffs, New Jersey: Prentice Hall.

Chopra, Anil K. 2001. *Dynamics of structures; theory and applications to earthquake engineering*, second edition, Englewood Cliffs, New Jersey: Prentice Hall.

Clough, Ray W., and Joseph Penzien. 1993. *Dynamics of structures*, Second edition, New York, NY: McGraw-Hill, Inc.

Computers and Structures, Inc. 2003. SAP2000 static and dynamic finite element analysis of structures nonlinear 8.2.3, Berkeley, CA, 2003.

Craig, R. R. 1981. *Structural dynamics, an introduction to computer methods*, New York, NY: John Wiley & Sons, Inc.

Davisson, M. T. 1970. *Lateral load capacity of piles*, Highway Research Record, Number 133, Pile4 Foundations, Washington, D.C.: Highway Research Board.

Ebeling, Robert M., R. A. Green, and S. E. French. 1997. *Accuracy of response of single degree-of-freedom systems to ground motion*, Earthquake Engineering Research Program, TR ITL-97-7, Vicksburg, MS: U.S. Army Waterways Experiment Station.

Ebeling, Robert M., Barry C. White, Abdul N. Mohamed, and Bruce C. Barker. 2010. *Force time-history during the impact of a barge train impact with a approach lock wall using impact_force*, ERDC/ITL TR-10-1, Vicksburg, MS: U.S. Army Engineer Research and Development Center.

Ebeling, Robert M., Abdul N. Mohamed, Jose R. Arroyo, Barry C. White, Ralph W. Strom, and Bruce C. Barker. 2011. *Dynamic structural flexible-beam response to a moving barge train impact force time-history using impact_beam*, ERDC/ITL TR-11-1, Vicksburg, MS: U.S. Army Engineer Research and Development Center.

Ebeling, R. M., R. W. Strom, B. C. White, and K. Abraham. 2012. *Simplified Analysis Procedures for Flexible Approach Wall Systems Founded on Groups of Piles and Subjected to Barge Train Impact*, ERDC/ITL TR-12-3, Vicksburg, MS: U.S. Department of the Army, Army Corps of Engineers, Engineer Research and Development Center.

Hartman, J. P., Jaeger, J. J., Jobst, J. J., and Martin, D. K. 1989. *User's Guide: Pile Group Analysis (CPGA)*. Technical Report ITL-89-3. Vicksburg, MS: U.S. Army Engineer Waterways Experiment Station.

Hilber, H. M., T. J. R. Hughes, and R. L. Taylor. 1977. Improved Dissipation for Time Integration Algorithms in Structural Dynamics. *Earthquake Engineering and Structural Design*. 5:283-292.

MathCAD 8. 1998. Cambridge, MA: Mathsoft, Inc.

McGuire, W., and R. H. Gallagher. 1979. *Matrix structural analysis*, New York, NY: John Wiley & Sons, Inc.

Patev, Robert C., Bruce C. Barker, and Leo V. Koestler. 2003. *Prototype barge impact experiments, Allegheny lock and dam 2, Pittsburgh, Pennsylvania*, ERDC/ITL TR-03-2, Vicksburg, MS: U.S. Army Engineer Research and Development Center.

Paz, Mario. 1985. *Structural dynamics; theory and computation*, Second edition, New York, NY: Van Nostrand Reinhold Company.

Paz, Mario. 1991. *Structural dynamics; theory and computation*, Third edition, New York, NY: Van Nostrand Reinhold Company.

Press, W. H., S. A. Teukolsky, W. T. Vetterling, and B. P. Flannery. 1996. *Numerical recipes in Fortran 77, the art of scientific computing*, Second edition, New York, NY.

Reddy, J. N. 1993. *An introduction to the finite element method*, Second edition, McGraw-Hill, Inc.

Rangan, B. V., and M. Joyce. 1992. Strength of eccentrically loaded slender steel tubular columns filled with high-strength concrete, *ACI Structural Journal*, 89(6): 676-681.

Ross, C. T. F. 1991. Finite element programs for structural vibrations, New York, NY: Springer-Verlag Berlin Heidelberg.

Saul, W. E. 1968. Static and dynamic analysis of pile foundations, *Journal of the Structural Division*, ASCE, Volume 94, Number St5, Proceeding Paper 5936.

Stadler, W., and R. W. Shreeves. 1970. The transient and steady-state response of the infinite Bernoulli-Euler beam with damping and an elastic foundation. *Quarterly Journal of Mechanics and Applied Mathematics,* **23**(2): 197-208.

Tedesco, J., W. G. McDougal, and C. A. Ross. 1999. *Structural dynamics-theory and applications*, Menlo Park, California: Addison Wesley Longman, Inc.

Terzaghi, K. 1955. Evaluation of coefficient of subgrade reaction, *Geotechnique*, Vol. 5, pp. 297-326.

Yang, N. C. 1966. *Buckling strength of pile*, Highway Research Record, Number 147, Bridges and Structures, Washington, D.C.: Highway Research Board.

Wilson, E. L. 2002. Three-dimensional static and dynamic analysis of structures-A physical approach with emphasis on earthquake engineering, Berkeley, California: Computer and Structures, Inc.

Wilson, E. L. 2010. *Static & Dynamic Analysis of Structures: A Physical Approach with Emphasis on Earthquake Engineering,* 4th edition, p. 394, Berkeley, CA: Computers and Structures, Inc.

Weaver, W., and P. Johnston. 1984. *Finite elements for structural analysis*, Englewood Cliffs, New Jersey: Prentice Hall.

Appendix A: Lock and Dam 3 – Equations of Motion for the Mathematical Model

In structural dynamics, the mathematical model of bodies of finite dimensions undergoing translational motion are governed by Newton's Second Law of Motion, expressed as

$$\sum F = m \bullet a \tag{1.1 bis}$$

at each time step *t* during motion. In the mathematical model of transverse vibration, the forces acting on the flexible impact beam mass at each time step *t* include (1) the impact force at time step *t*, (2) the elastic restoring forces (of the beam), and (3) the damping forces (of the beam). The mathematical model of the beam in the engineering formulation described in this appendix has a finite number of degrees of freedom (DOF) because it is discretized using the finite element formulation. The engineering formulations of equations of motion are solved using a numerical solution method to determine the displacement and response forces at each pile bent support feature. Each group of clustered piles is modeled as transverse and longitudinal elastic/plastic springs. This is a dynamic process, with the response forces responding to an impact pulse force time history and each calculation of the equations of motion occurring at each time step. The applied impact force can be given a constant velocity parallel to the approach wall so that it is changing position with time. The responses of the elastic beam over elastic or plastic springs can be obtained by the use of the Multi-Degrees-of-Freedom model (MDOF) and the finite element formulation of the beam element. The Impact_Deck software includes damping forces by using the Rayleigh damping model. The response is obtained using either the HHT-α method (Appendix F) or the well-known Wilson-θ method (Appendix G). By using the Newton's Second law and applying it to a MDOF system, the resulting equations of motion can be expressed as,

$$[M]\{\ddot{u}(t)\} + [C]\{\dot{u}(t)\} + [K]\{u(t)\} = \{F(t)\} \tag{2.1 bis}$$

where,

[M] = global mass matrix
[C] = global damping matrix

[K] = global stiffness matrix
{F(t)} = global vector of external forces and moments
$\{\ddot{u}(t)\},\{\dot{u}(t)\},\{u(t)\}$ = relative acceleration, relative velocity, and relative displacement for each DOF.

This appendix discusses the various relationships used in this engineering methodology that are implemented in Impact_Deck.

A.1 Element degrees of freedom (DOF) and interpolation functions

Consider a straight-beam element of length L, mass per unit length $m(x)$, and flexural rigidity $EI(x)$. The two nodes by which the 2-D finite element can be assembled into a structure are located at its ends. If only planar displacements are considered, each node has three DOF: the longitudinal displacement, the transverse displacement, and rotation.

The longitudinal displacement (i.e., axial direction) of the beam element is related to its two DOF:

$$u(x,t)=\sum_{i=1}^{2}u_i(t)\phi_i(x) \tag{A.1}$$

where the function $\phi_i(x)$ defines the displacement of the element due to unit displacement u_i, while constraining other DOF to zero. Thus $\phi_i(x)$ satisfies the following boundary conditions and are shown in Figure A.1,

$$i=1:\psi_1(0)=1,\ \psi_1(L)=0 \tag{A.2}$$

$$i=2:\psi_2(0)=0,\ \psi_2(L)=1 \tag{A.3}$$

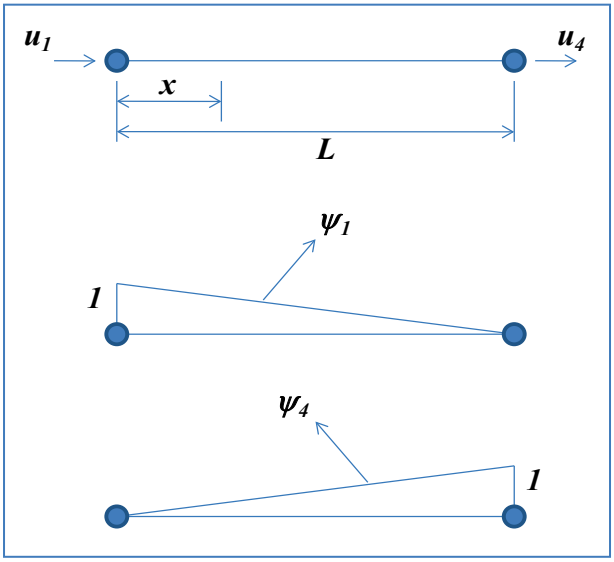
Note that these DOF subscript values i = 1 and 2 correspond to Figure A.1 DOF subscripts i = 1 and 4.

The transverse displacement and rotation of the beam element is related to its four DOF,

$$u(x,t)=\sum u_i(t)\psi_i(x)\therefore i=2,3,5,6 \tag{A.4}$$

where the function $\psi_i(x)$ defines the displacement of the element due to unit displacement $u_{i,}$ while constraining other DOF to zero. Thus, $\psi_i(x)$ satisfies the following boundary conditions

Figure A.1 Shape function for axial displacement effect.



$$i = 1 : \psi_1(0)=1, \psi'_1(0)=\psi_1(L)=\psi'_1(L)=0 \quad \text{(A.5)}$$

$$i = 2 : \psi'_2(0) = 1, \psi_2(0)=\psi_2(L)=\psi'_2(L)=0 \quad \text{(A.6)}$$

$$i = 3 : \psi_3(L)=1, \psi_3(0)=\psi'_3(0)=\psi'_3(L)=0 \quad \text{(A.7)}$$

$$i = 4 : \psi'_4(L) = 1, \psi_4(0)=\psi'_4(0)=\psi_4(L)=0 \quad \text{(A.8)}$$

Note that these DOF subscript values i = 1, 2, 3 and 4 correspond to Figure A.2 DOF subscripts i = 2, 3, 5, and 6.

These interpolation functions could be any arbitrary shapes satisfying the boundary conditions. One possibility is the exact deflected shapes of the beam element due to the imposed boundary conditions, but these are difficult to determine if the flexural rigidity varies over the length of the element. However, they can conveniently be obtained for a uniform beam as illustrated next for the transverse displacement and rotation. Neglecting shear deformations, the equilibrium equation for a beam loaded only at its ends is

$$EI\frac{d^4u}{dx^4}=0 \tag{A.9}$$

The general solution of Equation (A.9) for a uniform beam is a cubic polynomial

$$u(x)=a_1+a_2\left(\frac{x}{L}\right)+a_3\left(\frac{x}{L}\right)^2+a_4\left(\frac{x}{L}\right)^3 \tag{A.10}$$

The constants a_i can be determined for each of the four sets of boundary conditions of Equations (A.5) to (A.8), to obtain

$$\psi_1(x)=1-3\left(\frac{x}{L}\right)^2+2\left(\frac{x}{L}\right)^3 \tag{A.11}$$

$$\psi_2(x)=L\left(\frac{x}{L}\right)-2L\left(\frac{x}{L}\right)^2+L\left(\frac{x}{L}\right)^3 \tag{A.12}$$

$$\psi_3(x)=3\left(\frac{x}{L}\right)^2-2\left(\frac{x}{L}\right)^3 \tag{A.13}$$

$$\psi_4(x)=-L(x/L)^2+L(x/L)^3 \tag{A.14}$$

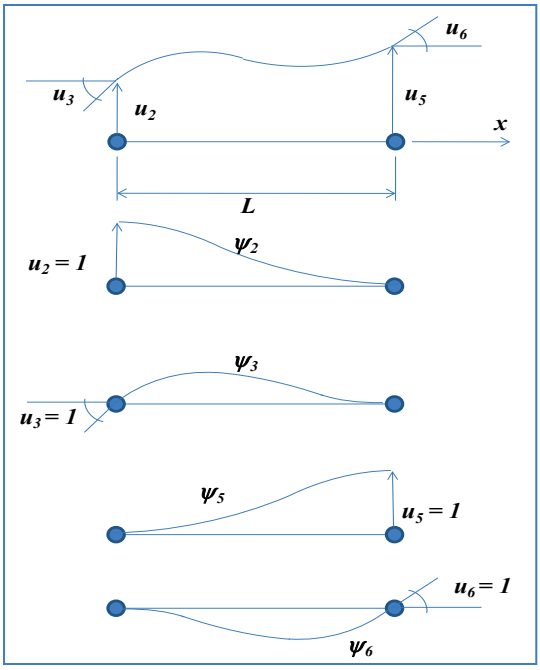
These interpolation functions, illustrated in Figure A.2, can be used in formulating the element matrices. The same process can be done with the axial effect to obtain the basic interpolation functions,

$$\psi_1(x)=1-\frac{x}{L} \tag{A.15}$$

$$\psi_2(x)=\frac{x}{L} \tag{A.16}$$

The finite element method is based on assumed relationships between the displacements at interior points of the element and the displacements at the nodes. Proceeding in this manner makes the problem tractable but introduces approximations in the solution.

Figure A.2 Shape function for transverse displacement and rotation effect.



A.2 Element stiffness matrix

Consider a beam element of length L with flexural rigidity $EI(x)$. By definition, the stiffness influence coefficient k_{ij} of the beam element is the force in the DOF i due to unit displacement in DOF j. Using the principle of virtual displacement, the general equation for k_{ij}, which is the stiffness term for the transverse displacement and rotation, in the element stiffness matrix is

$$k_{ij} = \int_0^L EI(x)\psi''_i(x)\psi''_j(x)dx \tag{A.17}$$

The symmetric form of this equation shows that the element stiffness matrix is symmetric, $k_{ij} = k_{ji}$. Equation (A.17) is a general result in the sense that it is applicable to elements with arbitrary variation of flexural rigidity $EI(x)$, although the interpolation functions of Equations (A.11) to (A.14) are exact only for uniform elements. The associated errors can be reduced to any desired degree by reducing the element size and increasing the number of finite elements in the structural idealization. For a uniform finite element with $EI(x) = EI$, the integral of Equation (A.17) can be evaluated analytically for $i, j = 2, 3, 5,$ and 6, resulting in the corresponding terms in the element stiffness matrix.

In the same way, for the axial contribution, the general equation for k_{ij}, which is the stiffness term for the axial displacement in the element stiffness matrix is

$$k_{ij} = \int_0^L EA(x)\psi'_i(x)\psi'_j(x)dx \tag{A.18}$$

For a uniform finite element with $EA(x) = EA$, the integral of Equation (A.18) can be evaluated analytically for $i, j = 1, 4$ resulting in the corresponding terms in the element stiffness matrix. Finally, when all terms are calculated, the element stiffness matrix can be obtained as,

$$\left[K'\right] = \begin{bmatrix} \frac{AE}{L} & 0 & 0 & -\frac{AE}{L} & 0 & 0 \\ 0 & \frac{12EI}{L^3} & \frac{6EI}{L^2} & 0 & -\frac{12EI}{L^3} & \frac{6EI}{L^2} \\ 0 & \frac{6EI}{L^2} & \frac{4EI}{L} & 0 & -\frac{6EI}{L^2} & \frac{2EI}{L} \\ -\frac{AE}{L} & 0 & 0 & \frac{AE}{L} & 0 & 0 \\ 0 & -\frac{12EI}{L^3} & -\frac{6EI}{L^2} & 0 & \frac{12EI}{L^3} & -\frac{6EI}{L^2} \\ 0 & \frac{6EI}{L^2} & \frac{2EI}{L} & 0 & -\frac{6EI}{L^2} & \frac{4EI}{L} \end{bmatrix} \tag{A.19}$$

These stiffness coefficients are the exact values for a uniform beam, neglecting shear deformation, because the interpolation functions are the true deflection shapes for this case. Observe that the stiffness matrix of Equation (A.19) is equivalent to the force-displacement relations for a uniform beam that are familiar from classical structural analysis.

A.3 Member end-releases

When a structure has an internal pin (i.e., no moment transfer from one element to the adjacent element), the DOF associated to the rotation must have a stiffness value of zero for that DOF. In that way, the element will keep the ability to transfer the axial and shear force but not the bending moment. That process of assigning a zero value to one term in the stiffness matrix will affect the other terms because equilibrium has to be maintained.

For a beam element, the six equilibrium equations in the local reference system can be written as

$$f_{ij} = k_{ij} u_{ij} \tag{A.20}$$

If one end of the member has a hinge, or other type of release that causes the corresponding force to be equal to zero, Equation (A.20) requires modification. A typical equation is of the following form:

$$f_n = \sum_{j=1}^{12} k_{nj} u_j \tag{A.21}$$

If we know a specific value of f_n is zero because of a release, the corresponding displacement u_n can be written as

$$u_n = \sum_{j=1}^{n-1} \frac{k_{nj}}{k_{nn}} u_j + \sum_{j=n+1}^{12} \frac{k_{nj}}{k_{nn}} u_j + r_n \tag{A.22}$$

Therefore, by substitution of Equation (A.22) into the other five equilibrium equations, the unknown u_n can be eliminated and the corresponding row and column set to zero, or

$$\overline{f}_{ij} = \overline{k}_{ij} u_{ij} + \overline{r}_{ij} \tag{A.23}$$

The terms $f_n = 0$ and the new stiffness terms are equal to

$$\overline{k}_{ij} = k_{ij} - k_{in} \frac{k_{nj}}{k_{nn}} \tag{A.24}$$

This procedure can be repeatedly applied to the element equilibrium equations for all releases. The repeated application of the simple numerical equation is sometimes called the ***static condensation or partial Gauss elimination***.

There is a special case when the load is applied at the end release node. In this case, the load must be altered to maintain the 0 moment transfer. This special case is discussed in Appendix H.

A.4 Element mass matrix

The mass influence coefficient m_{ij} for a structure is the force in the i^{th} DOF due to unit acceleration in the j^{th} DOF. Applying this definition to a beam element with distributed mass *m (x)* and using the principle of virtual displacement, a general equation for m_{ij} can be derived:

$$m_{ij} = \int_0^L m(x)\psi_i(x)\psi_j(x)dx \tag{A.25}$$

The symmetric form of this equation shows that the mass matrix is symmetric; $m_{ij} = m_{ji}$. If we use the same interpolation functions of Equations (A.11) to (A.16) as were used to derive the element stiffness matrix into Equation (A.20), the result obtained is known as the *consistent mass matrix*. The integrals of Equation (A.20) are evaluated numerically or analytically depending on the function $m(x)$. For an element with uniform mass per unit length (i.e., $m(x) = m$), the integrals can be evaluated analytically to obtain the element (consistent) mass matrix as

$$\bar{m}_e = mL\begin{bmatrix} \frac{1}{3} & 0 & 0 & \frac{1}{6} & 0 & 0 \\ 0 & \frac{156}{420} & \frac{22L}{420} & 0 & \frac{54}{420} & \frac{-13L}{420} \\ 0 & \frac{22L}{420} & \frac{4L^2}{420} & 0 & \frac{13L}{420} & \frac{-3L^2}{420} \\ \frac{1}{6} & 0 & 0 & \frac{1}{3} & 0 & 0 \\ 0 & \frac{54}{420} & \frac{13L}{420} & 0 & \frac{156}{420} & \frac{-22L}{420} \\ 0 & \frac{-13L}{420} & \frac{-3L^2}{420} & 0 & \frac{-22L}{420} & \frac{4L^2}{420} \end{bmatrix} \tag{A.26}$$

A.5 Element (applied) force vector

If the external forces $p_i(t), i = 1, 2, 3, 4, 5, and\ 6$ are applied along the six DOF at the two nodes of the finite element, the element force vector can be written directly. On the other hand, if the external forces are concentrated forces $p_j'(t)$ at locations x_j, the nodal force in the i^{th} DOF is

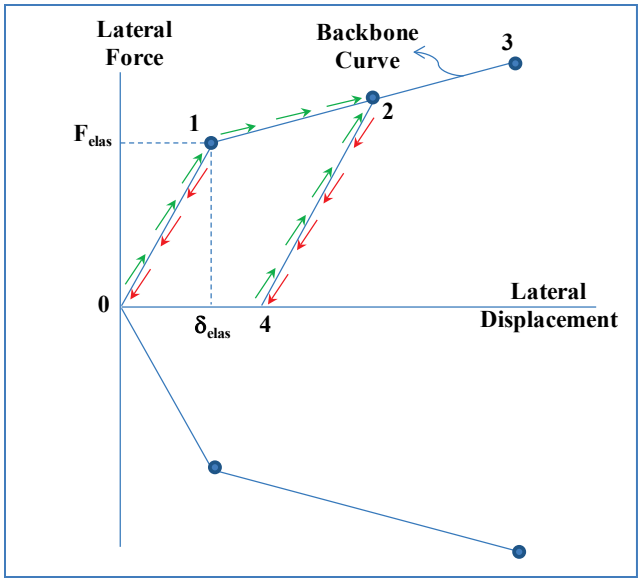
$$p_i(t) = \sum_j p_j' \psi_i(x_j) \tag{A.27}$$

This equation can be obtained by the principle of virtual displacement. If the same interpolation functions of Equations (A.11) to (A.16), are used to derive the element stiffness matrix as used here, the results obtained are called *consistent nodal forces*.

A.6 Nonlinear force-deflection relationship for the springs supports

The software Impact_Deck has the capability to calculate the response of spring supports if the springs develop plastic behavior in the force-displacement relationship. The spring can be considered as linear if the load in the spring is below the elastic displacement δ_{elas} and the elastic force F_{elas} as shown in Figure A.3. If the load is reduced and the force-displacement is below point 1, the unload returns along the same path as the loading phase. The loading phase is shown using green arrows and the unloading phase is shown using red arrows. However, if the load is greater than the elastic displacement and it is in the loading stage, it follows the green arrows until reaching the maximum force-displacement, point 2. If the unload occurs from this point, it will unload following a slope specified by the user. In this case, the slope proceeds from point 2 to point 4. If the force never increases to point 2 again, the force-displacement will remain along the line from point 2 to point 4. If the force decreases to point 4, zero force is reached with a plastic permanent deflection. If the load increases again until point 2 is reached, the original backbone is rejoined, proceeding from point 2 towards point 3. If the force reaches a maximum on the line between point 2 and 3 and starts to decrease again, the load-deflection will follow the same unload slope as the slope from point 2 to point 4 but starting from the new maximum force-deflection. If the force-deflection is greater than point 3, Impact_Deck assigns a zero value to this spring because the maximum value was reached and failure occurs.

Figure A.3 Force-displacement relation of the spring support.



Appendix B: McAlpine Alternative Flexible Wall – Equations of Motion for the Mathematical Model

In structural dynamics the mathematical model of bodies of finite dimensions undergoing translatory motion are governed by Newton's Second Law of Motion, expressed as

$$\sum F = m \bullet a \tag{1.1 bis}$$

at each time step *t* during motion. In the mathematical model of transverse vibration, the forces acting on the flexible impact beam mass at each time step *t* include (1) the impact force at time step *t*, (2) the elastic restoring forces (of the beam), and (3) the damping forces (of the beam). The mathematical model of the beam in the engineering formulation described in this section has a finite number of degrees of freedom (DOF) because it is discretized using the finite element formulation. The engineering formulation of equations of motion are solved using a numerical solution method to determine the displacement and response forces at each pile bent support feature. Each group of clustered piles is modeled as transverse, longitudinal, and rotational elastic/plastic springs. This is a dynamic process, with the response forces responding to an impact pulse force time history and each calculation of the equations of motion occurring at each time step. The applied impact force can be given a constant velocity parallel to the approach wall so that it is changing its position with time. The responses of the elastic beam over elastic or plastic springs can be obtained by the use of the multiple degrees of freedom model (MDOF) and the finite element formulation of the beam element. Impact_Deck includes the damping forces by using the Rayleigh damping model. The response is obtained using the HHT- α method (Appendix F) or the well-known Wilson-θ method. By using the Newton's Second law and applying it to a MDOF system, the resulting equations of motion can be expressed as

$$[M]\{\ddot{u}(t)\} + [C]\{\dot{u}(t)\} + [K]\{u(t)\} = \{F(t)\} \tag{2.1 bis}$$

where:

[M] = global mass matrix

[C] = global damping matrix
[K] = global stiffness matrix
{F(t)} = global vector of external forces and moments
$\{\ddot{u}(t)\},\{\dot{u}(t)\},\{u(t)\}$ = relative acceleration, relative velocity, and relative displacement for each DOF.

This appendix discusses the various relationships used in this engineering methodology that are implemented in Impact_Deck.

B.1 Element degrees of freedom (DOF) and interpolation functions

Consider a straight-beam element of length L, mass per unit length *m(x)*, and flexural rigidity *EI (x)*. The two nodes by which the 2-D finite element can be assembled into a structure are located at its ends. If only planar displacements are considered, each node has three DOF: the longitudinal displacement, the transverse displacement, and rotation.

The longitudinal displacement (i.e., axial direction) of the beam element is related to its two DOF:

$$u(x,t)=\sum_{i=1}^{2}u_i(t)\phi_i(x) \tag{B.1}$$

where the function $\phi_i(x)$ defines the displacement of the element due to unit displacement u_i while constraining other DOF to zero. Thus, $\phi_i(x)$ satisfies the following boundary conditions and are shown in Figure B.1,

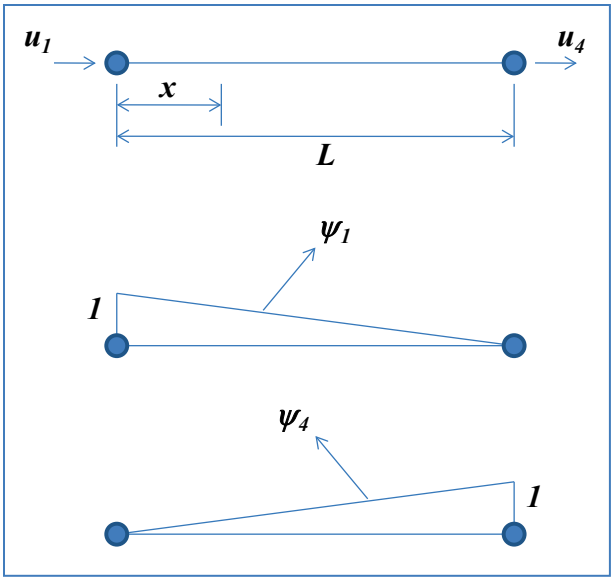
$$i = 1 : \psi_1(0)=1,\ \psi_1(L)=0 \tag{B.2}$$

$$i = 2 : \psi_2(0)=0,\ \psi_2(L)=1 \tag{B.3}$$

Note that these DOF subscript values i = 1 and 2 correspond to Figure B.1 DOF subscripts i = 1 and 4.

The transverse displacement and rotation of the beam element is related to its four DOF,

Figure B.1 Shape function for axial displacement effect.



$$u(x,t) = \sum u_i(t)\psi_i(x) \therefore i = 2,3,5,6 \tag{B.4}$$

where the function $\psi_i(x)$ defines the displacement of the element due to unit displacement u_i, while constraining other DOF to zero. Thus, $\psi_i(x)$ satisfies the following boundary conditions,

$$i = 1 : \psi_1(0) = 1, \psi'_1(0) = \psi_1(L) = \psi'_1(L) = 0 \tag{B.5}$$

$$i = 2 : \psi'_2(0) = 1, \psi_2(0) = \psi_2(L) = \psi'_2(L) = 0 \tag{B.6}$$

$$i = 3 : \psi_3(L) = 1, \psi_3(0) = \psi'_3(0) = \psi'_3(L) = 0 \tag{B.7}$$

$$i = 4 : \psi'_4(L) = 1, \psi_4(0) = \psi'_4(0) = \psi_4(L) = 0 \tag{B.8}$$

Note that these DOF subscript values i = 1, 2, 3, and 4 correspond to Figure B.2 DOF subscripts i = 2, 3, 5, and 6.

These interpolation functions could be any arbitrary shapes satisfying the boundary conditions. One possibility is the exact deflected shapes of the beam element due to the imposed boundary conditions, but these are difficult to determine if the flexural rigidity varies over the length of the element. However, they can conveniently be obtained for a uniform beam

as illustrated next for the transverse displacement and rotation. Neglecting shear deformations, the equilibrium equation for a beam loaded only at its ends is

$$EI\frac{d^4u}{dx^4}=0 \tag{B.9}$$

The general solution of Equation (B.9) for a uniform beam is a cubic polynomial

$$u(x)=a_1+a_2\left(\frac{x}{L}\right)+a_3\left(\frac{x}{L}\right)^2+a_4\left(\frac{x}{L}\right)^3 \tag{B.10}$$

The constants a_i can be determined for each of the four sets of boundary conditions of Equations (B.5) to (B.8), to obtain

$$\psi_1(x)=1-3\left(\frac{x}{L}\right)^2+2\left(\frac{x}{L}\right)^3 \tag{B.11}$$

$$\psi_2(x)=L\left(\frac{x}{L}\right)-2L\left(\frac{x}{L}\right)^2+L\left(\frac{x}{L}\right)^3 \tag{B.12}$$

$$\psi_3(x)=3\left(\frac{x}{L}\right)^2-2\left(\frac{x}{L}\right)^3 \tag{B.13}$$

$$\psi_4(x)=-L\left(\frac{x}{L}\right)^2+L\left(\frac{x}{L}\right)^3 \tag{B.14}$$

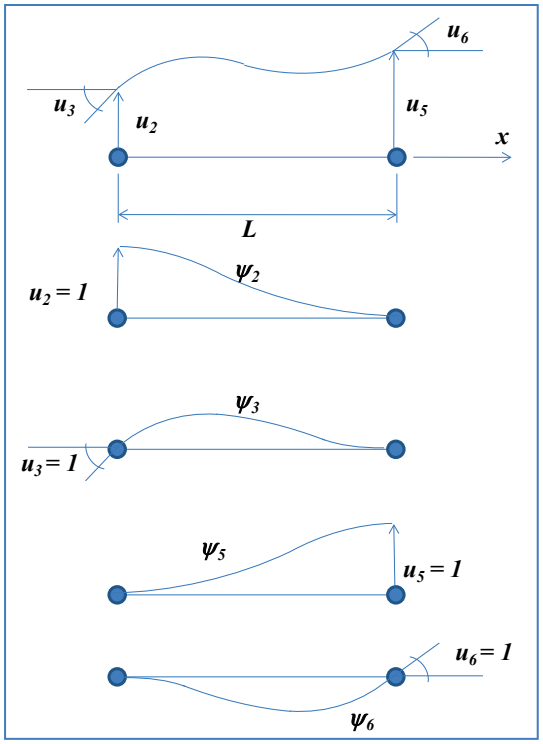
These interpolation functions, illustrated in Figure B.2, can be used in formulating the element matrices. The same process can be done with the axial effect to obtain the basic interpolation functions,

$$\psi_1(x)=1-\frac{x}{L} \tag{B.15}$$

$$\psi_2(x)=\frac{x}{L} \tag{B.16}$$

The finite element method is based on assumed relationships between the displacements at interior points of the element and the displacements at the nodes. Proceeding in this manner makes the problem tractable but introduces approximations in the solution.

Figure B.2 Shape function for transverse displacement and rotation effect.



B.2 Element stiffness matrix

Consider a beam element of length L with flexural rigidity $EI(x)$. By definition, the stiffness influence coefficient k_{ij} of the beam element is the force in the DOF i due to unit displacement in DOF j. Using the principle of virtual displacement, the general equation for k_{ij}, which is the stiffness term for the transverse displacement and rotation, in the element stiffness matrix is:

$$k_{ij} = \int_0^L EI(x)\psi''_i(x)\psi''_j(x)dx \tag{B.17}$$

The symmetric form of this equation shows that the element stiffness matrix is symmetric; $k_{ij} = k_{ji}$. Equation (B.17) is a general result in the sense that it is applicable to elements with arbitrary variation of flexural rigidity $EI(x)$, although the interpolation functions of Equations (B.11) to (B.14) are exact only for uniform elements. The associated errors can be reduced to any desired degree by reducing the element size and increasing the number of finite elements in the structural idealization. For a uniform finite element with $EI(x) = EI$, the integral of Equation (B.17) can be

evaluated analytically for $i, j = 2, 3, 5,$ and 6, resulting in the corresponding terms in the element stiffness matrix.

In the same way, for the axial contribution, the general equation for k_{ij}, which is the stiffness term for the axial displacement in the element stiffness matrix is

$$k_{ij} = \int_0^L EA(x)\psi'_i(x)\psi'_j(x)dx \tag{B.18}$$

For a uniform finite element with $EA(x) = EA$, the integral of Equation (B.18) can be evaluated analytically for $i, j = 1, 4$ resulting in the corresponding terms in the element stiffness matrix. Finally, when all terms are calculated, the element stiffness matrix can be obtained as

$$\left[K'\right] = \begin{bmatrix} \frac{AE}{L} & 0 & 0 & -\frac{AE}{L} & 0 & 0 \\ 0 & \frac{12EI}{L^3} & \frac{6EI}{L^2} & 0 & -\frac{12EI}{L^3} & \frac{6EI}{L^2} \\ 0 & \frac{6EI}{L^2} & \frac{4EI}{L} & 0 & -\frac{6EI}{L^2} & \frac{2EI}{L} \\ -\frac{AE}{L} & 0 & 0 & \frac{AE}{L} & 0 & 0 \\ 0 & -\frac{12EI}{L^3} & -\frac{6EI}{L^2} & 0 & \frac{12EI}{L^3} & -\frac{6EI}{L^2} \\ 0 & \frac{6EI}{L^2} & \frac{2EI}{L} & 0 & -\frac{6EI}{L^2} & \frac{4EI}{L} \end{bmatrix} \tag{B.19}$$

These stiffness coefficients are the exact values for a uniform beam, neglecting shear deformation, because the interpolation functions are the true deflection shapes for this case. Observe that the stiffness matrix of Equation (B.19) is equivalent to the force-displacement relations for a uniform beam that are familiar from classical structural analysis.

B.3 Member end-releases

When a structure has an internal pin (i.e., no moment transfer from one element to the adjacent element), the DOF associated to the rotation must have a stiffness value of zero for that DOF. In that way the element will keep the ability to transfer the axial and shear force but not the bending

moment. That process of assigning a zero value to one term in the stiffness matrix will affect the others terms because equilibrium has to be maintained.

For a beam element, the six equilibrium equations in the local reference system can be written as

$$f_{ij} = k_{ij} u_{ij} \tag{B.20}$$

If one end of the member has a hinge, or other type of release that causes the corresponding force to be equal to zero, Equation (B.20) requires modification. A typical equation is of the following form:

$$f_n = \sum_{j=1}^{12} k_{nj} u_j \tag{B.21}$$

If we know a specific value of f_n is zero because of a release, the corresponding displacement u_n can be written as

$$u_n = \sum_{j=1}^{n-1} \frac{k_{nj}}{k_{nn}} u_j + \sum_{j=n+1}^{12} \frac{k_{nj}}{k_{nn}} u_j + r_n \tag{B.22}$$

Therefore, by substitution of Equation (B.22) into the other five equilibrium equations, the unknown u_n can be eliminated and the corresponding row and column set to zero, or

$$\overline{f}_{ij} = \overline{k}_{ij}\, u_{ij} + \overline{r}_{ij} \tag{B.23}$$

The terms $f_n = 0$ and the new stiffness terms are equal to

$$\overline{k}_{ij} = k_{ij} - k_{in} \frac{k_{nj}}{k_{nn}} \tag{B.24}$$

This procedure can be repeatedly applied to the element equilibrium equations for all releases. The repeated application of the simple numerical equation is sometimes called the ***static condensation or partial Gauss elimination***.

There is a special case when the load is applied at the end release node. In this case, the load must be altered to maintain the 0 moment transfer. This special case is discussed in Appendix H.

B.4 Element mass matrix

The mass influence coefficient m_{ij} for a structure is the force in the i^{th} DOF due to unit acceleration in the j^{th} DOF. Applying this definition to a beam element with distributed mass *m (x)* and using the principle of virtual displacement, a general equation for m_{ij} can be derived

$$m_{ij} = \int_0^L m(x)\psi_i(x)\psi_j(x)dx \tag{B.25}$$

The symmetric form of this equation shows that the mass matrix is symmetric; $m_{ij} = m_{ji}$. If we use the same interpolation functions of Equations (B.11) to (B.16) as were used to derive the element stiffness matrix into Equation (B.23), the result obtained is known as the *consistent mass matrix*. The integrals of Equation (B.23) are evaluated numerically or analytically depending on the function $m(x)$. For an element with uniform mass per unit length (i.e., $m(x) = m$), the integrals can be evaluated analytically to obtain the element (consistent) mass matrix as

$$\bar{m}_e = mL\begin{bmatrix} \frac{1}{3} & 0 & 0 & \frac{1}{6} & 0 & 0 \\ 0 & \frac{156}{420} & \frac{22L}{420} & 0 & \frac{54}{420} & \frac{-13L}{420} \\ 0 & \frac{22L}{420} & \frac{4L^2}{420} & 0 & \frac{13L}{420} & \frac{-3L^2}{420} \\ \frac{1}{6} & 0 & 0 & \frac{1}{3} & 0 & 0 \\ 0 & \frac{54}{420} & \frac{13L}{420} & 0 & \frac{156}{420} & \frac{-22L}{420} \\ 0 & \frac{-13L}{420} & \frac{-3L^2}{420} & 0 & \frac{-22L}{420} & \frac{4L^2}{420} \end{bmatrix} \tag{B.26}$$

B.5 Element (applied) force vector

If the external forces $p_i(t), i = 1, 2, 3, 4, 5\ and\ 6$ are applied along the six DOF at the two nodes of the finite element, the element force vector can be

written directly. On the other hand, if the external forces are concentrated forces $p_j^{'}(t)$ at locations x_j, the nodal force in the i^{th} DOF is

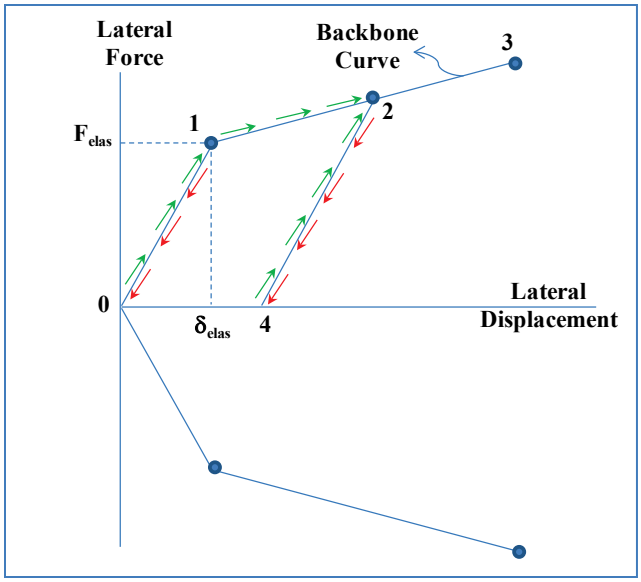
$$p_i(t) = \sum_j p_j^{'} \psi_i(x_j) \tag{B.27}$$

This equation can be obtained by the principle of virtual displacement. If the same interpolation functions of Equations (B.11) to (B.16) are used to derive the element stiffness matrix as used here, the results obtained are called *consistent nodal forces*.

B.7 Nonlinear force-deflection relationship for the springs supports

The Impact_Deck software has the capability to calculate the response of spring supports if the springs develop plastic behavior in the force-displacement relationship. The spring can be considered as linear if the load in the spring is below the elastic displacement δ_{elas} and the elastic force F_{elas} as shown in Figure B.3. If the load is reduced and the force-displacement is below point 1, the unload process returns along the same path as the loading phase. The loading phase is shown using green arrows and the unloading phase is shown using red arrows. However, if the load is greater than the elastic displacement and it is in the loading stage, it follows the green arrows until reaching the maximum force-displacement, point 2. If the unload occurs from this point, it will unload following a slope specified by the user. In this case, the slope proceeds from point 2 to point 4. If the force never increases to point 2 again, the force-displacement will remain along the line from point 2 to point 4. If the force decreases to point 4, zero force is reached with a plastic permanent deflection. If the load increases again until point 2 is reached, the original backbone curve is rejoined, proceeding from point 2 towards point 3. If the force reaches a maximum on the line between point 2 and 3 and starts to decrease again, the load-deflection will follow the same unload slope as the slope from point 2 to point 4, but starting from the new maximum force-deflection. If the force-deflection is greater than point 3, Impact_Deck assigns a zero value to this spring because the maximum value was reached and failure occurs.

Figure B.3 Force-displacement relation of the spring support.



B.8 Transformation of the stiffness matrix from local to global coordinate system

The Impact_Deck computer program has the option to calculate the dynamic response of a flexible wall system such as the McAlpine alternative flexible wall system when subjected to an impact load. The McAlpine alternative flexible wall consists of a series of elastic beams supported over a series of clustered pile groups. The beams transfer the axial and shear forces to the pile cap by means of a shear key. Due to the fact that the beams are not directly connected between the impact beams, that is, they are connected by means of the cap beam shear key, the mathematical model has to include a rigid beam element to model the distance, stiffness, and mass of the shear key. Assuming that a barge train moving at 3 ft/sec impacts the flexible wall at the end of a beam, and with a time history duration of 3 sec, the whole impact process will have 9 ft of length in contact, which occurs inside the shear key model length (i.e., contact solely with the concrete cap to the three-pile group) and not over the beams. A typical McAlpine alternative flexible wall is presented in Figure B.4, and this arrangement of the structural system can be observed.

Impact_Deck also models the effect of a shear key and pile cap along two consecutive beams. Two rigid beam elements are used to model the end-points of the two incoming beams to the center of the pile cap along the longitudinal center-line of the beams. However, the triangular arrangement

Figure B.4 Typical McAlpine flexible wall system.

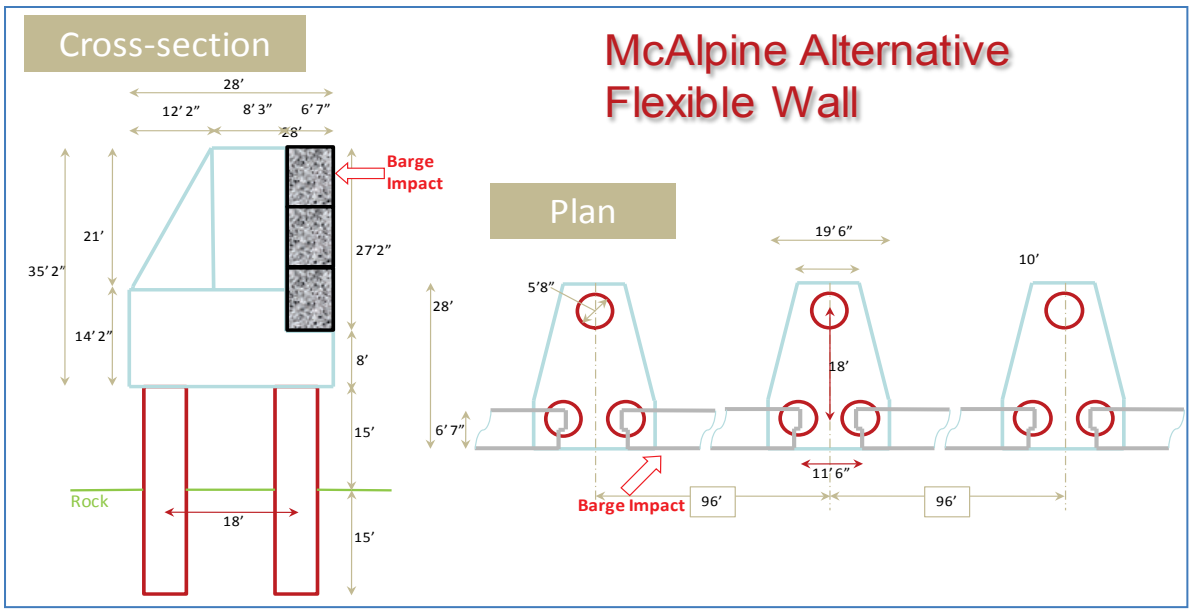
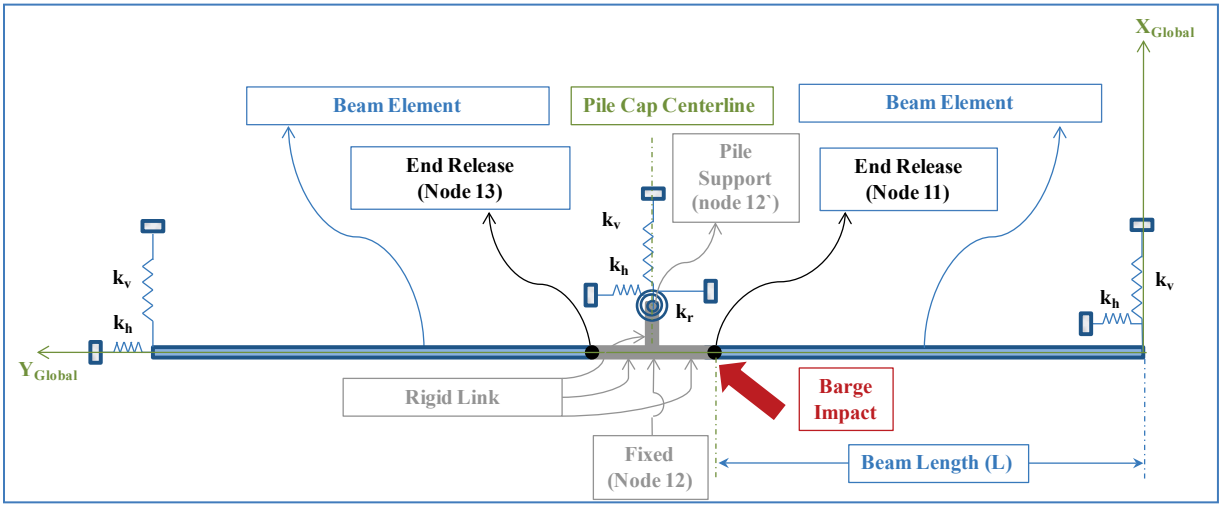


Figure B.5 McAlpine flexible wall mathematical model.



of piles allows the introduction of a possible rotation of the pile cap. That rotation occurs at the center of rigidity of the pile cap with respect to its supporting piles. In this case, the center of rigidity is at the center of the pile cap, but along the transverse direction (perpendicular to the center-line of the beams). To see the calculation of the center of rigidity, please refer to Appendix E. The correct position of the equivalent translational and rotational spring is at this center of rigidity, which does not coincide with the longitudinal global axis of the beams. To connect the springs located at the center of rigidity to the flexible beam elements and rigid beam element (shear key), an additional rigid beam element is included

perpendicular to the longitudinal beam (in the transverse direction) and connected to a node at the center of rigidity of the pile cap. This concept can be visualized in Figure B.5.

This rigid beam element has the same stiffness matrix in local coordinates as a general beam element which stiffness matrix is

$$\left[K'\right]=\begin{bmatrix} \frac{AE}{L} & 0 & 0 & -\frac{AE}{L} & 0 & 0 \\ 0 & \frac{12EI}{L^3} & \frac{6EI}{L^2} & 0 & -\frac{12EI}{L^3} & \frac{6EI}{L^2} \\ 0 & \frac{6EI}{L^2} & \frac{4EI}{L} & 0 & -\frac{6EI}{L^2} & \frac{2EI}{L} \\ -\frac{AE}{L} & 0 & 0 & \frac{AE}{L} & 0 & 0 \\ 0 & -\frac{12EI}{L^3} & -\frac{6EI}{L^2} & 0 & \frac{12EI}{L^3} & -\frac{6EI}{L^2} \\ 0 & \frac{6EI}{L^2} & \frac{2EI}{L} & 0 & -\frac{6EI}{L^2} & \frac{4EI}{L} \end{bmatrix} \tag{B.28}$$

If the local axis of the element does not coincide with the global axis of the transformation of axis has to be done to assemble the global stiffness matrix of the structure. The transformation from local coordinate system to global coordinate system, as shown in Figure B.5 can be done by the transformation matrix.

First, let the equilibrium equations in local coordinates be,

$$\left\{F'\right\}=\left[K'\right]\left\{\Delta'\right\} \tag{B.29}$$

If each side of Equation (B.29) is pre-multipled by transformation matrix, it results in,

$$[\Gamma]\{F\}=\left[K'\right][\Gamma]\{\Delta\} \tag{B.30}$$

If Equation (B.30) is again pre-multipled by the transpose of the transformation matrix,

$$[\Gamma]^T[\Gamma]\{F\}=[\Gamma]^T\left[K'\right][\Gamma]\{\Delta\} \tag{B.31}$$

And noting that the transformation matrix is orthonormal, that is,

$$[\Gamma]^T[\Gamma]=[I] \tag{B.32}$$

$$[I]\{F\}=\{F\} \tag{B.33}$$

then,

$$\{F\}=[\Gamma]^T\left[K'\right][\Gamma]\{\Delta\} \tag{B.34}$$

Equation (B.34) relates the forces in global coordinates to the stiffness matrix in local coordinates and the displacements in global coordinates. Equation (B.34) can be expressed as

$$\{F\}=[K]\{\Delta\} \tag{B.35}$$

where *[K]* is the global stiffness matrix of the element. Finally, the stiffness matrix in global coordinates can be expressed as multiplication of three matrices, the transpose of the transformation matrix by the stiffness matrix in local coordinates, and by the transformation matrix as

$$[K]=[\Gamma]^T\left[K'\right][\Gamma] \tag{B.36}$$

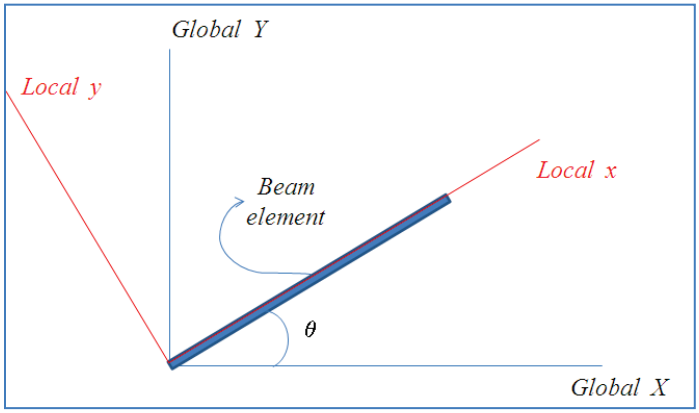
It can be demonstrated by the equilibrium equations that the transformation matrix has the form

$$[\Gamma]=\begin{bmatrix}\gamma & 0\\ 0 & \gamma\end{bmatrix}=\begin{bmatrix} cos\theta & sin\theta & 0 & 0 & 0 & 0\\ -sin\theta & cos\theta & 0 & 0 & 0 & 0\\ 0 & 0 & 1 & 0 & 0 & 0\\ 0 & 0 & 0 & cos\theta & sin\theta & 0\\ 0 & 0 & 0 & -sin\theta & cos\theta & 0\\ 0 & 0 & 0 & 0 & 0 & 1\end{bmatrix} \tag{B.37}$$

The Impact_Deck computer program performs this matrix calculation to transform the stiffness matrix in local coordinate system to global coordinate system for the rigid beam element which is perpendicular to the beam alignment as shown in Figure B.6. In that case, Equation (B.8) uses a value of $\theta = 90$ degrees (the angle between the local axis to the

global axis). The same transformation procedure is done for the element mass matrix to transform from local to global coordinate system for the perpendicular rigid beam element.

Figure B.6 Transformation of beam element coordinate system (Local-Global).



Appendix C: Guard wall – Equations of Motion for the Mathematical Model

In structural dynamics the mathematical model of bodies of finite dimensions undergoing translatory motion are governed by Newton's Second Law of Motion, expressed as

$$\sum F = m \bullet a \tag{1.1 bis}$$

at each time step *t* during motion. In the mathematical model of transverse vibration, the forces acting on the flexible impact beam mass at each time step *t* include (1) the impact force at time step *t*, (2) the elastic restoring forces (of the beam), and (3) the damping forces (of the beam). The mathematical model of the beam in the engineering formulation described in this has a finite number of degrees of freedom (DOF) because it is discretized using the finite element formulation. The engineering formulations of equations of motion are solved using a numerical solution method to determine the displacement and response forces at each pile bent support feature. Each group of clustered piles is modeled as transverse and longitudinal elastic/plastic springs. This is a dynamic process, with the response forces responding to an impact pulse force time history and each calculation of the equations of motion occurring at each time step. The applied impact force can be given a constant velocity parallel to the approach wall so that it is changing position with time. The responses of the elastic beam over elastic or plastic springs can be obtained by the use of the multiple degrees of freedom model (MDOF) and the finite element formulation of the beam element. Impact_Deck includes the damping forces by using the Rayleigh damping model. The response is obtained using either the HHT-α method (Appendix F) or the well-known Wilson-θ method (Appendix G). By using the Newton's Second law and applying it to a MDOF system, the resulting equations of motion can be expressed as

$$[M]\{\ddot{u}(t)\} + [C]\{\dot{u}(t)\} + [K]\{u(t)\} = \{F(t)\} \tag{2.1 bis}$$

where:

[M] = global mass matrix
[C] = global damping matrix

[K] = global stiffness matrix
{F(t)} = global vector of external forces and moments
$\{\ddot{u}(t)\},\{\dot{u}(t)\},\{u(t)\}$ = relative acceleration, relative velocity, and relative displacement for each DOF.

This appendix discusses the various relationships used in this engineering methodology that are implemented in Impact_Deck.

C.1 Element degrees of freedom (DOF) and interpolation functions

Consider a straight-beam element of length L, mass per unit length $m(x)$, and flexural rigidity $EI(x)$. The two nodes by which the 2-D finite element can be assembled into a structure are located at its ends. If only planar displacements are considered, each node has three DOF: the longitudinal displacement, the transverse displacement, and rotation.

The longitudinal displacement (i.e., axial direction) of the beam element is related to its two DOFs:

$$u(x,t)=\sum_{i=1}^{2}u_i(t)\phi_i(x) \tag{C.1}$$

where the function $\phi_i(x)$ defines the displacement of the element due to unit displacement $u_{i,}$ while constraining other DOF to zero. Thus $\phi_i(x)$ satisfies the following boundary conditions and are shown in Figure C.1,

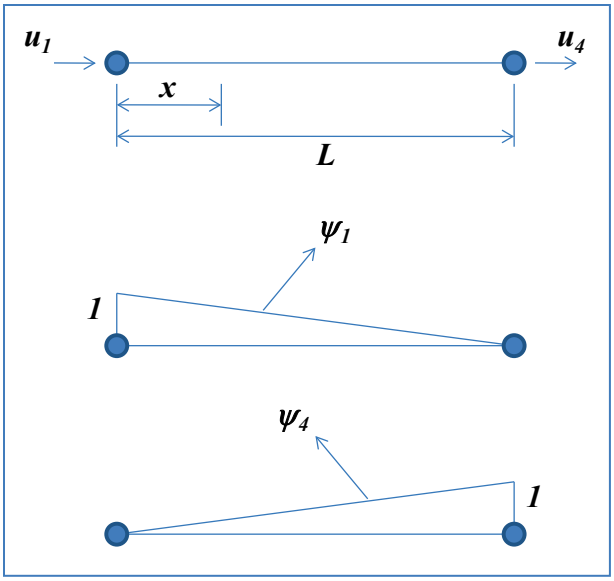
$$i=1:\psi_1(0)=1,\ \psi_1(L)=0 \tag{C.2}$$

$$i=2:\psi_2(0)=0,\ \psi_2(L)=1 \tag{C.3}$$

Note that these DOF subscript values i = 1 and 2 correspond to Figure C.1 DOF subscripts i = 1 and 4.

The transverse displacement and rotation of the beam element is related to its four DOF,

Figure C.1 Shape function for axial displacement effect.



$$u(x,t) = \sum u_i(t)\psi_i(x) \therefore i = 2,3,5,6 \tag{C.4}$$

where the function $\psi_i(x)$ defines the displacement of the element due to unit displacement $u_{i,}$ while constraining other DOF to zero. Thus, $\psi_i(x)$ satisfies the following boundary conditions,

$$i = 1 : \psi_1(0) = 1, \psi'_1(0) = \psi_1(L) = \psi'_1(L) = 0 \tag{C.5}$$

$$i = 2 : \psi'_2(0) = 1, \psi_2(0) = \psi_2(L) = \psi'_2(L) = 0 \tag{C.6}$$

$$i = 3 : \psi_3(L) = 1, \psi_3(0) = \psi'_3(0) = \psi'_3(L) = 0 \tag{C.7}$$

$$i = 4 : \psi'_4(L) = 1, \psi_4(0) = \psi'_4(0) = \psi_4(L) = 0 \tag{C.8}$$

Note that these DOF subscript values i = 1, 2, 3, and 4 correspond to Figure C.2 DOF subscripts i = 2, 3, 5, and 6.

These interpolation functions could be any arbitrary shapes satisfying the boundary conditions. One possibility is the exact deflected shapes of the beam element due to the imposed boundary conditions, but these are difficult to determine if the flexural rigidity varies over the length of the element. However, they can conveniently be obtained for a uniform beam

as illustrated next for the transverse displacement and rotation. Neglecting shear deformations, the equilibrium equation for a beam loaded only at its ends is

$$EI\frac{d^4u}{dx^4}=0 \tag{C.9}$$

The general solution of Equation (C.9) for a uniform beam is a cubic polynomial

$$u(x)=a_1+a_2\left(\frac{x}{L}\right)+a_3\left(\frac{x}{L}\right)^2+a_4\left(\frac{x}{L}\right)^3 \tag{C.10}$$

The constants a_i can be determined for each of the four sets of boundary conditions of Equations (C.5) to (C.8), to obtain

$$\psi_1(x)=1-3\left(\frac{x}{L}\right)^2+2\left(\frac{x}{L}\right)^3 \tag{C.11}$$

$$\psi_2(x)=L\left(\frac{x}{L}\right)-2L\left(\frac{x}{L}\right)^2+L\left(\frac{x}{L}\right)^3 \tag{C.12}$$

$$\psi_3(x)=3\left(\frac{x}{L}\right)^2-2\left(\frac{x}{L}\right)^3 \tag{C.13}$$

$$\psi_4(x)=-L\left(\frac{x}{L}\right)^2+L\left(\frac{x}{L}\right)^3 \tag{C.14}$$

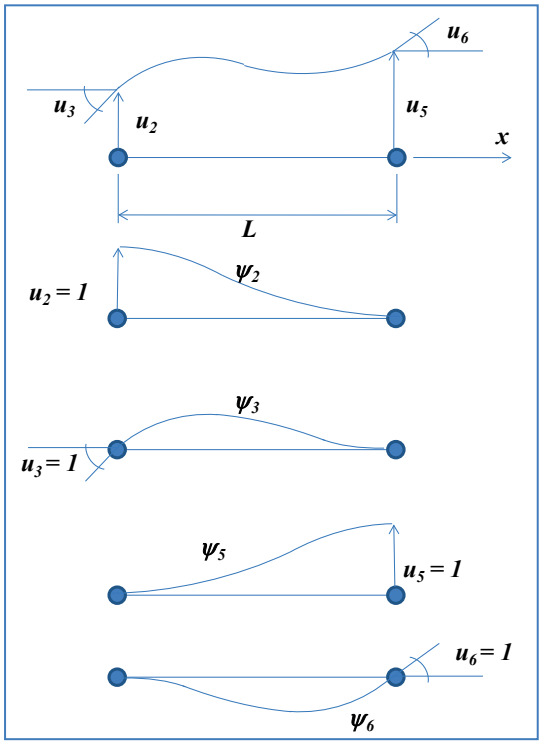
These interpolation functions, illustrated in Figure C.2, can be used in formulating the element matrices. The same process can be done with the axial effect to obtain the basic interpolation functions,

$$\psi_1(x)=1-\frac{x}{L} \tag{C.15}$$

$$\psi_2(x)=\frac{x}{L} \tag{C.16}$$

The finite element method is based on assumed relationships between the displacements at interior points of the element and the displacements at the nodes. Proceeding in this manner makes the problem tractable but introduces approximations in the solution.

Figure C.2 Shape function for transverse displacement and rotation effect.



C.2 Element stiffness matrix

Consider a beam element of length L with flexural rigidity $EI(x)$. By definition, the stiffness influence coefficient k_{ij} of the beam element is the force in the DOF i due to unit displacement in DOF j. Using the principle of virtual displacement, the general equation for k_{ij}, which is the stiffness term for the transverse displacement and rotation, in the element stiffness matrix is

$$k_{ij} = \int_0^L EI(x)\psi''_i(x)\psi''_j(x)dx \tag{C.17}$$

The symmetric form of this equation shows that the element stiffness matrix is symmetric; $k_{ij} = k_{ji}$. Equation (C.19) is a general result in the sense that it is applicable to elements with arbitrary variation of flexural

rigidity $EI(x)$, although the interpolation functions of Equations (C.11) to (C.14) are exact only for uniform elements. The associated errors can be reduced to any desired degree by reducing the element size and increasing the number of finite elements in the structural idealization. For a uniform finite element with $EI(x) = EI$, the integral of Equation (C.17) can be evaluated analytically for $i, j = 2, 3, 5,$ and 6, resulting in the corresponding terms in the element stiffness matrix.

In the same way, for the axial contribution, the general equation for k_{ij}, which is the stiffness term for the axial displacement in the element stiffness matrix is

$$k_{ij} = \int_0^L EA(x)\psi'_i(x)\psi'_j(x)dx \tag{C.18}$$

For a uniform finite element with $EA(x) = EA$, the integral of Equation (C.18) can be evaluated analytically for $i, j = 1, 4$ resulting in the corresponding terms in the element stiffness matrix. Finally, when all terms are calculated, the element stiffness matrix can be obtained as

$$\left[K'\right] = \begin{bmatrix} \frac{AE}{L} & 0 & 0 & -\frac{AE}{L} & 0 & 0 \\ 0 & \frac{12EI}{L^3} & \frac{6EI}{L^2} & 0 & -\frac{12EI}{L^3} & \frac{6EI}{L^2} \\ 0 & \frac{6EI}{L^2} & \frac{4EI}{L} & 0 & -\frac{6EI}{L^2} & \frac{2EI}{L} \\ -\frac{AE}{L} & 0 & 0 & \frac{AE}{L} & 0 & 0 \\ 0 & -\frac{12EI}{L^3} & -\frac{6EI}{L^2} & 0 & \frac{12EI}{L^3} & -\frac{6EI}{L^2} \\ 0 & \frac{6EI}{L^2} & \frac{2EI}{L} & 0 & -\frac{6EI}{L^2} & \frac{4EI}{L} \end{bmatrix} \tag{C.19}$$

These stiffness coefficients are the exact values for a uniform beam, neglecting shear deformation, because the interpolation functions are the true deflection shapes for this case. Observe that the stiffness matrix of Equation (C.19) is equivalent to the force-displacement relations for a uniform beam that are familiar from classical structural analysis.

C.3 Member end-releases

When a structure has an internal pin (i.e., no moment transfer from one element to the adjacent element), the DOF associated to the rotation must have a stiffness value of zero for that DOF. In that way the element will keep the ability to transfer the axial and shear force but not the bending moment. That process of assigning a zero value to one term in the stiffness matrix will affect the others terms because equilibrium has to be maintained.

For a beam element, the six equilibrium equations in the local reference system can be written as

$$f_{ij} = k_{ij} u_{ij} \tag{C.20}$$

If one end of the member has a hinge, or other type of release that causes the corresponding force to be equal to zero, Equation (C.20) requires modification. A typical equation is of the following form:

$$f_n = \sum_{j=1}^{12} k_{nj} u_j \tag{C.21}$$

If we know a specific value of f_n is zero because of a release, the corresponding displacement u_n can be written as

$$u_n = \sum_{j=1}^{n-1} \frac{k_{nj}}{k_{nn}} u_j + \sum_{j=n+1}^{12} \frac{k_{nj}}{k_{nn}} u_j + r_n \tag{C.22}$$

Therefore, by substitution of Equation (C.21) into the other five equilibrium equations, the unknown u_n can be eliminated and the corresponding row and column set to zero, or

$$\overline{f}_{ij} = \overline{k}_{ij} u_{ij} + \overline{r}_{ij} \tag{C.23}$$

The terms $f_n = 0$ and the new stiffness terms are equal to

$$\overline{k}_{ij} = k_{ij} - k_{in} \frac{k_{nj}}{k_{nn}} \tag{C.24}$$

This procedure can be repeatedly applied to the element equilibrium equations for all releases. The repeated application of the simple numerical equation is sometimes called the ***static condensation or partial Gauss elimination***.

There is a special case when the load is applied at the end release node. In this case, the load must be altered to maintain the 0 moment transfer. This special case is discussed in Appendix H.

C.4 Element mass matrix

The mass influence coefficient m_{ij} for a structure is the force in the i^{th} DOF due to unit acceleration in the j^{th} DOF. Applying this definition to a beam element with distributed mass *m (x)* and using the principle of virtual displacement, a general equation for m_{ij} can be derived

$$m_{ij} = \int_0^L m(x)\psi_i(x)\psi_j(x)dx \tag{C.25}$$

The symmetric form of this equation shows that the mass matrix is symmetric; $m_{ij} = m_{ji}$. If we use the same interpolation functions of Equations (C.11) to (C.16) as were used to derive the element stiffness matrix into Equation (C.20), the result obtained is known as the *consistent mass matrix*. The integrals of Equation (C.20) are evaluated numerically or analytically depending on the function $m(x)$. For an element with uniform mass per unit length (i.e., $m(x) = m$), the integrals can be evaluated analytically to obtain the element (consistent) mass matrix as

$$\bar{m}_e = mL \begin{bmatrix} \frac{1}{3} & 0 & 0 & \frac{1}{6} & 0 & 0 \\ 0 & \frac{156}{420} & \frac{22L}{420} & 0 & \frac{54}{420} & \frac{-13L}{420} \\ 0 & \frac{22L}{420} & \frac{4L^2}{420} & 0 & \frac{13L}{420} & \frac{-3L^2}{420} \\ \frac{1}{6} & 0 & 0 & \frac{1}{3} & 0 & 0 \\ 0 & \frac{54}{420} & \frac{13L}{420} & 0 & \frac{156}{420} & \frac{-22L}{420} \\ 0 & \frac{-13L}{420} & \frac{-3L^2}{420} & 0 & \frac{-22L}{420} & \frac{4L^2}{420} \end{bmatrix} \quad \text{(C.26)}$$

C.5 Element (applied) force vector

If the external forces $p_i(t), i = 1, 2, 3, 4, 5, and\ 6$ are applied along the six DOF at the two nodes of the finite element, the element force vector can be written directly. On the other hand, if the external forces are concentrated forces $p_j^{'}(t)$ at locations x_j, the nodal force in the i^{th} DOF

$$p_i(t) = \sum_j p_j^{'} \psi_i(x_j) \quad \text{(C.27)}$$

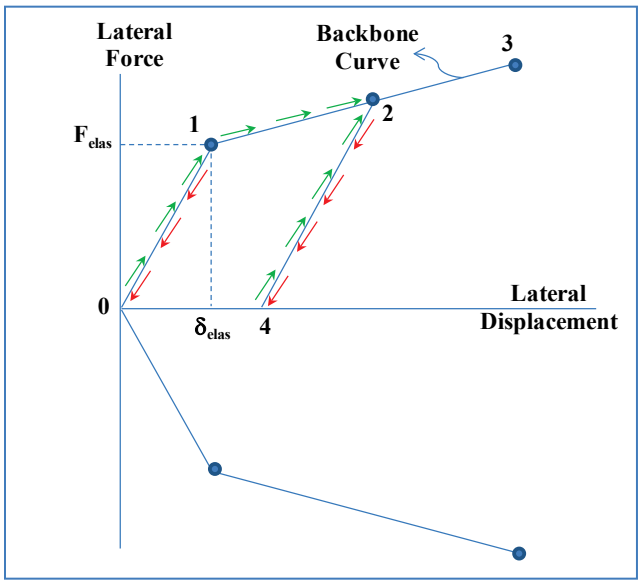
This equation can be obtained by the principle of virtual displacement. If the same interpolation functions of Equations (C.11) to (C.16) are used to derive the element stiffness matrix as used here, the results obtained are called *consistent nodal forces*.

C.6 Nonlinear force-deflection relationship for the springs supports

Impact_Deck has the capability to calculate the response of spring supports if the springs develop plastic behavior in the force-displacement relationship. The spring can be considered as linear if the load in the spring is below the elastic displacement δ_{elas} and the elastic force F_{elas} as shown in Figure C.3. If the load is reduced and the force-displacement is below point 1, the unload returns along the same path as the loading phase. The loading phase is shown using green arrows and the unloading phase is shown using red arrows. However, if the load is greater than the elastic displacement and it is in the loading stage, it follows the green arrows until reaching the maximum force-displacement, point 2. If the

unload occurs from this point, it will unload following a slope specified by the user. In this case, the slope proceeds from point 2 to point 4. If the force never increases to point 2 again, the force-displacement will remain along line from point 2 to point 4 until zero force is reached with a plastic permanent deflection. If the load increases again until point 2 is reached, the original backbone curve is rejoined proceeding from point 2 towards point 3. If the force reaches a maximum on the line between point 2 and 3 and starts to decrease again, the load-deflection will follow the same unload slope as the slope from point 2 to point 4, but starting from the new maximum force-deflection. If the force-deflection is greater than point 3, Impact_Deck assigns a zero value to this spring because the maximum value was reached and failure occurs.

Figure C.3 Force-displacement relation of the spring support.

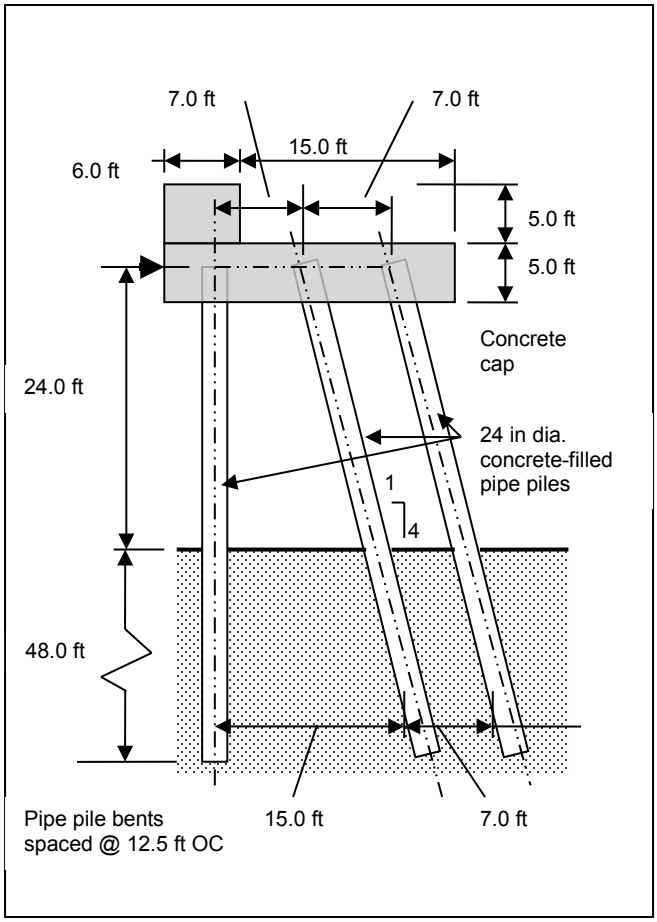


Appendix D Push-over analysis for batter-pile bent system

D.1 Bent geometry and analytical model used in the push-over analysis

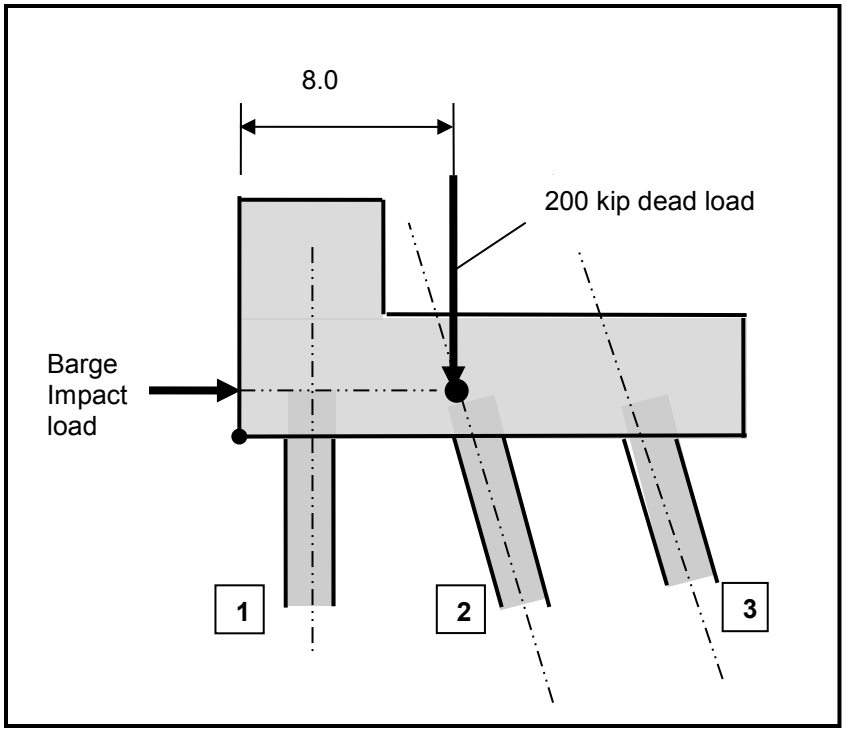
The pipe pile bent of Figure D.1 is examined by push-over analysis (Ebeling et al. 2012) to determine its load-displacement characteristics. The Saul (1968), CPGA analytical model used in the analysis is shown in Figure D.2.[1] The pipe pile bent is comprised of 24-inch-diameter, concrete-filled pipe piles. Load-displacement plots will be determined by push-over analysis for pinned-head and fixed-head conditions.

Figure D.1 Pipe pile approach wall.



[1] Pile numbers are reported in Figure D.2.

Figure D.2 CPGA analytical model.



D.2 Pipe pile properties

Pipe pile properties are presented below:

Diameter D_p of concrete-filled pipe pile = 2.0 ft = 24 in.

Area A_p of concrete-filled pipe pile = 3.142 ft^2 = 452 $in.^2$

Moment of inertia I_p of concrete-filled pipe pile = 0.785 ft^4 = 16300 $in.^4$

Radius of gyration = 0.50 ft = 6 in.

Distance from neutral axis to extreme fiber c = 1.0 ft. = 12 in.

Modulus of elasticity E_c = 504000 ksf = 3500 ksi

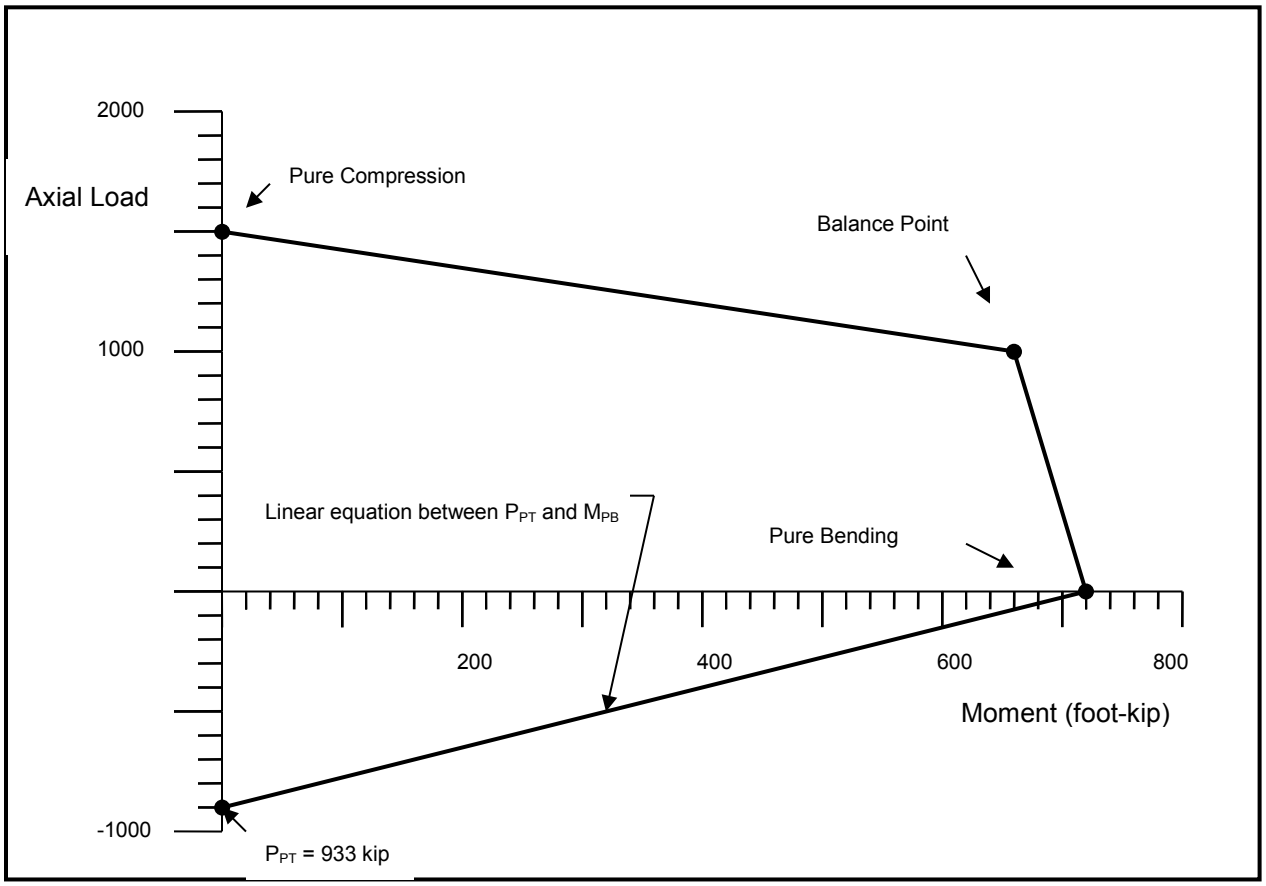
A simple interaction (axial load – moment) diagram is developed to help in assessing the conditions where piles reach their moment or axial load limits. The interaction diagram is based on the ultimate capacity of the pile members. The procedures described in Rangan and Joyce (1992) can be used to develop a simple interaction diagram for a concrete-filled pipe pile. The interaction diagram points are

- Pure axial compression
- Balance condition (axial compression and bending)
- Pure bending
- Pure axial tension

The value for pure axial compression is based only on the compressive strength of the concrete. The 0.375-inch thick steel pipe casing was not included in this calculation. The value for pure axial tension is based only on the tensile strength of the steel pipe. Balance point and pure moment conditions assumes the contribution only of the concrete in compression on the compressive side of the neutral axis and contribution only of the steel in tension on the tensile side of the neutral axis.

The interaction diagram for a 24-inch-diameter, concrete-filled pipe pile is presented in Figure D.3.

Figure D.3 Simple interaction diagram for 24-inch-diameter pipe pile.



The interaction diagram assumes that the pipe piles in axial compression fail as a result of the materials (i.e., concrete and steel) reaching their ultimate capacities, rather than by buckling. However buckling computations will be needed to assure that this is the case. If buckling loads are less than the ultimate axial compressive loads predicted by the interaction diagram, then the buckling loads are to be used in the push-over analysis.

Piles are generally founded in soils that will not allow them to develop their ultimate capacities. It is up to the engineer performing the push-over analysis to consider axial load limitations imposed by the foundation materials. This example also considers pile axial capacities that are limited by side friction and tip resistance provided by the soil foundation.

D.3 Soil properties

A sand foundation with a stiffness that varies linearly with depth is investigated. The coefficient of subgrade reaction (n_h) is assumed to be 50 pci. This value for n_h is corresponds to Terzaghi's (1955) "recommended" value for a moist medium-dense sand and within the scatter considering n_h values cited in other technical literature (e.g., Davisson 1970). There is no water table present in this case (i.e., a "dry" site).

The axial capacity based on soil limitations are 250 kips for piles in tension and 1000 kips for piles in compression.

Relative stiffness factor (T):

$$T = \sqrt[5]{\frac{E_c I_p}{n_h}} = 5.4 \text{ ft}$$

D.4 Buckling evaluation

Buckling loads for the concrete-filled pipe piles are determined using methods described in Yang (1996). Figures D.4 and D.5, after Figures 3 and 9 of Yang (1966), are provided for use in the analysis.

The coefficient of free standing length m is equal to the free standing length L_o divided by the relative stiffness factor T, or $m = L_o \div T = 24 \div 5.4 = 4.45$.

Figure D.4 (After Figure 3 Yang 1966) Coefficient of critical buckling strength.

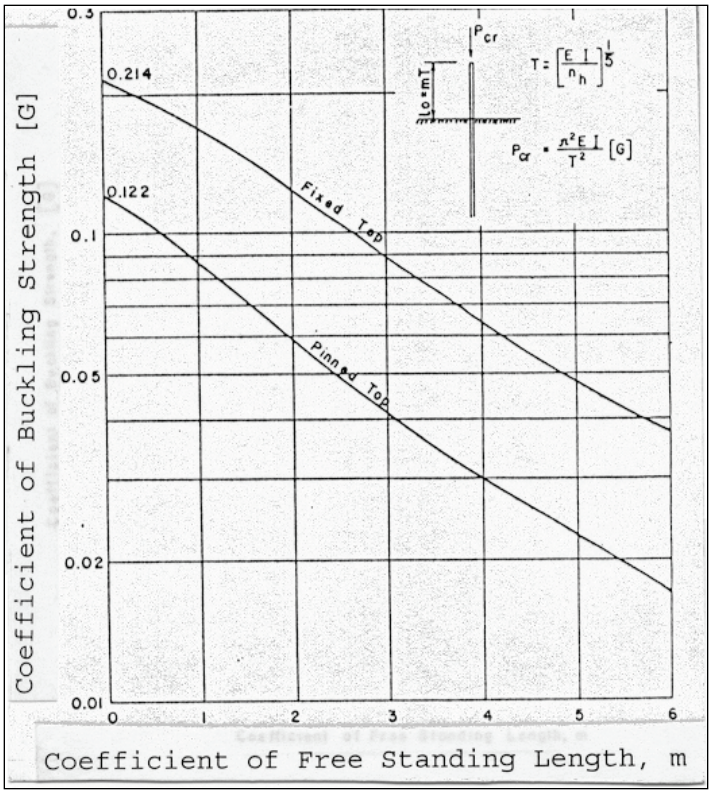
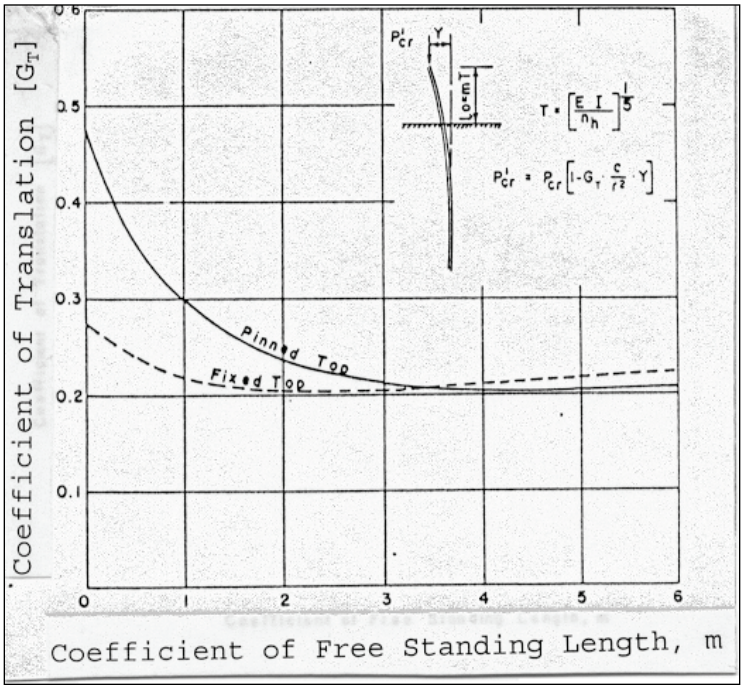


Figure D.5 (After Figure 9 Yang 1966) Coefficient decrement of buckling strength.



The critical buckling load assuming no translation can be determined using Figure D.4 (after Figure 3 in Yang 1966).

For pinned-top non-translating pile cap for Figure D.4, the coefficient of critical buckling strength [*G*] is equal to 0.026 and the Euler critical buckling load is

$$P_{CR} = \frac{\pi^2 E_c I_p}{T^2}[G] = 3847 \text{ kips}$$

For fixed-top non-translating pile cap from Figure D.4, the coefficient of critical buckling strength [*G*] is equal to 0.056 and the Euler critical buckling load is

$$P_{CR} = \frac{\pi^2 E_c I_p}{T^2}[G] = 7509 \text{ kips}$$

The critical buckling load with translation can be determined using Figure D.5 (after Figure 9 of Yang 1966). Entering Figure D.5 with a coefficient of free standing length (m) equal to 4.45, the coefficient of translation [G_T] is approximately equal to 0.21 for both pinned-head and fixed-head piles. The critical buckling load assuming a translation ($P_{CR\Delta}$) is

$$P_{CR\Delta} = P_{CR}\left[1 - G_T\left(\frac{c}{r^2}\right)\Delta\right]$$

It is desirable for the push-over analysis to have the critical buckling load for various lateral displacements when performing a push-over analysis. This has been accomplished with the aid of MathCAD (1998) for pinned-head piles (Table D.1) and fixed-head piles (Table D.2).

D.5 Push-over analysis for pinned-head condition – dry site

The first push-over analysis is performed for a pinned-head condition at a dry site using Saul's (1968) method and the CPGA software. The results are summarized in this section. The first incremental analysis was run using an axial stiffness modifier (C_{33}) for the embedded portion of the pile with a value of 1.00 for compression piles and 0.50 for tension piles where:

$$C_{33} = \frac{\Delta}{\delta}$$

Where:

$$\Delta = \frac{PL}{AE}$$

This assumes that the pile is supported at its tip with all axial load (P) transferred to the tip and:

δ = actual displacement of the pile under axial load (P)

Table D.1 Euler critical buckling load – translating pile top – pinned head condition

Euler critical buckling load - Translating pile top

$G_T := 0.21$ Figure 9, Reference 1
Pinned top

$r := \left(\frac{I_p}{A_p}\right)^{0.5}$ $r = 0.5 \cdot ft$ $c := 1.0 \cdot ft$

$\Delta := 3 \cdot in, 4 \cdot in .. 14 \cdot in$

$P_{cr\Delta}(\Delta) := P_{cr} \cdot \left(1 - G_T \cdot \frac{c}{r^2} \cdot \Delta\right)$ $\Delta_x(\Delta) := \Delta$

$P_{cr\Delta}(\Delta) =$ kip	$\Delta_x(\Delta) =$ in
$2.754 \cdot 10^3$	3
$2.51 \cdot 10^3$	4
$2.266 \cdot 10^3$	5
$2.022 \cdot 10^3$	6
$1.778 \cdot 10^3$	7
$1.534 \cdot 10^3$	8
$1.29 \cdot 10^3$	9
$1.046 \cdot 10^3$	10
801.897	11
557.842	12
313.786	13
69.73	14

Table D.2 Euler critical buckling load – translating pile top – fixed head condition.

Euler critical buckling load - Translating pile top

$G_T := 0.21$ Figure 9, Reference 1
Fixed top

$r := \left(\frac{I_p}{A_p}\right)^{0.5}$ $r = 0.5 \cdot ft$ $c := 1.0 \cdot ft$

$\Delta := 3 \cdot in, 4 \cdot in .. 14 \cdot in$

$P_{cr\Delta}(\Delta) := P_{cr} \cdot \left(1 - G_T \cdot \frac{c}{r^2} \cdot \Delta\right)$ $\Delta_x(\Delta) := \Delta$

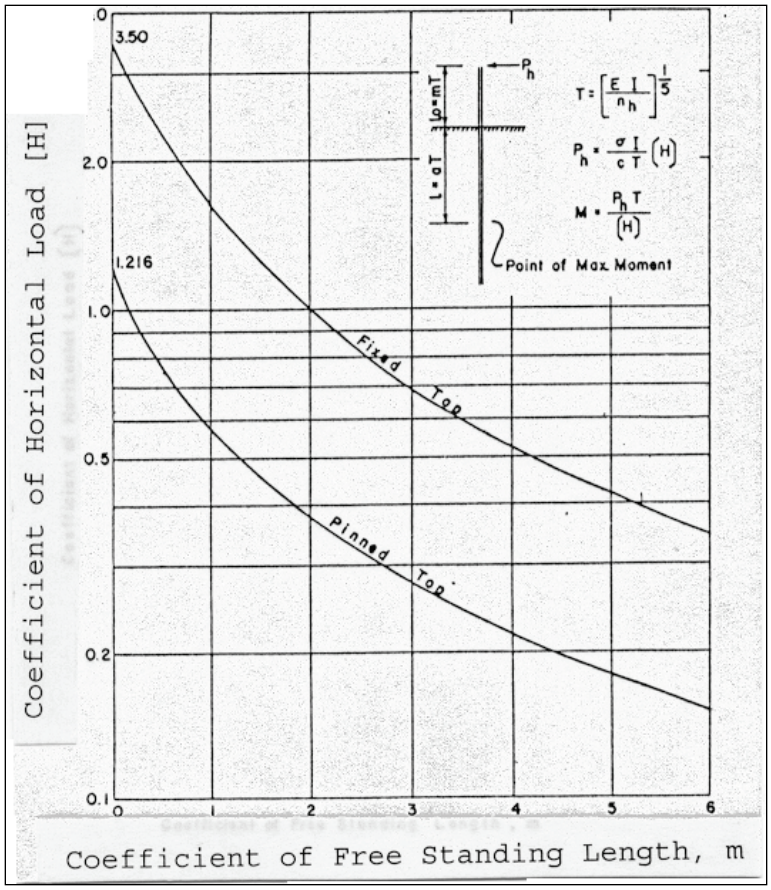
$P_{cr\Delta}(\Delta) =$ •kip	$\Delta_x(\Delta) =$ •in
$5.932 \cdot 10^3$	3
$5.407 \cdot 10^3$	4
$4.881 \cdot 10^3$	5
$4.355 \cdot 10^3$	6
$3.83 \cdot 10^3$	7
$3.304 \cdot 10^3$	8
$2.778 \cdot 10^3$	9
$2.253 \cdot 10^3$	10
$1.727 \cdot 10^3$	11
$1.202 \cdot 10^3$	12
675.846	13
150.188	14

This is a crude approximation of axial stiffness used to illustrate the push-over method. The actual value of the stiffness modifier (C_{33}) should be determined by appropriate analytical t-z models and/or pile load tests. To obtain the maximum moment below the mudline it is necessary to include a PMAXMOM data line where:

$$PMAXMOM = \frac{T}{[H_p]}$$

And $[H_p]$, the coefficient of horizontal load for pinned-head conditions, is obtained from Figure D.6 (after Figure 7 of Yang 1966) and is equal to 0.20.

Figure D.6, (After Figure 7 Yang 1966) Coefficient of horizontal load capacity.



Therefore:

$$PMAXMOM = \frac{T}{\left[H_p\right]} = \frac{5.4}{0.20} = 27 \text{ ft} = 324 \text{ in.}$$

The "ALLOW" and UNSP" data lines for CPGA do not represent actual allowable loads and buckling loads but were included only to obtain pile force and displacement results.

For the first increment of lateral loading, a trial and error process is used to determine the lateral load driving Pile #3 to its axial tensile capacity of 250 kips. This is accomplished with a lateral load of 88 kips. The CPGA input and output for this loading increment is presented below.

CPGA INPUT FOR RUN #1 Pinned-head piles

```
10 BATTER PILE BENT PINNED TOP FILE:BP4

15 PROP 3834. 16300. 16300. 453. 0.5 0.0 1 3

20 PROP 3834. 16300. 16300. 453. 1.0 0.0 2

30 SOIL NH .050 L 72. 24. 1 TO 3

40 PIN 1 TO 3

50 ALLOW R 1000. 242. 1485. 933. 8544. 8544. 1 TO 3

70 UNSP S 0.6 0.6 500. 500. N 1 TO 3

80 PMAXMOM 324. 324. 1 TO 3
```

CPGA LOAD-DISPLACEMENT OUTPUT FOR RUN #1 Pinned-head piles

```
PILE CAP DISPLACEMENTS

 LOAD

 CASE DX DZ R

 IN IN RAD

 1 .3079E+01 -.3695E-01 .5633E-02

 PILE FORCES IN LOCAL GEOMETRY

 M1 & M2 NOT AT PILE HEAD FOR PINNED PILES

 PILE F1 F2 F3 M1 M2

 K K K IN-K IN-K

 1  Pile #3 reaches its axial load capacity of 250 kips

 2
```

Horizontal displacement equals 3.1 inch

Maximum moments below the mudline

By trial-and-error push-over investigations, it can be shown that the next failure mechanism will occur due to flexural yielding of the piles below the mudline. This will be followed by buckling of Pile 2 followed by buckling of Pile 1 as load is shifted from Pile 2 to Pile 1. In the next CPGA run, a low stiffness modifier (C_{33} = 0.0001) is given to Pile 3 to eliminate its ability to attract axial load. This amounts to releasing Pile 3 in its axial direction since it has reached 250 kips of axial tensile capacity.

The CPGA analysis is performed with a final incremental barge impact load of 54 kips producing a total axial load in Pile 2 of: 506.4 + 14.2 = 520.6 kips (compression). This is less than the 1000 kips axial compressive capacity due to skin friction and end bearing. The additional barge impact load of 54 kips brings the flexural demand on the piles below the mudline to their yield capacities. Referring to the Figure D.3 interaction diagram for a compressive axial load of 500 kips the flexural yield capacity of the piling is 700 ft-k (8400 in.-k) and the flexural demand on Pile #2 is 2817 in.-k + 5524 in.-k = 8341 in.-k. This occurs at a total lateral displacement of 3.1 + 6.0 = 9.1 in. Referring to previous buckling calculations, an axial compressive load of 558 kip with 12.0 in. of lateral displacement will induce buckling. Therefore, when subjected to an additional 3 in. of lateral displacement, buckling of Pile #2 is expected to be followed by buckling of Pile #3. It should be noted that CPGA does not have the capability to introduce below mudline flexural hinges and therefore it will be assumed for the purpose of constructing the load-deformation curve that the stiffness of the system remains unchanged between the points below mudline where flexural hinging develops and buckling takes place.

A load-displacement plot for the pinned-head bent (solid blue curve) at a dry site is presented in Figure D.8 that is located at the end of this Appendix. This figure summarizes the resulting load displacement curves from this and three other CPGA analyses that will be discussed subsequently for pinned-head and fixed-head conditions at dry and wet sand sites. These other three push-over analyses will be summarized prior to discussing the resulting push-over load-displacement curves so that comparisons can be made among the results four analyses.

```
CPGA INPUT FOR RUN #2 Pinned-head piles

10 CANTILEVER BATTER PILE BENT FILE:BP5

15 PROP 3834. 16300. 16300. 453. 0.0001 0.0 3

20 PROP 3834. 16300. 16300. 453. 1.0 0.0 1 2

30 SOIL NH .047 L 72. 24. 1 TO 3

40 PIN 1 TO 3

50 ALLOW R 1000. 242. 1485. 933. 8544. 8544. 1 TO 3

70 UNSP S 0.6 0.6 500. 500. N 1 TO 3

80 PMAXMOM 324. 324. 1 TO 14
```

```
CPGA LOAD-DISPLACEMENT OUTPUT FOR RUN #2 Pinned-head piles

PILE CAP DISPLACEMENTS

 LOAD

 CASE DX DZ R

 IN IN RAD

 1 .5986E+01 .9708E-01 .1889E-01

 PILE FORCES IN LOCAL GEOMETRY

 PILE F1 F2 F3 M1 M2

 K K K IN-K IN-K
```

D.6 Push-over analysis for fixed-head condition – dry site

This section summarizes a second push-over analysis conducted for a fixed-head condition at a dry site using the CPGA software. The first incremental analysis was run using an axial stiffness modifier (C_{33}) for the

embedded portion of the pile with a value of 1.00 for compression piles and 0.50 for tension piles. This is a crude approximation of axial stiffness used to illustrate the push-over method. The actual value of the stiffness modifier (C_{33}) should be determined by appropriate analytical *t-z* models and/or pile load tests. To obtain the maximum moment below the mudline it is necessary to include a FUNSMOM data line where:

$$FUNSMOM = \frac{T}{[H_f]} + \frac{L_O + aT}{2}$$

Where [H_f], the coefficient of horizontal load for fixed-head conditions, is obtained from Figure D.6 (after Figure 7 of Yang 1966) and is equal to 0.47, and

L_O = free standing length = 24 ft
a = coefficient of effective embedment obtained from Figure D.7 for "fixed top translating" = 1.7

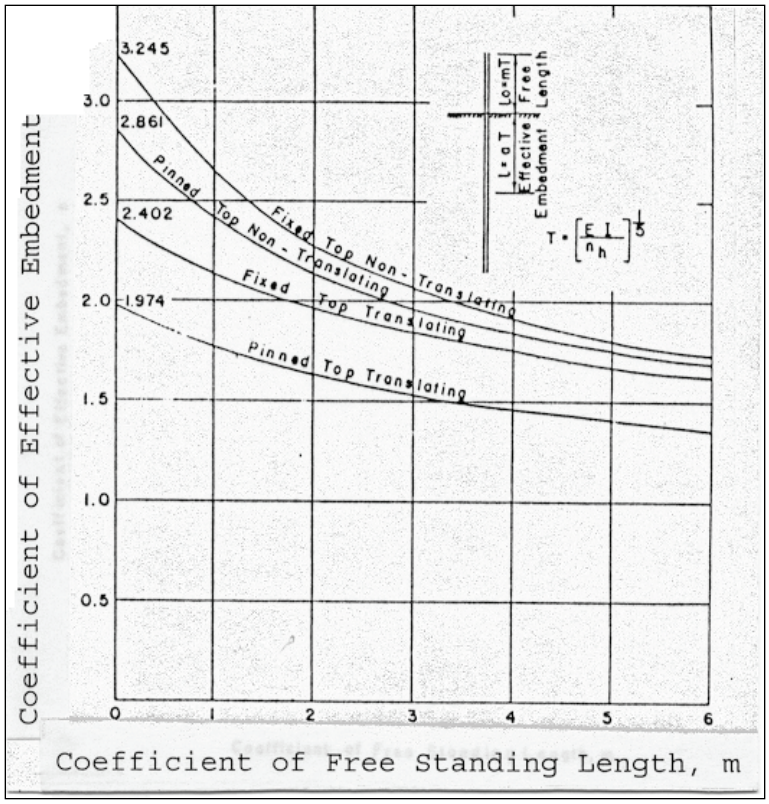
Therefore,

$$FUNSMOM = \frac{T}{[H_f]} + \frac{L_O + aT}{2} = \frac{5.4}{0.47} + \frac{24 + 1.7(5.4)}{2} = 28.1 \text{ ft} = 337 \text{ in.}$$

As before, the "ALLOW" and UNSP" data lines for CPGA do not represent actual allowable loads and buckling loads but were included only to obtain pile force and displacement results.

For the first increment of lateral loading, a trial-and-error process is used to determine the lateral load causing the pile to reach their moment capacities at the pile to pile cap connection. This is accomplished with a lateral load of 180 kips. CPGA input and output for this loading increment is presented below.

Figure D.7 (After Figure 2 Yang 1966) Effective embedment of pile at buckling.




```
CPGA INPUT FOR RUN #1 Fixed-head piles

10 BATTER PILE BENT FIXED TOP FILE:BF4

15 PROP 3834. 16300. 16300. 453. 0.5 0.0 1 3

20 PROP 3834. 16300. 16300. 453. 1.0 0.0 2

30 SOIL NH .050 L 72. 24. 1 2 3

40 FIX 1 TO 3

50 ALLOW R 1000. 242. 1485. 933. 8544. 8544. 1 2 3

70 UNSP S 0.6 0.6 1000. 1000. N 1 2 3

80 FUNSMOM 337. 337. 1 3
```

```
CPGA LOAD-DISPLACEMENT OUTPUT FOR RUN #1 Fixed-head piles

PILE CAP DISPLACEMENTS

 LOAD
 CASE DX DY DZ RX RY RZ
 IN IN IN RAD RAD RAD

 1 .2309E+01 .0000E+00 -.1013E+00 .0000E+00 .3155E-02 .0000E+00

 PILE FORCES IN LOCAL GEOMETRY
 PILE F1 F2 F3 M1 M2
 K K K IN-K IN-K
       1 32.1 .0 -122.1 .0 7002.7
 FUNSMOM .0 -3817.5
 2 32.3 .0 411.6 .0 7046.6
 FUNSMOM .0 -3846.5
 3 33.0 .0 -63.2 .0 7188.6
 FUNSMOM .0 -3940.4
```

From Figure B-3 (interaction diagram) for a tensile load of 122 kips the moment capacity ≈ 610 ft-k (7330 in-k). Therefore moment demand ≈ moment capacity at pile to pile cap connection.

For the second increment of lateral loading, a trial-and-error process is used to determine the lateral load causing pile #3 to reach its tensile load capacity (250 k). This occurs with a lateral load increase of 64 kips. The pile-to-pile cap connection is changed from fix to pin to capture the yielding that occurred in Run #1.

```
CPGA INPUT FOR RUN #2 Fixed-head piles
10 BATTER PILE BENT FIXED TOP FILE:BF5
15 PROP 3834. 16300. 16300. 453. 0.5 0.0 1 3
20 PROP 3834. 16300. 16300. 453. 1.0 0.0 2
30 SOIL NH .050 L 72. 24. 1 TO 3
40 PIN 1 TO 3
50 ALLOW R 1000. 242. 1485. 933. 8544. 8544. 1 TO 3
70 UNSP S 0.6 0.6 500. 500. N 1 TO 3
80 PMAXMOM 324. 324. 1 TO 3
90 BATTER 4. 2 TO 3
100 ANGLE 0. 1 2 3
110 PILE 1 0. 0. 0.
120 PILE 2 7. 0. 0.
130 PILE 3 14. 0. 0.
140 LOAD 1 64. 0. 200. 0. 0. 0.
190 TOUT 1 2 3 4 5 6 7
200 FOUT 1 2 3 4 5 6 7
210 PFO 1 TO 3
```

```
CPGA LOAD-DISPLACEMENT OUTPUT FOR RUN #2 Fixed-head piles

PILE CAP DISPLACEMENTS

 LOAD
 CASE DX DZ R
 IN IN RAD

 1 .2121E+01 .1493E-01 .4192E-02

PILE FORCES IN LOCAL GEOMETRY
 PILE F1 F2 F3 M1 M2
 K K K IN-K IN-K
       1 5.9 .0 18.0 .0 -1920.8
       2 6.0 .0 376.7 .0 -1937.50
       3 6.2 .0 -186.0 .0 -2014.8
```

Pile #3 has a tensile load of 63.2 k from Run #1 and 186.0 k from Run #2 giving a total axial tensile load of 249.2 k ≈ 250 k. tensile capacity reached.

By trial-and-error push-over investigations, it can be seen that next failure mechanism will occur due to flexural yielding of the piles below the mudline. This will be followed by buckling of Pile 2 followed by buckling of

Pile 1 as load is shifted from Pile 2 to Pile 1. In the next CPGA run, a low stiffness modifier (C_{33} = 0.0001) is given to Pile 3 to eliminate its ability to attract axial load. This amounts to releasing Pile 3 in its axial direction since it has reached 250 kips of axial tensile capacity.

The CPGA analysis is performed with a final incremental barge impact load of 22 kips producing a total axial load in Pile 2 of 411.6 + 376.7 + 5.8 = 794.1 kip (compression). This is less than the 1000 kip axial compressive capacity due to skin friction and end bearing. The additional barge impact load of 22 kips brings the flexural demand on the piles below the mudline to their yield capacities. Referring to the Figure D.3 interaction diagram for a compressive axial load of 800 kips, the flexural yield capacity of the piling is 670 ft-k (8040 in.-k) and the flexural demand on Pile #2 is 3846 in.-k + 1937 in.-k + 2246 in.-k = 8029 in.-k indicating demand is approximately equal to capacity. This occurs at a total lateral displacement of 2.3+ 2.1 + 2.4 = 6.8 in. Referring to previous buckling calculations, an axial compressive load of 800 kips at about 12.5 in. of lateral displacement will cause buckling. Therefore when subjected to an additional 6 in. of lateral displacement, buckling of Pile #2 is expected to be followed by buckling of Pile #3. It should be noted that CPGA does not have the capability to introduce below-mudline flexural hinges; therefore, it will be assumed for the purpose of constructing the load-deformation curve that the stiffness of the system remains unchanged between the points below mudline where flexural hinging develops and buckling takes place.

```
CPGA INPUT FOR RUN #3 Fixed-head piles
10 BATTER PILE BENT FIXED TOP FILE:BF6
15 PROP 3834. 16300. 16300. 453. 1.0 0.0 1 2
20 PROP 3834. 16300. 16300. 453. 0.0001 0.0 3
30 SOIL NH .050 L 72. 24. 1 TO 3
40 PIN 1 TO 3
50 ALLOW R 1000. 242. 1485. 933. 8544. 8544. 1 TO 3
70 UNSP S 0.6 0.6 500. 500. N 1 TO 3
80 PMAXMOM 324. 324. 1 TO 3
90 BATTER 4. 2 TO 3
100 ANGLE 0. 1 2 3
110 PILE 1 0. 0. 0.
120 PILE 2 7. 0. 0.
130 PILE 3 14. 0. 0.
140 LOAD 1 22. 0. 200. 0. 0. 0.
190 TOUT 1 2 3 4 5 6 7
200 FOUT 1 2 3 4 5 6 7
210 PFO 1 TO 3
```

```
CPGA OUTPUT FOR RUN #3 Fixed-head piles
PILE CAP DISPLACEMENTS

 LOAD
 CASE DX DZ R
 IN IN RAD

 1 .2407E+01 .9850E-01 .9300E-02

 PILE FORCES IN LOCAL GEOMETRY
 PILE F1 F2 F3 M1 M2
 K K K IN-K IN-K


      1 6.7 .0 198.0 .0 -2179.2
 2 6.9 .0 5.8 .0 -2245.7
 3 7.4 .0 -.2 .0 -2398.8
```

A load-displacement plot for the fixed-head bent (solid green curve) at a dry site is presented in Figure D.8.

D.7 Submerged Site

A submerged sand foundation with a stiffness that varies linearly with depth is investigated. The coefficient of subgrade reaction (n_h) is assumed to be 30 pci. This value for n_h is corresponds to Terzaghi's (1955) "recommended" value for a submerged medium-dense sand per Table 3.2 of Section 3 in Ebeling, et al. (2012). This is sometimes referred to as a "wet" site in that report.

The axial capacity based on soil limitations are 250 kips for piles in tension and 1000 kips for piles in compression.

Relative stiffness factor (T):

$$T = \sqrt[5]{\frac{E_c I_p}{n_h}} = 6.0 \text{ ft}$$

D.8 Buckling evaluation

Buckling loads for the concrete-filled pipe piles are determined using methods described in Yang (1996). Figures D.4 and D.5, after Figures 3 and 9 of Yang (1966), are provided for use in the analysis.

The coefficient of free standing length m is equal to the free standing length L_o divided by the relative stiffness factor T, or $m = L_o \div T = 24 \div 6.0 = 4.0$.

Assuming no translation, the critical buckling load can be determined using Figure D.4 (after Figure 3 in Yang 1966).

For pinned-top non-translating pile cap from Figure D.4, the coefficient of critical buckling strength [G] is equal to 0.030 and the Euler critical buckling load is

$$P_{CR} = \frac{\pi^2 E_c I_p}{T^2}[G] = 3256 \text{ kips}$$

For fixed-top non-translating pile cap from Figure D.4, the coefficient of critical buckling strength [G] is equal to 0.062 and the Euler critical buckling load is

$$P_{CR} = \frac{\pi^2 E_c I_p}{T^2}[G] = 6728 \text{ kips}$$

The critical buckling load with translation can be determined using Figure D.5 (after Figure 9 of Yang 1966). Entering Figure D.5 with a coefficient of free standing length (m) equal to 4.0, the coefficient of translation [G_T] is approximately equal to 0.20 for both pinned-head and fixed-head piles. Assuming a translation ($P_{CR\Delta}$), the critical buckling load is

$$P_{CR\Delta} = P_{CR}\left[1 - G_T\left(\frac{c}{r^2}\right)\Delta\right]$$

It is desirable for the push-over analysis to have the critical buckling load for various lateral displacements when performing a push-over analysis. This has been accomplished with the aid of MathCAD (1998) for pinned-head piles (Table D.3) and fixed-head piles (Table D.4).

Table D.3 Euler critical buckling load – translating pile top – pinned head condition.

Euler critical buckling load - Translating pile top

$G_T := 0.20$ Figure 9, Reference 1
Pinned top

$r := \left(\frac{I_p}{A_p}\right)^{0.5}$ $r = 0.5 \cdot ft$ $c := 1.0 \cdot ft$

$\Delta := 3 \cdot in, 4 \cdot in .. 14 \cdot in$

$P_{cr\Delta}(\Delta) := P_{cr} \cdot \left(1 - G_T \cdot \frac{c}{r^2} \cdot \Delta\right)$ $\Delta_x(\Delta) := \Delta$

$P_{cr\Delta}(\Delta) =$ •kip	$\Delta_x(\Delta) =$ •in
$2.605 \cdot 10^3$	3
$2.387 \cdot 10^3$	4
$2.17 \cdot 10^3$	5
$1.953 \cdot 10^3$	6
$1.736 \cdot 10^3$	7
$1.519 \cdot 10^3$	8
$1.302 \cdot 10^3$	9
$1.085 \cdot 10^3$	10
868.176	11
651.132	12
434.088	13
217.044	14

Table D.4 Euler critical buckling load – translating pile top – fixed head condition.

Euler critical buckling load - Translating pile top

$G_T := 0.20$ Figure 9, Reference 1
Fixed top

$r := \left(\frac{I_p}{A_p}\right)^{0.5}$ $r = 0.5 \cdot ft$ $c := 1.0 \cdot ft$

$\Delta := 3 \cdot in, 4 \cdot in .. 14 \cdot in$

$P_{cr\Delta}(\Delta) := P_{cr} \cdot \left(1 - G_T \cdot \frac{c}{r^2} \cdot \Delta\right)$ $\Delta_x(\Delta) := \Delta$

$P_{cr\Delta}(\Delta) =$ •kip	$\Delta_x(\Delta) =$ •in
$5.383 \cdot 10^3$	3
$4.934 \cdot 10^3$	4
$4.486 \cdot 10^3$	5
$4.037 \cdot 10^3$	6
$3.588 \cdot 10^3$	7
$3.14 \cdot 10^3$	8
$2.691 \cdot 10^3$	9
$2.243 \cdot 10^3$	10
$1.794 \cdot 10^3$	11
$1.346 \cdot 10^3$	12
897.115	13
448.557	14

D.9 Push-over analysis for pinned-head condition – wet site

This section summarizes a third push-over analysis conducted for a pinned-head condition at a wet site using Saul's (1968) method and the CPGA software. The first incremental analysis was run using an axial stiffness modifier (C_{33}) for the embedded portion of the pile with a value of 1.00 for compression piles and 0.50 for tension piles where:

$$C_{33} = \frac{\Delta}{\delta}$$

Where:

$$\Delta = \frac{PL}{AE}$$

This assumes that the pile is supported at its tip with all axial load (P) transferred to the tip and:

δ = actual displacement of the pile under axial load (P)

This is a crude approximation of axial stiffness used to illustrate the push-over method. The actual value of the stiffness modifier (C_{33}) should be determined by appropriate analytical *t-z* models and/or pile load tests. To obtain the maximum moment below the mudline, it is necessary to include a PMAXMOM data line where:

$$PMAXMOM = \frac{T}{[H_p]}$$

Where $[H_p]$, the coefficient of horizontal load for pinned-head conditions, is obtained from Figure D.6 (after Figure 7 of Yang 1966) and is equal to 0.21.

Therefore:

$$PMAXMOM = \frac{T}{[H_p]} = \frac{6.0}{0.21} = 28.57 \text{ ft} = 343 \text{ in.}$$

The "ALLOW" and UNSP" data lines for CPGA do not represent actual allowable loads and buckling loads but were included only to obtain pile force and displacement results.

For the first increment of lateral loading, a trial-and-error process is used to determine the lateral load driving Pile #3 to its axial tensile capacity of 250 kips. This is accomplished with a lateral load of 88 kips. CPGA input and output for this loading increment is presented below.

```
CPGA INPUT FOR RUN #1 Pinned-head piles
10 BATTER PILE BENT PINNED TOP FILE:BP8
15 PROP 3834. 16300. 16300. 453. 0.5 0.0 1 3
20 PROP 3834. 16300. 16300. 453. 1.0 0.0 2
30 SOIL NH .030 L 72. 24. 1 TO 3
40 PIN 1 TO 3
50 ALLOW R 1000. 242. 1485. 933. 8544. 8544. 1 TO 3
70 UNSP S 0.6 0.6 500. 500. N 1 TO 3
80 PMAXMOM 343. 343. 1 TO 3
90 BATTER 4. 2 TO 3
100 ANGLE 0. 1 2 3
110 PILE 1 0. 0. 0.
120 PILE 2 7. 0. 0.
130 PILE 3 14. 0. 0.
140 LOAD 1 88. 0. 200. 0. 0. 0.
190 TOUT 1 2 3 4 5 6 7
200 FOUT 1 2 3 4 5 6 7
210 PFO 1 TO 3
```

```
*****************************************************************
************

 PILE CAP DISPLACEMENTS
                                                  Horizontal
                                                  displacement
 LOAD                                             equals 3.1 inch

 CASE DX DZ R

 IN IN. RAD

 1 .3096E+01 -.3789E-01 .5660E-02


*****************************************************************
***********
                                                    Maximum moments
 PILE FORCES IN LOCAL GEOMETRY                      below the mudline

 LOAD CASE - 1
```

```
PILE F1 F2 F3 M1 M2

K K K IN.-K IN.-K


     1 7.9 .0 -45.7 .0 -2700.6

2 8.0 .0 508.5 .0 -2728.53

3 8.2 .0 -251.2 .0 -2829.1

            Pile #3 reaches its axial load
            capacity of 250 kips

**************************************************************
******
```

By trial-and-error push-over investigations, it can be shown that the next failure mechanism will occur due to flexural yielding of the piles below the mudline. This will be followed by buckling of Pile 2 followed by buckling of Pile 1 as load is shifted from Pile 2 to Pile 1. In the next CPGA run a low stiffness modifier (C_{33} = 0.0001) is given to Pile 3 to eliminate its ability to attract axial load. This amounts to releasing Pile 3 in its axial direction since it has reached 250 kips of axial tensile capacity.

The CPGA analysis is performed with a final incremental barge impact load of 52 kips producing a total axial load in Pile 2 of 508.5 + 13.8 = 522.3 kips (compression). This is less than the 1000 kips axial compressive capacity due to skin friction and end bearing. The additional barge impact load of 52 kips brings the flexural demand on the piles below the mudline to their yield capacities. Referring to the Figure D.3 interaction diagram for a compressive axial load of 500 kips, the flexural yield capacity of the piling is 700 ft-k (8400 in.-k) and the flexural demand on Pile #2 is 2728.5 in.-k + 5630.7 in.-k = 8359.2 in.-k. This occurs at a total lateral displacement of 3.1 + 6.3 = 9.4 in. Referring to previous buckling calculations, an axial compressive load of 560 kip with 12.0 in. of lateral displacement will induce buckling. Therefore, when subjected to an additional 3 in. of lateral displacement, buckling of Pile #2 is expected to be followed by buckling of Pile #3. It should be noted that CPGA does not have the capability to introduce below mudline flexural hinges; therefore, it will be assumed for

the purpose of constructing the load-deformation curve that the stiffness of the system remains unchanged between the points below mudline where flexural hinging develops and buckling takes place.

```
CPGA INPUT FOR RUN #2 Pinned-head piles
10 CANTILEVER BATTER PILE BENT FILE:BP5
15 PROP 3834. 16300. 16300. 453. 0.0001 0.0 3
20 PROP 3834. 16300. 16300. 453. 1.0 0.0 1 2
30 SOIL NH .030 L 72. 24. 1 TO 3
40 PIN 1 TO 3
50 ALLOW R 1000. 242. 1485. 933. 8544. 8544. 1 TO 3
70 UNSP S 0.6 0.6 500. 500. N 1 TO 3
80 PMAXMOM 343. 343. 1 TO 14
90 BATTER 4. 2 TO 3
100 ANGLE 0. 1 2 3
110 PILE 1 0. 0. 0.
120 PILE 2 7. 0. 0.
130 PILE 3 14. 0. 0.
140 LOAD 1 52. 0. 200. 0. 0. 0.
190 TOUT 1 2 3 4 5 6 7
200 FOUT 1 2 3 4 5 6 7
210 PFO 1 TO 3
```

```
*****************************************************************
******

 PILE CAP DISPLACEMENTS

 LOAD

 CASE DX DZ R

 IN IN. RAD

 1 .6265E+01 .9716E-01 .1972E-01

*****************************************************************
******
```

```
 PILE FORCES IN LOCAL GEOMETRY

 LOAD CASE - 1

 PILE F1 F2 F3 M1 M2

 K K K IN.-K IN.-K

 1 15.9 .0 195.3 .0 -5464.0

 2 16.4 .0 13.8 .0 -5630.7

 3 17.4 .0 -.5 .0 -5981.1

************************************************************************
******
```

A load-displacement plot for the pinned-head bent (dashed blue curve) at the wet site is presented in Figure D.8.

D.10 Push-over analysis for fixed-head condition – wet site

This section summarizes a fourth push-over analysis conducted for a fixed-head condition at a wet site using Saul's (1968) method and the CPGA software. The first incremental analysis was run using an axial stiffness modifier (C_{33}) for the embedded portion of the pile with a value of 1.00 for compression piles and 0.50 for tension piles. This is a crude approximation of axial stiffness used to illustrate the push-over method. The actual value of the stiffness modifier (C_{33}) should be determined by appropriate analytical *t-z* models and/or pile load tests. To obtain the maximum moment below the mudline, it is necessary to include a FUNSMOM data line where:

$$FUNSMOM = \frac{T}{[H_f]} + \frac{L_O + aT}{2}$$

Where $[H_f]$, the coefficient of horizontal load for fixed-head conditions, is obtained from Figure D.6 (after Figure 7 of Yang 1966) and is equal to 0.52, and:

L_O = free standing length = 24 ft

a = coefficient of effective embedment obtained from Figure D.7 for "fixed top translating" = 1.75

Therefore,

$$FUNSMOM = \frac{T}{\left[H_f\right]} + \frac{L_O + aT}{2} = \frac{6.0}{0.52} + \frac{24 + 1.7(6.0)}{2} = 28.6 \text{ ft} = 344 \text{ in.}$$

As before, the "ALLOW" and UNSP" data lines for CPGA do not represent actual allowable loads and buckling loads but were included only to obtain pile force and displacement results.

For the first increment of lateral loading, a trial-and-error process is used to determine the lateral load causing the pile to reach their moment capacities at the pile to pile cap connection. This is accomplished with a lateral load of 180 kips. CPGA input and output for this loading increment is presented below.

```
CPGA INPUT FOR RUN #1 Fixed-head piles
10 BATTER PILE BENT FIXED TOP FILE:BF7
15 PROP 3834. 16300. 16300. 453. 0.5 0.0 1 3
20 PROP 3834. 16300. 16300. 453. 1.0 0.0 2
30 SOIL NH .030 L 72. 24. 1 2 3
40 FIX 1 TO 3
50 ALLOW R 1000. 242. 1485. 933. 8544. 8544. 1 2 3
70 UNSP S 0.6 0.6 1000. 1000. N 1 2 3
80 FUNSMOM 344. 344. 1 3
85 FUNSMOM 344. 344. 2
90 BATTER 4. 2 TO 3
100 ANGLE 0. 1 2 3
110 PILE 1 0. 0. 0.
120 PILE 2 7. 0. 0.
130 PILE 3 14. 0. 0.
140 LOAD 1 180. 0. 200. 0. 0. 0.
190 TOUT 1 2 3 4 5 6 7
200 FOUT 1 2 3 4 5 6 7
210 PFO 1 TO 3
```

```
*****************************************************************
******

 PILE CAP DISPLACEMENTS

 LOAD

 CASE DX DY DZ

 IN IN IN

 1 .2462E+01 .0000E+00 -.1102E+00


*****************************************************************
******

 PILE FORCES IN LOCAL GEOMETRY

 LOAD CASE - 1

 PILE F1 F2 F3 M1 M2

 K K K IN.-K IN.-K

 1 31.2 .0 -132.9 .0 7045.0

 FUNSMOM .0 -3699.8

 2 31.5 .0 431.9 .0 7090.5

 FUNSMOM .0 -3729.1

 3 32.1 .0 -72.9 .0 7232.5

 FUNSMOM .0 -3820.5

*****************************************************************
```

From Figure B-3 (interaction diagram) for a tensile load of 122 kips the moment capacity ≈ 610 ft-k (7330 in-k). Therefore moment demand ≈ moment capacity at pile to pile cap connection.

For the second increment of lateral loading, a trial-and-error process is used to determine the lateral load causing pile #3 to reach its tensile load capacity (250 k). This occurs with a lateral load increase of 70 kips. The

pile-to-pile cap connection is changed from fix to pin to capture the yielding that occurred in Run #1.

```
CPGA INPUT FOR RUN #2 Fixed-head piles
10 BATTER PILE BENT FIXED TOP FILE:BF8
15 PROP 3834. 16300. 16300. 453. 0.5 0.0 1 3
20 PROP 3834. 16300. 16300. 453. 1.0 0.0 2
30 SOIL NH .030 L 72. 24. 1 TO 3
40 PIN 1 TO 3
50 ALLOW R 1000. 242. 1485. 933. 8544. 8544. 1 TO 3
70 UNSP S 0.6 0.6 500. 500. N 1 TO 3
80 PMAXMOM 344. 344. 1 TO 3
90 BATTER 4. 2 TO 3
100 ANGLE 0. 1 2 3
110 PILE 1 0. 0. 0.
120 PILE 2 7. 0. 0.
130 PILE 3 14. 0. 0.
140 LOAD 1 70. 0. 200. 0. 0. 0.
190 TOUT 1 2 3 4 5 6 7
200 FOUT 1 2 3 4 5 6 7
210 PFO 1 TO 3
```

```
*****************************************************************
******

 PILE CAP DISPLACEMENTS

 LOAD

 CASE DX DZ R

 IN IN. RAD

 1 .2437E+01 -.2179E-02 .4668E-02


*****************************************************************
************
```

```
PILE FORCES IN LOCAL GEOMETRY

LOAD CASE - 1

PILE F1 F2 F3 M1 M2

K K K IN.-K IN.-K

1 6.2 .0 -2.6 .0 -2131.9

2 6.3 .0 419.3 .0 -2151.91

3 6.5 .0 -207.2 .0 -2235.1
```

Pile #3 has a tensile load of 32.1 k from Run #1 and 207.2 k from Run #2 giving a total axial tensile load of 239.3 k ≈ 250 k. tensile capacity reached.

```
*****************************************************************
******
```

By trial-and-error push-over investigations it can be seen that next failure mechanism will occur due to flexural yielding of the piles below the mudline. This will be followed by buckling of Pile 2 followed by buckling of Pile 1 as the load is shifted from Pile 2 to Pile 1. In the next CPGA run, a low stiffness modifier (C_{33} = 0.0001) is given to Pile 3 to eliminate its ability to attract axial load. This amounts to releasing Pile 3 in its axial direction since it has reached 250 kips of axial tensile capacity.

The CPGA analysis is performed with a final incremental barge impact load of 22 kips producing a total axial load in Pile 2 of 431.9 + 419.3 + 5.9 = 857.1 kips (compression). This is less than the 1000 kips axial compressive capacity due to skin friction and bearing. The additional barge impact load of 22 kips brings the flexural demand on the piles below the mudline to their yield capacities. Referring to the Figure D.3 interaction diagram for a compressive axial load of 800 kips the flexural yield capacity of the piling is 675 ft-k (8100 in. k) and the flexural demand on Pile #2 is 3729 in. k + 2152 in. k + 2385 in. k = 8266 in. k which indicates that the demand is slightly greater than the capacity. This occurs at a total lateral displacement of 2.5 + 2.4 + 2.6 = 7.5 in. Referring to previous buckling calculations an axial compressive load of 857 kips at about 13 in. of lateral displacement will cause buckling. Therefore when subjected to an additional 5.5 in. of lateral displacement, buckling of Pile #2 is expected to be followed by buckling of Pile #3. It should be noted that CPGA does not have the capability to introduce below mudline

flexural hinges and therefore it will be assumed for the purpose of constructing the load-deformation curve that the stiffness of the system remains unchanged between the points below mudline where flexural hinging develops and buckling takes place.

```
CPGA INPUT FOR RUN #3 Fixed-head piles
10 BATTER PILE BENT FIXED TOP FILE:BF6
15 PROP 3834. 16300. 16300. 453. 1.0 0.0 1 2
20 PROP 3834. 16300. 16300. 453. 0.0001 0.0 3
30 SOIL NH .030 L 72. 24. 1 TO 3
40 PIN 1 TO 3
50 ALLOW R 1000. 242. 1485. 933. 8544. 8544. 1 TO 3
70 UNSP S 0.6 0.6 500. 500. N 1 TO 3
80 PMAXMOM 344. 344. 1 TO 3
90 BATTER 4. 2 TO 3
100 ANGLE 0. 1 2 3
110 PILE 1 0. 0. 0.
120 PILE 2 7. 0. 0.
130 PILE 3 14. 0. 0.
140 LOAD 1 22. 0. 200. 0. 0. 0.
190 TOUT 1 2 3 4 5 6 7
200 FOUT 1 2 3 4 5 6 7
210 PFO 1 TO 3
```

```
*****************************************************************
******

 PILE CAP DISPLACEMENTS

 LOAD

 CASE DX DZ R

 IN IN RAD

 1 .2645E+01 .9849E-01 .9010E-02

*****************************************************************
******
```

```
 PILE FORCES IN LOCAL GEOMETRY

 LOAD CASE - 1

 PILE F1 F2 F3 M1 M2

 K K K IN.-K IN.-K


      1 6.7 .0 198.0 .0 -2314.0

 2 6.9 .0 5.9 .0 -2384.5

 3 7.4 .0 -.2 .0 -2545.1


**********************************************************************
******
```

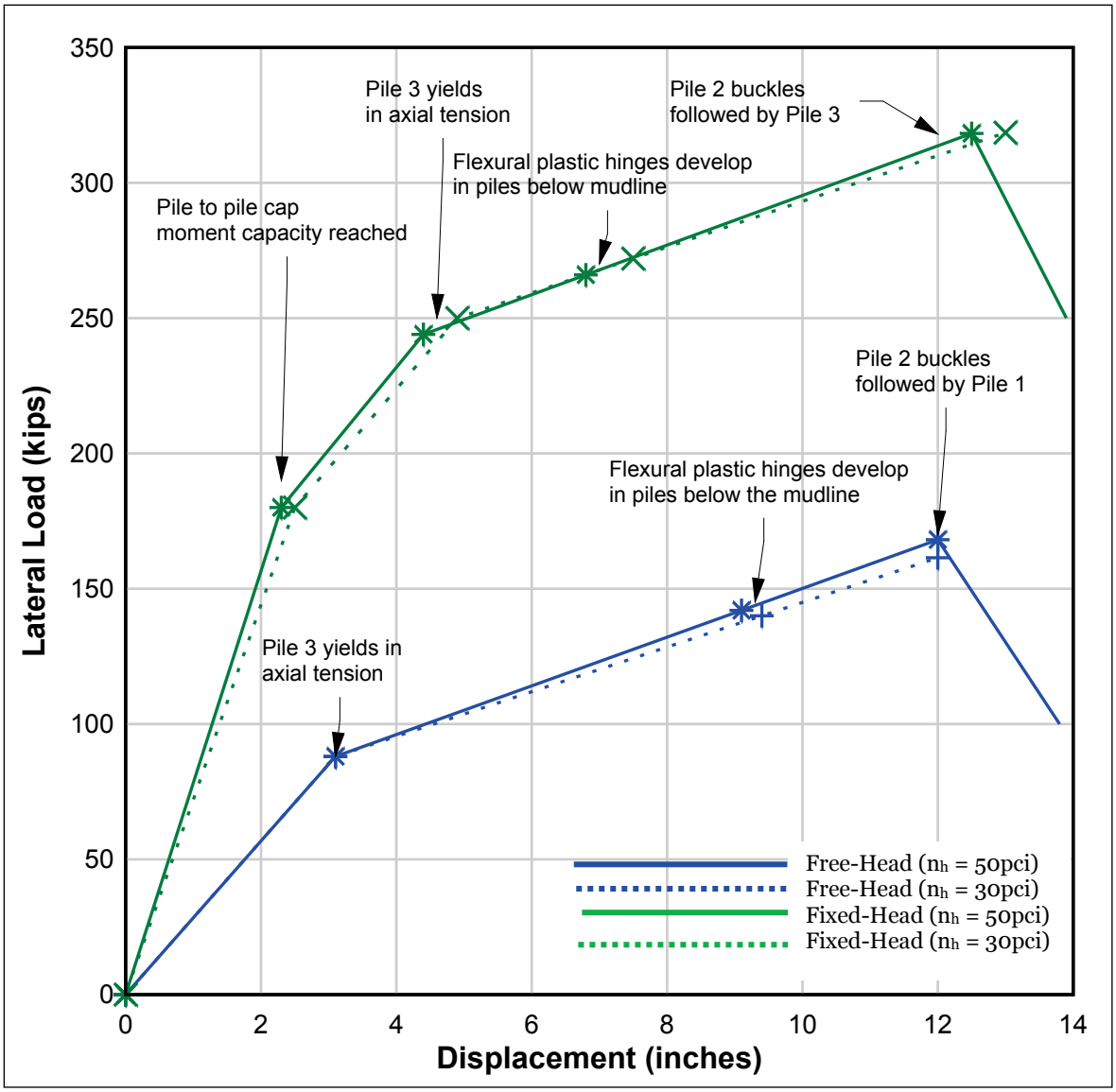
A load-displacement plot for the fixed-head bent (dashed green curve) at the wet site is presented in Figure D.8. The resulting structural system versus displacement plots characterizes the potential energy capacity of the particular batter pile bent being analyzed. The push-over results for four systems are shown in this figure.

In Figure D-8 the load-displacement results by the Saul (1968) method for a dry site (n_h = 50 pci) are represented by solid line and those for a submerged or wet site (n_h = 30 pci) by dashed lines. Yang (1966) and COM624G methods cannot be used for batter-pile systems because they are only applicable to single vertical pile analysis. The methods can be used for systems comprised of multiple vertical piles since a single pile from the system can be analyzed and the load-displacement results for the entire system derived based on the behavior of that single pile.

The load-displacement curves for the fixed-head pile system have four break points designating places where pile or soil yielding occurs. The number of yield points and the type of yielding will be pile bent and foundation dependent. For the particular pile-bent–foundation system investigated, the first break point (one with lowest displacement demand) occurs when flexural yielding takes place at the pile-to-pile cap connection. The second breakpoint occurs when Pile 3 yields in axial

tension (a foundation to pile transfer mechanism).[1] The third breakpoint occurs when flexural yielding takes place in the piles below the mudline. The fourth breakpoint occurs when Pile 2 buckles. Pile buckling quickly results in pile-bent system failure with little reserve potential energy capacity in the system.

Figure D.8 Load – displacement plot for pipe pile system.



There is little difference between the behaviors of submerged (wet) sites and dry sites, recognizing of course that lock approach wall bent systems will always be submerged. With batter-pile systems, the resistance to

[1] Recall pile numbers are reported in Figure D.2.

lateral load comes principally from pile axial stiffness and not from flexural stiffness, as is the case with vertical pile systems. Therefore, changes in lateral subgrade resistance (e.g., n_h) have little effect on system load-displacement behavior.

It can easily be recognized from Figure D-8 that the fixed-head system (green curves) has much greater potential energy capacity than the free-head system (blue curves). The free-head system does not possess the added lateral force resistance provided by rigid pile-to-pile cap connections (which is the first break point for the fixed-head system).

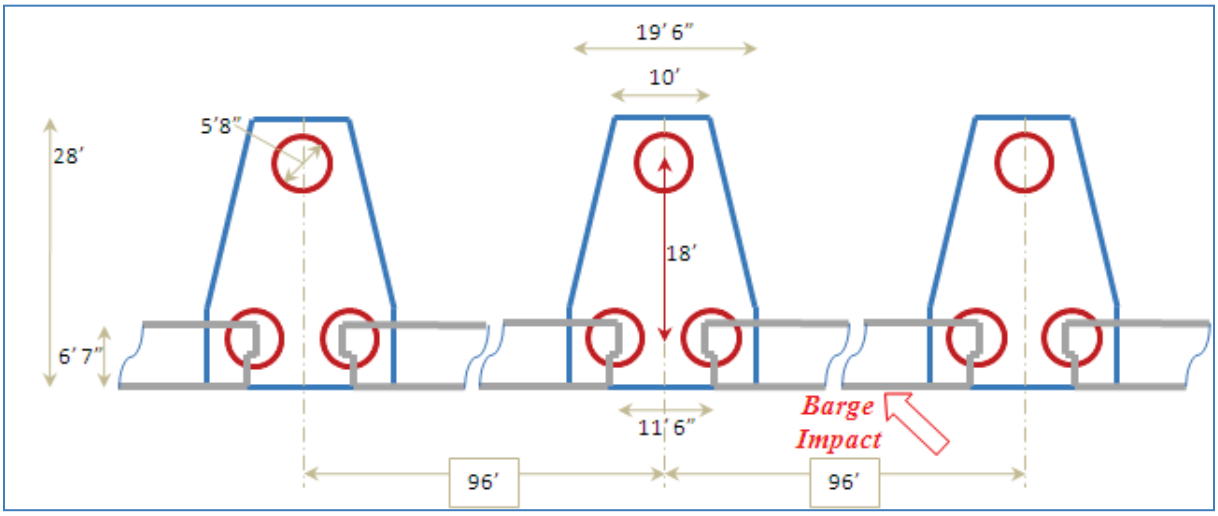
The information contained in this appendix illustrates the push-over analysis for a pinned-head and fixed-head batter pile bent using the Corps computer program CPGA (X0080) for wet and dry sites (i.e., n_h = 30 pci and 50 pci, respectively). Note that potential failure mechanisms and the sequence in which they form will likely be different for other batter-pile bent system groups and pile configurations.

Appendix E: Formulation for the rotational spring stiffness for the McAlpine flexible approach wall clustered group of vertical piles model

E.1 Calculation of the Center of Rigidity of a pile group for the McAlpine flexible wall model

The McAlpine flexible wall system is supported over pile groups consisting of three piles in a triangular arrangement as shown in Figure E.1. Impact_Deck computer program has the capability to perform a dynamic analysis of this structure that introduces an important change to the finite element model from the other two types of approach wall (i.e., guard wall and impact deck) structural configurations. This model change is the inclusion of a rotational spring at the central rigid link, in addition to moving the two translational elastic-plastic springs to the central rigid link. This addition is needed because the piles in the group are not in line with each other and a torsional resistance is provided by this configuration, which means that the pile bent rotates about a Center of Rigidity (C.R.), which is not in line with the wall beam. First, the location of the C.R. calculation must be performed because the C.R. position identifies the length of the rigid element which is perpendicular to the beam alignment.

Figure E.1. Plan view of the McAlpine flexible alternative approach wall system.



The length of the rigid element, which is perpendicular to the beam elements, is calculated as the distance between C.R. and the central blue

cross as shown in Figure E.2. Figure E.2 also shows the relation between the pile cap local axis and the beam global axis. This Figure also demonstrates that the alignment of the centerline of the beam does not coincide with the location of the piles.

Figure E.2 Relation between Global-Axis and central support Local-Axis.

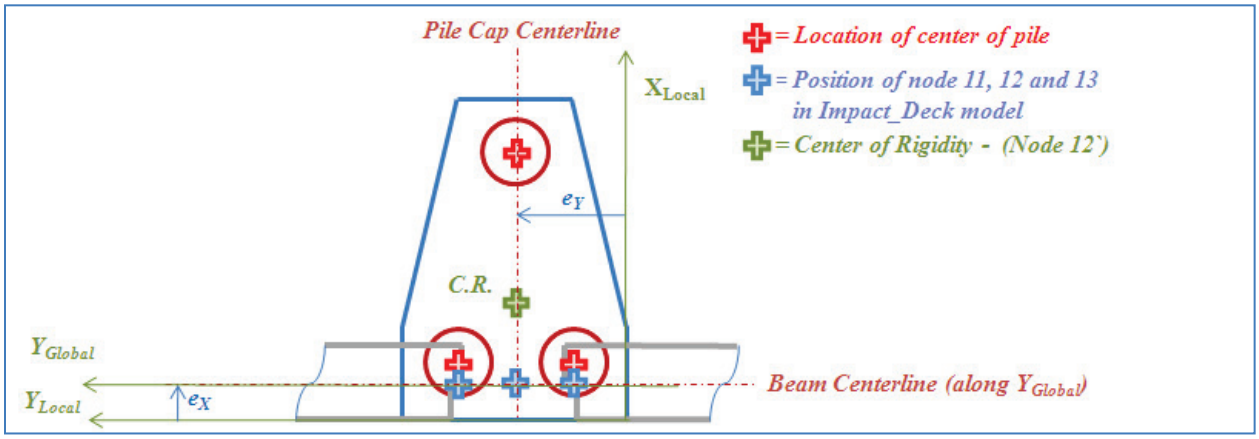
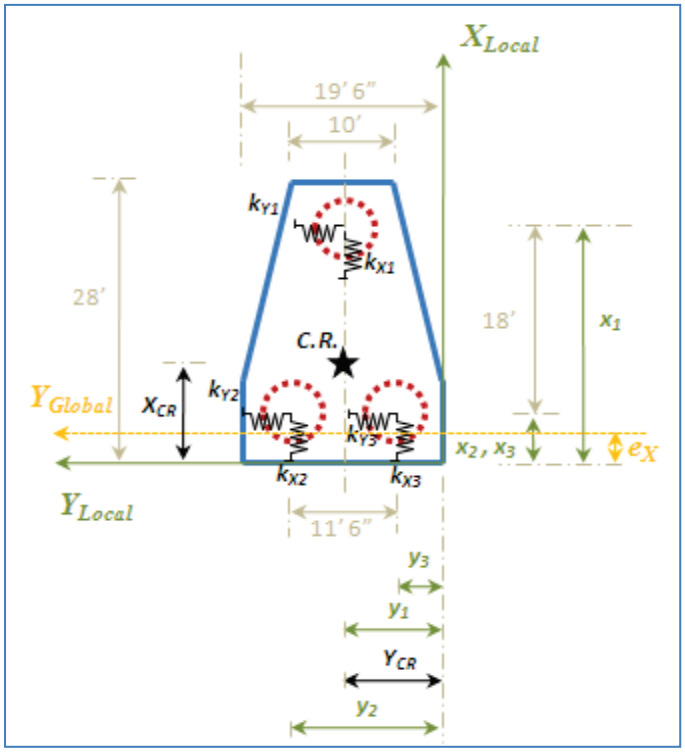


Figure E.3 shows the dimensions and the distances needed to calculate the center of rigidity

Figure E.3 Location of the Center of Rigidity.



The equations to calculate the C.R. are the following. First, the moment of inertia for an element with a circular cross-sectional is

$$I = \frac{\pi}{64} * d^4 \tag{E.1}$$

The translational elastic stiffness of the pile fixed at bottom and top is

$$k_{pile} = \frac{12 * E * I}{L^3} \tag{E.2}$$

If the piles have the same cross-sectional area, same modulus of elasticity, and same length then, following the notation presented in Figure E.3, the coordinates of the Center of Rigidity are

$$\begin{aligned} X_{CR} &= \frac{\sum_{i=1}^{n} k_{Yi} * x_i}{\sum_{i=1}^{n} k_{Yi}} \\ Y_{CR} &= \frac{\sum_{i=1}^{n} k_{Xi} * y_i}{\sum_{i=1}^{n} k_{Xi}} \end{aligned} \tag{E.3}$$

Following the same notation, the equivalent translational spring stiffness in the global coordinate system are calculated as

$$\left(k_X\right)_{eq.} = \sum_{i=1}^{n} k_{Xi} \tag{E.4}$$

$$\left(k_Y\right)_{eq.} = \sum_{i=1}^{n} k_{Yi} \tag{E.5}$$

where $n = number\ of\ piles$. Finally, the length of the rigid element which is perpendicular to the beam can be calculated as

$$L_{Rigid\ Link} = X_{CR} - e_X \tag{E.6}$$

E.2 Numerical example for the calculation of the Center of Rigidity

The definitions of the variables are presented in Figure E.3.

Data:

d = 5 ft 8 in. = pile diameter

f'c = 5,000 psi

E = 57,000(5,000)$^{1/2}$ = 4,030,508.65 psi = 580,393.25 ksf = Modulus of elasticity*

L = 20 ft = height of the pile above ground

e_X = beam width / 2 = 3 ft – 3.5 in.

Calculations:

*I = π * (5.6666)^4 / 64 = 50.613 ft^4*

*k_{pile} = 12 * 580,393.25* 50.613 / (20)^3*

= 44,063.16 kip / ft

k_{X1} = k_{X2} = k_{X3} = 44,063.16 kip / ft

k_{Y1} = k_{Y2} = k_{Y3} = 44,063.16 kip / ft

x_1 = (28 – 18) / 2 + 18 = 23 ft

x_2 = (28 – 18) / 2 = 5 ft

x_3 = (28 – 18) / 2 = 5 ft

y_1 = 19.5 / 2 = 9.75 ft

y_2 = (19.5 – 11.5) / 2 + 11.5 = 15.5 ft

y_3 = (19.5 – 11.5) / 2 = 4 ft

*X_{CR} = (44,063.16 *(23 + 5 + 5)) / 132,189.5*

$= 11\ ft$

$Y_{CR} = (44{,}063.16 * (9.75+15.5+4)) / 132{,}189.5 = 9.75\ ft$

$(k_X)_{eq.} = 132{,}189.5\ kip / ft$

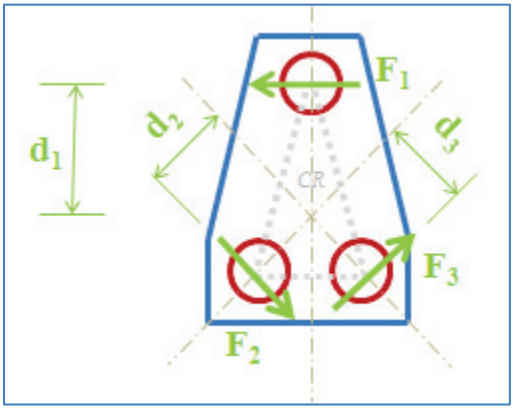
$(k_Y)_{eq.} = 132{,}189.5\ kip / ft$

$L_{Rigid\ Link} = 11 - 3.291666 = 7.708333\ ft$

E.3 Calculation of the rotational spring stiffness of a pile group for the McAlpine flexible wall model

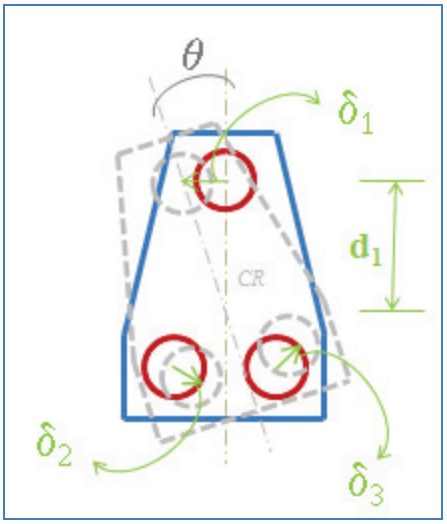
The rotational stiffness is developed in a pile group when the response forces are not aligned to the center of rigidity, forming moment arms from the line of action of the forces and the center of rigidity. That concept is presented in Figure E.4. Each one of the forces contributes to the resultant moment around the axis normal to the plan view.

Figure E.4 Definition of the forces and distances generated when the pile cap rotate.



The resultant moment creates a rotation in the structure. This angle of rotation is associated to the ratio of the lateral displacement to the distance from the center of each pile to the center of rigidity, as shown in Figure E.5.

Figure E.5 Rotational angle definition when the pile cap rotate.



The governing equations to calculate the rotational spring stiffness are the following. The distance from the line of action of the shear forces in the piles to the center of rigidity are,

$$d_1 = x_1 - X_{CR} \tag{E.7}$$

$$d_2 = d_3 = \sqrt{\left(y_2 - Y_{CR}\right)^2 + \left(X_{CR} - x_2\right)^2} \tag{E.8}$$

The resultant moment (torsion) due to the shear forces in the piles is

$$M_{CR} = \sum_{i=1}^{n} F_i d_i \tag{E.9}$$

where the forces in pile number one can be defined as the translational stiffness times the displacement achieved,

$$F_1 = k_1 * \delta_1 \tag{E.10}$$

and the rotation of the pile cap can be calculated as

$$tan(\theta) = \frac{\delta_1}{d_1} \tag{E.11}$$

this assumes that all piles will rotate the same amount (i.e., rigid body motion). Following that concept, the lateral displacement and shear forces at piles two and three are

$$\delta_2 = \theta * d_2 \tag{E.12}$$

$$F_2 = k_2 * \delta_2 \tag{E.13}$$

$$\delta_3 = \theta * d_3 \tag{E.14}$$

$$F_3 = k_3 * \delta_3 \tag{E.15}$$

Finally, the rotational spring stiffness can be calculated as the ratio of the resultant moment divided by the angle of rotation, as

$$k_r = \frac{M_{CR}}{\theta} \tag{E.16}$$

E.4 Numerical example of the calculation of the rotational spring stiffness of a pile group for the McAlpine flexible wall model

Using the numerical results obtained in section E.2, the calculation of the center of rigidity is presented next.

Data:

$k_{X1} = k_{X2} = k_{X3} = 44{,}063.16$ kip / ft

$k_{Y1} = k_{Y2} = k_{Y3} = 44{,}063.16$ kip / ft

$d_1 = 23 - 11 = 12$ ft

$d_2 = d_3 = (5.75^2 + 6^2)^{1/2} = 8.310$ ft

$\Delta_1 = 0.063$ ft

Calculations:

$F_1 = 44{,}063.16 * 0.063 = 2{,}775.98$ kips

tan ϑ = 0.063 / 12 = 0.00525

θ *= arctan (0.00525) = 0.00525 (small angle)*

d_2 *= 0.00525 * 8.310 = 0.0436 ft*

F_2 *= 44,063.16* 0.0436 = 1,921.15 kips*

d_3 *= 0.00525 * 8.310 = 0.0436 ft*

F_3 *= 44,063.16* 0.0436 = 1,921.15 kips*

M_{CR} *= 2,775.98* 12 + 1,921.15* 8.310*

+ 1,921.15 8.310 = 65,241.27 kip * ft*

k_r *= 65,241.27 / 0.00525 =* ***12,426,909 kip * ft /rad***

Appendix F: HHT-α method

In many structural dynamics applications, only low mode response is of interest. For these cases, the use of implicit unconditionally stable algorithms is generally preferred over conditionally stable algorithms. For unconditionally stable algorithms, a time step may be selected independent of stability considerations, thus results in a substantial saving of computational effort. In addition to being unconditionally stable, when only low mode response is of interest, it is often advantageous for an algorithm to possess some form of numerical dissipation to damp out any spurious participation of the higher modes. Examples of algorithms commonly used in structural dynamics which possess these properties are the Wilson-θ method and the Newmark-β method restricted to parameter values of $\gamma > \frac{1}{2}$ and $\beta \geq \frac{\left(\gamma+\frac{1}{2}\right)^2}{4}$. The Newmark family of methods allows the amount of dissipation to be continuously controlled by a parameter other than the time step. On the other hand, the dissipative properties of this family of algorithms are considered to be inferior to the Wilson method, since the lower modes are affected too strongly (Hilber et al. 1977).

In the Wilson-θ method, θ must be selected greater than or equal to 1.37 to maintain unconditional stability. It is recommended to use a value of $\theta = 1.42$, as further increasing θ reduces accuracy and further increases dissipation; but even for $\theta = 1.42$ the method is highly dissipative. *A well known deficiency of the Wilson-θ method is that it is generally too dissipative in the lower modes, requiring a time step to be taken that is smaller than that needed for accuracy. In addition, the Wilson-θ method tends to damp out the higher modes and could produce large errors when contributions of higher modes are significant* (Wilson 2010). Therefore, the use of Wilson-θ method has limited applications. Despite its shortcoming, the Wilson-θ method is considered by many to be the best available unconditionally stable one-step algorithm when numerical dissipation is desired.

Since it seemed that the commonly used unconditionally stable, dissipative algorithms of structural dynamics all possessed some drawbacks, in 1977 Hilber, Hughes, and Taylor presented a method called the HHT-α method. They were looking for an improved one-step method with the following requirements: a) it should be unconditionally stable when applied to linear problems, b) it should possess numerical dissipation which can be

controlled by a parameter other than the time step, (i.e., no numerical dissipation should be possible), and c) the numerical dissipation should not affect the lower modes too strongly. The resulting new algorithm, which consists of a combination of positive Newmark β-dissipation and negative α-dissipation, is shown to have improved characteristics when compared to the Wilson-θ method.

The Hilber, Hughes, and Taylor HHT-α method is a generalization of the Newmark-β method. The finite-difference equations for the HHT-α method are identical to those of the Newmark-β method. However, the equations of motion has to be modified using the parameter α, as follows,

$$\boldsymbol{m}\ddot{\boldsymbol{u}}_{t+\Delta t} + (1+\alpha)\boldsymbol{c}\dot{\boldsymbol{u}}_{t+\Delta t} - \alpha\boldsymbol{c}\dot{\boldsymbol{u}}_{t} + (1+\alpha)\boldsymbol{k}\boldsymbol{u}_{t+\Delta t} - \alpha\boldsymbol{k}\boldsymbol{u}_{t} = (1+\alpha)\boldsymbol{f}_{t+\Delta t} - \alpha\boldsymbol{f}_{t} \quad \text{(F.1)}$$

where α, β, and γ are free parameters, which govern the stability and numerical dissipation of the algorithm. If α = 0 this family of algorithms reduces to the Newmark family. In this case if $\gamma = \frac{1}{2}$ the algorithms possess no numerical dissipation whereas if $\gamma > \frac{1}{2}$ numerical dissipation is present and if $\beta \geq \frac{\left(\gamma+\frac{1}{2}\right)^2}{4}$ the new algorithm is unconditionally stable. However, by appropriately combining negative α-dissipation with particular values of β and γ, a one-parameter family of algorithms with the attributes previously enumerated can be developed. Hilber, Hughes, and Taylor in 1977 used $\beta = \frac{(1-\alpha)^2}{4}$ and $\gamma = \frac{1}{2} - \alpha$. They found by numerical experimentation that the range of practical interest was $-\frac{1}{3} \leq \alpha \leq 0$. This ensures adequate dissipation in the higher modes and at the same time guarantees that the lower modes are not affected too strongly. Finally, if α, β, and γ have the following expressions, $-\frac{1}{3} \leq \alpha \leq 0, \beta = \frac{(1-\alpha)^2}{4}$, and $\gamma = \frac{1}{2} - \alpha$, the HHT-α method is second-order accurate and unconditionally stable. With $\alpha = 0$ the HHT-α method reduces to the constant acceleration method. The HHT-α method is useful in structural dynamics simulations incorporating many degrees of freedom (DOF), and in which it is desirable to numerically attenuate the response at high frequencies. Decreasing α below zero decreases the response at frequencies above $\frac{1}{2\Delta t}$, provided that β and γ are defined as above. The procedure of the HHT-α method is summarized in Table F.1.

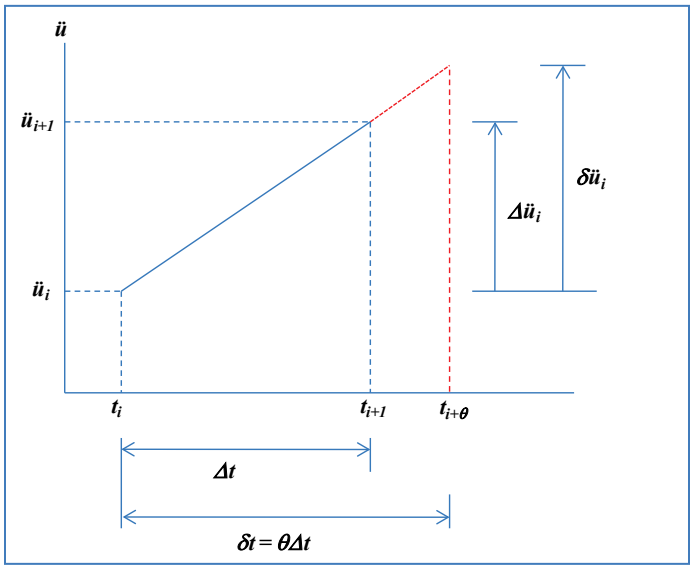
Table F.1. HHT-α Method.

1. Initial calculations
1.1 Select Δt and α, $(-\frac{1}{3} \le \alpha \le 0)$.
1.2 Calculate $\beta = \frac{(1-\alpha)^2}{4}$ and $\gamma = \frac{1}{2} - \alpha$.
1.3 Solve for $\ddot{\boldsymbol{u}}_0 \therefore \ \boldsymbol{m}\ddot{\boldsymbol{u}}_0 = (1+\alpha)(\boldsymbol{p}_0 - \boldsymbol{c}\dot{\boldsymbol{u}}_0 - \boldsymbol{k}\boldsymbol{u}_0)$.
1.4 Calculate $\bar{\boldsymbol{c}} = (1+\alpha)\boldsymbol{c} \therefore \bar{\boldsymbol{k}} = (1+\alpha)\boldsymbol{k}$
1.5 $\hat{\mathbf{k}} = \bar{\boldsymbol{k}} + \frac{\gamma}{\beta\Delta t}\bar{\boldsymbol{c}} + \frac{1}{\beta(\Delta t)^2}\boldsymbol{m}$
1.6 $\boldsymbol{a} = \frac{1}{\beta\Delta t}\boldsymbol{m} + \frac{\gamma}{\beta}\bar{\boldsymbol{c}}; and\ \boldsymbol{b} = \frac{1}{2\beta}\boldsymbol{m} + \Delta t\left(\frac{\gamma}{2\beta} - 1\right)\bar{\boldsymbol{c}}$.
2. Calculations for each time step, *i*
2.1 $\bar{\bar{\boldsymbol{c}}} = \alpha\boldsymbol{c}(\dot{\boldsymbol{u}}_{\boldsymbol{i}} - \dot{\boldsymbol{u}}_{\boldsymbol{i-1}}) \therefore \bar{\bar{\boldsymbol{k}}} = \alpha\boldsymbol{k}(\boldsymbol{u}_{\boldsymbol{i}} - \boldsymbol{u}_{\boldsymbol{i-1}}) \therefore \bar{\boldsymbol{f}} = (1+\alpha)\boldsymbol{f}_{i+1} - (1+2\alpha)\boldsymbol{f}_i + \alpha\boldsymbol{f}_{i-1}$.
2.2 $\Delta\boldsymbol{p}_{\boldsymbol{i}} = \bar{\boldsymbol{f}} + \bar{\bar{\boldsymbol{c}}} + \bar{\bar{\boldsymbol{k}}} \ \therefore \ \Delta\hat{\boldsymbol{p}}_i = \Delta\boldsymbol{p}_i + \boldsymbol{a}\dot{\boldsymbol{u}}_i + \boldsymbol{b}\ddot{\boldsymbol{u}}_i$.
2.3 Solve for $\Delta\boldsymbol{u}_i$ from $\hat{\boldsymbol{k}}\Delta\boldsymbol{u}_i = \Delta\hat{\boldsymbol{p}}_i$.
2.4 $\Delta\dot{\boldsymbol{u}}_i = \frac{\gamma}{\beta\Delta t}\Delta\boldsymbol{u}_i - \frac{\gamma}{\beta}\dot{\boldsymbol{u}}_\iota + \Delta t\left(1 - \frac{\gamma}{2\beta}\right)\ddot{\boldsymbol{u}}_i$.
2.5 $\Delta\ddot{\boldsymbol{u}}_i = \frac{1}{\beta(\Delta t)^2}\Delta\boldsymbol{u}_i - \frac{1}{\beta\Delta t}\dot{\boldsymbol{u}}_\iota - \frac{1}{2\beta}\ddot{\boldsymbol{u}}_\iota$.
2.6 $\boldsymbol{u}_{i+1} = \boldsymbol{u}_i + \Delta\boldsymbol{u}_i, \dot{\boldsymbol{u}}_{i+1} = \dot{\boldsymbol{u}}_i + \Delta\dot{\boldsymbol{u}}_i, and\ \ddot{\boldsymbol{u}}_{i+1} = \ddot{\boldsymbol{u}}_i + \Delta\ddot{\boldsymbol{u}}_\iota$.
3. Repetition for the next time step. Replace *i* by i+1 and implement steps 2.1 to 2.6 for the next time step.

Appendix G: Wilson-θ Method

In Impact_Deck, the solution of the MDOF equations of motion is obtained by applying the Wilson-θ method. This method, developed by E.L. Wilson (2002), is a modification of the conditionally stable linear acceleration method that makes it unconditionally stable. This modification is based on the assumption that the acceleration varies linearly over an extended time step $\delta_t = \theta \Delta t$, as shown in Figure G.1. The accuracy and stability properties of the method depend on the value of the parameter θ, which is always greater than 1.

Figure G.1 Linear variation of acceleration over normal and extended time steps.



The numerical procedure can be derived merely by rewriting the basic relationship of the linear acceleration method. The corresponding matrix equations that apply to MDOF systems are

$$\Delta \dot{u}_i = (\Delta t)\ddot{u}_i + \frac{\Delta t}{2}\Delta \ddot{u}_i \qquad \Delta u_i = (\Delta t)\dot{u}_i + \frac{(\Delta t)^2}{2}\ddot{u}_i + \frac{(\Delta t)^2}{6}\Delta \ddot{u}_i \quad \text{(G.1)}$$

Replacing Δt by δt and the incremental responses by u_i, $\delta \dot{u}_i$, and $\delta \ddot{u}_i$, as shown in Figure G.1 gives the corresponding equations for the extended time step:

$$\delta \dot{u}_i = (\delta t)\ddot{u}_i + \frac{\delta t}{2}\delta \ddot{u}_i \therefore \delta u_i = (\delta t)\dot{u}_i + \frac{(\delta t)^2}{2}\ddot{u}_i + \frac{(\delta t)^2}{6}\delta \ddot{u}_i \quad \text{(G.2)}$$

The right equation in Equation (G.2) can be solved for

$$\delta \ddot{u}_i = \frac{6}{(\delta t)^2}\delta u_i - \frac{6}{\delta t}\dot{u}_i - 3\ddot{u}_i \quad \text{(G.3)}$$

Substituting Equation (G.3) into the left equation of Equation (G.2) gives

$$\delta \dot{u}_i = \frac{3}{\delta t}\delta u_i - 3\dot{u}_i - \frac{\delta t}{2}\ddot{u}_i \quad \text{(G.4)}$$

Next, Equations (G.3) and (G.4) are substituted into the incremental (over the extended time step) equation of motion:

$$m\delta \ddot{u}_i + c\delta \dot{u}_i + k_i \delta u_i = \delta p_i \quad \text{(G.5)}$$

where, based on the assumption that the exciting force vector also varies linearly over the extended time step.

$$\delta p_i = \theta(\Delta p_i) \quad \text{(G.6)}$$

This substitution leads to

$$\hat{k}_i \delta u_i = \delta \hat{p}_i \quad \text{(G.7)}$$

where:

$$\hat{k}_i = k_i + \frac{3}{\theta \Delta t}c + \frac{6}{(\theta \Delta t)^2}m \quad \text{(G.8)}$$

$$\delta \hat{p}_i = \theta\left(\Delta \hat{p}_i\right) + \left(\frac{6}{\theta \Delta t}m + 3c\right)\dot{u}_i + \left(3m + \frac{\theta \Delta t}{2}c\right)\ddot{u}_i \quad \text{(G.9)}$$

Equation (G.7) is solved for δu_i, and $\delta \ddot{u}_i$ is computed from Equation (G.3). The incremental acceleration over the normal time step is then given by

$$\Delta \ddot{u}_i = \frac{1}{\theta}\delta \ddot{u}_i \tag{G.10}$$

And the incremental velocity and displacement are determined from Equation (G.1). The procedure is summarized in Table G.1.

Table G.1 Wilson's Method: Nonlinear Systems

1. Initial calculations
1.1 Solve $m\ddot{u}_0 = p_0 - c\dot{u}_0 - (f_s)_0 \Rightarrow \ddot{u}_0$.
1.2 Select Δt and θ.
1.3 $\boldsymbol{a} = \frac{6}{\theta \Delta t}\boldsymbol{m} + 3\boldsymbol{c}; and\ \boldsymbol{b} = 3\boldsymbol{m} + \frac{\theta \Delta t}{2}\boldsymbol{c}$.
2. Calculations for each time step, *i*
2.1 $\delta \widehat{\boldsymbol{p}}_{\boldsymbol{i}} = \theta(\Delta \widehat{\boldsymbol{p}}_{\boldsymbol{i}}) + \boldsymbol{a}\dot{\boldsymbol{u}}_{\boldsymbol{i}} + \boldsymbol{b}\ddot{\boldsymbol{u}}_{\boldsymbol{i}}$.
2.2 Determine the tangent stiffness matrix $\boldsymbol{k}_{\boldsymbol{i}}$.
2.3 $\widehat{\boldsymbol{k}_{\boldsymbol{i}}} = \boldsymbol{k}_{\boldsymbol{i}} + \frac{3}{\theta \Delta t}\boldsymbol{c} + \frac{6}{(\theta \Delta t)^2}\boldsymbol{m}$.
2.4 Solve for δu_i from $\hat{k}_i\ and\ \delta \hat{p}_i$
2.5 $\boldsymbol{\delta \ddot{u}_i} = \frac{6}{(\theta \Delta t)^2}\boldsymbol{\delta u_i} - \frac{6}{\theta \Delta t}\boldsymbol{\dot{u}_i} - 3\boldsymbol{\ddot{u}_i}$; and $\Delta \boldsymbol{\ddot{u}_i} = \frac{1}{\theta}\boldsymbol{\delta \ddot{u}_i}$.
2.6 $\Delta \boldsymbol{\dot{u}_i} = (\Delta t)\boldsymbol{\ddot{u}_i} + \frac{\Delta t}{2}\Delta \boldsymbol{\ddot{u}_i}; and\ \Delta \boldsymbol{u_i} = (\Delta t)\boldsymbol{\dot{u}_i} + \frac{(\Delta t)^2}{2}\boldsymbol{\ddot{u}_i} + \frac{(\Delta t)^2}{6}\Delta \boldsymbol{\ddot{u}_i}$.
2.7 $\boldsymbol{u}_{i+1} = \boldsymbol{u}_i + \Delta \boldsymbol{u}_i, \dot{\boldsymbol{u}}_{i+1} = \dot{\boldsymbol{u}}_i + \Delta \dot{\boldsymbol{u}}_i, and\ \ddot{\boldsymbol{u}}_{i+1} = \ddot{\boldsymbol{u}}_i + \Delta \ddot{\boldsymbol{u}}_i$.
3. Repetition for the next time step. Replace *i* by i+1 and implement steps 2.1 to 2.7 for the next time step.

As mentioned earlier, the value of θ governs the stability characteristics of Wilson's method. If θ = 1, then this method reverts to the linear acceleration method, which is stable if $\Delta t < 0.551 T_N$, where T_N is the shortest natural period of the system. If θ ≥ 1.37, the Wilson-θ method is unconditionally stable, making it suitable for direct solution of the equations of motion and θ = 1.42 gives optimal accuracy.

Appendix H: Member End Release Details for Load Applied at the End Release Node

Member end release occurs in the Impact_Deck software when there is no moment transfer from one node to the next, because of an internal pin from one beam or deck to the next. Member end release details are discussed in Appendices A, B, and C for the generic case when the load is not applied at the end release node.

When the load is applied at the end release node, an additional term is required for the end release equations and the load is altered to accomplish the lack of moment transfer. This Appendix extends the equations to include these terms.

For a beam element, the six equilibrium equations in the local reference system can be written as

$$f_n = \sum_{j=1}^{6} k_{nj} u_j + r_n \therefore n = 1,2,\ldots,6 \tag{H.1}$$

If one end of the member has a hinge, or other type of release that causes the corresponding force to be equal to zero, Equation (H-1) requires modification. If we know that a specific value of f_n is zero because of a release, the corresponding displacement u_n can be written as:

$$u_n = \sum_{j=1}^{n-1} \frac{k_{nj}}{k_{nn}} u_j + \sum_{j=n+1}^{12} \frac{k_{nj}}{k_{nn}} u_j + r_n \tag{H.2}$$

Therefore, by substitution of equation (H.2) into the other five equilibrium equations, the unknown u_n can be eliminated and the corresponding row and column set to zero. Or:

$$\overline{f}_{ij} = \overline{k}_{ij}\, u_{ij} + \overline{r}_{ij} \tag{H.3}$$

The terms $f_n = r_n = 0$ and the new stiffness and load terms are equal to:

$$\overline{k}_{ij} = k_{ij} - k_{in} \frac{k_{nj}}{k_{nn}} \tag{H.4}$$

$$\overline{r}_i = r_i - r_n \frac{k_{in}}{k_{nn}} \tag{H.5}$$

This procedure can be repeatedly applied to the element equilibrium equations for all releases. The repeated application of the simple numerical equation is sometimes called the ***static condensation or partial Gauss elimination***.

Appendix I: Rayleigh Damping

In this Appendix, the implementation of damping in the numerical procedures used in the computer software Impact_Deck will be discussed. Rayleigh damping is the method used.

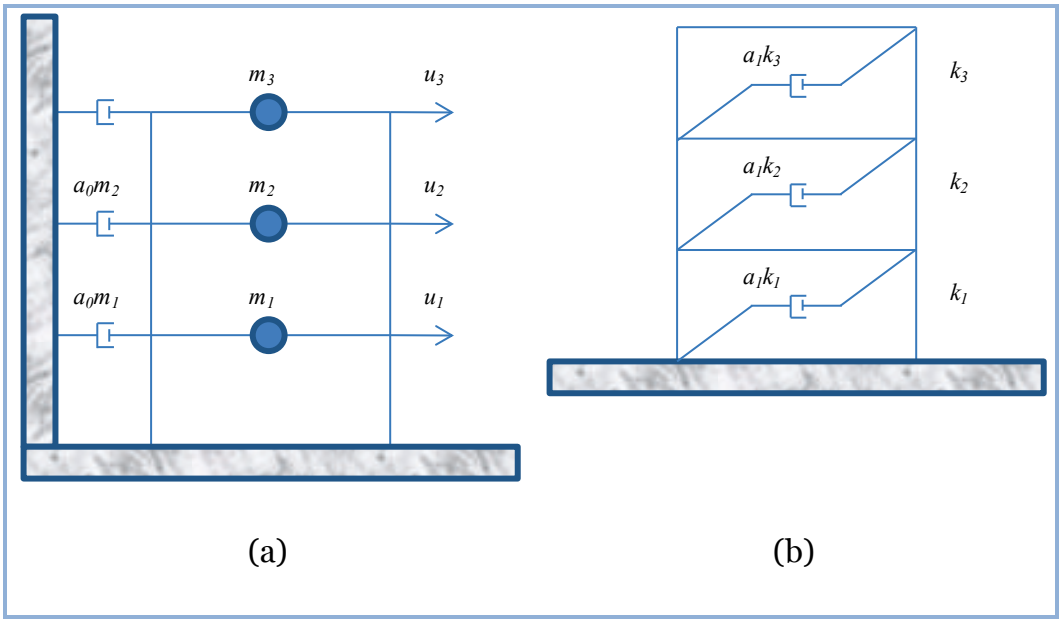
I.1 Method

Consider first mass-proportional damping and stiffness-proportional damping:

$$c = a_0 m \text{ and } c = a_1 k \tag{I.1}$$

Where the constants a_0 and a_1 have units of sec^{-1} and sec, respectively. Physically, they represent the damping models shown in Figure I.1 for a multistory building. Stiffness-proportional damping appeals to intuition because it can be interpreted to model the energy dissipation arising from story deformations. In contrast, mass-proportional damping is difficult to justify physically because the mass of the air damping the structure, compared to the structural mass, is negligibly smaller. Later we shall see that, by themselves, neither of the two damping models are appropriate for practical application.

Figure I.1 (a) Mass-proportional damping; (b) stiffness-proportional damping.



We now relate the modal damping ratios for a system with mass-proportional damping to the coefficient a_0. The generalized damping for the n^{th} mode, Equation (I.1) is

$$C_n = a_0 M_n \tag{I.2}$$

and the modal damping ratio is

$$\beta_n = \frac{a_0}{2}\frac{1}{\omega_n} \tag{I.3}$$

The damping ratio is inversely proportional to the natural frequency. The coefficient a_0 can be selected to obtain a specified value of damping ratio in any one mode, say β_i for the i^{th} mode. Equation (I.3) then gives

$$a_0 = 2\beta_i\omega_i \tag{I.4}$$

When a_0 has been computed, the damping matrix c can be determined from Equation (I.1). The damping ratio in any other mode, say the n^{th} mode, is given by Equation (I.3). Similarly, the modal damping ratios for a system with stiffness-proportional damping can be related to the coefficient a_1 . In this case

$$C_n = a_1\omega_n^2 M_n \text{ and } \beta_n = \frac{a_1}{2}\omega_n \tag{I.5}$$

The damping ratio increases linearly with the natural frequency. The coefficient a_1 can be selected to obtain a specified value of the damping ratio in any one mode, say β_i for the j^{th} mode. Equation (I.5) then gives

$$a_1 = \frac{2\zeta_j}{\omega_j} \tag{I.6}$$

When a_1 has been computed, the damping matrix $\boldsymbol{c}$ can be determined from Equation (I.1), and the damping ratio in any other mode is given by Equation (I.5). Neither of the damping matrices defined by the previous matrices is appropriate for practical analysis of MDOF systems. The variations of modal damping ratios with the natural frequencies they

represent are not consistent with experimental data indicating roughly the same damping ratios for several vibration modes of a structure.

As a first step toward constructing a classical damping matrix somewhat consistent with experimental data, we consider *Rayleigh damping*

$$c = a_0 m + a_1 k \tag{I.7}$$

The damping ratio for the n^{th} mode of such a system is

$$\beta_n = \frac{a_0}{2}\frac{1}{\omega_n} + \frac{a_1}{2}\omega_n \tag{I.8}$$

The coefficients a_0 and a_1 can be determined from specified damping ratios β_i and β_j for the i^{th} and j^{th} modes, respectively. Expressing Equation (I.8) for these two modes in matrix from leads to

$$\frac{1}{2}\begin{bmatrix} 1/\omega_i & \omega_i \\ 1/\omega_j & \omega_j \end{bmatrix}\begin{Bmatrix} a_0 \\ a_1 \end{Bmatrix} = \begin{Bmatrix} \beta_i \\ \beta_j \end{Bmatrix} \tag{I.9}$$

These two algebraic equation can be solved to determine the coefficients a_0 and a_1. If both modes are assumed to have the same damping ratio β, which is reasonable based on experimental data, then

$$a_0 = \beta\frac{2\omega_i\omega_j}{\omega_i + \omega_j} \quad a_1 = \beta\frac{2}{\omega_i + \omega_j} \tag{I.10}$$

The damping matrix is then computed from Equation (I.7) and the damping ratio for any other mode, given by Equation (I.8), varies with natural frequency.

When applying this procedure to a practical problem, the modes i and j along with specified damping ratios should be chosen to ensure reasonable values for the damping ratios in all the modes contributing significantly to the response.

In the Impact_Deck computer program this type of damping model is implemented to obtain the dynamic response. The user assigns a fixed

damping ratio and Impact_Deck estimates the natural frequencies and calculate the coefficients a_0 and a_1, and assemble the damping matrix of the system based on Equation (A.31).

I.2 Impact Deck frequency estimates

For the model of an impact deck or beam directly mounted on a cluster of piles specified in Appendix A, Impact_Deck estimates the first two natural frequencies as follows:

$$\omega_1 = \omega_2 = \sqrt{\frac{\bar{k}}{\bar{m}}} \tag{I.11}$$

where:

$\bar{k}$ =spring transverse stiffness per unit length of the beam = (total number of springs * linear stiffness of one spring) / total length of the beam

$\bar{m}$ =the mass per unit length of the beam = mass density of the beam * cross-sectional area of the beam

This estimate is based on SAP2000 models for a similar structure, and guidance from Chopra (2001).

I.3 Guard Wall frequency estimates

For the model of a guard wall consisting of simply supported beams specified in Appendix B, Impact_Deck estimates the first two natural frequencies as follows,

$$\omega_1 = \sqrt{\frac{2.5 * k}{m}} \therefore \omega_2 = \sqrt{\frac{3.0 * k}{m}} \tag{I.12}$$

where:

k =the transverse elastic stiffness of the center pile group

m =the total mass of the two beams = mass density of the beam * cross-sectional area of the beam * total length of the structure

This estimate is based on SAP2000 models for a similar structure.

I.4 Flexible Wall frequency estimates

For the flexible wall problem specified in Appendix C, Impact_Deck estimate the first two natural frequencies as follows:

$$\omega_1 = 0.5 * \sqrt{\frac{k}{m}} \therefore \omega_2 = \sqrt{\frac{k}{2.0 * m^*}} \tag{I.13}$$

where:

$\bar{k}$ =the transverse elastic stiffness of the center pile group
m =total mass of one beam = mass density of the beam * cross-sectional area of the beam * length of one beam
m^* =total mass of the two beams = mass density of the beam * cross-sectional area of the beam * total length of the system including the length of the shear key.

This estimate is based on SAP2000 models for a similar structure.

Appendix J: Key Impact_Deck Program Variables

NSTU mode of operation:

1. Flexible Wall
2. Guard Wall
3. Impact Deck

DS<X,Y,R>() Input displacements (fixed)

FS<X,Y,R>() Input force/moment (fixed)

These variables describe a user-defined, piece-wise linear, force displacement curve for piles.

SPRING_K<X,Y,R>() Computed tangent stiffness of a pile group

SPRING_B<X,Y,R>() Computed force axis intercept a pile group

These variables return the tangent stiffness and force intercept (deflection=0) at each part of the user-defined, piece-wise linear, force displacement curve described by DS<X,Y,R>() and FS<X,Y,R>(). By working from the force intercept, the appropriate force for an absolute displacement can be computed

SK_SPRING() Current stiffness tangent at pile locations

SB_SPRING() Current stiffness force axis intercept at pile locations

Returned from the **stiffness()** function, these values return the current tangent stiffness and intercept that the pile is under. This value takes into considerations whether the pile is under an unload/reload cycle where the resisting force is less than the maximum force achieved to that point.

NELAS() Flag for elastic loading condition:

1. Load

2. Unload/Reload

UELAS<X,Y,R>	Greatest deflection to this point – for unload/reload cycle
X_LOAD()	The x-position of the applied load over time (along the wall)

This is pre-computed as a linear increment from the start point to the end point of the simulation, given in block 4 of the input file

U(,)	The absolute displacement of each pile over time
UD(,)	The absolute velocity of each pile over time
UDD(,)	The absolute acceleration of each pile over time
SK(,)	Element stiffness matrix
SM(,)	Element mass matrix
SKM(,)	Global stiffness matrix
SMM(,)	Global mass matrix
SKMM(,)	The global stiffness matrix (sans restraints on DOF)
SKMMS(,)	Intermediate matrix multi value
SMMM(,)	The global mass matrix (sans restraints on DOF)
SCMM(,)	The global damping matrix
ALFAA	Rayleigh damping term for mass – a0
BETAA	Rayleigh damping term for stiffness – a1

These variables are determined from the natural frequencies of the structure and □ (EFI1 in Block 5 of the Input File)

P_LOAD(,)	Force acting at nodes of the element at each time step (spread to adjacent nodes to the impact)
FOR_SPRING(,)	Element spring forces occurring at each node at each time step
ELENGTH()	Length of each wall segment (in the X direction only)
NRES	Total number of array indexes (~= number of nodes*number of DOF)
NODF<1,2,3>()	Index for DOF for node number
NOND	Number of nodes

NOTE: may not be the number of pile groups

NPS()	Indices for DOF information for pile groups (Flexible and Guard Walls)

REPORT DOCUMENTATION PAGE

Form Approved
OMB No. 0704-0188

Public reporting burden for this collection of information is estimated to average 1 hour per response, including the time for reviewing instructions, searching existing data sources, gathering and maintaining the data needed, and completing and reviewing this collection of information. Send comments regarding this burden estimate or any other aspect of this collection of information, including suggestions for reducing this burden to Department of Defense, Washington Headquarters Services, Directorate for Information Operations and Reports (0704-0188), 1215 Jefferson Davis Highway, Suite 1204, Arlington, VA 22202-4302. Respondents should be aware that notwithstanding any other provision of law, no person shall be subject to any penalty for failing to comply with a collection of information if it does not display a currently valid OMB control number. **PLEASE DO NOT RETURN YOUR FORM TO THE ABOVE ADDRESS.**

1. REPORT DATE *(DD-MM-YYYY)*	2. REPORT TYPE	3. DATES COVERED *(From - To)*
July 2016		

4. TITLE AND SUBTITLE

Simplified Dynamic Structural Time-History Response Analysis of Flexible Approach Walls Founded on Clustered Pile Groups Using Impact_Deck

5a. CONTRACT NUMBER

5b. GRANT NUMBER

5c. PROGRAM ELEMENT NUMBER

6. AUTHOR(S)

Barry C. White, José Ramón Arroyo, and Robert M. Ebeling

5d. PROJECT NUMBER

5e. TASK NUMBER

5f. WORK UNIT NUMBER
448769

7. PERFORMING ORGANIZATION NAME(S) AND ADDRESS(ES)

Information Technology Laboratory
U.S. Army Engineer Research and Development Center
3909 Halls Ferry Road, Vicksburg, MS 39180-6199;
Department of General Engineering
University of Puerto Rico, Mayagüez, PR 00681

8. PERFORMING ORGANIZATION REPORT NUMBER

ERDC/ITL TR-16-1

9. SPONSORING / MONITORING AGENCY NAME(S) AND ADDRESS(ES)

U.S. Army Corps of Engineers
441 G. Street NW
Washington, DC 20314-1000

10. SPONSOR/MONITOR'S ACRONYM(S)

11. SPONSOR/MONITOR'S REPORT NUMBER(S)

12. DISTRIBUTION / AVAILABILITY STATEMENT
Approved for public release; distribution is unlimited.

13. SUPPLEMENTARY NOTES

14. ABSTRACT

Flexible approach walls are being considered for retrofits, replacements, or upgrades to Corps lock structures that have exceeded their economic lifetime. This report discusses a new engineering software tool to be used in the design or evaluation of flexible approach walls founded on clustered pile groups and subjected to barge train impact events.

This software tool, Impact_Deck, is used to perform a dynamic, time-domain analysis of three different types of pile-founded flexible approach walls: an impact deck, an alternative flexible approach wall, and a guard wall. Dynamic loading is performed using impact-force time histories (Ebeling et al. 2010). This report covers the numerical methods used to create this tool, a discussion of the graphical user interface for the tool, and an analysis of results for the three wall systems.

The results of analyzing the three wall systems reveals that dynamic evaluations should be performed for these structures because of inertial effects occurring in the wall superstructure and substructure. These inertial effects can cause overall and individual response forces that are greater than the peak force from the impact-force time history.

This report also discusses the advantages of load sharing between multiple pile groups in an approach wall substructure. In the case of Lock and Dam 3, the peak reaction force for any individual pile group was 11% of the peak impact load.

15. SUBJECT TERMS
See reverse

16. SECURITY CLASSIFICATION OF:			17. LIMITATION OF ABSTRACT	18. NUMBER OF PAGES	19a. NAME OF RESPONSIBLE PERSON
a. REPORT	b. ABSTRACT	c. THIS PAGE			19b. TELEPHONE NUMBER *(include area code)*
Unclassified	Unclassified	Unclassified		264	

15. SUBJECT TERMS (concluded)

Barge impact
Barge train impact
Flexible lock approach wall
Impact_Deck
Impact_Force
Flexible approach wall
Guide wall
Guard wall
Pile groups
Clustered pile groups
Glancing blow
Impact Deck
Time-history analysis
Force time-history
Dynamic analysis
Dynamic structural analysis
Simply supported beam